MOUNTAIN-PLAINS CONSORTIUM

MPC 24-534 | E. Lawton, S. Maringanti and A. Jones

LOADING AND WETTING-INDUCED SETTLEMENT OF BRIDGE APPROACH EMBANKMENT MATERIALS IN UTAH

MOUNTAIN-PLAINS CONSORTIUM REGION 8

A University Transportation Center sponsored by the U.S. Department of Transportation serving the Mountain-Plains Region. Consortium members:

Colorado State University
North Dakota State University
South Dakota State University
University of Colorado Denver
University of Denver
University of Utah
Utah State University
University of Wyoming

Technical Report Documentation Page

1. Report No.	2. Government Accession No.	3. Recipient's Catalog No.
MPC-607		

4. Title and Subtitle	5. Report Date
Loading and Wetting-induced Settlement of Bridge Approach Embankment Materials in Utah	July 2024
	6. Performing Organization Code

7. Author(s)	8. Performing Organization Report No.
Evert Lawton, Professor Emeritus Sai Sravan Maringanti, Graduate Research Assistant Adam C. Jones, Graduate Research Assistant	MPC 24-534

9. Performing Organization Name and Address	10. Work Unit No. (TRAIS)
University of Utah Civil & Environmental Engineering 110 Central Campus Dr., Room 2000 Salt Lake City, Utah 84112	11. Contract or Grant No.

12. Sponsoring Agency Name and Address	13. Type of Report and Period Covered
Mountain-Plains Consortium North Dakota State University PO Box 6050, Fargo, ND 58108	Final Report
	14. Sponsoring Agency Code

15. Supplementary Notes

Supported by a grant from the US DOT, University Transportation Centers Program

16. Abstract

Often engineers and maintenance personnel are faced with a serious problem in the maintenance of bridges due to excessive settlement of approach embankments near bridge abutments, causing bumps at the ends of the bridges. These settlements result from loading-induced and sometimes wetting-induced strains within the native material at the site caused by the weight of the embankment and loading and wetting-induced strains within the embankment material itself. The primary objectives of this research were to (a) determine the loading-wetting stress-strain properties of 10 selected embankment materials under varying conditions of density, load, and moisture; (b) identify potential problems for each type of embankment material in terms of contributing to settlement that may exacerbate the “bump at the end of the bridge” problem; and (c) recommend changes to Utah Department of Transportation specifications for embankment materials used in bridge approaches. These objectives were achieved by conducting one-dimensional compression-wetting tests on compacted specimens of the materials using standard and larger consolidometers. Based on results and analyses from these tests, recommendations were made to change the current specifications regarding grain-size distribution, plasticity of the materials; shape of the particles; moisture condition during processing, transport, and compaction; allowable compaction during freezing or snowy conditions, and the method used for quality control.

17. Key Word	18. Distribution Statement
bridge approaches, deformation curve, embankments, laboratory tests, load tests, settlement (structures), specifications, wetting	Public distribution

19. Security Classif. (of this report)	20. Security Classif. (of this page)	21. No. of Pages	22. Price
Unclassified	Unclassified	218	n/a

Form DOT F 1700.7 (8-72) Reproduction of completed page authorized

Loading and Wetting-induced Settlement of Bridge Approach Embankment Materials in Utah

Evert Lawton
Professor Emeritus

Sai Sravan Maringanti
Graduate Student

Adam C. Jones
Graduate Student

Department of Civil and Environmental Engineering
The University of Utah

July 2024

Acknowledgements

The authors sincerely appreciate and acknowledge the financial support for this research project provided by the Mountain Plains Consortium (MPC) under Contract No. MPC-607 and the Utah Department of Transportation (UDOT) under Contract No. 208178 (Research PIC No. UT 19.406). The authors also gratefully acknowledge the help and guidance provided by the following individuals from UDOT who served on the Technical Advisory Committee:

- Grant Gummow
- James Corney
- Jim Higbee
- Lonnie Marchant
- Travis Gerber (Consultant)
- Mark Daniels
- Ken Talbot
- Cheryl Hersh Simmons
- Keith Brown
- Scott Nussbaum.

The assistance provided by Lonnie, Jim, and Grant in identifying sources and providing contact information for the borrow materials used to manufacture the soils studied in this research project is also truly appreciated. Sincere thanks are due to David Stevens of UDOT Research and Innovation for managing this project. Cort Van Gorder from the Kilgore Ready Mix Plant graciously donated a sufficient amount of their 3/8" screen fines to fill 33 five-gallon buckets to this project. This material was used to manufacture all or parts of several of the soils tested in this project, and this donation is sincerely appreciated.

Disclaimer

ABSTRACT

Often engineers and maintenance personnel are faced with a serious problem in the maintenance of bridges due to excessive settlement of approach embankments near bridge abutments, causing bumps at the ends of the bridges. These settlements result from loading-induced and sometimes wetting-induced strains within the native material at the site caused by the weight of the embankment and loading and wetting-induced strains within the embankment material itself. The primary objectives of this research were to (a) determine the loading-wetting stress-strain properties of 10 selected embankment materials under varying conditions of density, load, and moisture; (b) identify potential problems for each type of embankment material in terms of contributing to settlement that may exacerbate the "bump at the end of the bridge" problem; and (c) recommend changes to Utah Department of Transportation specifications for embankment materials used in bridge approaches. These objectives were achieved by conducting one-dimensional compression-wetting tests on compacted specimens of the materials using standard and larger consolidometers. Based on results and analyses from these tests, recommendations were made to change the current specifications regarding grain-size distribution, plasticity of the materials; shape of the particles; moisture condition during processing, transport, and compaction; allowable compaction during freezing or snowy conditions, and the method used for quality control.

TABLE OF CONTENTS

LIST OF TABLES

LIST OF FIGURES

UNIT CONVERSION FACTORS

SI* (MODERN METRIC) CONVERSION FACTORS

APPROXIMATE CONVERSIONS TO SI UNITS

Symbol	When You Know	Multiply By	To Find	Symbol
		LENGTH		
in	inches	25.4	millimeters	mm
ft	feet	0.305	meters	m
yd	yards	0.914	meters	m
mi	miles	1.61	kilometers	km
		AREA		
in^2	square inches	645.2	square millimeters	mm^2
ft^2	square feet	0.093	square meters	m^2
yd^2	square yard	0.836	square meters	m^2
ac	acres	0.405	hectares	ha
mi^2	square miles	2.59	square kilometers	km^2
		VOLUME		
fl oz	fluid ounces	29.57	milliliters	mL
gal	gallons	3.785	liters	L
ft^3	cubic feet	0.028	cubic meters	m^3
yd^3	cubic yards	0.765	cubic meters	m^3
		NOTE: volumes greater than 1000 L shall be shown in m^3		
		MASS		
oz	ounces	28.35	grams	g
lb	pounds	0.454	kilograms	kg
T	short tons (2000 lb)	0.907	megagrams (or "metric ton")	Mg (or "t")
		TEMPERATURE (exact degrees)		
°F	Fahrenheit	5 (F-32)/9 or (F-32)/1.8	Celsius	°C
		ILLUMINATION		
fc	foot-candles	10.76	lux	lx
fl	foot-Lamberts	3.426	$candela/m^2$	cd/m^2
		FORCE and PRESSURE or STRESS		
lbf	poundforce	4.45	newtons	N
lbf/in^2	poundforce per square inch	6.89	kilopascals	kPa

APPROXIMATE CONVERSIONS FROM SI UNITS

Symbol	When You Know	Multiply By	To Find	Symbol
		LENGTH		
mm	millimeters	0.039	inches	in
m	meters	3.28	feet	ft
m	meters	1.09	yards	yd
km	kilometers	0.621	miles	mi
		AREA		
mm^2	square millimeters	0.0016	square inches	in^2
m^2	square meters	10.764	square feet	ft^2
m^2	square meters	1.195	square yards	yd^2
ha	hectares	2.47	acres	ac
km^2	square kilometers	0.386	square miles	mi^2
		VOLUME		
mL	milliliters	0.034	fluid ounces	fl oz
L	liters	0.264	gallons	gal
m^3	cubic meters	35.314	cubic feet	ft^3
m^3	cubic meters	1.307	cubic yards	yd^3
		MASS		
g	grams	0.035	ounces	oz
kg	kilograms	2.202	pounds	lb
Mg (or "t")	megagrams (or "metric ton")	1.103	short tons (2000 lb)	T
		TEMPERATURE (exact degrees)		
°C	Celsius	1.8C+32	Fahrenheit	°F
		ILLUMINATION		
lx	lux	0.0929	foot-candles	fc
cd/m^2	$candela/m^2$	0.2919	foot-Lamberts	fl
		FORCE and PRESSURE or STRESS		
N	newtons	0.225	poundforce	lbf
kPa	kilopascals	0.145	poundforce per square inch	lbf/in^2

*SI is the symbol for the International System of Units. (Adapted from FHWA report template, Revised March 2003)

LIST OF ACRONYMS AND TERMS

AASHTO: American Association of State Highway and Transportation Officials
ASTM: American Society for Testing and Materials
C: Clay fraction
CP: Collapse potential
C_u: Coefficient of uniformity
e_0: Initial void ratio
FHWA: Federal Highway Administration
G_s: Specific gravity of soil solids
I_e: Collapse Index
LSC: Large-Scale Consolidometer
p_A: atmospheric pressure
PI: Plasticity Index
p_w Pressure at wetting
R_c Relative compaction
R_m As-compacted relative compaction based on Modified Proctor test (AASHTO T 180)
R_s As-compacted relative compaction based on Standard Proctor test (AASHTO T 99)
S Sand fraction
SC Standard Consolidometer
S_L Loading-induced settlement
S_w Wetting-induced settlement
S_r Degree of saturation
UDOT Utah Department of Transportation
w As-compacted water content
w_i Initial water content
w_{opt} Optimum moisture content
ε_L Loading-induced strain
ε_v Vertical strain
ε_w Wetting-induced strain
γ_d Dry unit weight
γ_{dmax} Maximum dry unit weight
γ_w Unit weight of water
σ_3 Minor principal stress
σ_v Total vertical stress

EXECUTIVE SUMMARY

Often, engineers are faced with a serious problem in the maintenance of bridges due to the excessive settlement of the approach embankments near the bridge abutments, causing bumps at the ends of the bridges. These settlements result from loading-induced strains and, sometimes, wetting-induced strains within the native material at the site caused by the weight of the embankment, and loading and wetting-induced strains within the embankment material itself. The primary objectives in this research project were (a) to determine the loading-wetting stress-strain properties of 10 selected embankment materials under varying conditions of density, load, and moisture, (b) identify potential problems for each type of embankment material in terms of contributing to settlement that may exacerbate the "bump at the end of the bridge" problem, and (c) recommend changes to the specifications for embankment materials used in bridge approaches.

To achieve these objectives, one-dimensional compression-wetting tests were conducted on compacted specimens of the 10 selected materials using standard-size consolidometers and a large-scale consolidometer. A total of 181 tests were conducted - 154 tests were conducted on nine different soils using standard consolidometers, and 27 tests were conducted on three different soils using the large-scale consolidometer. The large-scale consolidometer was fabricated by the University of Utah as part of this project. Both single consolidometer tests (loading-wetting of single as-compacted specimens) and double consolidometer tests (loading nominally identical as-compacted and soaked specimens) were performed. For the standard-size consolidometer tests, specimens of granular soil were compacted using vibration from a vibrating table and specimens of cohesive soil were compacted using kneading compaction (Harvard miniature tamper). For the large-scale consolidometer tests, specimens were prepared using a rammer with a flat plate for granular soils and a plate with protruding feet for cohesive soils.

Based on the data obtained from the standard consolidometer tests, equations were developed for each soil type using multiple parameter linear regression to estimate the loading and wetting-induced strains at specified values of overburden pressure, as-compacted relative compaction and water content. In general, a better correlation was observed for the regression equations developed using the as-compacted degree of saturation instead of the as-compacted relative compaction and water content of the fill material.

Analysis of the results from the standard consolidometer tests showed that the cohesive soils — even those with low plasticity — would be susceptible to unacceptable loading and wetting-induced time-dependent strains that make these materials unacceptable for bridge approach embankments. Therefore, the decision was made to conduct most of the large-scale consolidometer tests on specimens of two nonplastic, well-graded granular soils. Analysis of the results from the large-scale consolidometer tests showed the wetting-induced strains for a 30-foot-tall embankment comprised on the two granular soils tested would be very small, even from full wetting of the embankment. In contrast, the loading-induced strains were large enough to cause significant settlement from strains within the embankment itself. However, these settlements would occur quickly in the field (during the construction process) and would not likely contribute to the bumps at the ends of the bridges.

No comparisons could be made for tests conducted in the Standard Consolidometer (SC) and those conducted in the large-scale consolidometer for which all materials and conditions were nominally identical. However, reasonably close comparisons showed the strains in LSC tests were several times greater than the strains in the SC tests. These very large differences are likely attributable to the differences in boundary constraints related to the different sizes of the specimens.

Based on results from these tests, and analysis of those results, recommendations were made to change the current specifications regarding grain-size distribution and plasticity of the materials; shape of the particles; moisture condition during processing, transport, and compaction; and allowable compaction during freezing or snowy conditions. In addition, a recommendation was made to change the method used for quality control of the compacted embankment material from Proctor-type tests to cyclic plate-load tests.

1. INTRODUCTION

Collapse can be defined as the subsidence of soil due to an increase in the water content from its natural state without any change in the overburden pressure. Contrary to popular belief that collapse only occurs in certain types of collapsible soils like loess or laterites, it can occur in any type of soil when it is subjected to saturation. Collapse not only occurs in naturally deposited soils but also in compacted soils.

Compacted fill is mainly used as an embankment for pavement systems, earthen dams and as a backfill beneath bridge approaches and other structures. They can be subjected to either saturation or increase in the water content due to increase in the level of groundwater table, leakage in underground water pipelines, storm water drainage, etc., which can cause collapse to occur within the fill and lead to problems, like excessive settlement, cracking and failure of slopes, pavement distress and damage to the underground utilities.

One such problem that can be caused in bridges is the excessive settlement of the bridge approaches, often referred to as the "Bump at the end of the bridge" or more simply the "Bump at the bridge." Bridge approach slabs which serve as a transition between the pavement and the bridge deck are built on an embankment constructed using a select fill material. This embankment — if constructed without conforming to proper compaction specifications — can cause collapse to occur when the soil is subjected to an increase in the water content. According to a survey, this problem affects about 25 percent of the bridges in United States and the estimated maintenance cost is at least 100 million per year nationwide (Briaud, 1997).

When expansive soils are used for the construction of compacted fills, the vertical movements are caused due to swelling and collapse. Swelling usually occurs at low overburden stresses, which are observed in the upper layers of the fill, and collapse occurs at higher overburden stresses (usually in the range of 2–3 tsf), which are observed in the lower layers of the fill. Sometimes, this can be beneficial if the overall vertical profile of the fill is taken into account, as the negative effects of swelling and collapse counteract each other, depending on the magnitudes of swelling and collapse.

Apart from the settlements caused due to wetting-induced collapse and swelling embankments are subjected to strains due to loading-induced stresses from self-weight and loads from the traffic above the pavement. Unlike granular soils, in cohesive soils most of the strength to resist loading-induced strains is derived from the cementation between the soil particles caused due to matric suction. This strength in cohesive soils is drastically lost when the water content is even increased slightly. In granular soils, however, the interlocking between the soil particles is the main root cause for the strength against loading-induced strains.

One of the long-term problems compacted fills are prone to is excessive settlement caused due to secondary compression. Sometimes, this problem is referred to as the "creep settlement" as it occurs when the soil is subjected to a constant overburden stress over a long period of time. Secondary compression occurs after the completion of the primary consolidation of soil under a constant uniform stress. In compacted granular soils, it is difficult to distinguish the secondary compression from primary consolidation — both occur almost instantaneously within the first few minutes of loading the specimen. However, in cohesive soils, the distinction between primary consolidation and secondary compression can be clearly observed by the characteristic reverse "S" shape for the loading-induced strain vs. logarithm of time plot.

This research project is aimed at studying the negative effects caused due to all the three components of settlement in compacted fills namely: wetting-induced, loading-induced and secondary compression and providing appropriate measures toward mitigating this problem that is affecting the maintenance of bridges for many state departments of transportation across the country.

2. LITERATURE REVIEW

2.1 Introduction

Much of the research on collapsible soils in the literature has emphasis on the wetting-induced collapse of compacted cohesive soils. However, the mechanisms of collapse and the laboratory methodologies for prediction of collapse settlement of cohesive soils are also applicable to compacted granular soils. Since it is possible that even clean sands and soils containing a substantial amount of gravel content are also susceptible to wetting-induced strains at certain conditions, the method of analysis and the equations developed to estimate the collapse of cohesive soils do not apply for compacted granular soils.

2.2 Previous Research on Loading and Wetting-induced Collapse

Booth (1977) published a report on the adverse effects of wetting-induced collapse in compacted fills across Southern Africa. He was among the first to conduct an investigation to examine factors influencing the effects of wetting-induced collapse in compacted soils. Before that, there had been research on wetting-induced collapse of naturally deposited soils by conducting double consolidometer experiments on undisturbed soil samples (Jennings and Knight, 1957). Booth adopted those same laboratory techniques and collapse mechanisms in his research on compacted soil samples collected from different roadway embankment fills across South Africa. The specimens were compacted in the consolidometer rings using a static method of compaction. Booth's research has revealed that collapse settlement can occur in almost any type of soil that has low relative density. It also points out that a critical moisture content exists for every soil, which is in the range of one to two percent more than Proctor optimum. No collapse settlement was observed above this critical moisture content. He also discusses the effects of clay mineralogy and soil gradation, but both factors seem less important than the initial dry density.

Lawton (1986) conducted approximately 150 wetting-induced volume change tests on an expansive soil compacted in laboratory using static, impact and kneading methods of compaction. Consolidometer tests were used to model the one-dimensional strain conditions e.g., very wide fills, which are rarely observed in the field, and triaxial tests were conducted to model the effects of principal stress ratio on the wetting-induced volume changes of the compacted soils. The soil used in this research was primarily cohesive and had significant amounts of plastic fines in it. Major observations from the consolidometer tests were: (1) There existed a crossover pressure below which swelling was observed when the soil was wetted, and collapse was observed when the overburden stress increased beyond the crossover pressure. (2) Zero collapse was observed when the soil was compacted at a molding water content wet of optimum. (3) The magnitude of collapse for all conditions of relative compaction and molding water content is only slightly dependent on the compaction method.

Basma and Tuncer (1992) investigated the effect of soil type, compaction water content, initial dry unit weight and applied pressure at wetting on collapse potential by conducting single consolidometer tests on eight different types of soil. A majority of the different soil types used in their study were categorized as silty clays and had a significant fraction of cohesive material. Static method of compaction was used to compact the soil directly into the consolidometer rings. From the experimental results of the consolidometer tests, they proposed two collapse predictive models by performing multiple linear regression analysis and are given by Equations 2.1 and 2.2.

$$CP = 48.496 + 0.102C_u - 0.457w_i - 3.533\gamma_d + 2.80\ln(p_w) \quad (2.1)$$

where

CP = the collapse potential in percent;
C_u = the coefficient of uniformity of the soil;
w_i = the initial water content in percent;
γ_d = the compaction dry unit weight in kN/m^3;
p_w = the pressure at wetting in kPa.

$$CP = 47.506 - 0.072(S - C) - 0.439w_i - 3.123\gamma_d + 2.851\ln(p_w) \quad (2.2)$$

where

S = percentage of sand fraction;
C = percentage of clay fraction.

Sasitharan et al. (1993) have conducted triaxial tests on loose cohesionless sands and characterized their behavior under static and dynamic loading conditions. The soil samples collected for the purpose of this research were from Ottawa, Illinois. The specimens were compacted in layers using tamping method of compaction with a small drop hammer. The behavior of loose sands, when subjected to a variety of stress paths using both drained and undrained loading conditions that can cause collapse, was studied using a conventional triaxial apparatus setup. The major finding from results of the triaxial test were that the post peak portion of the constant void ratio test defines a state-boundary surface, and when the loading exceeds beyond this surface, collapse of loose cohesionless material may occur. Although this study was more concentrated on the liquefaction phenomenon observed in loose sands when subjected to dynamic loading, it gives certain information about the loading-induced collapse of loose sands when different stress paths are followed. However, the findings were pertinent to loose sands and may not be applicable to compacted cohesionless soils.

Moisture condition has a significant influence on compressibility and strength of compacted cohesive soils. It was observed that the matric suction was reduced by almost 78% due to just an increase of 6% in moisture content (Lawton, 2001). The strength of well-compacted cohesive soils is derived from matric suction to such an extent that they are virtually incompressible at extremely low water contents. However, the compressibility of these soils increases with an increase in the moisture content. Thus, when cohesive soils are compacted at a higher moisture content, they will become more susceptible to loading-induced strains. In cohesive soils, the initial dry density of the soil also plays a vital role in determining the strength against loading-induced strains. It was observed that an increase in the density of compacted cohesive soils increased the stiffness and strength and decreased the compressibility of the soil. Also, the compactive prestress increased with increasing density at the same water content as more energy was required to achieve a higher density. It should be noted these observations were made specifically for compacted cohesive soils and should not be generalized for granular soils. Since the particle size of granular soils is considerably higher than cohesive soils, matric suction is negligible and does not contribute toward the loading induce strength or compressibility.

Lim and Miller (2004) studied the wetting-induced compression of compacted Oklahoma soils by conducting single consolidometer tests on a variety of soils consisting of highly plastic clays, low plastic silts, weather shales, non-plastic sands, and weathered sandstone. The majority of soils tested in this study were classified as AASHTO A-3, A-4, A-6 and A-7-6, with just one soil type falling in the category of A-1-b. Empirical relations were developed based on the statistical analysis of the data from the experiments. The collapse index was evaluated by taking the Clay-size fraction, Plasticity Index, Liquid Limit and Activity as the predictor parameters. A collapse index (I_e), predictive model was also proposed in terms of compaction moisture content (w), dry unit weight (γ_d), plasticity index (PI), and clay-size fraction (C), and is given in the Equation 2.3.

$$I_e(\%) = 9.805 - 0.261w\ (\%) - 0.424\gamma_d\left(\frac{kN}{m^3}\right) + 0.058PI\ (\%) + 0.0697C\ (\%) \quad (2.3)$$

Sridharan and Gurtug (2004) have performed a series of consolidometer tests on three different types of Cyprus fine-grained soils to study the long-term swelling behavior of cohesive soils with a plasticity index ranging from 7 to 58. To get a full spectrum picture of how plasticity affects the swelling behavior of compacted clays, two additional soil samples, consisting of low plasticity Kaolinite and highly plastic Montmorillonite clays, were used. The specimens used for the swell test were prepared by impact method of compaction at three different compaction energy levels i.e., Standard Proctor, Reduced Modified Proctor and Modified Proctor. The consolidometer tests were continued until each of the specimens reached equilibrium under a specified level of applied pressure. It was observed that after inundation, the low plastic soil specimen reached equilibrium within 24 hours, while the highly plastic specimens took 7 days or more to attain equilibrium prior to loading. The specimens were then loaded gradually to reach their original volume. From the results of the consolidometer tests they have conducted, it was observed that swelling potential increases linearly with log of time in the secondary portion, and the slope of that line increased as the soil plasticity increased. The rate of secondary swelling was also observed to be more than the rate of secondary compression.

Cerato et al. (2009) have conducted single and double consolidometer tests to determine the effects of the clod size and soil structure on wetting-induced collapse in cohesive soils. The samples used in this research program were collected from nine different natural soil deposits located across Oklahoma. The soil samples were majorly cohesive in nature with only one clayey sand and one clayey silt samples. The specimens used for consolidometer tests were prepared by two methods of compaction: 1) By direct compaction of soil into the consolidometer rings using tamper rod to imitate Proctor compaction and 2) Trimming the soil specimen from a compacted soil sample extracted from a Standard Proctor mold. The soil structure was associated to the specimen preparation methods and several other factors such as compaction methods, clod size, moisture condition of the clods, etc. They found that the differences in evaluating the collapse settlement caused due to soil structure influenced clayey soils more than silts and clayey sands with low plasticity. Their research has pointed out the necessity for the specimen preparation and compaction methods used in the laboratory to model the actual field compaction methods as close as possible to minimize the differences in predicting the actual field settlement from the laboratory experimental results.

Ashour et al. (2020) developed a collapse potential predictive model based on the experimental data gathered from Basma & Tuncer (1992), Habibagahi (2004) and Qian et al. (2014). The database for modeling the behavior of inundated soils in their study consisted of results from 339 single consolidometer tests conducted on undisturbed samples of different types of soils. The collapse predictive model they developed was based on the initial soil properties, which they identified as the most critical in affecting the wetting-induced collapse of soils, and multiple linear regression analysis was employed with those particular soil parameters. The predictive model for collapse settlement they proposed is given in the Equation 2.4. This model was developed primarily based on naturally deposited soils, since the experiments were conducted on undisturbed samples and not on compacted collapsible soils.

$$CP = -17.373 + 1.355\ln\sigma_3 + 16.156e_0 + 21.366e^{-5.5S_r} + 0.00088C_u^2 \quad (2.4)$$

where

CP = the collapse potential in percent;
σ_3 = applied pressure in kPa;
e_0 = initial void ratio;

S_r = degree of saturation in percent;
C_u = the coefficient of uniformity of the soil

2.3 Conclusions

A significant amount of research has already been done on loading-induced settlement and wetting-induced collapse of compacted soils. The following are observations and conclusions from works reported in the literature review:

- There are reports of wetting-induced collapse occurring not only in naturally deposited soils but also in compacted fills.
- The wetting-induced collapse potential of the compacted soil decreases with decreasing overburden stress, increasing water content and increasing relative compaction.
- The wetting-induced collapse increases with increasing plasticity index and increasing clay fraction.
- The wetting-induced collapse potential for uniformly graded soils is more than well-graded soils.
- The loading-induced compressibility and strength of compacted cohesive soils depends on the as-compacted moisture condition of the soil. Increasing the compaction water content of soil increases its susceptibility toward loading-induced strains.
- Apart from moisture condition, the initial dry density also affects the compressibility of compacted cohesive soils, especially at small magnitudes (5%) of loading-induced strains. With increasing dry density, the soil will be less compressible and is more resistant toward loading-induced strains. Also, a higher compactive prestress is needed to produce such a soil.
- The swelling potential of compacted cohesive soils increases linearly with log of time, and the rate of swelling increases with increasing plasticity of the soils.
- The rate of secondary swelling was observed to be more than the rate of secondary compression under loading, indicating that swelling is more detrimental compared to collapse in highly plastic soils.

While a vast amount about collapse in compacted fills is known, there are some research gaps that the current research program was designed to fill.

- Although granular soils have been known to pose fewer problems regarding wetting-induced collapse, there is very little evidence available in the literature about their wetting-induced stress-strain characteristics, especially that of A-1 soils compacted at very low water contents.
- There is limited research regarding the loading-induced stress-strain characteristics of compacted soils, and most of the research available was pertinent to only cohesive soils.
- None of the previous works have included the specimen preparation using the vibratory method of compaction for granular soil types in consolidometer testing.
- The regression analysis done in most of the previous works included primarily cohesive soils and whether those models are valid for predicting collapse in granular soils is unknown.

3. METHODOLOGY FOR STANDARD CONSOLIDOMETER TESTS

This research project consisted of 70 double consolidometer tests (35 sets of two tests) and 84 single consolidometer tests conducted on soil collected from various borrow pits across Northern Utah. The one-dimensional consolidometer tests are used to model one-dimensional strain conditions often observed in very wide embankments. However, the field situations may vary as the highway embankments are not usually wide enough that only plane-strain is observed.

In subsequent sections, the soils used for the consolidometer testing, their visual and engineering properties, the equipment used for testing, testing and data analysis methods will be discussed in detail.

3.1 Soil Description

The research project required that nine (9) different soil grades be manufactured for the standard consolidometer tests, according to the specifications summarized in Table 3.1. Three different samples of soil having the desired levels of plasticity, as shown in Figure 3.1, were collected from the borrow pits and brought to the laboratory, where the soil was air-dried for several days. When the soil samples were dry enough that they could be sieved, the soil agglomerates were broken down to individual particles sizes by hand crushing, and the soil was poured into a testing screen shown in Figure 3.2, which was used to divide the soil into the required particle sizes.

The soil gradation was then adjusted to manufacture the required soil grade for testing. For the soil grades containing plastic fines, hydrometer analysis was conducted on the fraction passing through the No. 200 US sieve size according to ASTM D7928-17 standard. The grain size distribution curves for the different grades of soil used in the research are shown in Figure 3.3. Additionally, Atterberg limits tests have been conducted on the soil grades having plastic fines according to ASTM D4318-17e1 standard. The results of both hydrometer analysis and Atterberg's limits tests have also been summarized in Table 3.1.

To achieve homogeneity while reducing the soil sample from bulk to the test size, a gate-operated universal sample splitter, shown in Figure 3.4, was used. The manufactured soil was split several times until the sample is reduced to the weight required for each test (approximately 500g). The test samples, which are homogenous after splitting, are then placed in two plastic bags with air extracted from the bags and stored in a dry, cool place prior to testing.

To determine the optimum moisture content (w_{opt}) and the maximum dry density (γ_{dmax}) for each of the test materials, proctor tests were conducted on the different soil grades used in the consolidometer testing. According to Section 02056:1.5.A.4 of the UDOT 2017 Standard Specifications for Road and Bridge Construction, Modified Proctor (ASTM D1557-12e1) was used for A-1 soils and Standard Proctor (ASTM D698-12e2) was used for all other soils. The results of the Proctor tests are summarized in Table 3.2. The compaction curves for all the soil grades are shown in Figures A.1 through A.9 in Appendix A.

Table 3.1 Gradation of the Soil Used for Standard Consolidometer Testing

Particle size (mm)	Sieve No.	Percentage finer (%)								
		A-1-a (SP or SW)	A-1-a (SM)	A-1-a (SC - SM)	A-1-b (SM)	A-1-b (SC - SM)	A-3 (SP - SM)	A-2 (SC)	A-2 (SC)	A-4 (CL)
19	3/4 in.									
4.75	No. 4	100	100	100						
2.00	No. 10	50	50	50	100	100				
0.425	No. 40	30	30	30	50	50	100	100	100	
0.075	No. 200	5	15	15	25	25	10	35	35	100
0.040	40µm			7		11		30	30	85
0.020	20µm			6		10		28	28	79
0.010	10µm			5		9		23	23	65
0.005	5µm			4		7		15	15	44
0.002	2µm			3		4		6	6	18
0.001	1µm			2		3		4	4	10
Liquid Limit, LL		N/A	N/A	19	N/A	19	N/A	30	42	42
Plasticity Limit PL		NP	NP	15	NP	15	NP	20	22	22
Plasticity Index, PI		N/A	N/A	4	N/A	4	N/A	10	20	20

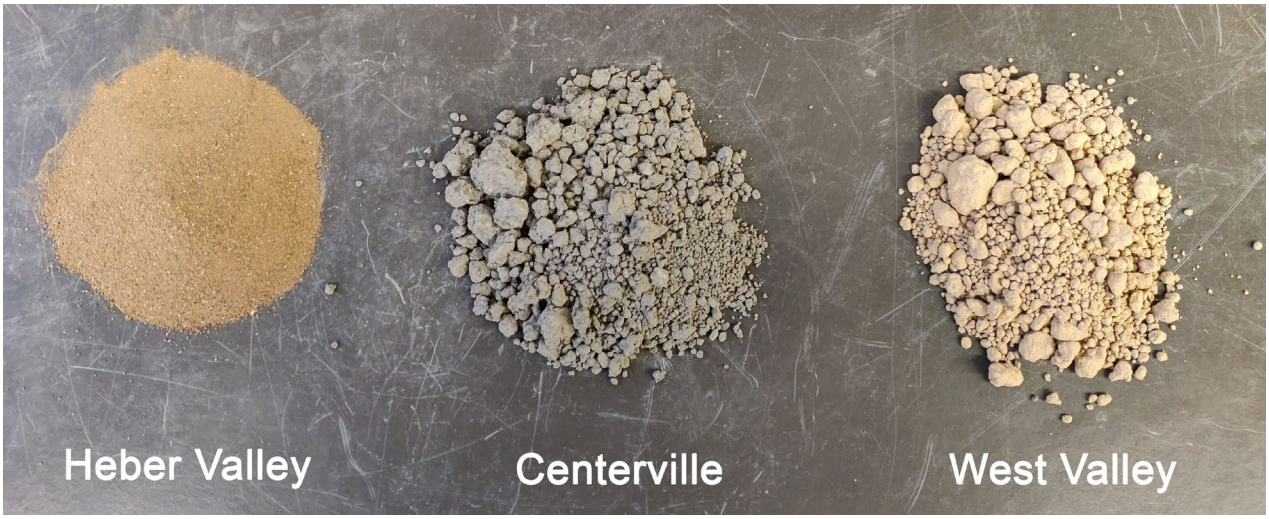

Figure 3.1 Different Soil Samples Collected From Borrow Pits in Northern Utah

Figure 3.2 Testing Screen Used In Sieving the Soil. (*Testing Screen*, n.d.)

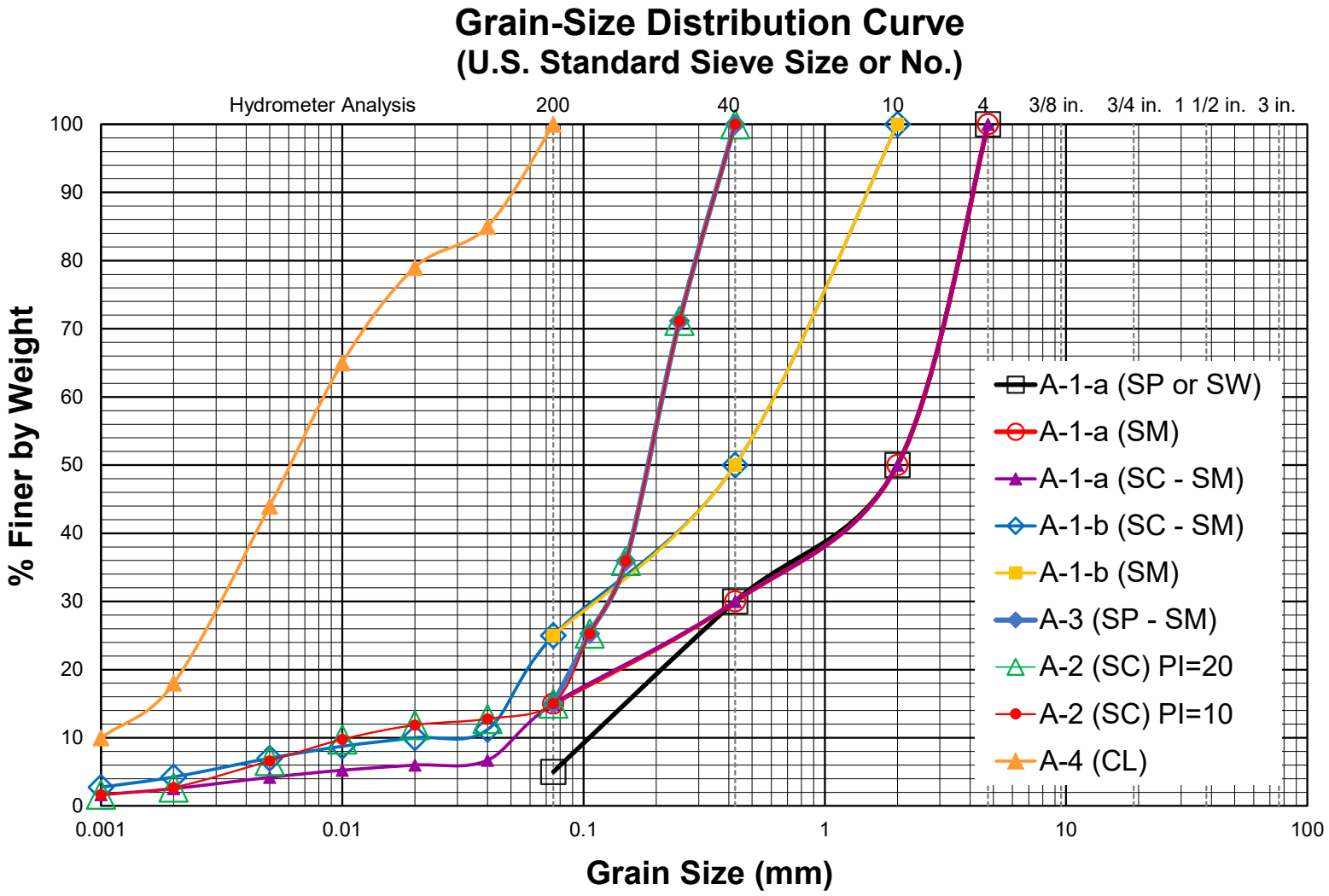

Figure 3.3 Grain Size Distribution of the Test Materials for the Standard Consolidometer Tests

Figure 3.4 Universal Sample Splitter (*Sample Splitter*, n.d.)

Table 3.2 Proctor Test Results for Each of the Test Materials

No.	Description of the test	Soil Type	γ_{dmax} (pcf)	w_{opt} (%)
1	Modified Proctor Test	A-1-a (SP or SW)	129	10.1
		A-1-a (SC-SM)	142	6.3
		A-1-a (SM)	128	10.0
		A-1-b (SC-SM)	137	6.7
		A-1-b (SM)	123	12.0
2	Standard Proctor Test	A-2 (SC) PI>>11	109	19.0
		A-2 (SC) PI=10	112	15.5
		A-3 (SP-SM)	112	16.0

3.2 Preparation of Soil Before Compaction.

A small amount of the test sample — enough to determine the air-dried moisture content of the soil — was removed from the storage bag and placed in a moisture tin after the empty weight of the tin was measured. The weight of the moisture tin containing the air-dried soil was measured. The moisture tin with the soil was then placed in the oven at 210° C for 15 minutes. The moisture tin was removed from the oven and the weight of the moisture tin containing the oven-dried soil was measured. The air-dried moisture content was determined from the above-mentioned weights.

A sufficient amount of soil was then removed from the storage bag and taken into a ceramic dish. It was noted that this amount accounted for some wastage of the soil that can occur due to the compaction process. The appropriate amount of deionized water to be added to the air-dried soil to achieve the desired level of moisture content was then calculated and added to the soil in the ceramic dish and mixed using a metal spoon. In some cases, when the soil has significant amounts of cohesive material in it, the soil forms moist agglomerates when mixed with water. These moist agglomerates were broken down by hand as much as possible and mixed thoroughly to achieve a uniform moisture content throughout the soil sample. The amount of water added was a little more than required to account for the moisture losses that may occur during the compaction process when the soil is exposed to atmosphere. The moist soil was then placed into two storage bags and sealed, removing all the air from the bags. The moist soil was left in the bags for 24 hours (or overnight) to cure.

3.3 Consolidometer Test Procedures

3.3.1 Description of the Equipment

The consolidometer tests were conducted using six dead-weight consolidation frames equipped with digital dial gauges to take the specimen deformation readings. Fixed ring consolidation cells, with porous stones on top and bottom of the specimen, were used. Stainless steel rings, with a nominal diameter of 2.5 inches and a nominal height of one inch, were used inside the consolidation cells.

3.3.2 Vibratory Compaction for Double Consolidometer Specimens

The field compaction method generally used for granular soils is compaction by using vibratory smooth-drum rollers. To model this type of compaction method in the laboratory, the soil was compacted directly inside the consolidation cell using a Relative Density Vibrating Table, shown in Figure 3.5.

A funnel-like apparatus that fits into the saturation tank of the consolidation cell and has the same inside diameter as that of the consolidation ring (as shown in Figure 3.6) was 3D-printed using ABS (Acrylonitrile Butadiene Styrene) plastic filament. This apparatus was used to prevent the soil from overflowing from the lip of the ring and to allow application of additional loading discs on top of the soil during the compaction process.

The soil was compacted in two to four lifts, depending on the level of relative compaction desired to achieve for a particular test. First, the soil required to achieve the desired level of relative compaction at a specified moisture condition relative to the optimum moisture content is calculated. Then, the required amount of moist soil was weighed and divided into equal parts, depending on the number of lifts in which the soil was to be compacted.

Figure 3.5 Relative Density Vibrating Table. (*Vibrating Table*, n.d.)

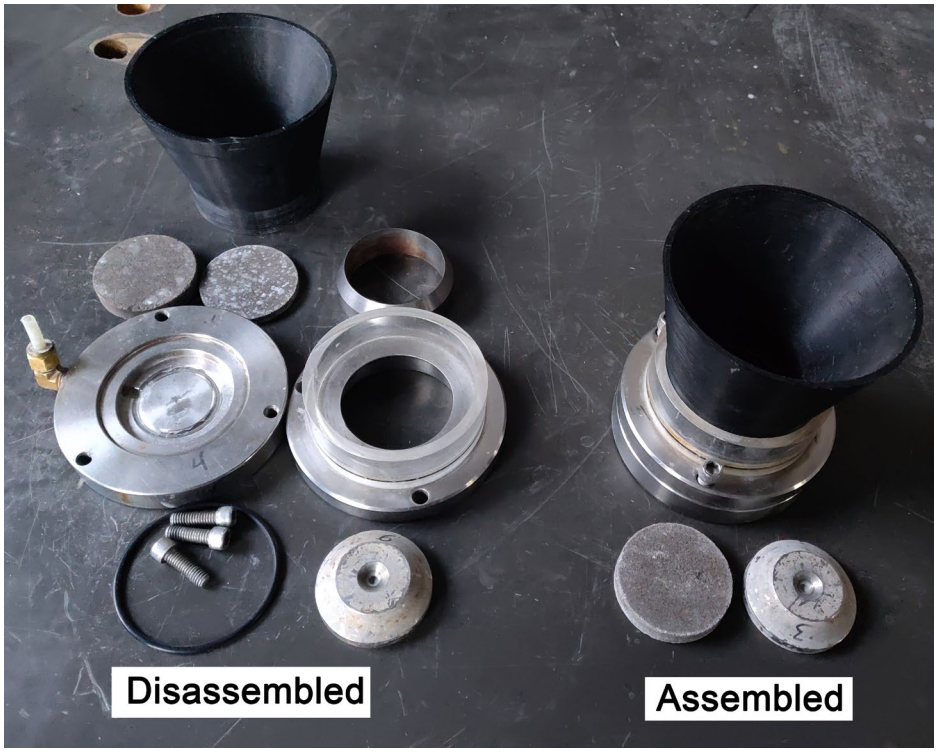

Figure 3.6 Figure Showing the Consolidation Cell Assembly and the Funnel Apparatus

The inside wall of the consolidation ring was sprayed with silicone lubricant to reduce the side friction between the ring and the soil specimen. The consolidation cell was then assembled. The empty weight of the consolidation cell with the bottom porous stone was noted. Next, the funnel apparatus was fitted on top of the consolidation cell, as shown in Figure 3.6, and the first portion of the soil was then poured into the consolidation ring. The soil was leveled by tapping gently with a glass rod. The entire assembly was then placed on the surface of the vibrating table. Solid stainless steel discs having a diameter slightly smaller than the inside diameter of the consolidation ring and a height of 1.0 inch were used as static weights. These static weights were placed on top of the soil surface inside the consolidation ring, and the vibrating table was turned on. The frequency of the vibrating table was set in the range of 20 Hz – 50 Hz, depending on the level of relative compaction. Over-compaction of the soil was avoided by periodically stopping the compaction process, removing the discs used as weights, and visually monitoring the height of the lift. The vibration was stopped when the height of the lift reached the desired height noted by markings made on the wall of the consolidation ring. The same procedure, as described above, was followed for all the subsequent lifts.

The funnel tool was detached from the top of the consolidation cell after the compaction process was finished. The consolidation cell with the soil specimen compacted in place was then weighed, and the weight was noted. This method of vibratory compaction was adopted for all the soil grades except for A-2 (SC) with PI>>11 and A-4 (CL). Since the two grades of soil had significant amount of cohesive material, vibratory compaction would have been inefficient and would not have modelled the field compaction method accurately.

3.3.3 Kneading Compaction for Single Consolidometer Specimens

Generally, fills consisting of cohesive soils are compacted in the field using a Sheepsfoot roller. To model the kneading compaction method of a Sheepsfoot roller, the Harvard miniature tamper shown in Figure 3.7 was used in the laboratory to compact the cohesive samples.

Only the soil grades A-2 (SC) with PI >>11 and A-4 (CL) have been compacted using this method. The soil was compacted directly into the consolidometer rings placed inside the consolidation cells. The same funnel apparatus used for compaction in vibratory method was also used in this method of compaction to facilitate ease of compaction without the wastage of soil.

The Harvard miniature tamper achieves compaction through a spring-loaded steel rod that simulates the compaction by the feet of a Sheepsfoot roller. The tamper was equipped with a 40-pound spring, as it was observed that the desired levels of relative compaction were not achieved with a lower capacity spring.

The tamper was sprayed with silicone lubricant, so the soil would not stick to it during the compaction process. After the measured amount of moist soil required for each lift was poured into the consolidation ring with the funnel in place, the soil was given blows with the Harvard miniature tamper by pushing down the handle until the spring deflects and releasing instantly. The blows were applied uniformly in a circular pattern throughout the surface of the soil — at high moisture contents, the soil is bound to stick to the tamper rod. The soil stuck to the tamper rod was removed carefully by using a metal spatula to scrape the surface of the tamper, and the soil was placed back into the consolidation ring.

As it is difficult to obtain a level surface by using this method, a final phase of ironing was done by placing the cylindrical static weight on top of the compacted soil and gently tapping it using a rubber mallet to obtain a flat, even surface suitable for the consolidometer testing.

Figure 3.7 Harvard Miniature Tamper

3.3.4 As-compacted Testing Conditions

3.3.4.1 Double Consolidometer Tests

The double consolidometer technique was used for the preliminary set of tests on granular soil grades having a low plasticity index ranging from 0 to 10. For A-1 and A-3 soil grades, the double consolidometer tests were conducted at different levels of relative compaction ranging between 90% and 95% for the following as-compacted moisture conditions:

- At optimum moisture condition (w_{opt}).
- 2% drier than the w_{opt}.

Since the γ_{dmax} for A-1 soils was based on the Modified Proctor test, it was difficult to achieve a relative compaction higher than 95% using the equipment available in the laboratory.

For A-2 (SC) soil grade having PI=10, the double consolidometer tests were conducted at the same moisture conditions, as mentioned above, but at three different levels of relative compaction (92%, 96% and 100%). Since the γ_{dmax} for A-2 soils is based on Standard Proctor test a relative compaction of 100% was achievable in the laboratory.

3.3.4.2 Single Consolidometer Tests

After the preliminary test results from the double consolidometer tests, which showed a significant amount of swell for soil grades having very high plasticity, it was decided that single consolidometer tests must be conducted for those soils with very high fraction of plastic fines.

For the soil grade A-2 (SC) with PI>>11, the single consolidometer tests were conducted at two different levels of relative compaction (92% and 96%) for the following as-compacted moisture conditions:

- at optimum moisture condition (w_{opt})
- 3% drier than the w_{opt}.
- 5% drier than the w_{opt}.
- 7% drier than the w_{opt}.

For the soil grade A-4 (CL), the same set of tests were conducted at three different levels of compaction (92%, 96% and 100%) for the following as-compacted moisture conditions:

- At optimum moisture condition (w_{opt}).
- 4% drier than the w_{opt}.

It is to be noted, as discussed in the previous section, all the specimens used in the single consolidometer tests were compacted using the Harvard miniature tamper equipped with a 40-pound spring. Since the γ_{dmax} of A-4 soil grade was lower than the A-2 soil grade, 100% relative compaction was achievable with the Harvard miniature tamper.

3.3.5 Double Consolidometer Test Procedure

The double consolidometer tests conducted in this research project followed the procedure as described in this section. Two nominally identical specimens were prepared using vibratory compaction method as described previously in section 3.3.2. A consolidation cell assembly with the specimen compacted in place on the platform of the consolidometer loading frame is shown in Figure 3.8. The air dried top porous stone was placed on the specimen surface making sure that the porous stone aligns centrally with the consolidation ring. The loading cap was placed centrally on top of the porous stone. The loading arm of the frame was then seated on top of the loading cap.

A digital dial gauge was used to take the deformation readings of the specimen. The needle of the dial gauge was placed at the center of the loading arm and all the screws of the apparatus were tightened after making sure that the loading arm was level. The dial gauge was turned on and zeroed at this point. A seating load of 0.01 tsf (1 kPa) was placed on the lever arm for a period of 30 minutes. The specimen was then inundated with de-ionized water until the water level reaches above the top porous stone. This water level was maintained throughout the test until the last dial gauge reading was taken at the last loading increment. The dial gauge readings were taken at times 0.1, 0.25, 0.5, 1, 2, 4, 8, 15, 30, 60, 120 minutes, etc., until the specimen reached equilibrium after the addition of water (meaning consecutive dial gauge readings are the same over a long period of time). After the equilibrium dial gauge reading was taken, a stress of 0.25 tsf was applied to the specimen instantaneously and the dial gauge readings were taken at the same intervals, as described previously.

Figure 3.8 Consolidometer Loading Frames Used for the Standard Tests

The loading sequence adopted was such that the current stress on the specimen was double that of the previous stress level, when the specimen reached equilibrium, resulting in stresses of 0.5 tsf, 1 tsf, 2 tsf, 4 tsf and 8 tsf applied sequentially.

At the end of the test, the consolidation cell was drained and water content of the specimen at the end of the test was determined. The entire specimen and the consolidation ring was dried in the oven at 110^{o} C for a period of 24 hours for accurate measurement of the dry weight of the specimen. The actual as-compacted moisture content and dry unit weight were determined from the dry weight of the specimen at the end of test and the as-compacted moist weight of the specimen before the commencement of the test.

The second consolidation cell assembly was used to test the soil specimen kept at a constant as-compacted moisture condition throughout the test. To achieve this, the specimen was placed between the top and bottom porous stones to allow air to escape from the specimen during the consolidation, and the top porous stone was covered with a plastic wrap. The loading cap was placed on top of the porous stone with the plastic wrap in between them. After verifying the assembly was sealed from any leaks that might cause a change in the moisture condition, it was placed on the platform of the loading frame. The procedure and loading sequence followed for taking the dial gauge readings of the soaked specimen was also adopted for the as-compacted specimen kept at its initial moisture condition throughout the test. At the end of the test, the specimen and the ring were weighed and oven-dried at 110^{o} C for 24 hours. The water content of the specimen at the end of the test was determined and compared to the actual as-compacted water content to see whether the moisture condition has changed during the test.

All the double consolidometer tests were corrected for compression of the apparatus and seating of the porous stones on the specimen. The correction values were obtained by simulating the same procedures followed for the soaked and as-compacted specimens and replacing the specimen with a dummy specimen made out of stainless steel.

3.3.6 Single Consolidometer Test Procedure

The single consolidometer test requires much more material for the test sample and is also much more time consuming than the double consolidometer test. However, results from the single consolidometer tests are more accurate and reliable as both the soaked and the as-compacted tests are performed on the same specimen. So, for the soil grades highly susceptible to both swell and collapse, the single consolidometer test was chosen to predict the wetting and loading-induced strains.

For the single consolidometer tests, seven (7) nominally identical specimens were prepared following the compaction method described in Section 3.3.3. The first specimen was placed on the loading platform, and the top porous stone was placed on top of the soil specimen in as-compacted state. The loading cap was then placed on top of the porous stone. The loading arm was brought into position and the dial gauge was placed, making sure that the loading arm was level. The screws were then tightened, and the dial gauge was switched on and zeroed. The seating load of 0.01 tsf was placed on the lever arm for a period of 30 minutes. The specimen was then inundated with deionized water until the water level reached a little above the top of the porous stone. The dial gauge readings were taken at times 0.1, 0.25, 0.5, 1, 2, 4, 8, 15, 30, 60, 120 minutes, etc., followed by readings at every 24 hours from the time the specimen was inundated, until the specimen reached equilibrium.

The other six specimens were tested at 0.25, 0.5, 1, 2, 4 and 8 tsf stress levels simultaneously. The as-compacted specimen was instantaneously loaded to the desired stress levels and the dial gauge readings were taken at times 0.1, 0.25, 0.5, 1, 2, 4, 8, 15, 30, 60, 120 minutes, etc. After the as-compacted specimens reached equilibrium, the specimen was inundated and the dial gauge readings were taken again at times 0.1, 0.25, 0.5, 1, 2, 4, 8, 15, 30, 60, 120 minutes, etc. followed by readings at every 24 hours from

the time the specimen was inundated, until the specimen reached equilibrium. The dial gauge readings were also corrected for compression of the apparatus, and the seating of the porous stones was done in the same manner as for the double consolidometer tests.

4. RESULTS AND ANALYSIS FOR STANDARD CONSOLIDOMETER TESTS

4.1 Introduction

The purpose of the consolidometer tests was to analyze the effect of compaction specifications for different soil grades on the settlement of approach embankments of bridges, often referred to as the "Bump at the bridge" problem. The results from the double and the single consolidometer tests are presented in the following sections with a brief description of the effects of various factors that are taken into consideration while writing the compaction specifications for embankment fills. Also, the results from the regression analysis and the theory behind the development of the data analysis models are discussed in the subsequent sections.

4.2 Results from the Double Consolidometer Tests

4.2.1 One-Dimensional Loading-Induced Vertical Strain

The equilibrium dial gauge readings from the double consolidometer tests conducted on the specimen kept at a constant as-compacted moisture content throughout the test were used to predict the one-dimensional loading-induced vertical strain.

Typically, results from the double consolidometer tests are plotted, as shown in the Figure 4.1. Similar graphs for all the soil grades tested using the double consolidometer technique at different levels of relative compaction and moisture condition are shown in Figures B.1 through B.32 in Appendix B.

Effect of overburden pressure: Overburden pressure refers to the stress the soil experiences due to its self-weight and external loads. From Figure 4.2, it can be observed that, as the magnitude of overburden pressure increases, the magnitude of the loading-induced vertical strain also increases for both as-compacted and soaked specimens.

Effect of Soil Gradation and Plasticity Index: The loading-induced stress-strain characteristics of different soil grades are plotted in Figure 4.2 through Figure 4.5. Data from the double consolidometer tests in which the soil specimens are compacted to similar levels of relative compaction and as-compacted moisture condition were compared to observe the effect of the soil gradation on the loading-induced vertical strain. Since the γ_{dmax} and w_{opt} of A-1 soils are based on the Modified Proctor test, and that of all the other soils are based on Standard Proctor test, the comparative graphs are plotted separately for all the A-1 grade soils and the rest of the soil grades.

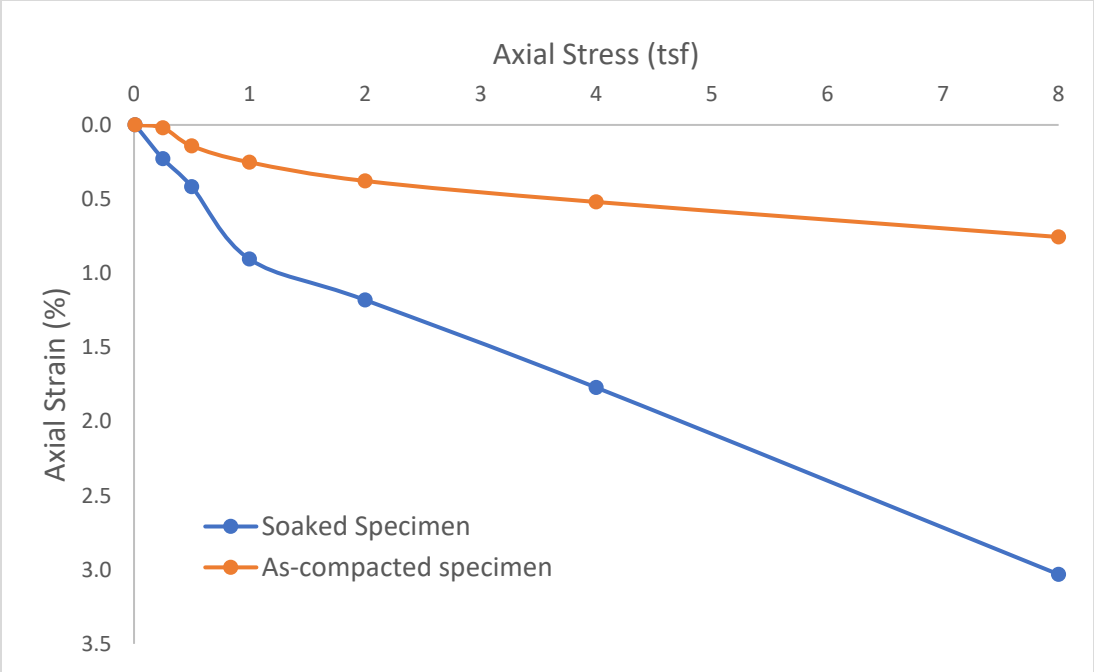

Figure 4.1 Comparison of Stress-strain Characteristics Between Soaked and As-compacted Specimens for A-1-a (SP or SW) Soil at R_m = 90%, w = 8.1%

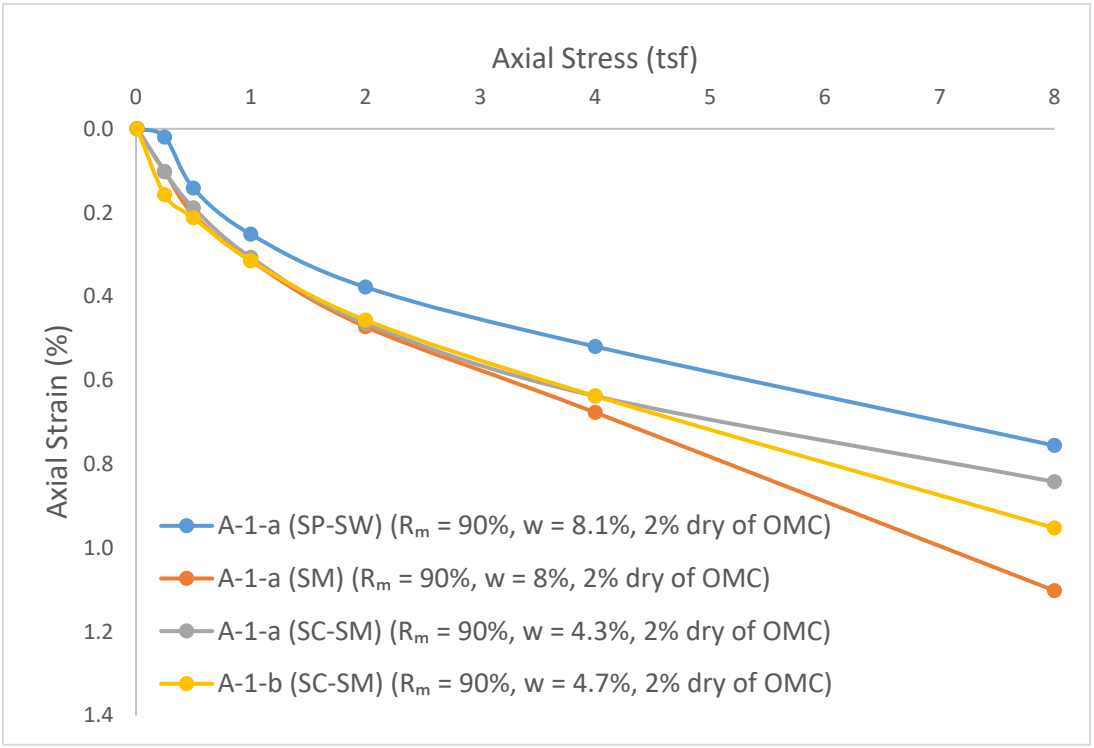

Figure 4.2 Comparison of Stress-strain Characteristics of Nominally Identical As-compacted Specimens among the A-1 Soil Types

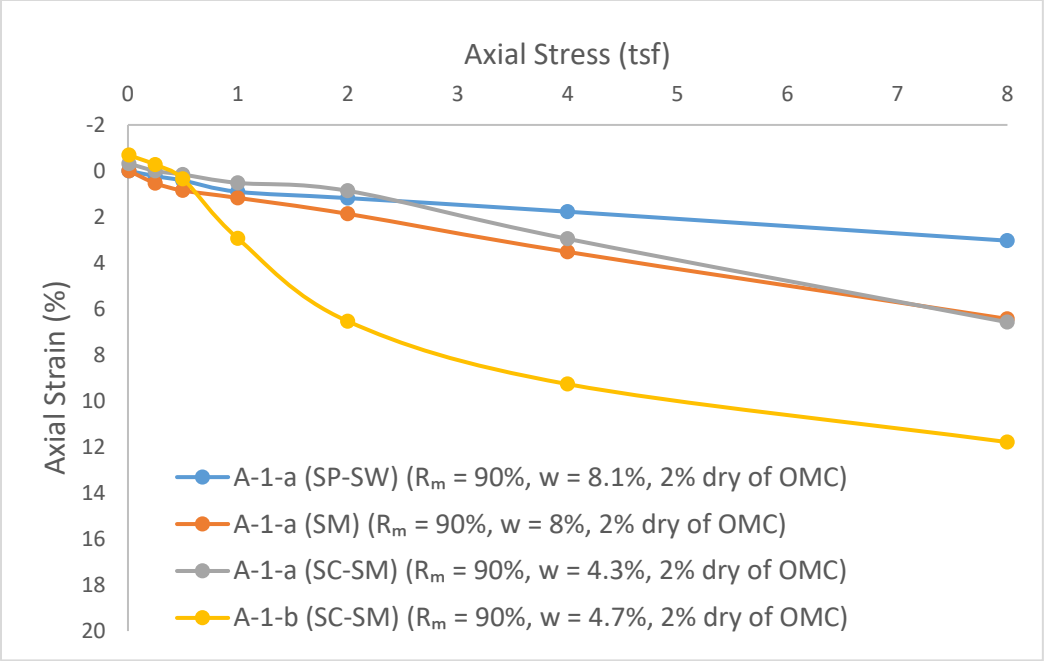

Figure 4.3 Comparison of Stress-strain Characteristics of Nominally Identical Soaked Specimens among the A-1 Soil Types

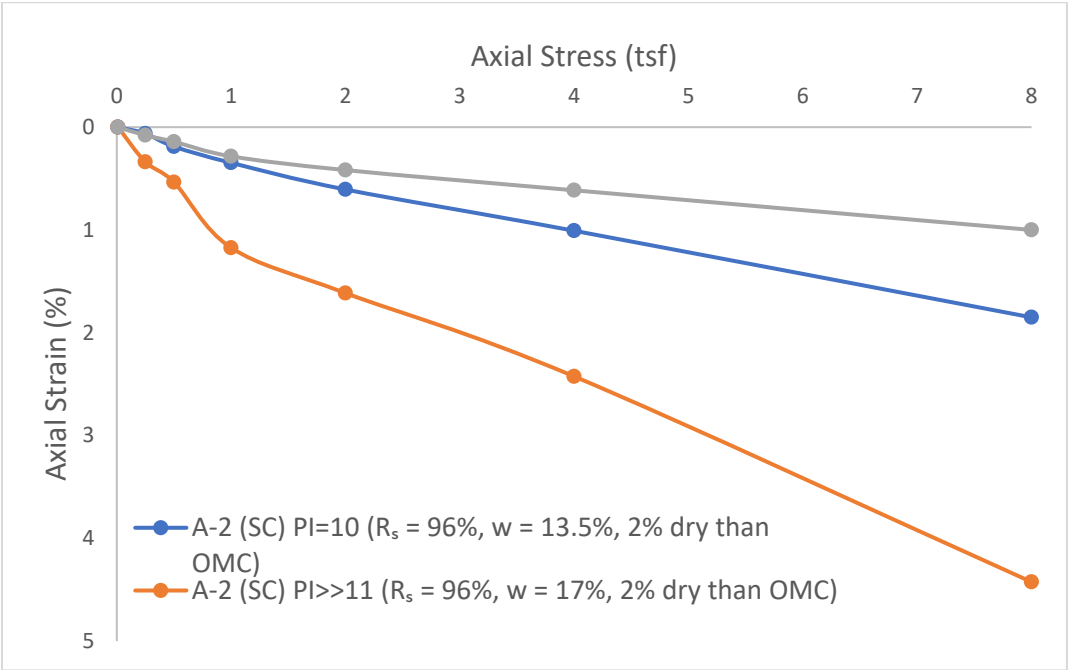

Figure 4.4 Comparison of Stress-strain Characteristics of Nominally Identical As-compacted Specimens of Soil Types Other Than A-1

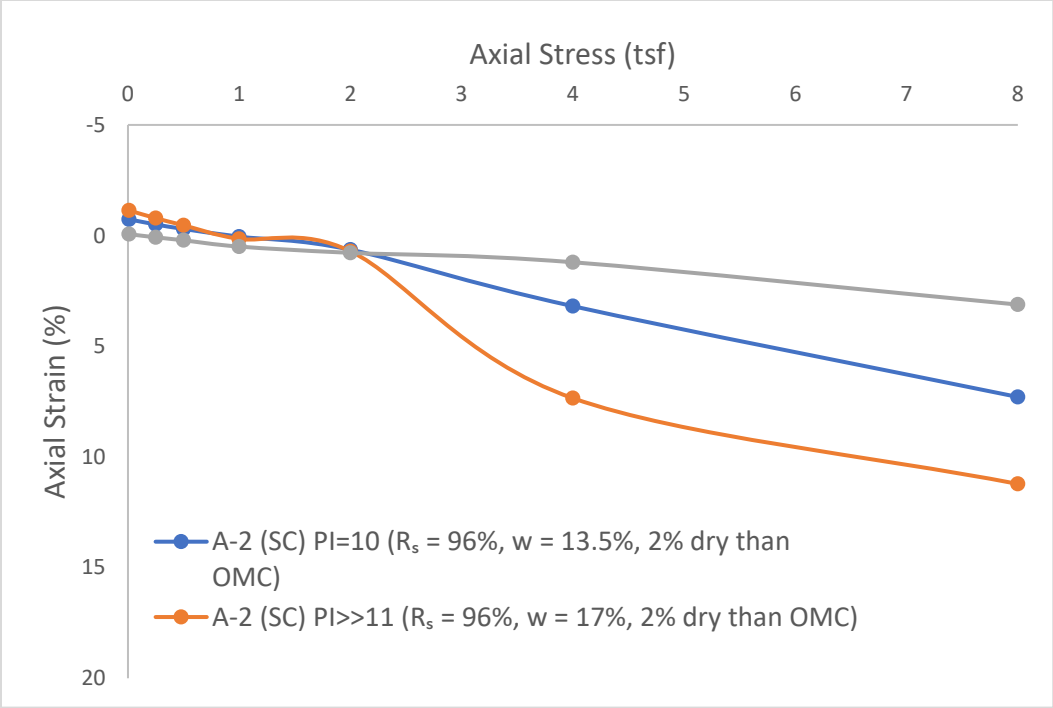

Figure 4.5 Comparison of Stress-strain Characteristics of Nominally Identical Soaked Specimens of Soil Types Other Than A-1

From Figure 4.2, it can be observed that among the soil grades A-1-a (SP-SW) and A-1-a (SM) the as-compacted specimen of the former soil type is compressing less, as it has a better soil gradation than A-1-a (SM). On the contrary, even though the as-compacted specimen of A-1-a (SM) has a better soil gradation than that of A-1-b (SC-SM) soil, it is compressing more, as the γ_{dmax} of A-1-b (SC-SM) soil type was much higher than that of A-1-a (SM). In other words, although both soil types are compacted to the same level of relative compaction, since the γ_{dmax} of A-1-b (SC-SM) soil is higher, it is in a more densified form and compressing lesser than A-1-a (SM) soil. Among the soil grades A-1-a (SC-SM) and A-1-b (SC-SM), which have similar γ_{dmax} values, the as-compacted specimen of the former soil type is compressing less, as it has a better soil gradation than A-1-b (SC-SM). This reiterates that among the soils having comparable γ_{dmax} values, the soil that is well-graded compresses the least in their as-compacted state. The value of PI does not seem to have any effect on the loading-induced strain of the as-compacted specimens of A-1 soils.

Figure 4.3 shows the comparison of the stress-strain characteristics of the soaked specimen for the different A-1 soil grades. As expected, the soaked specimen for A-1-b (SM) soil compressed the most among the A-1 soils, since the soil gradation was inferior to the other soil grades under comparison. The soaked specimen for A-1-a (SC-SM) and A-1-a (SM) soils showed similar stress-strain characteristics, as the soil gradation of both the soils was almost identical. The soaked specimen for A-1-a (SP-SW) soil compressed the least, which was also expected. The soaked specimens of both A-1-a (SC-SM) and A-1-b (SC-SM) soils having a PI of 4 compressed less than the soil types having non-plastic fines at low overburden pressures.

For soils other than the A-1 grade, plasticity index seems to have a greater effect on the loading-induced vertical strain of the as-compacted specimens. From Figure 4.4, the as-compacted specimen for A-2 (SC) with PI>>11 was compressed more than A-2 (SC) with PI=10, as it has a greater value of PI, although the

soil gradations for both soils are similar. The A-3 (SP-SM) soil compressed the least, as it contained non-plastic fines.

At low overburden pressures, the soaked specimen of A-2 (SC) with PI>>11 swelled the most, as it contains the greatest amount of plastic fines among the soils under comparison (shown in the Figure 4.5). In the compression region, the soaked specimens exhibited a similar trend followed by the as-compacted specimens of the same soil types.

Effect of Relative Compaction and As-Compacted Moisture Content: Relative compaction is the ratio of the as-compacted dry density of the soil specimen to the maximum dry density obtained from the control test (Modified Proctor test for A-1 soils and Standard Proctor test for all the other soils). Figure 4.6 shows the loading-induced stress-strain characteristics of the as-compacted specimens at different levels of relative compaction and as-compacted moisture content for A-1-a (SP or SW) soil.

From Figure 4.6, it was observed that, for a given as-compacted moisture condition and overburden pressure, the specimen compacted at a higher level of relative compaction compressed less than the specimen compacted at a lower level of relative compaction. Since the specimen compacted at a higher level of relative compaction would have less voids at the same moisture content, this behavior aligned with what is known in theory.

It can also be observed from Figure 4.6 that, at a given level of relative compaction and overburden pressure, the specimen compacted at w_{opt}, compressed more than the specimen compacted 2% drier than the w_{opt}.

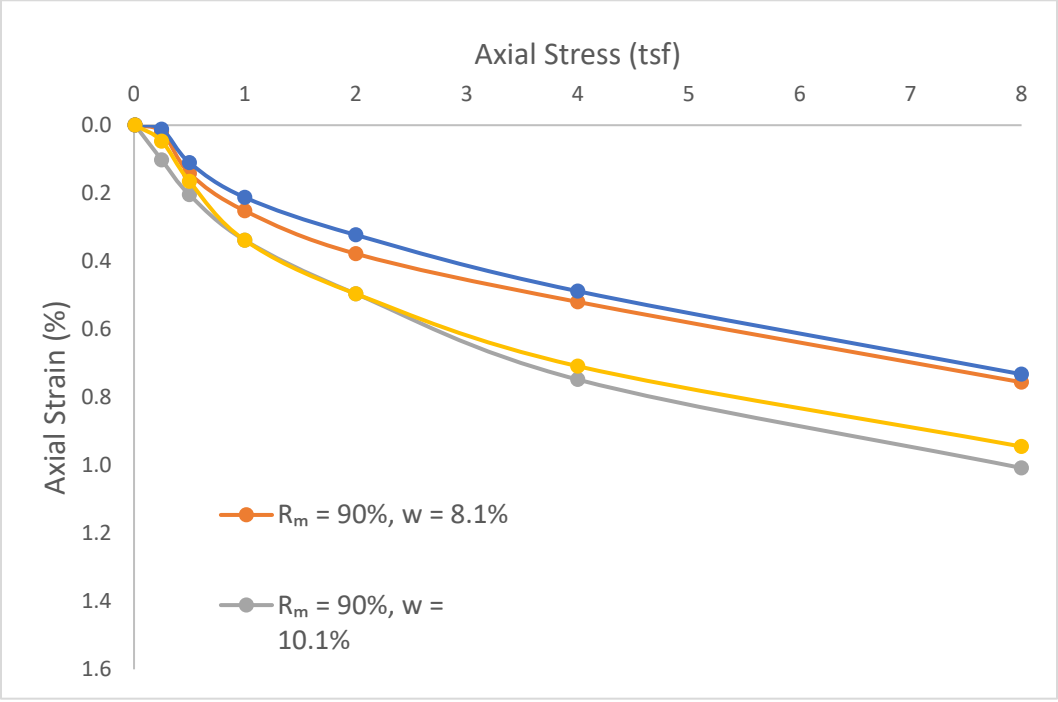

Figure 4.6 Loading-Induced Stress-strain Characteristics of A-1-a (SP or SW) As-compacted Specimen

Figure 4.7 shows the loading-induced stress-strain characteristics for the soaked specimens for A-1-a (SP or SW) soil. It was observed that at a given as-compacted moisture condition and overburden pressure, the soaked specimen compacted to a higher level of relative compaction compressed less than the specimen compacted to a lower level of relative compaction.

The variation of loading-induced strain with varying moisture content can also be observed from Figure 4.7. For a given level of relative compaction and overburden pressure, the soaked specimen, which was compacted at w_{opt}, compressed less than the specimen compacted at 2% drier than the w_{opt} value. This trend opposes what was observed for the as-compacted specimens. Comparison graphs, similar to Figure 4.6 and Figure 4.7, are provided in Appendix B in Figures B.33 through B.44 for all the soils that have been tested using the double consolidometer technique.

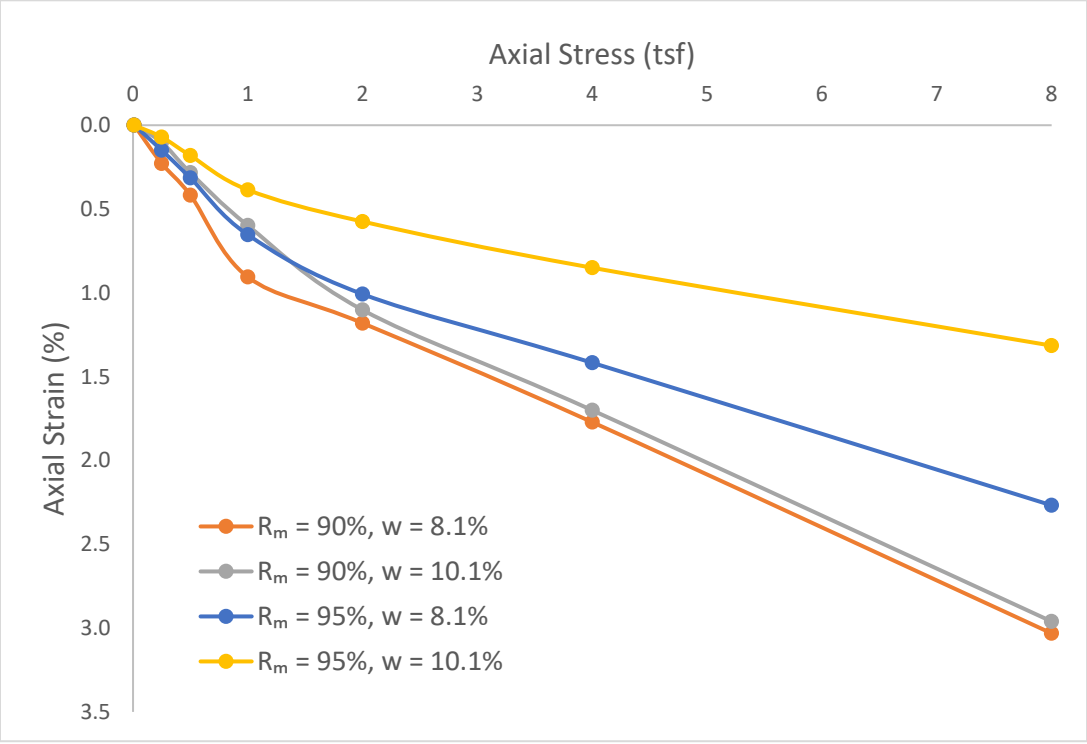

Figure 4.7 Loading-Induced Stress-strain Characteristics of A-1-a (SP or SW) Soaked Specimen

4.2.2 One-dimensional Wetting-induced Strain

The wetting-induced strain for a particular soil at a specified as-compacted condition was predicted from the double consolidometer test results as the difference between the loading-induced strains of the soaked and the as-compacted specimens. The effects of various factors influencing the magnitude of wetting-induced strain are discussed below.

Effect of overburden pressure: The wetting-induced stress-strain characteristics for the A-1-a (SP or SW) soil at 90% R_m and an as-compacted moisture content of 8.1% is shown in the Figure 4.8. From Figure 4.8, it is clear that as the overburden stress was increased, the wetting-induced strain also increased in the direction of the applied overburden stress (collapse). Although, this trend was observed for most of the soils tested using double consolidometer technique, for A-2 (SC) soil with PI=10 at low levels of relative compaction, the wetting-induced strain increased with an increase in the overburden stress to a maximum critical value and beyond that value the wetting-induced strain decreased with an increase in the overburden stress as shown in the Figure 4.9.

Effect of Relative Compaction and As-compacted Moisture Content: The wetting-induced stress-strain characteristics for A-1-a (SP or SW) soil at different levels of relative compaction and as-compacted moisture content are shown in the Figure 4.10 at the same as-compacted moisture content, it was predicted that the soil would collapse less when it was compacted to a higher level of relative compaction as shown in Figure 4.10.

It was also observed that, at the same level of relative compaction, the soil would collapse more when it was compacted at low moisture content relative to the optimum moisture content (w_{opt}) than when it was compacted at the w_{opt}. The comparative graphs similar to the Figure 4.10 are provided in the Appendix B from Figure B.45 through B,50.

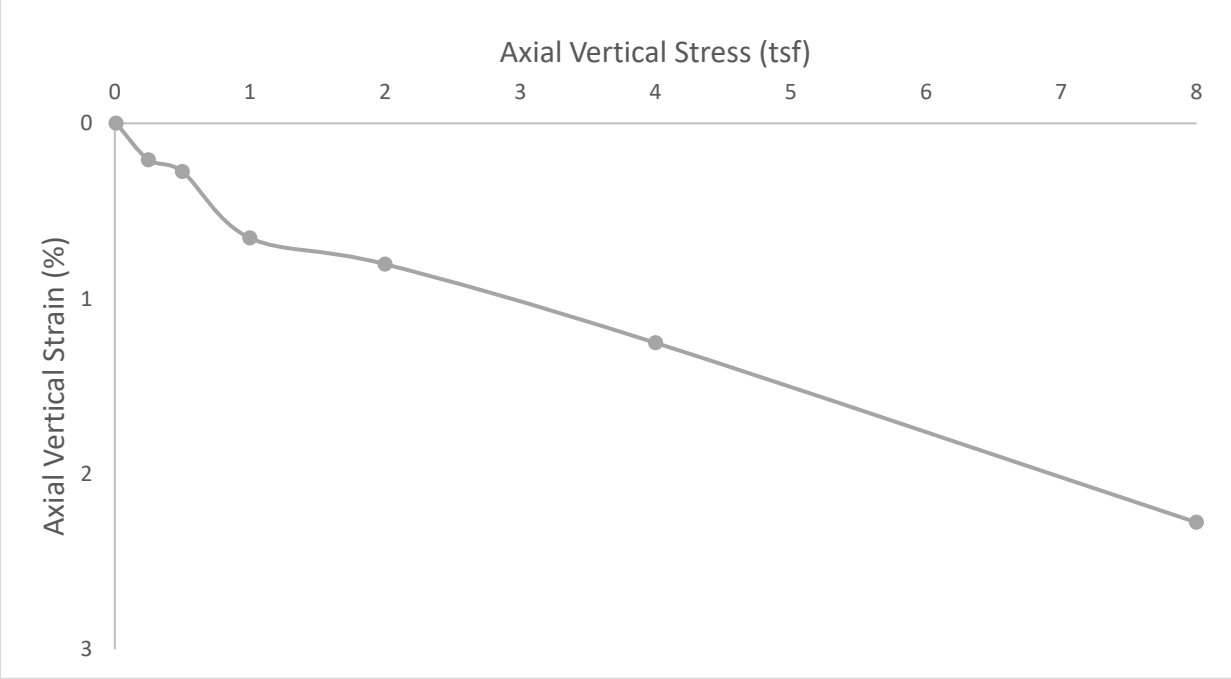

Figure 4.8 Predicted Wetting-induced Stress-strain Characteristics for A-1-a (SP or SW) Soil at R_m = 90%, w = 8.1%

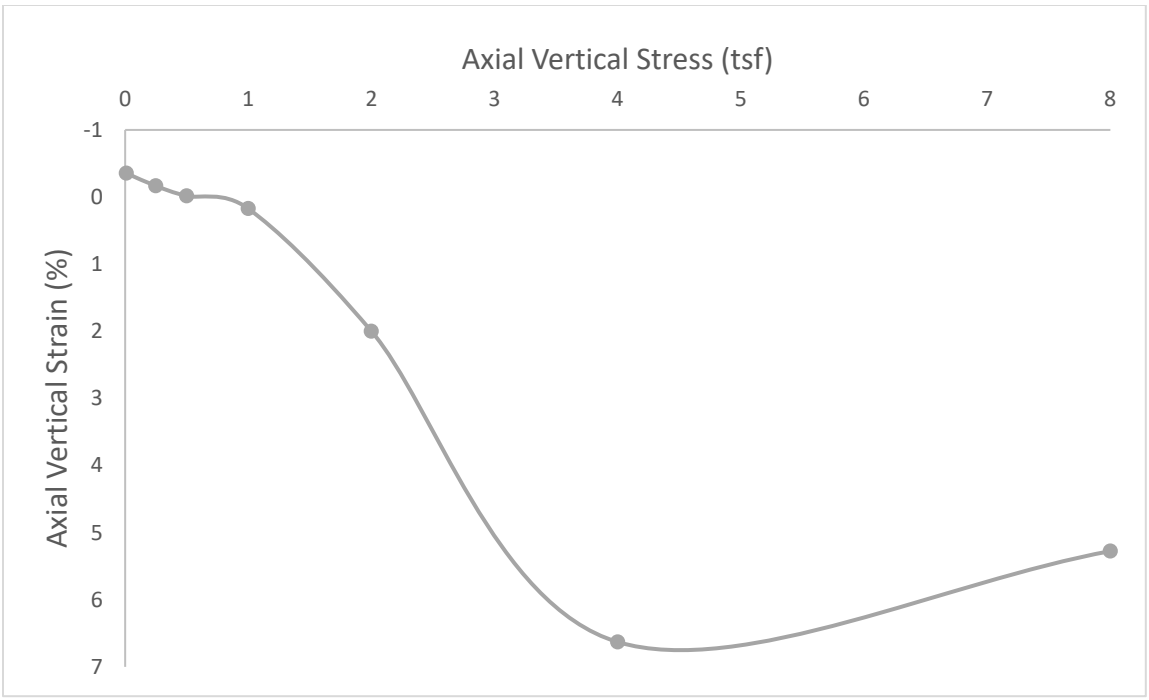

Figure 4.9 Predicted Wetting-induced Stress-strain Characteristics for A-2 (SC) PI=10 Soil at R_s = 92%, w = 13.5%

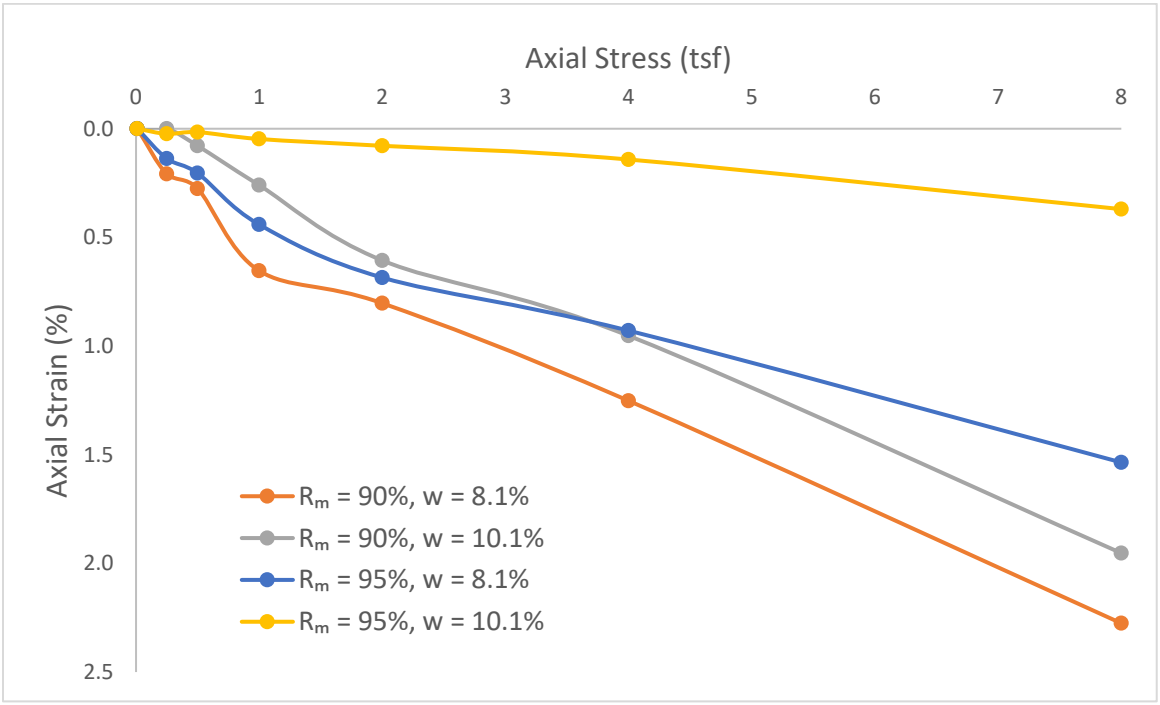

Figure 4.10 Comparison of the Magnitude of Wetting-induced Stress-strain Characteristics of A-1-a (SP or SW) at Different As-compacted Conditions

4.3 Results from Single Consolidometer Tests

4.3.1 One-dimensional Loading-induced Vertical Strain

The equilibrium dial gauge reading when the specimen was compressed at a constant stress before it was saturated was used to estimate the loading-induced vertical strain at that particular overburden stress level. To get the complete profile of the stress-strain characteristics, the dial gauge readings were taken for all the desired overburden stress levels, as described previously in the methodology carried out for the single consolidometer tests. The effects of factors influencing the loading-induced strain of A-2 (SC) with PI>>11 and A-4 (CL) soils are discussed below.

Effect of overburden stress: As the overburden stress increased, the loading-induced strain for both A-2 (SC) with PI>>11 and A-4 (CL) soils increased. Although, A-2 (SC) soil contained high amounts of plastic fines, the loading-induced strain increased gradually with increasing overburden pressure, as shown in the Figure 4.11 which was similar to the as-compacted specimen behavior of the granular soils tested using the double consolidometer tests.

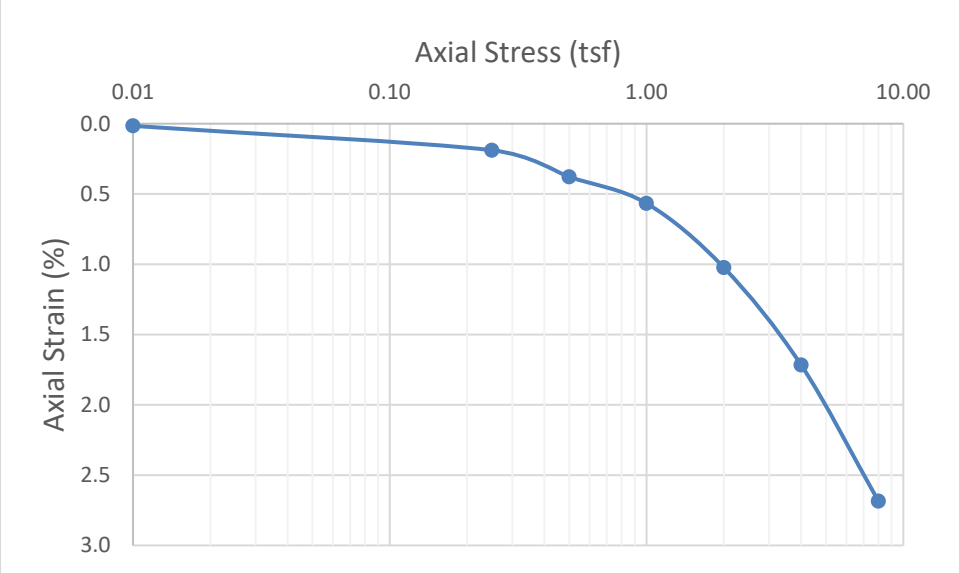

Figure 4.11 Loading-induced Stress-strain Characteristics of A-2 (SC) Soil at R_s = 96% and w = 20%

The A-4 (CL) soil showed a loading-induced stress-strain behavior similar to that of purely cohesive over-consolidated soils. The loading-induced strain increased gradually until a certain critical value of overburden stress and increased rapidly after the stress surpassed that value, as shown in the Figure 4.12. This critical value of overburden stress is called as the pre-compactive stress and is equal to the stress at which the soil was compacted using the Harvard Miniature tamper.

Effect of as-compacted moisture content: The loading-induced stress-strain characteristics for A-2 (SC) soil with PI>>11 compacted at a constant level of relative compaction and different values of as-compacted moisture content, are shown in Figure 4.13. It was observed that the soil compacted at a higher moisture content compressed more at high overburden stresses. At low over-burden stresses, significant deviations from this trend occurred for the soil compacted at 17% and 20% moisture content.

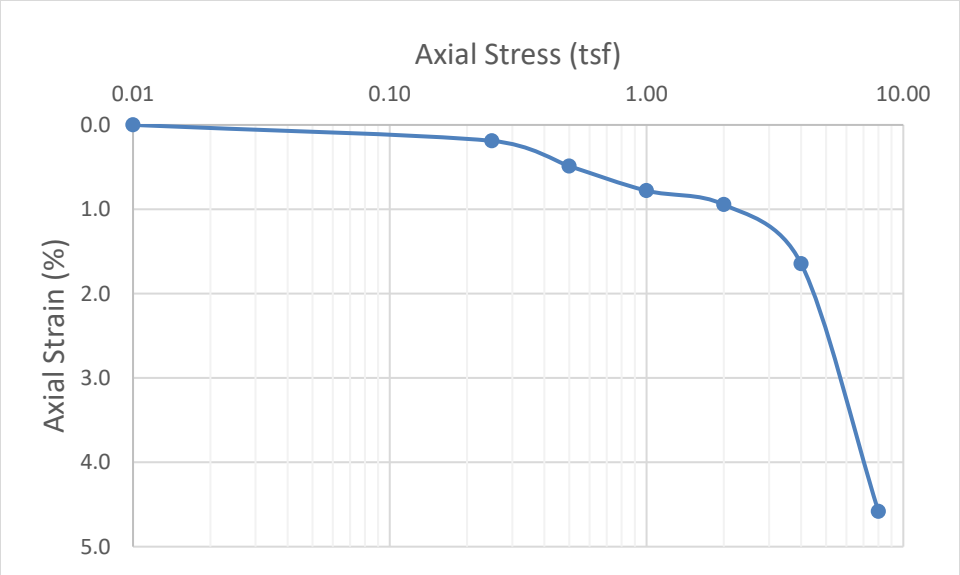

Figure 4.12 Loading-Induced Stress-strain Characteristics of A-4 (CL) Soil at R_s = 100% and w = 21%

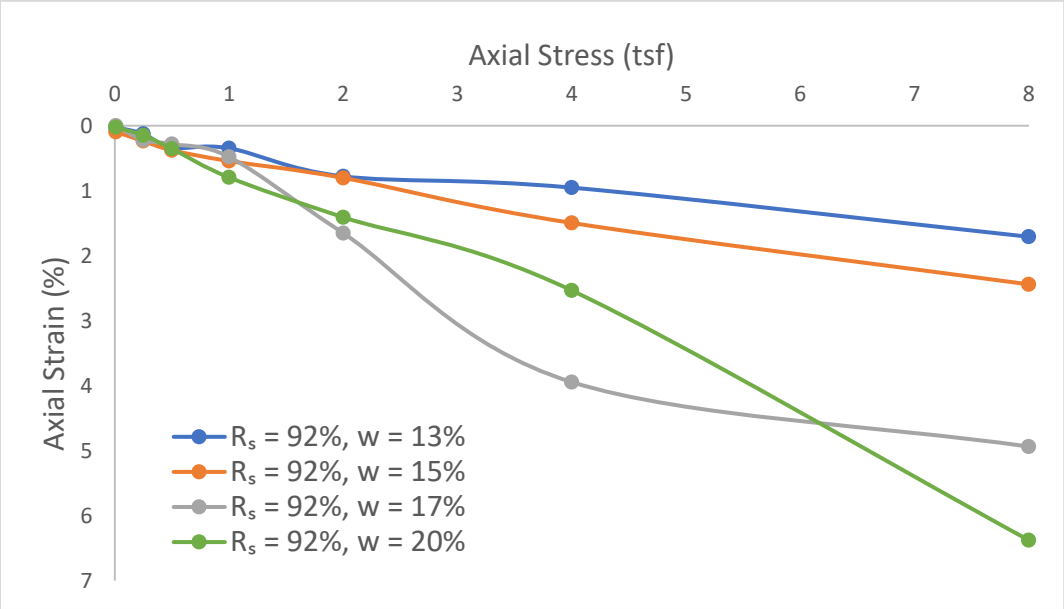

Figure 4.13 Comparison of Loading-induced Stress-strain Characteristics for A-2 (SC) PI>>11 Soil at a Constant Relative Compaction R_s = 92%

The loading-induced stress-strain characteristics for the A-4 (CL) soil at three different levels of relative compaction (92%, 96%, and 100%) are shown in Figure 4.14–Figure 4.16. It was observed that at any given level of relative compaction, the soil compacted at a higher moisture content compressed more than the soil compacted at a lower moisture content. Minor deviations from this trend can be observed at low overburden stresses, which might be caused by minor inconsistencies in specimen preparation, as it was difficult to prepare perfectly identical specimens.

Effect of Relative Compaction: In Figure 4.17 and Figure 4.18, the loading-induced stress-strain characteristics for A-2 (SC) soil with PI>>11 at two different as-compacted moisture contents (17% and 20%) are plotted. It was clear from these figures that loading-induced strain was greater for the soil that was compacted to a lower level of relative compaction, with the exception of minor inconsistencies at the low overburden stresses.

The loading-induced stress-strain characteristics for the A-4 (CL) soil at the two different moisture contents (17% and 21%) are shown in the Figure 4.19 and Figure 4.20, respectively. It was observed for A-4 (CL) soil also that the loading-induced strain for the soil compacted to a higher level of relative compaction was much less than the soil compacted to a lower level of relative compaction.

4.3.2 One-Dimensional Wetting-Induced Vertical Strain

After the as-compacted specimen reached equilibrium under a constant stress, the specimen was saturated, and the soaked readings were taken, as previously mentioned, in the methodology for the single consolidometer tests. The dial gauge readings, after the specimen reaches equilibrium under the constant stress after soaking, were used to estimate the wetting-induced strains for the A-2 (SC) soil with PI>>11 and the A-4 (CL) soil. Discussed below are the effects of the various factors influencing the wetting-induced collapse or swell of the above-mentioned soils.

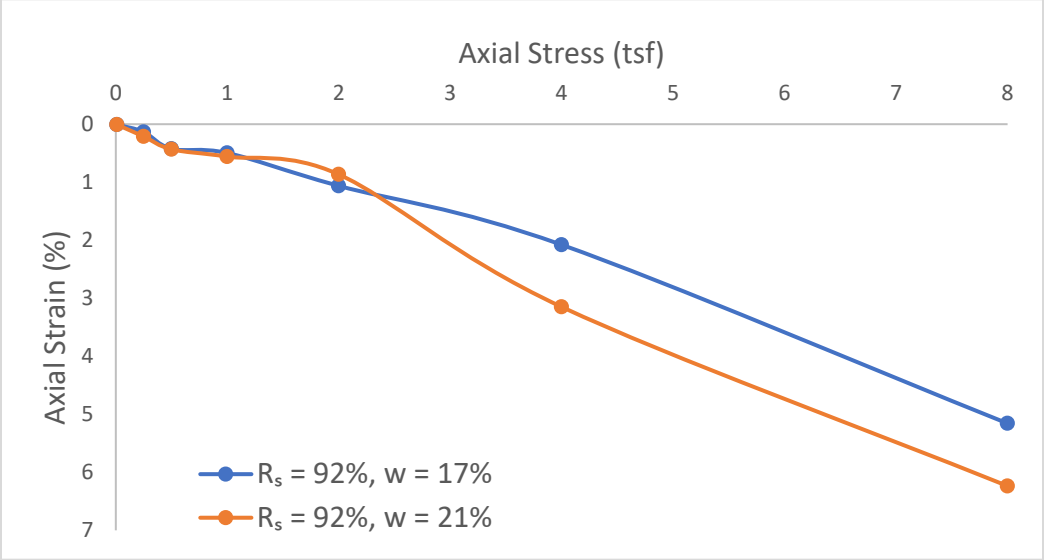

Figure 4.14 Comparison of Loading-induced Stress-strain Characteristics for A-4 (CL) Soil at a Constant Relative Compaction R_s = 92%

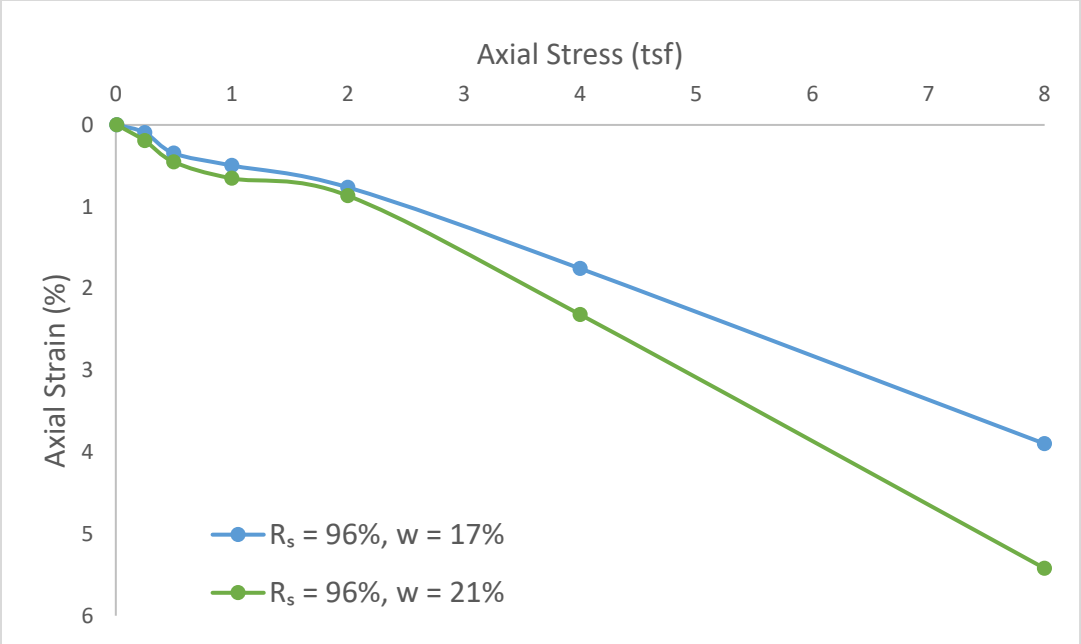

Figure 4.15 Comparison of Loading-induced Stress-strain Characteristics for A-4 (CL) Soil at a Constant Relative Compaction R_s = 96%

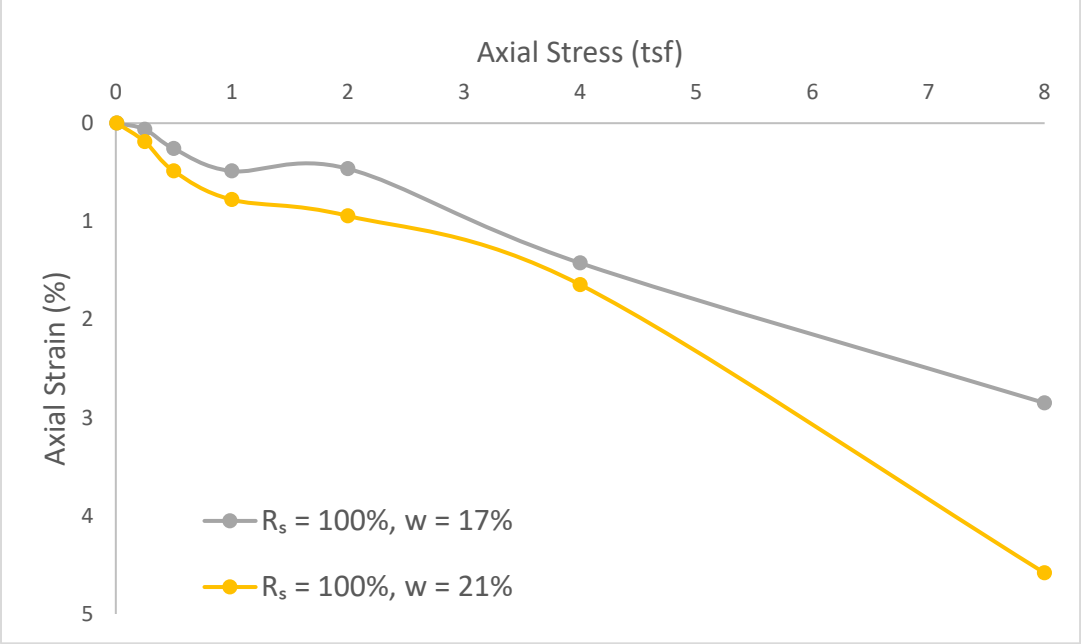

Figure 4.16 Comparison of Loading-induced Stress-strain Characteristics for A-4 (CL) Soil at a Constant Relative Compaction R_s = 100%

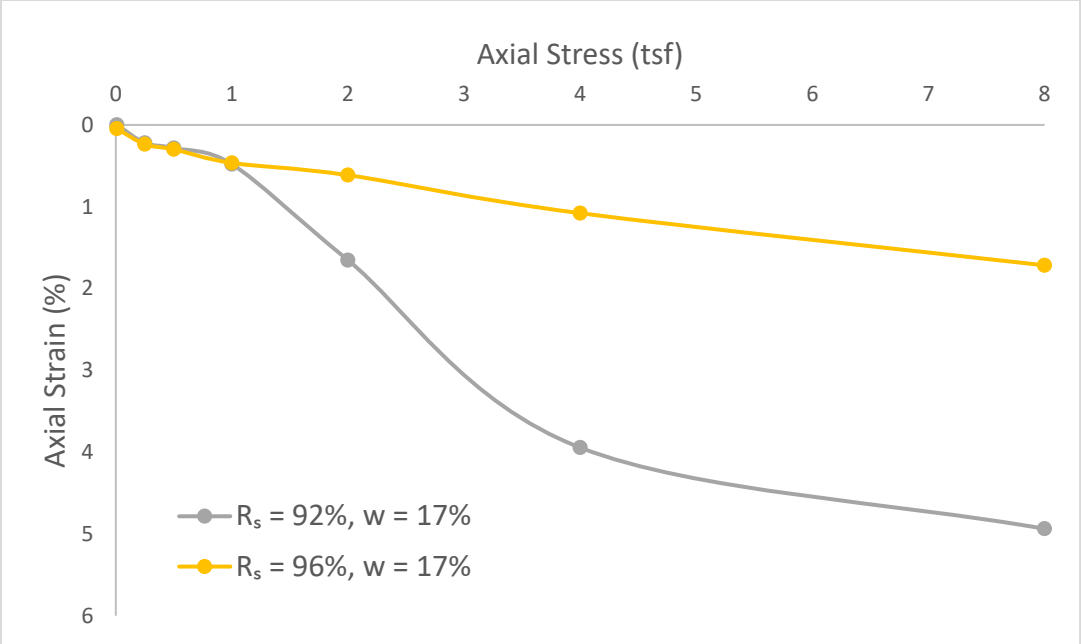

Figure 4.17 Comparison of Loading-induced Stress-Strain Characteristics for A-2 (SC) PI>>11 Soil at a Constant As-compacted Moisture Content w = 17%

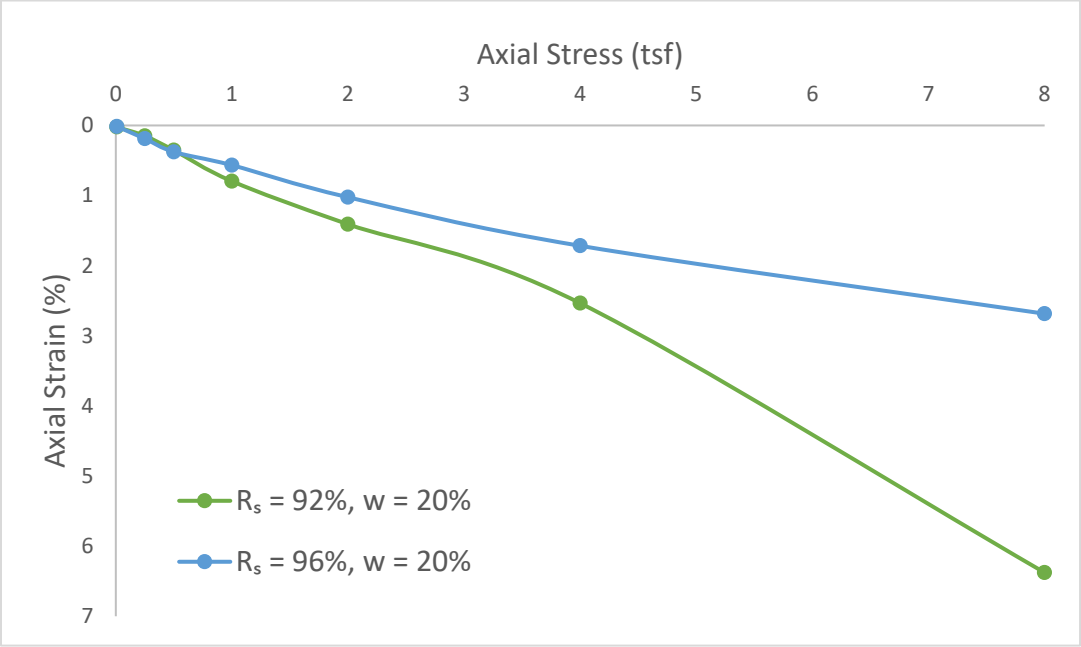

Figure 4.18 Comparison of Loading-induced Stress-strain Characteristics for A-2 (SC) PI>>11 Soil at a Constant As-compacted Moisture Content w = 20%

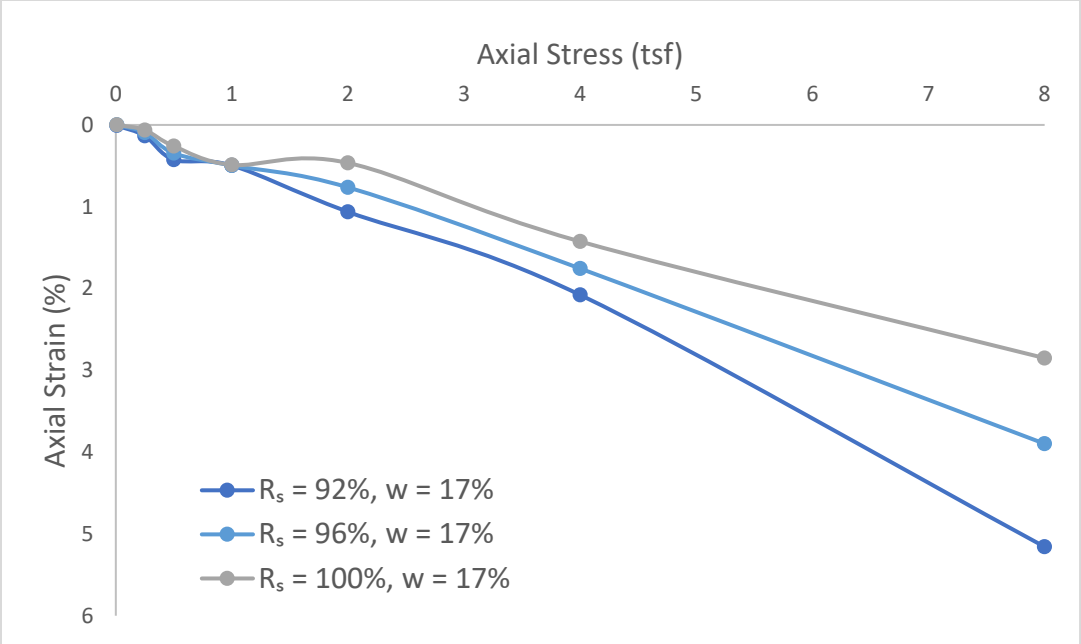

Figure 4.19 Comparison of Loading-induced Stress-strain Characteristics for A-4 (CL) Soil at a Constant As-compacted Moisture Content w = 17%

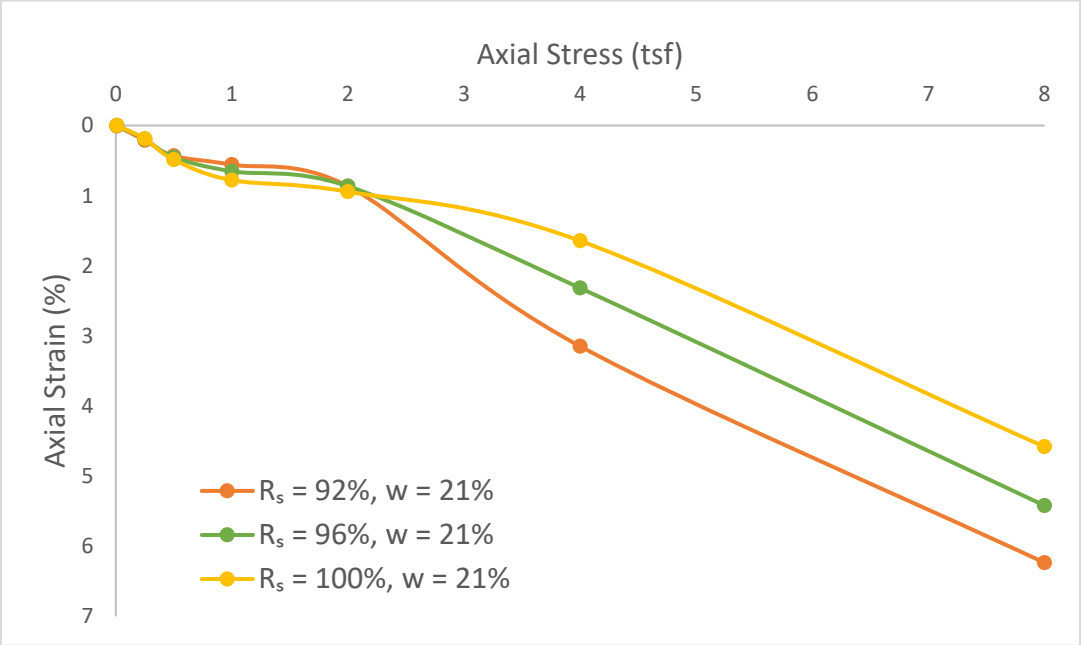

Figure 4.20 Comparison of Loading-induced Stress-strain Characteristics for A-4 (CL) Soil at a Constant As-compacted Moisture Content w = 17%

Effect of overburden pressure: It was observed that for soils containing high amounts of plastic fines, an increase in the volume (swell) of the soil specimen was observed when the soil was saturated with water at low overburden stresses. As the overburden stress increased, the amount of swell decreased and after a certain a certain value the soil specimen started to collapse, i.e., a decrease in the volume of the specimen was observed up to a maximum value, and the specimen started to swell again when the stress was increased beyond this point as shown in Figure 4.21.

Effect of as-compacted moisture content: The wetting-induced stress-strain characteristics for A-2 (SC) soil with PI>>11 compacted at a constant level of relative compaction and different values of as-compacted moisture content, are shown in Figure 4.22. It was observed that the soil compacted at a high moisture content was subjected to less swelling and collapse potential.

The wetting-induced stress-strain characteristics for the A-4 (CL) soil at three different levels of relative compaction (92%, 96% and 100%) are shown in the Figure 4.23 throughFigure 4.25. It was observed that for any given level of relative compaction, the soil compacted at w_{opt}showed a lower swelling potential at the low overburden stresses, and also showed a lower collapse potential at high overburden stresses than the soil compacted at a moisture content 4% drier than w_{opt}.

Effect of Relative Compaction: In Figure 4.26 and Figure 4.27, the wetting-induced stress-strain characteristics for A-2 (SC) soil with PI>>11 at two different as-compacted moisture contents (17% and 20%) are plotted. At any given as-compacted moisture content, the soil compacted at a lower level of relative compaction was more susceptible to swell at low overburden stresses and also was more susceptible to collapse at high over burden stresses up to a maximum critical value and then decreases with an increase in the overburden stress, than the soil compacted to a higher level of relative compaction at the same as-compacted moisture content.

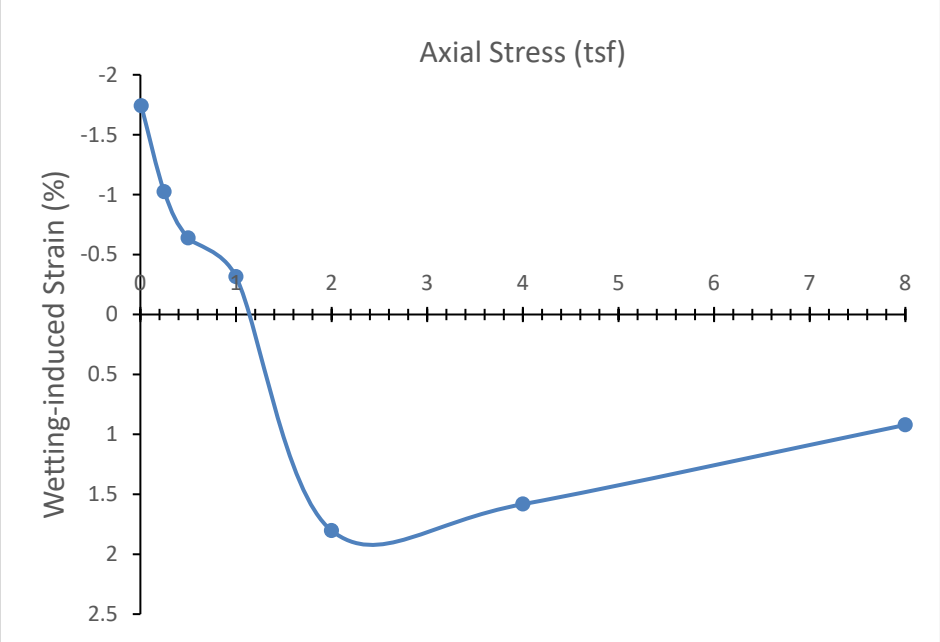

Figure 4.21 Wetting-induced Stress-strain Characteristics of A-2 (SC) Soil at R_s = 92% and w = 20%

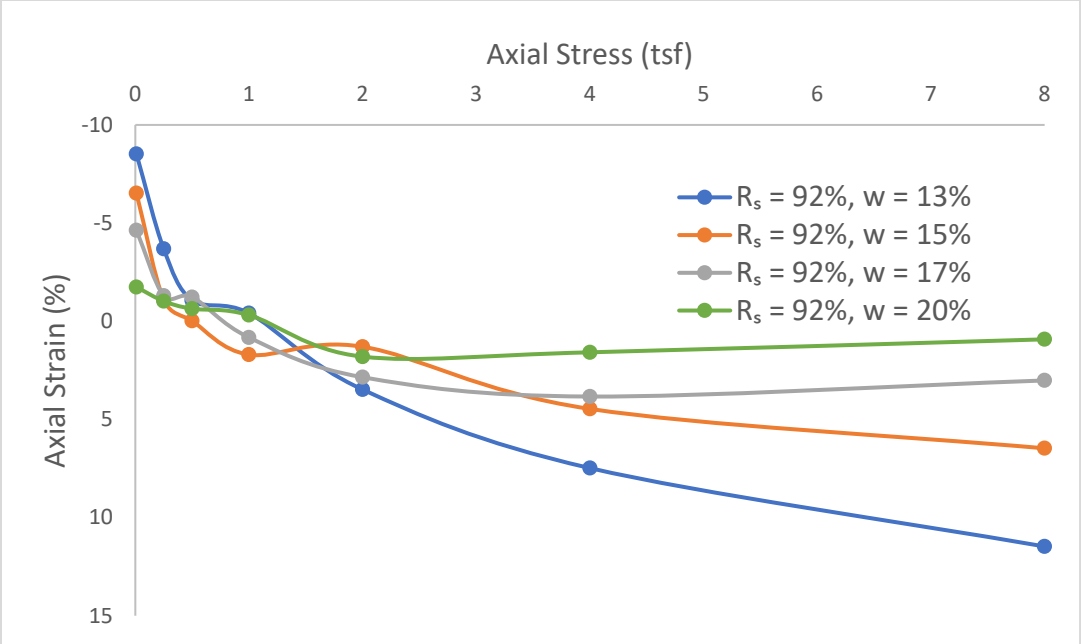

Figure 4.22 Comparison of Wetting-induced Stress-strain Characteristics for A-2 (SC) PI>>11 Soil at a Constant Relative Compaction R_s = 92%

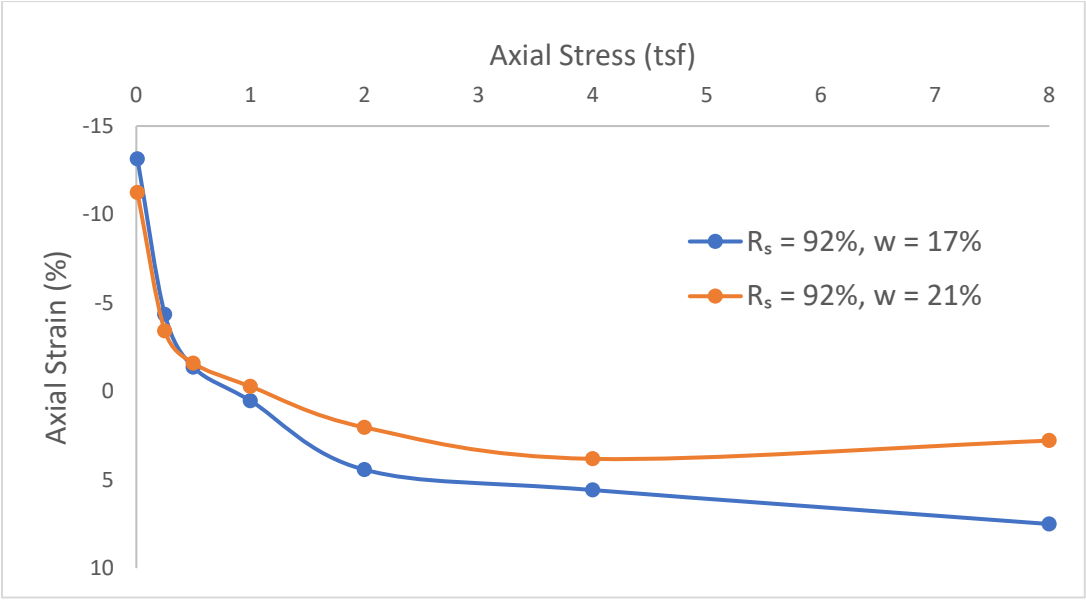

Figure 4.23 Comparison of Wetting-induced Stress-strain Characteristics for A-4 (CL) Soil at a Constant Relative Compaction R_s = 92%

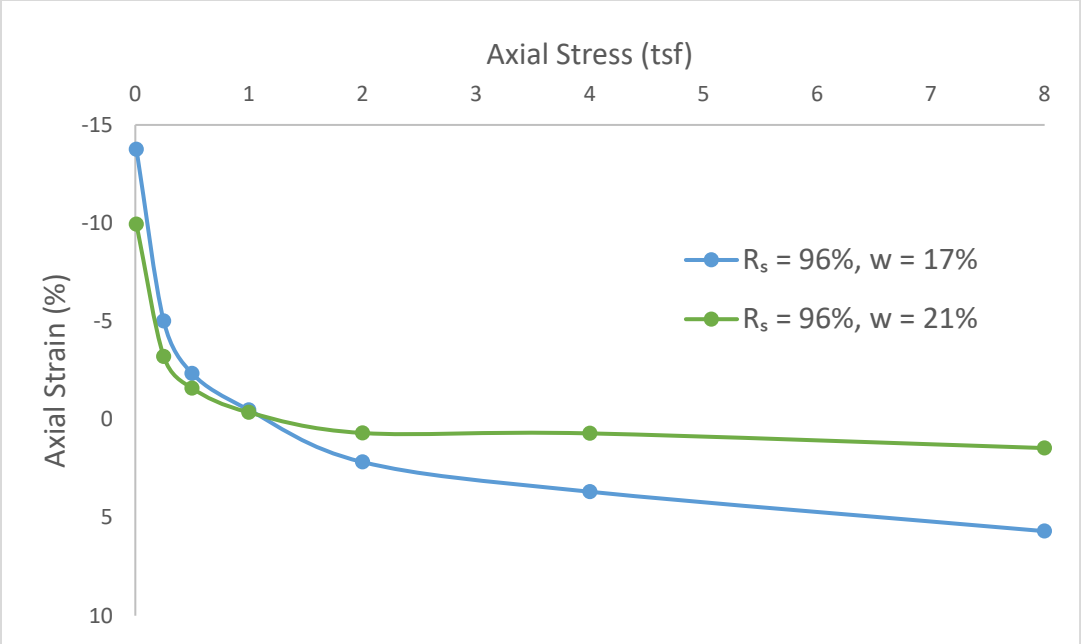

Figure 4.24 Comparison of Wetting-induced Stress-strain Characteristics for A-4 (CL) Soil at a Constant Relative Compaction R_s = 96%

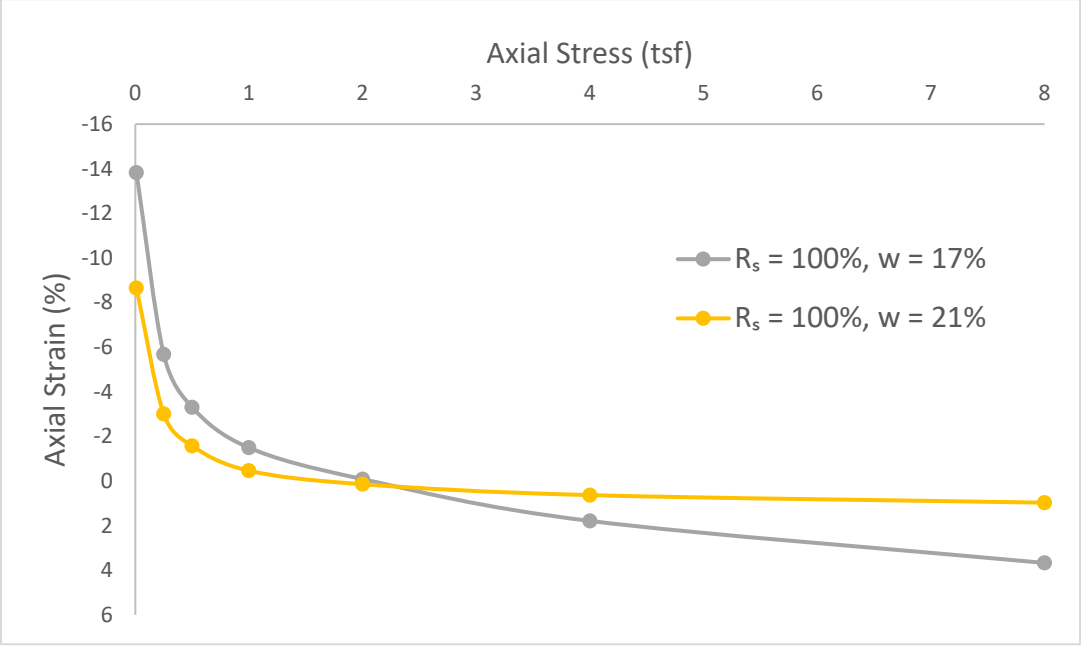

Figure 4.25 Comparison of Wetting-induced Stress-strain Characteristics for A-4(CL) Soil at a Constant Relative Compaction R_s = 100%

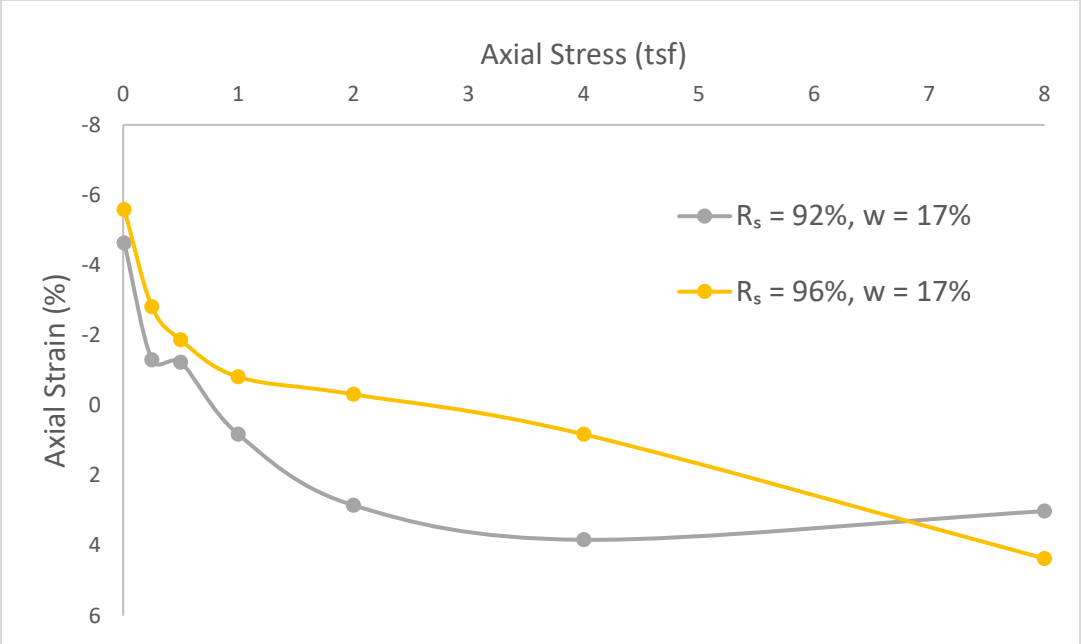

Figure 4.26 Comparison of Wetting-induced Stress-strain Characteristics for A-2(SC) PI>>11 Soil at a Constant As-compacted Moisture Content w = 17%

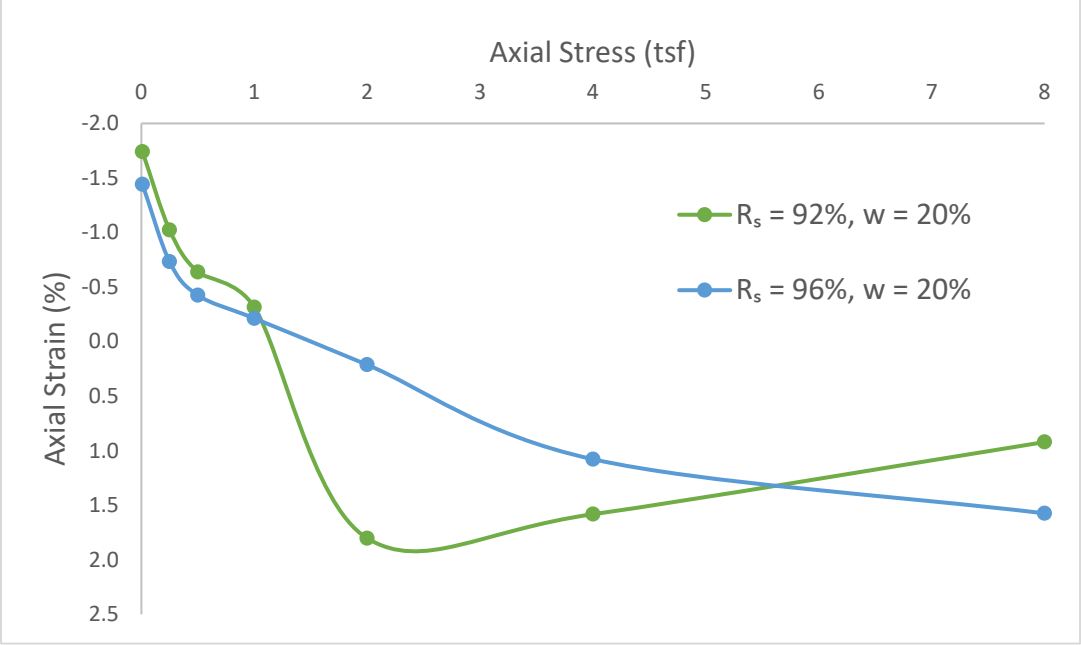

Figure 4.27 Comparison of Wetting-induced Stress-strain Characteristics for A-2(SC) PI>>11 Soil at a Constant As-compacted Moisture Content w = 20%

The wetting-induced stress-strain characteristics for the A-4 (CL) soil at the two different moisture contents (17% and 21%) are shown in the Figure 4.28 and Figure 4.29, respectively. It was observed that A-4 (CL) soil exhibited a huge amount of negative wetting-induced strain (swell) at low overburden stresses, even when the soil was compacted at a high relative compaction and moisture content values, as shown in Figure 4.29.

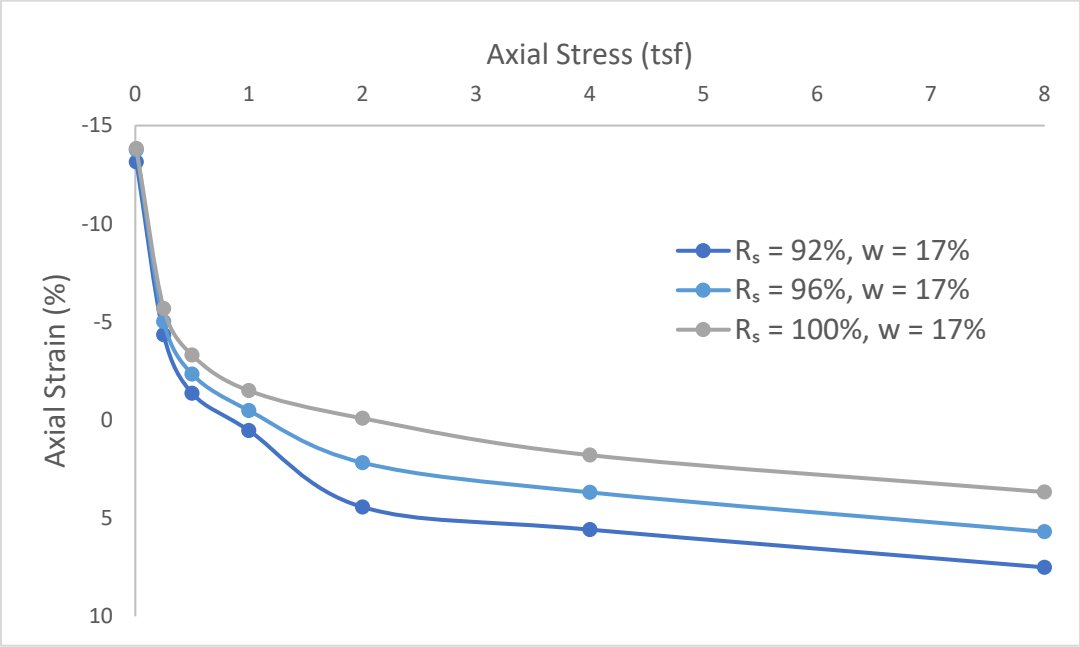

Figure 4.28 Comparison of Wetting-induced Stress-strain Characteristics for A-4 (CL) Soil at a Constant As-compacted Moisture Content w = 17%

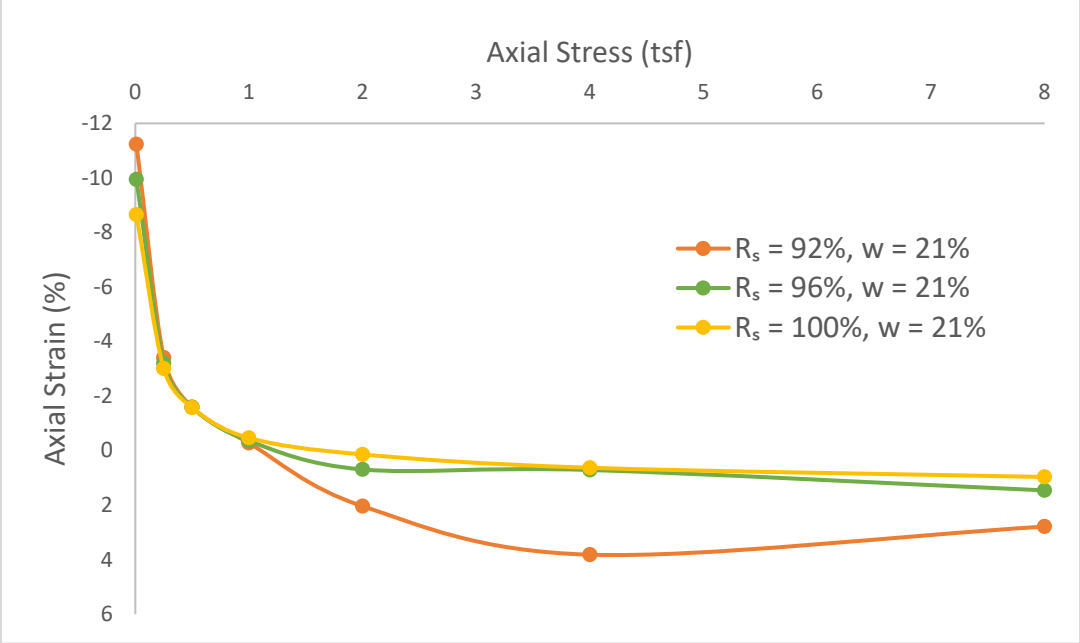

Figure 4.29 Comparison of Wetting-induced Stress-strain Characteristics for A-4 (CL) Soil at a Constant As-compacted Moisture Content w = 21%

4.3.3 Secondary Compression of A-4 (CL) soil

After examining the time rate compression of the different soil types, it was determined that the A-4 (CL) soil was most susceptible to settlement from secondary compression, as it contained the highest amount of cohesive material. The excess pore water pressures generated during the loading of soil took a long time to dissipate for this soil type. The same procedure adopted for determining the wetting-induced collapse using single consolidometer test was followed for a longer duration i.e., up to eight days after soaking the specimen, to determine the secondary compression of the soil. Since most of the embankment heights are in the range of 20–30 feet, an overburden stress of 2 tsf was chosen to conduct these tests, which represents the range of stress that the embankments are usually subject to under their self-weight.

For each of the testing conditions established for A-4 (CL), the specimen was left for a period of up to eight days after soaking and appropriate dial gauge reading were taken. In Figure 4.30, the plot between the axial strain after soaking and the logarithm of time for A-4 (CL) at 2 tsf overburden stress, 92% relative compaction and 4% drier than the optimum moisture condition is shown. It can be observed from Figure 4.30 that the plot follows a "reverse S-shape," which is characteristic of cohesive soils at the above-specified testing conditions, the axial strain value ceased to increase after a period of 48 hours. This shows that wetting-induced settlements caused were predominantly due to primary consolidation and the settlements due to secondary compression are negligible. However, the time taken for the A-4 (CL) soil to reach the completion of primary consolidation under the loading and wetting was much greater than the other soil grades. This trend was observed for most of the testing conditions and the strain-log of time characteristics are provided in the Figures B.51 through B.53.

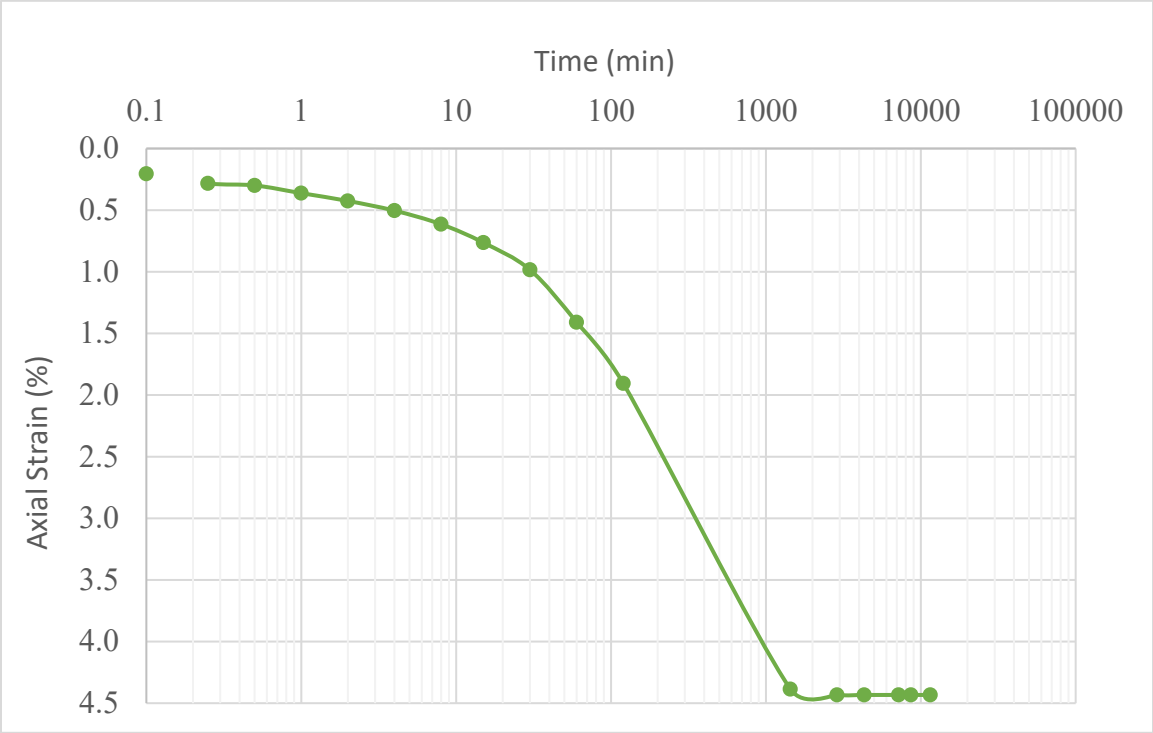

Figure 4.30 Strain vs. Logarithm of Time for Single-consolidometer Soaked Specimen A-4 (CL) - Rs = 92%, w = 17%, 2 tsf

Effect of Degree of Saturation: Figure 4.31 shows the variation of the secondary compression index with increasing as-compacted degree of saturation from left to right. It can be observed that with increasing as-compacted degree of saturation, the secondary compression index of the A-4 soil decreases to a certain critical value, and then increases with an increase in the as-compacted degree of saturation. Although the variation in the secondary compression index is really small, since the process of secondary compression occurs over a long period of time which is usually the design period of the structure, the settlements caused might pose a significant long-term effect. The calculated values of the secondary compression index of A-4 soil for the different placement conditions are summarized in Table 4.1.

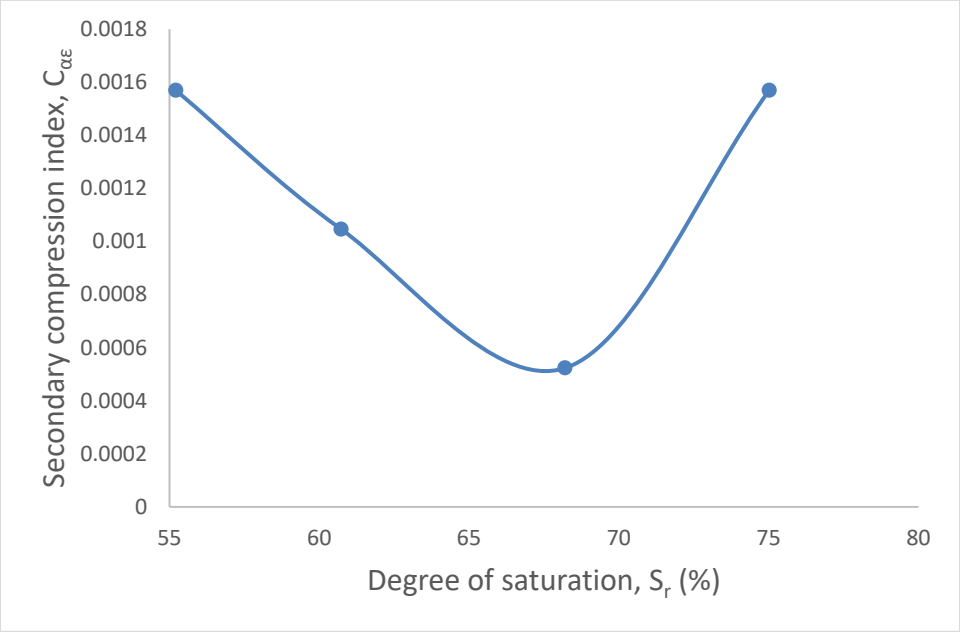

Figure 4.31 Graph Showing the Variation of Secondary Compression Index of A-4 (CL) Soil with Varying As-compacted Degree of Saturation

Table 4.1 Summary of Calculated $C_{\alpha\varepsilon}$ Values for Different Placement Conditions of A-4 (CL)

Soil condition	S_r (%)	$C_{\alpha\varepsilon}$
R_s = 92%, w = 17%	55.21	0.001569
R_s = 96%, w = 17%	60.73	0.001046
R_s = 92%, w = 21%	68.20	0.000523
R_s = 96%, w = 21%	75.02	0.001569
R_s = 100%, w = 17%	-	Swell
R_s = 100%, w = 21%	-	Swell

4.4 Regression Analysis for Evaluating Wetting-Induced Strain

Results from the consolidometer tests were used to develop a regression model for each type soil that evaluates the wetting-induced strain the soil is subjected to, as a function of the overburden stress, relative compaction and as-compacted water content.

The regression model was developed following the theory behind Multiple Linear Regression (Learn Something, 2015) and using Microsoft Excel's "Data Analysis" add-on feature. The general form of the equations obtained from this regression model is given in the Equation 4.1 below. The regression coefficients, significance indicators and the R^2 values for the regression model developed using Equation 4.1 for various soil types tested are summarized in Table 4.2.

$$\varepsilon_w = \beta_0 + \beta_1 \ln\left(\frac{\sigma_v}{p_A}\right) + \beta_2 R_c + \beta_3 w \quad (4.1)$$

where
ε_w = wetting-induced strain, (%)
σ_v = overburden stress, (kPa or tsf)
p_A = atmospheric pressure, (kPa or tsf)
R_c = Relative compaction, (%)
w = As-compacted water content, (%)
β_0, β_1, β_2, β_3 = Regression coefficients from Table 4.2

The significance level for the p-values of the regression coefficients was chosen to be equal to 0.1. Therefore, there can only be a maximum of 10% probability that the correlation between the response variable (wetting-induced strain) and the predictor variables (overburden stress, relative compaction or as-compacted water content) does not exist. In Table 4.2, the cells highlighted in red are the p-values for the predictor variable coefficients, which are greater than 0.1. Clearly, for all the soils except the A-1-a (SP or SW) soil, the p-value test fails for at least one of the predictor variable coefficients in the regression model developed using Equation 4.1. In Figure 4.32, the predicted wetting-induced strain from Equation 4.1 is plotted on the vertical axis against the observed wetting-induced strain on the horizontal axis for A-4 (CL) soil.

The scatter around the equality line (blue line) in Figure 4.32 provides a visual representation of how close the predicted values are to the observed values of wetting-induced strain. Similar graphs are provided for all the soils in Appendix C from Figures C.1 through C.8.

To achieve a better correlation, the general form of equations for the regression models included only the overburden stress and the as-compacted degree of saturation of the soil as the predictor variables, shown in the Equation 4.2 below. The as-compacted degree of saturation was calculated using the Equation 4.3 for each test. The regression coefficients, significance indicators and the R^2 values for the regression model developed using Equation 4.2 are summarized in Table 4.3 for all the soils.

$$\varepsilon_w = \beta_0 + \beta_1 \ln\left(\frac{\sigma_v}{p_A}\right) + \beta_2 e^{-\left(\frac{S_r}{100}\right)} \quad (4.2)$$

where
S_r = as-compacted degree of saturation, (%)
β_0, β_1, β_2 = Regression coefficients from Table 4.3

Table 4.2 Coefficients and Significance Indicators of the Regression Model Developed Using Equation 4.1

Soil Type	Regression coefficients				p - values for predictor coefficients			Overall Significance F-test	R^2
	b_0	b_1	b_2	b_3	b_1	b_2	b_3		
A-1-a (SP or SW)	8.3849	0.1947	-0.0673	-0.1741	3.56E-05	0.0434	0.0371	6.49E-05	0.5935
A-1-a (SM)	11.2505	0.3039	-0.0450	-0.6873	2.19E-03	0.5416	0.0009	4.05E-04	0.5243
A-1-a (SC - SM)	9.0372	0.2228	-0.0907	-0.0697	3.28E-02	0.2721	0.7325	1.18E-01	0.2135
A-1-b (SM)	1.1940	0.0824	0.0118	-0.1836	7.35E-05	0.6211	0.0000	4.57E-06	0.6756
A-1-b (SC-SM)	32.1681	0.7348	-0.2777	-0.8034	1.22E-03	0.1040	0.0623	1.91E-03	0.4561
A-2 (SC) PI 10	23.7005	0.5031	-0.2334	-0.0165	2.72E-04	0.0023	0.9491	1.54E-04	0.4737
A-2 (SC) high PI	-4.0744	1.4123	0.0937	-0.2013	1.72E-10	0.6371	0.1744	2.77E-09	0.6711
A-3 (SP-SM)	5.9576	0.2633	-0.0142	-0.2663	2.51E-04	0.7953	0.0520	1.20E-03	0.3381
A-4 (CL)	19.1011	2.3781	-0.1985	-0.0272	2.19E-22	0.0086	0.8176	5.79E-21	0.9208

Table 4.3 Coefficients and Significance Indicators of the Regression Model Developed Using Equation 4.2

Soil Type	Regression coefficients			p - values for predictor coefficients		Overall Significance F-test	R^2
	b_0	b_1	b_2	b_1	b_2		
A-1-a (SP or SW)	-2.0797	0.1947	4.9677	2.36E-05	0.0042	1.24E-05	0.5951
A-1-a (SM)	-5.8544	0.3039	12.3292	3.38E-03	0.0049	6.41E-04	0.4447
A-1-a (SC - SM)	-1.2102	0.2228	2.4727	3.14E-02	0.4049	7.03E-02	0.1914
A-1-b (SM)	-1.8719	0.0824	4.1794	3.41E-04	0.0011	4.43E-05	0.5515
A-1-b (SC-SM)	-7.8299	0.7348	15.9607	1.08E-03	0.0201	6.77E-04	0.4423
A-2 (SC) PI 10	-6.8159	0.5031	16.0165	3.71E-04	0.0099	1.55E-04	0.4220
A-2 (SC) high PI	-3.4846	1.3879	8.6038	1.58E-10	0.1222	6.65E-10	0.6616
A-3 (SP-SM)	-2.7835	0.2616	6.6090	1.90E-04	0.0968	3.24E-04	0.3377
A-4 (CL)	-5.2162	2.3781	9.3316	4.53E-22	0.0932	3.00E-21	0.9114

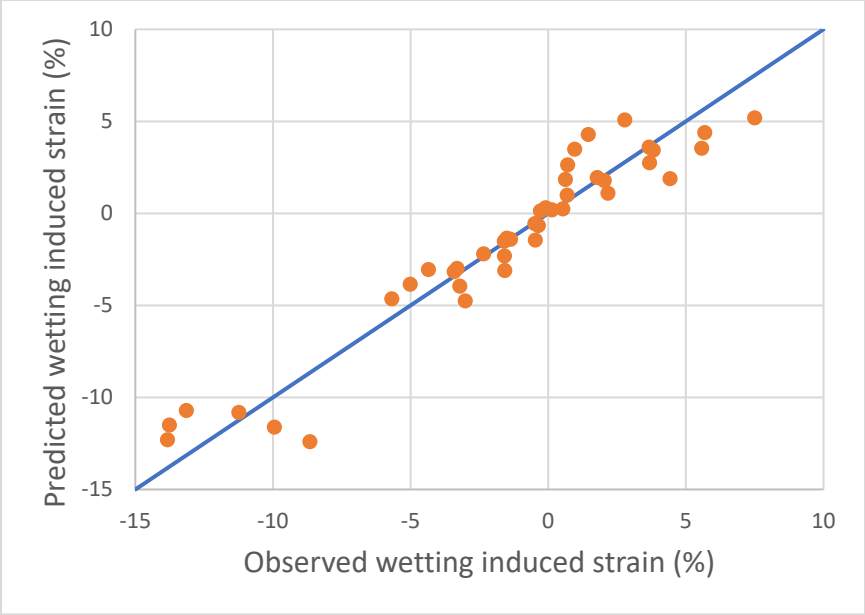

Figure 4.32 Predicted vs. Observed Wetting-induced Strain for A-4 (CL) Soil Using Equation 4.1

$$S_r = w\left(\frac{1}{\frac{100 * \gamma_w}{R_c * \gamma_{d,max}} - \frac{1}{G_s}}\right) \tag{4.3}$$

where
$\gamma_{d,max}$ = Maximum dry unit weight of the soil, (kN/m^3 or pcf)
γ_w = Unit weight of water, (kN/m^3 or pcf)
G_s = Specific Gravity of the soil solids

The same significance level of 0.1 was adopted for the p-values, as previously noted. As it is shown in the Table 4.3, only for soils A-1-a (SC-SM) and A-2 (SC) with PI>>11 the p-value cells for the β_2 term are highlighted in red, since only for those two soils the p-value test was not satisfied.

In Figure 4.33, the predicted wetting-induced strain from Equation 4.2 is plotted on the vertical axis against the observed wetting-induced strain on the horizontal axis for A-4 (CL) soil. Similar graphs are provided for all the soils in Appendix C from Figures C.9 through C.16.

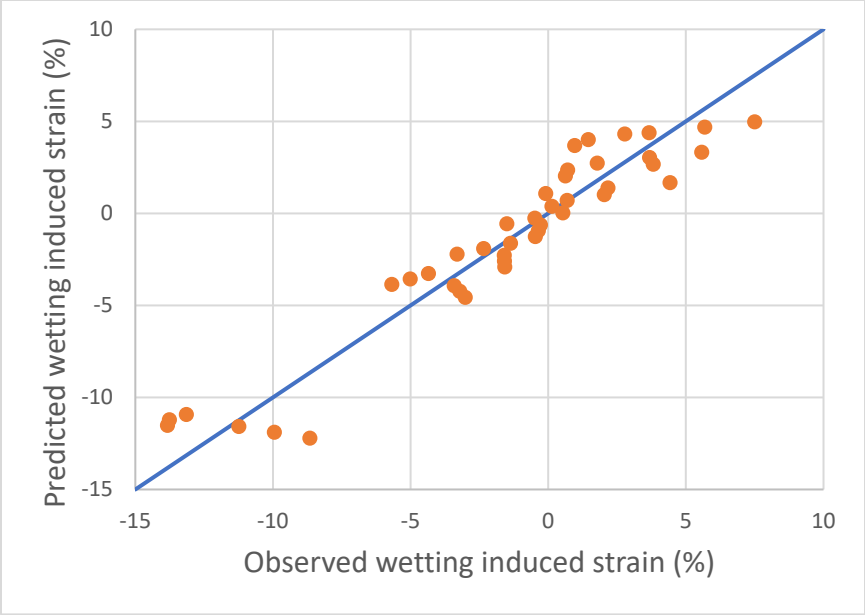

Figure 4.33 Predicted vs. Observed Wetting-induced Strain for A-4 (CL) Soil Using Equation 4.2

4.5 Regression Analysis for Evaluating Loading-induced Strain

Results from the consolidometer tests conducted on the specimen maintained at the as-compacted moisture content throughout the duration of the test were used to develop a regression model that evaluates the loading-induced strain the soil is subjected to, as a function of overburden stress and the as-compacted degree of saturation of the specimen.

The general form of equations for the loading-induced strain for different soil types obtained are given in the Equation 4.4, below. The regression coefficients, significance indicators and the R^2 values for the regression model developed using Equation 4.4 for various soil types tested are summarized in Table 4.4.

$$\varepsilon_L = \beta_0 + \beta_1 \, ln\left(\frac{\sigma_v}{p_A}\right) + \beta_2 e^{-\left(\frac{S_r}{100}\right)} \qquad (4.4)$$

where
ε_L = loading-induced strain, (%)
σ_v = overburden stress, (kPa or tsf)
p_A = atmospheric pressure, (kPa or tsf)
S_r = as-compacted degree of saturation, (%)
β_0, β_1, β_2 = Regression coefficients from Table 4.4

The degree of saturation for each test was calculated using Equation 4.3 previously given.

Table 4.4 Coefficients and Significance Indicators of the Regression Model Developed Using Equation 4.4

Soil Type	Regression coefficients			p - values for predictor coefficients		Overall Significance F-test	R^2
	b_0	b_1	b_2	b_1	b_2		
A-1-a (SP or SW)	0.7770	0.1232	-0.7183	2.49E-08	0.2775	1.14E-07	0.7217
A-1-a (SM)	0.4849	0.1439	-0.0405	1.32E-08	0.9569	7.24E-08	0.7316
A-1-a (SC - SM)	0.8424	0.2512	0.1295	3.06E-11	0.8482	1.77E-10	0.8341
A-1-b (SM)	0.5666	0.2364	0.3807	1.11E-07	0.8378	5.84E-07	0.6828
A-1-b (SC-SM)	0.6835	0.1868	-0.1592	2.77E-05	0.8938	1.29E-04	0.5115
A-2 (SC) PI 10	0.2800	0.4382	2.5661	1.14E-03	0.2044	2.57E-03	0.3111
A-2 (SC) high PI	0.5306	0.4330	1.0905	1.09E-05	0.7082	5.36E-05	0.3961
A-3 (SP-SM)	-3.6759	0.2696	8.9915	4.57E-06	0.0061	2.43E-06	0.4847
A-4 (CL)	1.8459	0.5382	-0.7399	7.95E-07	0.8602	4.36E-06	0.4690

4.6 Regression Analysis Comparison between Current and Existing Models

In this section, the comparison between the current regression model developed for each soil type and the existing regression models for the wetting-induced collapse potential developed by Basma and Tuncer, previously mentioned in the literature review will be discussed. The various soil properties used to estimate the collapse potential of the soil using Equations 2.1 and 2.2 developed by Basma and Tuncer are summarized in Table 4.5. The coefficient of uniformity, sand, and clay fractions for each soil type were obtained from their respective grain size distributions, shown in the Figure 3.3. The as-compacted dry unit weight of the soil was estimated using Equation 4.5. The values of pressure at wetting (p_w) in the Equations 2.1 and 2.2 were taken same as the values of the overburden stress (σ_v).

$$\gamma_d = \frac{R_c}{100} * \gamma_{d,max} \tag{4.5}$$

where
γ_d = as-compacted dry unit weight of the soil, (kN/m^3)
R_c = Relative compaction, (%)
$\gamma_{d,max}$ = Maximum dry unit weight of the soil, (kN/m^3)

In Figure 4.34, the observed vs. predicted collapse potential using the Equations 2.1, 2.2 and 4.2 are shown for the A-4 (CL) soil. From Figure 4.34, it was observed that the scatter is the least when the Equation 4.2 was used to predict the wetting-induced collapse of A-4 (soil). Similar graphs for all the soil types are shown in the Appendix D from Figures D.1 through D.8. It was observed, from all these graphs, that the Equations 2.1 and 2.2 were only valid for soils that contained high fractions of plastic fines, such as the A-4 (CL) soil. In all other soil types tested under this research program, the scatter in data from the equality line was so obvious,s as shown in Figures D.8, that the collapse potential calculated using Equations 2.1 and 2.2 would be massively incorrect. This makes sense to some extent because both the equations were developed using the experimental data for soils having a plasticity index ranging from 3.0 to as high as 28.9, and none of them contained non-plastic fines.

4.7 Estimated Loading and Wetting-induced Settlements for Different Embankment Heights, Soil Grades and Placement Conditions.

For each of the consolidometer tests conducted on the as-compacted specimen, from the stress-strain characteristics a best-fit regression equation for the loading-induced strain as a function of overburden stress was developed. This equation was then integrated with respect to the height of the embankment to get the loading-induced settlements for different embankment heights. The values of the estimated loading-induced settlements, using the procedure described above, are summarized in Table 4.6.

The wetting-induced settlements were also estimated by developing a best-fit regressing equation based on the tests conducted on the as-compacted and soaked specimens, since wetting-induced strain was estimated as the difference between the strains of soaked and as-compacted specimens. This equation was integrated with respect to the height of the embankment and the resulting collapse/swell are summarized in Table 4.7.

Table 4.5 Soil Properties Used in Equations 2.1 and 2.2

Soil Type	Soil Properties			
	C_u	$\gamma_{d,max}$ (kN/m^3)	S (%)	C (%)
A-1-a (SP or SW)	20.4	20.3	45	0
A-1-a (SM)	54.1	20.1	35	0
A-1-a (SC - SM)	54.1	22.3	35	3
A-1-b (SM)	17.8	19.3	25	0
A-1-b (SC-SM)	17.8	21.6	25	4
A-2 (SC) PI 10	56.7	17.7	65	6
A-2 (SC) high PI	56.7	17.1	65	6
A-3 (SP-SM)	2.6	17.6	90	0
A-4 (CL)	85.0	17.0	0	18

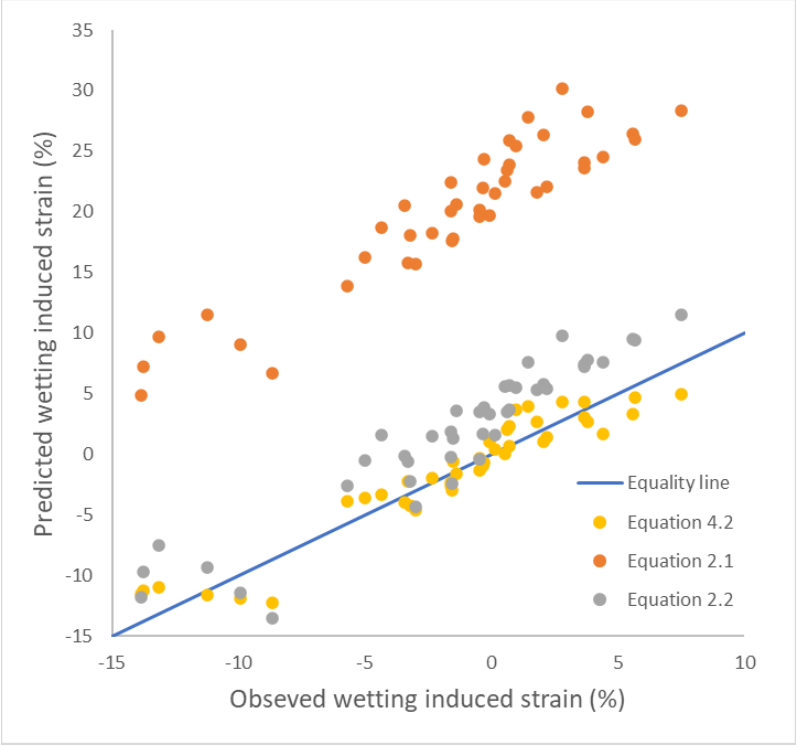

Figure 4.34 Predicted vs. Observed Wetting-induced Strain for A-4 (CL) Soil Using Equations 4.2, 2.1 and 2.2

Table 4.6 Estimated Loading-induced Settlement in Embankments Constructed to Various Heights and Placement Conditions for the Different Soil Grades

Soil Type and Testing Conditions	Predicted Loading-Induced Settlement for Various Embankment Heights (in.)							
	5 ft	10 ft	15 ft	20 ft	25 ft	30 ft	35 ft	40 ft
A-1-a (SC-SM)								
R_m = 90%, w = 4.3%	0.134	0.477	0.959	1.529	2.146	2.784	3.428	4.072
R_m = 90%, w = 6.3%	0.130	0.388	0.759	1.224	1.771	2.386	3.056	3.772
R_m = 95%, w = 4.3%	0.139	0.486	0.963	1.509	2.083	2.660	3.228	3.786
R_m = 95%, w = 6.3%	0.099	0.324	0.658	1.086	1.594	2.170	2.801	3.478
A-1-a (SM)								
R_m = 90%, w = 8%	0.040	0.134	0.276	0.462	0.685	0.942	1.226	1.535
R_m = 90%, w = 10%	0.042	0.156	0.328	0.545	0.798	1.078	1.380	1.701
R_m = 95%, w = 8%	0.020	0.093	0.212	0.374	0.572	0.804	1.065	1.350
R_m = 95%, w = 10%	0.037	0.137	0.292	0.496	0.740	1.020	1.330	1.664
A-1-a (SP-SW)								
R_m = 90%, w = 8.1%	0.016	0.080	0.186	0.329	0.505	0.707	0.934	1.180
R_m = 90%, w = 10.1%	0.040	0.137	0.285	0.479	0.713	0.985	1.288	1.621
R_m = 95%, w = 8.1%	0.013	0.067	0.158	0.282	0.434	0.612	0.813	1.034
R_m = 95%, w = 10.1%	0.024	0.110	0.258	0.466	0.733	1.057	1.437	1.873
A-1-b (SC-SM)								
R_m = 90%, w = 4.7%	0.071	0.190	0.350	0.548	0.779	1.038	1.321	1.626
R_m = 90%, w = 6.7%	0.068	0.231	0.476	0.790	1.163	1.584	2.044	2.538
R_m = 95%, w = 4.7%	0.042	0.151	0.319	0.541	0.811	1.123	1.473	1.857
R_m = 95%, w = 6.7%	0.041	0.140	0.290	0.484	0.717	0.982	1.276	1.594

A-1-b (SM)								
R_m = 90%, w = 10%	0.051	0.189	0.408	0.700	1.060	1.480	1.955	2.480
R_m = 90%, w = 12%	0.087	0.286	0.587	0.980	1.454	2.001	2.613	3.281
R_m = 95%, w = 10%	0.037	0.148	0.325	0.560	0.846	1.176	1.544	1.944
R_m = 95%, w = 12%	0.050	0.174	0.364	0.612	0.912	1.258	1.643	2.064
A-2 (SC) PI = 10								
R_s = 92%, w = 13.5%	0.128	0.254	0.386	0.535	0.708	0.916	1.169	1.474
R_s = 92%, w = 15.5%	0.073	0.229	0.462	0.769	1.145	1.587	2.095	2.668
R_s = 96%, w = 13.5%	0.038	0.122	0.251	0.425	0.642	0.902	1.205	1.549
R_s = 100%, w = 13.5%	0.047	0.148	0.300	0.504	0.758	1.060	1.409	1.804
R_s = 100%, w = 15.5%	0.034	0.118	0.249	0.428	0.651	0.919	1.229	1.581
A-2 (SC) PI>>11								
R_s = 96%, w = 13%	0.049	0.171	0.359	0.605	0.903	1.246	1.630	2.048
R_s = 96%, w = 15%	0.111	0.279	0.503	0.783	1.116	1.503	1.942	2.432
R_s = 96%, w = 17%	0.049	0.224	0.517	0.923	1.435	2.047	2.756	3.556
R_s = 96%, w = 20%	0.057	0.163	0.348	0.638	1.055	1.615	2.334	3.223
R_s = 96%, w = 17%	0.100	0.244	0.430	0.657	0.926	1.234	1.581	1.967
R_s = 96%, w = 20%	0.081	0.240	0.476	0.788	1.172	1.627	2.152	2.743
A-3 (SP-SM)								
R_s = 90%, w = 14%	0.121	0.418	0.876	1.480	2.216	3.071	4.031	5.086
R_s = 90%, w = 16%	0.125	0.412	0.845	1.412	2.101	2.898	3.793	4.775
R_s = 93%, w = 14%	0.048	0.168	0.341	0.554	0.796	1.059	1.338	1.628
R_s = 93%, w = 16%	0.072	0.251	0.508	0.819	1.166	1.534	1.914	2.299
R_s = 96%, w = 14%	0.026	0.098	0.210	0.360	0.543	0.755	0.994	1.255
R_s = 96%, w = 16%	0.038	0.136	0.286	0.481	0.715	0.982	1.277	1.596

A-4 (CL)								
R_s = 92%, w = 17%	0.080	0.223	0.430	0.703	1.045	1.459	1.945	2.507
R_s = 92%, w = 21%	0.111	0.243	0.413	0.638	0.935	1.318	1.800	2.394
R_s = 96%, w = 17%	0.058	0.172	0.340	0.566	0.850	1.192	1.594	2.058
R_s = 96%, w = 21%	0.091	0.245	0.463	0.750	1.106	1.534	2.036	2.615
R_s = 100%, w = 17%	0.053	0.144	0.274	0.447	0.666	0.931	1.245	1.610
R_s = 100%, w = 21%	0.150	0.344	0.583	0.871	1.210	1.603	2.052	2.561

Table 4.7 Estimated Wetting-induced Settlements in Embankments Constructed to Various Heights and Placement Conditions for the Different Soil Grades

Soil Type and Testing Conditions	Predicted Wetting-induced Settlement for Various Embankment Heights (in.)							
	5 ft	10 ft	15 ft	20 ft	25 ft	30 ft	35 ft	40 ft
A-1-a (SC-SM)								
R_m = 90%, w = 4.3%	-0.200	-0.463	-0.748	-1.020	-1.245	-1.391	-1.432	-1.344
R_m = 90%, w = 6.3%	-0.058	-0.089	-0.101	-0.099	-0.089	-0.074	-0.057	-0.041
R_m = 95%, w = 4.3%	-0.230	-0.531	-0.891	-1.298	-1.742	-2.209	-2.689	-3.170
R_m = 95%, w = 6.3%	0.005	0.007	0.003	-0.010	-0.034	-0.071	-0.121	-0.183
A-1-a (SM)								
R_m = 90%, w = 8%	0.169	0.450	0.842	1.346	1.962	2.689	3.528	4.479
R_m = 90%, w = 10%	0.020	0.072	0.144	0.227	0.313	0.398	0.480	0.558
R_m = 95%, w = 8%	0.155	0.399	0.733	1.155	1.666	2.265	2.954	3.732
R_m = 95%, w = 10%	0.004	0.012	0.022	0.036	0.051	0.069	0.087	0.107
A-1-a (SP-SW)								
R_m = 90%, w = 8.1%	0.070	0.238	0.493	0.825	1.225	1.685	2.196	2.752
R_m = 90%, w = 10.1%	0.019	0.080	0.185	0.332	0.523	0.756	1.032	1.351
R_m = 95%, w = 8.1%	0.044	0.173	0.376	0.644	0.968	1.340	1.753	2.200
R_m = 95%, w = 10.1%	-0.002	0.023	0.068	0.128	0.201	0.281	0.366	0.451
A-1-b (SC-SM)								
R_m = 90%, w = 4.7%	-0.456	-0.088	1.023	2.804	5.185	8.101	11.489	15.293
R_m = 90%, w = 6.7%	-0.025	-0.074	-0.116	-0.124	-0.075	0.054	0.280	0.619
R_m = 95%, w = 4.7%	-0.170	-0.310	-0.391	-0.389	-0.281	-0.049	0.325	0.855
R_m = 95%, w = 6.7%	0.335	0.923	1.585	2.282	2.998	3.724	4.453	5.182

A-1-b (SM)								
R_m = 90%, w = 10%	0.058	0.189	0.377	0.605	0.860	1.134	1.419	1.710
R_m = 90%, w = 12%	0.007	-0.003	-0.028	-0.066	-0.116	-0.175	-0.242	-0.314
R_m = 95%, w = 10%	0.076	0.205	0.381	0.599	0.853	1.137	1.448	1.781
R_m = 95%, w = 12%	0.005	0.017	0.043	0.087	0.151	0.234	0.337	0.456
A-2 (SC) PI = 10								
R_s = 92%, w = 13.5%	-0.152	-0.274	-0.306	-0.194	0.109	0.647	1.456	2.567
R_s = 92%, w = 15.5%	0.049	0.170	0.400	0.772	1.313	2.049	2.999	4.180
R_s = 96%, w = 13.5%	-0.366	-0.719	-1.037	-1.300	-1.491	-1.592	-1.588	-1.466
R_s = 100%, w = 13.5%	-0.317	-0.577	-0.788	-0.958	-1.094	-1.203	-1.290	-1.360
R_s = 100%, w = 15.5%	-0.050	-0.063	-0.057	-0.048	-0.045	-0.053	-0.075	-0.112
A-2 (SC) PI>>11								
R_s = 92%, w = 13%	-3.421	-5.637	-6.780	-6.975	-6.338	-4.978	-2.996	-0.486
R_s = 92%, w = 15%	-2.295	-2.452	-1.712	-0.792	-0.012	0.589	1.153	1.908
R_s = 92%, w = 17%	-1.915	-2.813	-2.914	-2.401	-1.429	-0.121	1.425	3.133
R_s = 92%, w = 20%	-0.889	-1.416	-1.625	-1.558	-1.254	-0.750	-0.081	0.722
R_s = 96%, w = 17%	-2.497	-3.801	-4.546	-5.097	-5.613	-6.113	-6.526	-6.744
R_s = 96%, w = 20%	-0.653	-1.041	-1.240	-1.313	-1.306	-1.252	-1.172	-1.075
A-3 (SP-SM)								
R_s = 90%, w = 14%	-0.005	-0.126	-0.325	-0.564	-0.808	-1.027	-1.190	-1.271
R_s = 90%, w = 16%	-0.012	0.004	0.043	0.104	0.181	0.274	0.379	0.494
R_s = 93%, w = 14%	-0.011	0.019	0.090	0.204	0.361	0.564	0.814	1.111
R_s = 93%, w = 16%	-0.031	-0.066	-0.096	-0.114	-0.112	-0.084	-0.023	0.077
R_s = 96%, w = 14%	-0.018	0.014	0.088	0.201	0.346	0.519	0.718	0.939
R_s = 96%, w = 16%	-0.006	-0.007	-0.004	0.004	0.016	0.033	0.054	0.080

A-4 (CL)								
R_s = 92%, w = 17%	-5.361	-7.152	-7.366	-7.131	-6.913	-6.709	-6.207	-4.941
R_s = 92%, w = 21%	-4.536	-6.088	-6.430	-6.566	-6.903	-7.426	-7.845	-7.725
R_s = 96%, w = 17%	-5.676	-7.815	-8.483	-8.822	-9.286	-9.835	-10.127	-9.678
R_s = 96%, w = 21%	-4.005	-5.390	-5.742	-5.948	-6.363	-6.972	-7.522	-7.647
R_s = 100%, w = 17%	-5.830	-8.342	-9.528	-10.478	-11.611	-12.882	-13.959	-14.388
R_s = 100%, w = 21%	-3.494	-4.743	-5.136	-5.432	-5.918	-6.559	-7.119	-7.278

5. LARGE-SCALE CONSOLIDOMETER TESTS

5.1 Overview

At a meeting of the Technical Advisory Committee (TAC) for this research project in December 2020, the researchers were encouraged by the TAC to concentrate the investigation on determining the best material for bridge approach embankments to help mitigate the problem of bumps at the bridges. The reasoning for this recommendation was the additional cost of using the best material would likely be insignificant compared to the total cost of the project. At the time of this recommendation the standard consolidometer tests had already been completed. Therefore, to pursue this goal, a total of 27 large-scale consolidometer (LSC) tests were conducted on the two materials, out of the 10 materials studied in this project determined to be the best embankment materials in terms of loading-induced and wetting-induced settlements. Both of these materials were granular. In addition, four (4) LSC tests were conducted on a cohesive soil for comparison with the LSC tests conducted on the two granular soils and also for comparison with results from Standard Consolidometer (SC) tests conducted on the same material. Results from these 27 LSC tests and analyses of the results from these tests are presented in this chapter.

5.2 Materials Tested in Large-scale Consolidometer

Of the 10 materials studied in this project, the two materials determined to be the least susceptible to loading and wetting-induced settlements are *Free-Draining Granular Backfill* (FDGW) and *A-1-a/SP or SW* (the first two materials listed in Table 5.1). Well-graded materials were chosen for both types because well-graded granular materials, in general, can be compacted to much denser states and, thus, are less susceptible to loading-induced and wetting-induced settlement than poorly-graded or uniform materials — all other factors being the same (mineral composition, relative compaction, angularity of particles, fabric, etc.). Evidence to support this statement is shown in Figure 5.1. Of the three non-plastic granular soils shown in Figure 5.1, the maximum dry densities for the two well-graded soils (about 2.18 and 2.03 Mg/m^3 = 136 and 127 pcf for Soils 1 and 2) are 36 and 27% greater than the maximum dry density for the one poorly-graded soil (1.60 Mg/m^3 = 100 pcf for Soil 8).

Because larger particles could be used in the LSC and still meet the requirement that the largest-sized particles could not be greater than one-sixth the smallest dimension of the specimen, it was decided to include the material passing the ¾-inch sieve in the A-1-a/SW soil tested in the LSC. Including the material passing the ¾-inch sieve allowed the use of more sizes from the original borrow material and to replicate more closely what would be used in the field if the same material was utilized. The material passing the #4 sieve was the nominally the same as used in the SC tests. Larger particles could have been used, but ¾-inch maximum size was selected to be consistent with the specifications for the free-draining granular backfill. In addition, only a small percentage of the material from the borrow pit was larger than ¾ inch. The acronym A1aSW is used for the material tested in the LSC to differentiate it from the A-1-a(SW) used in the SC tests. The grain-size distribution curves for the two A-1-a materials are compared in Figure 5.2. Due to the inclusion of the material passing the ¾-inch sieve in the A1aSW, the compaction curves for the two materials were different, as shown in Figure 5.3. The maximum dry density for the A1aSW material used in the LSC tests was 128 pcf, and the optimum water content was 8.4%. The maximum dry density for the A-1-a(SW) material used in the SC tests was 129 pcf and the optimum water content was 10.1%.

Table 5.1 Embankment Materials to Be Studied

Material	Meeting	Sieve Size (% Passing)					Plasticity Index**
		3/4 inch	No. 4	No. 10	No. 40	No. 200	
Free-Draining Granular Backfill	GP or GW	100	10	--	--	5	NP
A-1-a	SP or SW	--	100	50	30	5	NP
A-1-a	SM	--	100	50	30	15	NP
A-1-a	SC-SM	--	100	50	30	15	6
A-1-b	SM	--	--	100	50	25	NP
A-1-b	SC-SM	--	--	100	50	25	6
A-3	SP-SM	--	--	--	100	10	NP
A-2	SC	--	--	--	100	35	10
A-2	SC	--	--	--	100	35	>>11
A-4	CL	--	--	--	--	100	10

*In addition to the requirements shown in the table, the soil particles should be sub-angular

**LL and PL to be determined for fraction passing No. 40 sieve

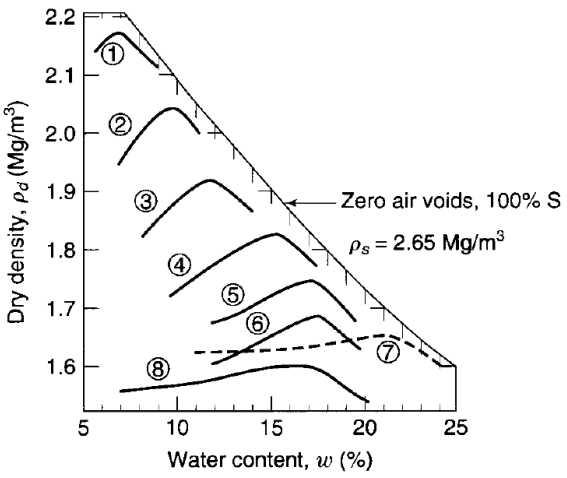

Soil No.	Description and USCS Symbol	Sand	Silt	Clay	LL	PI
1	Well-graded sand with silt SW-SM	88	10	2	16	NP
2	Well-graded silt SM	72	15	13	16	NP
3	Clayey sand SC	73	9	18	22	4
4	Sandy lean clay CL	32	33	35	28	9
5	Lean silty clay CL	5	64	31	36	15
6	Loessial silt ML	5	85	10	26	2
7	Fat clay CH	6	22	72	67	40
8	Poorly graded sand SP	94	6	—	NP	—

Figure 5.1 Water content-dry density relationships for eight soils compacted, according to the Standard Proctor method (after Johnson and Sallberg 1960 as cited in Holtz, Kovacs and Sheahan 2011)

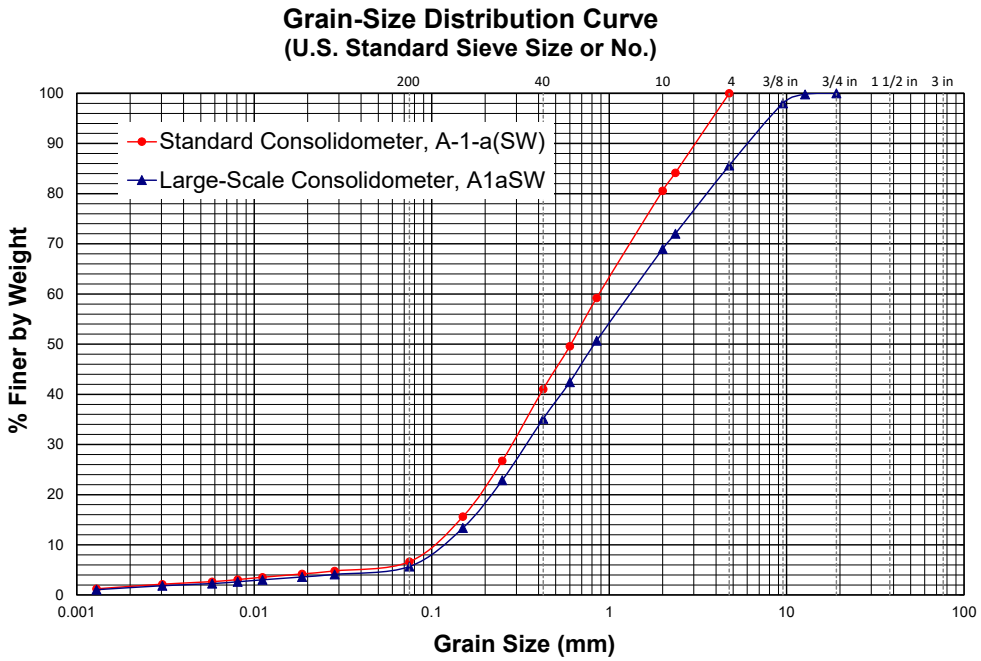

Figure 5.2 Grain-Size Distribution Curves for the A-1-a(SW) Material Used in the Standard Consolidometer Tests and the A1aSW Material Used in the Large-scale Consolidometer Tests

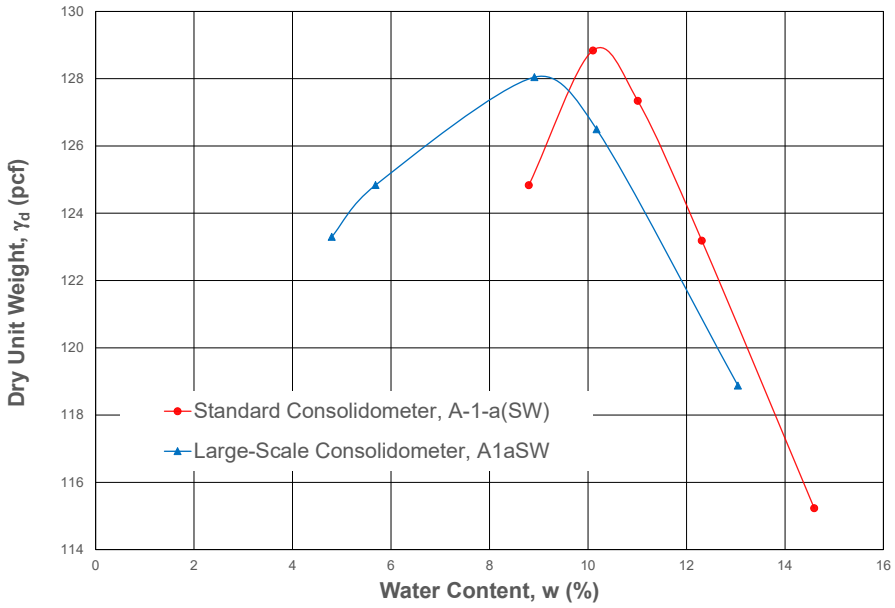

Figure 5.3 Modified Proctor Compaction Curves for the A-1-a(SW) Material Used in the Standard Consolidometer Tests and the A1aSW Material Used in the Large-scale Consolidometer Tests

The other granular material used in the LSC tests was the free-draining granular backfill, designated as FDGW. The grain-size distribution curve and the Modified Proctor compaction curve for the FDGW are shown in Figure 5.4 and Figure 5.5, respectively. The maximum dry unit weight for the FDGW was 142 pcf at an optimum water content of 6.6% (Figure 5.4). Standard consolidation tests were not performed on the FDGW tests, as the maximum particle size was too large for the standard consolidometer. The third material used in the LSC tests was the A2(SC, PI = 10) material, hereafter designated A2SCPI10, which was the same material used in the standard consolidation tests. The grain-size distribution curve for the A2SCPI10 is provided in Figure 3.3 (Chapter 3), and the Standard Proctor compaction curve is given in Figure A.6 (Appendix A). The Standard Proctor maximum dry density for the A2SCPI10 was 112 pcf at an optimum water content of 15.5%.

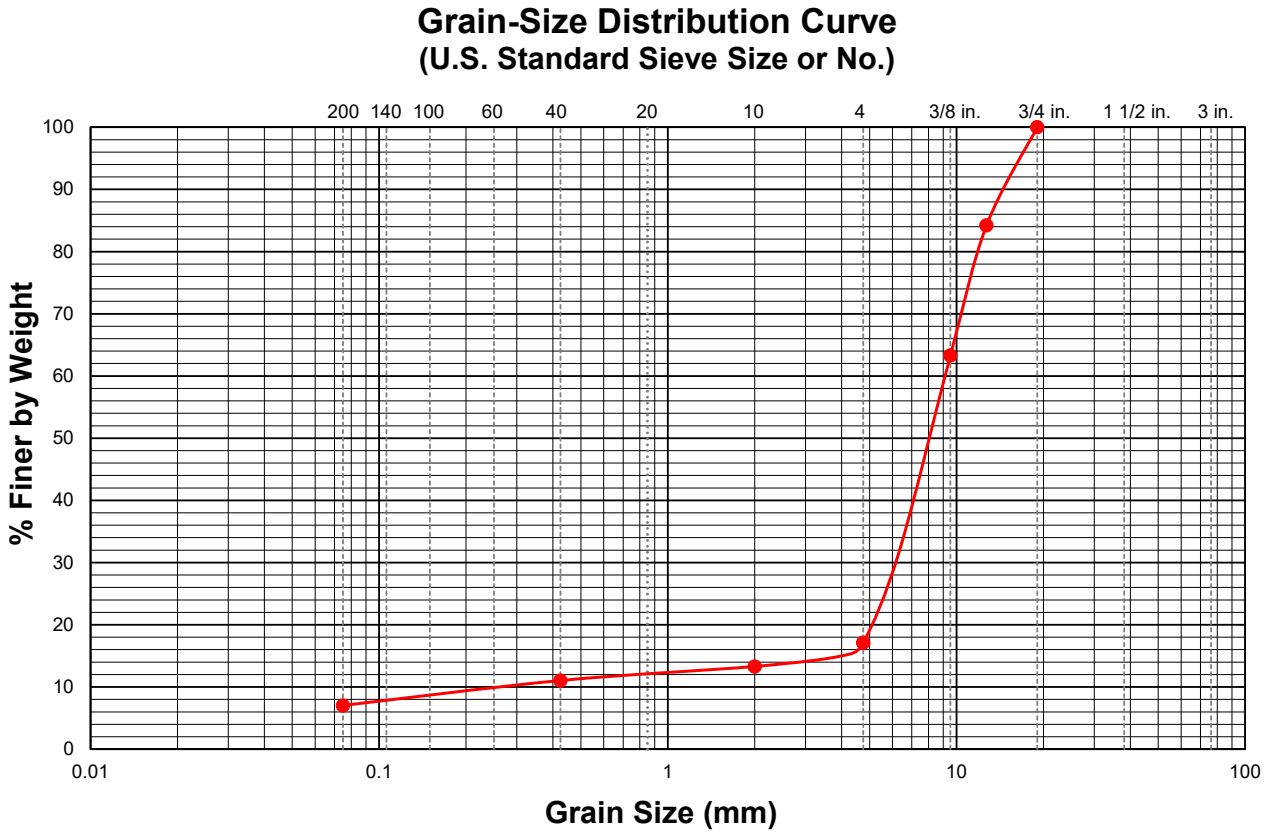

Figure 5.4 Grain-size Distribution Curve for the Free-draining Granular Backfill (FDGW) Used in the Large-scale Consolidometer Tests

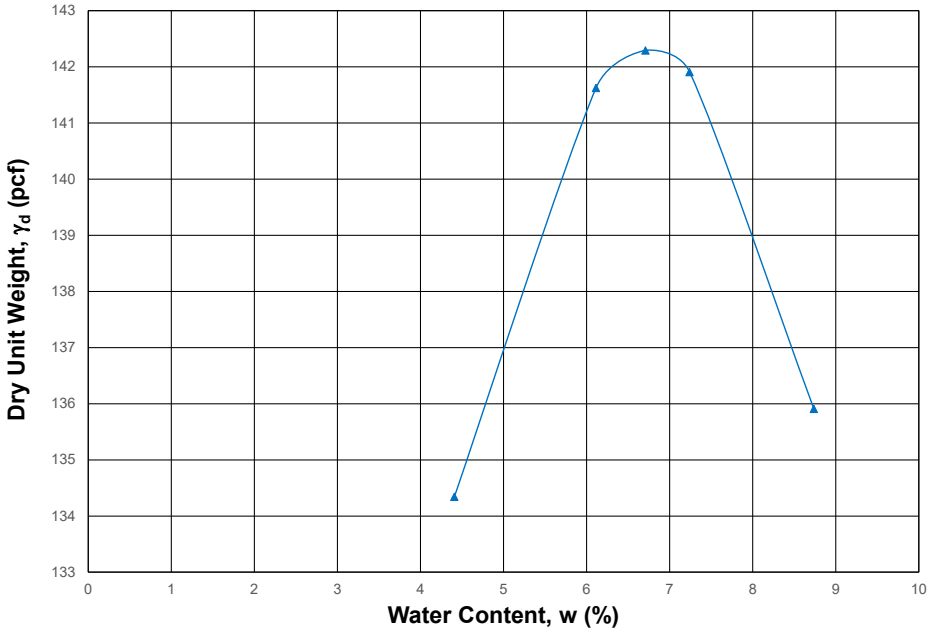

Figure 5.5 Modified Proctor Compaction Curve for the Free-draining Granular Backfill (FDGW) Used in the Large-scale Consolidometer Tests

5.3 Design and Construction of the Large-scale Consolidometer

The LSC was made from a section of nominal 12.75-inch O.D. steel pipe with a nominal I.D. of 11.5 inches. A full schematic of the design can be seen in Figure 5.6. The interior of the pipe was machined smooth, resulting in a final I.D. of 11.527 inches. The bottom plate of the LSC was bolted on using 12 bolts and was sealed with a nitrile gasket (see Figure 5.7 and Figure 5.8).

Two porous stones (see Figure 5.9) were machined to fit inside the LSC. The bottom porous stone sits directly on top of the bottom plate of the LSC (Figure 5.10). A piece of filter paper (see Figure 5.12) was then placed between the porous stone and the material being tested. Another filter paper can be placed on top of the material, and then the top porous stone rests on the filter paper. The top plate of the LSC fits inside the LSC on top of the porous stone or directly in contact with a material. Two handles made of #3 rebar were attached to the outside of the LSC (Figure 5.6 and Figure 5.10). The top plate is also made of steel and has a threaded hole in the center, so a rod can be threaded into it as a removable handle (Figure 5.11).

Four equally spaced threaded holes were tapped through the walls of the LSC. The holes were placed, so they open to the sides of the bottom porous stone. Brass tube fittings were threaded into these openings to attach hoses, which allowed water to be introduced to the bottom of a compacted material (Figure 5.12).

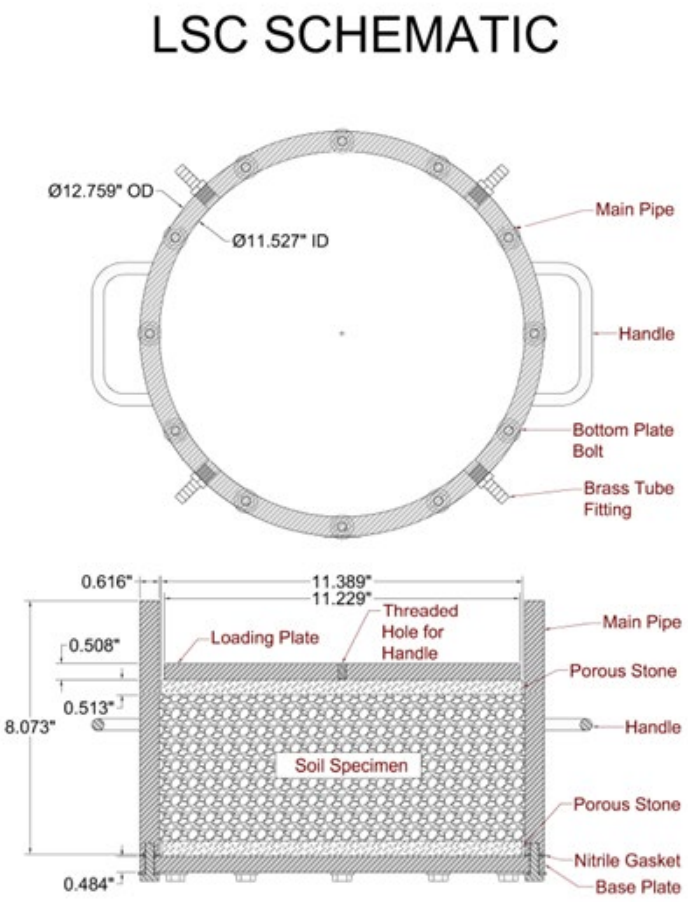

Figure 5.6 Schematic Diagram of Large-scale Consolidometer

Figure 5.7 Nitrile Gasket on Bottom of LSC

Figure 5.8 Bottom Plate of LSC Bolted On

Figure 5.9 Porous Stone for LSC

Figure 5.10 Porous Stone in Bottom of LSC

Figure 5.11 Top Plate of LSC with Removable Handle Installed

Figure 5.12 Filter Paper Placed in Bottom of LSC with Brass Fittings and Hoses Attached

5.4 Compaction of Granular (Cohesionless) Materials

First, the steel bottom plate of the LSC was bolted onto the body of the apparatus (Figure 5.13). A nitrile gasket was used to seal the bottom of the LSC. The exact volume of the LSC was determined by taking six measurements of its inner diameter and its height from the bottom of the inside of the LSC to the top rim using a set of calipers. These measurements were then averaged. Each sample compacted in the LSC was to be 4.5 inches thick. With this parameter, the volume of each sample would be 0.272 ft^3.

Figure 5.13 LSC with Bottom Plate Attached

To determine the amount of material needed for each sample, the volume of 0.272 ft^3 was multiplied by the dry unit weight of the material desired. Depending on the test, this value was either 90% of Modified Proctor or 96% of Modified Proctor. The moisture content of the material was also carefully controlled to match the desired moisture content for each test. The desired moisture content was achieved by oven drying the material at a low temperature (149° F), weighing out the appropriate amount of water, adding the water to the dried material and mixing the water and material using an electric mixer until the proper moisture content was achieved. The moisture content of the material was then determined by performing ASTM D2216-19 on a portion of it.

With the weight of the desired volume and density of the material determined and with the material at the proper moisture content, a sample of the material of the desired weight was obtained. Once a sample was weighed, the inside of the LSC was coated with a thin layer of silicone lubricant (Figure 5.14). The sample was placed in the LSC in three equal lifts by weight. Each lift was compacted by placing the top plate of the LSC inside the LSC on top of the sample. Each lift of the sample was then compacted using an electric jack hammer with a square compacting plate placed on top of the top plate of the LSC (Figure 5.15). To determine that the sample was compacted to the correct density, the volume of each lift after compaction was measured using six measurements taken around the rim of the LSC with a set of calipers, measuring from the top of the rim of the LSC to the top of the top plate placed on the sample. With the thickness of the top plate subtracted, the height of the sample could be determined inside of the LSC and the sample's volume. Some materials were difficult to compact to 96% of Modified Proctor. These materials were further aided in compaction by placing weights on top of the square compacting plate during compaction (Figure 5.15).

Figure 5.14 Silicone Lubricant

Figure 5.15 Electric Jack Hammer with Weights Attached to Square Compaction Plate

5.5 Compaction of Cohesive Material

The compaction procedure for cohesive materials was quite similar to the procedure for cohesionless materials, with a few variances. To ensure proper mixing of water into each material, water was added to the material, mixed with an electric mixer, and then allowed to sit overnight in a container with a sealed lid. The moisture content was also checked using ASTM D2216-19.

The use of porous stones and filter paper was not necessary for the cohesionless material but was needed for the cohesive material. Care had to be taken not to break the porous stones. To compact a sample, the LSC was filled in two lifts. The top plate of the LSC was placed in the bottom of the LSC. The LSC was then coated with silicone lubricant. One-half of the sample was placed in the LSC by weight. The cohesive sample was compacted using the electric jack hammer with a square compaction plate with nine four-inch long steel fingers welded onto its base (Figure 5.16). This allowed the sample to be kneaded during the compaction process. After compacting the sample, any material on the compaction plate and fingers was scraped off using a spatula and put back into the LSC. Next, a round plate attached to a handle was used to tamp down the sample and smooth the surface, filling in any of the indentions from the compaction plate. Six measurements of depth were taken using a pair of calipers, which were averaged to determine the volume of the compacted sample. Once the first lift was compacted to the appropriate density, the second lift was placed and compacted in the same manner.

Figure 5.16 Square Compaction Plate with Attached Feet for Cohesive Material

Once the sample was compacted in the LSC, the bottom plate of the LSC was removed, as shown in Figure 5.17. The top plate of the LSC, which was placed in the bottom of the LSC, was then removed by screwing a handle into it and then gently pulled out. After the top plate was removed, filter paper was placed on the bottom of the sample. The bottom porous stone was then placed on top of the filter paper. The bottom plate and gasket of the LSC were then reinstalled. Another filter paper was placed on top of the sample in the LSC, and then the top plate of the LSC was placed on top of the filter paper.

Figure 5.17 Bottom Plate and Top Plate Removed from LSC Containing Compacted Cohesive Material

5.6 Loading the Compacted Specimen

After compacting the sample, the LSC was placed in the loading frame within an hour of being compacted (Figure 5.18). A metal weight from a consolidometer, with a diameter slightly smaller than that of the top plate of the LSC, was placed on the top plate to help ensure an even distribution of load. A two-gallon bucket was used as a reservoir for water during the tests. It was attached to the hoses connected to the bottom of the LSC. The reservoir was filled with water with the valves leading to the LSC closed.

MTS software was used to control the loading protocol for each test. A load cell measured the load applied to the LSC, and an LVDT was utilized to measure the displacement of the sample vertically. A seating load of 120 pounds was used at the beginning of each test. Once the hydraulic ram was seated, the loading sequence was initiated. Real-time data of load and displacement were recorded using the MTS software.

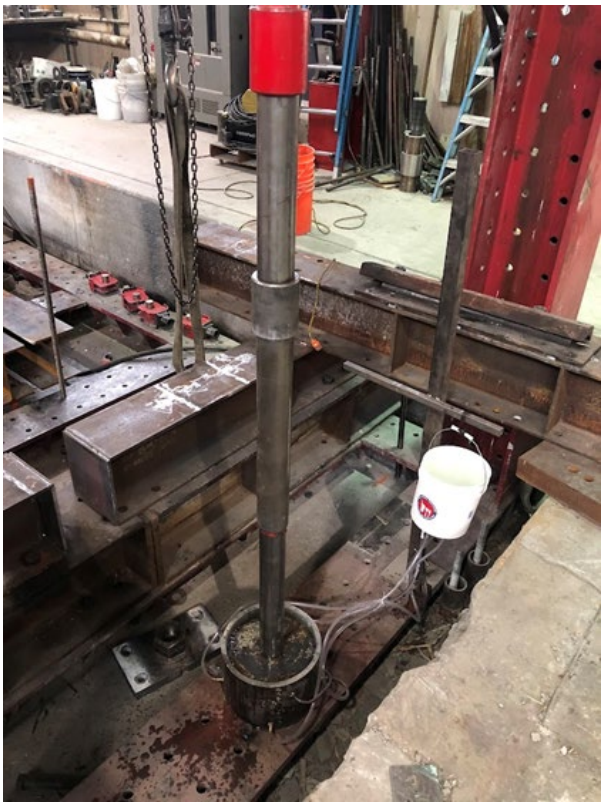

Figure 5.18 LSC in the Loading Frame

For the as-compacted tests, the valves allowing water to flow from the reservoir to the LSC remained closed during the initial loading procedure. The sample was loaded to ¼, ½, 1, 2, 4, and 8 tsf. Each dwell time was 10 minutes, except at the maximum stress of 8 tsf. The sample was loaded at 8 tsf for 30 minutes, and then the valves were opened to allow water to flow into the LSC. Air bubbles were removed from the hoses attached to the LSC by agitating them. After the valves were opened to allow water to flow into the LSC, the stress applied to the sample was maintained at 8 tsf for an additional 30 minutes. After this time, the sample was unloaded in the same way it was loaded.

In addition to the dwell times listed in the as-compacted test procedure, a dwell time was added to the beginning of the soaked test, which kept the sample at the seating load for 10 minutes before loading the sample to ¼ tsf. The valves were opened to allow water to flow into the sample throughout the duration of the test.

5.7 Tests Conducted and Nomenclature

A list of the 27 large-scale consolidometer tests conducted for this study are shown below in Table 5.2. In the following section, results from the tests will be provided graphically, and comparisons will be made to determine the effects of the following four parameters on the stress-strain results: (a) relative compaction (90 or 96%) of Modified Proctor maximum dry unit weight; (b) moisture content of the soil during compaction (dry of optimum, at optimum water content, or wet of optimum); (c) moisture condition of the soil during loading (loaded as-compacted or loaded after soaking); and (d) the type of soil (FDGW, A1aSW, or A2SCPI10). An acronym will be used in the legend of the graphs to describe the type of soil, relative compaction, moisture condition during compaction, and type of loading — in that order — using the following terminology:

Type of soil:
FDGW = Free-draining well-graded gravel (nonplastic)
A1aSW = Well-graded A-1-a gravelly sand (nonplastic)
A2SCPI10 = A-2 clayey sand with a Plasticity Index of 10 (plastic)

Relative Compaction: Percent relative compaction based on either Modified Proctor (M) or Standard Proctor (S) maximum dry unit weight.

Moisture Content during Compaction: Air-dry (Dry) or Modified Proctor optimum water content (Opt) or wet of optimum. The A1aSW soil could not be compacted in the air-dry condition with the equipment used for these tests due to a large percentage of fines becoming airborne during the compaction process. Therefore, the "dry" tests for this soil were done at the minimum water content for which the loss of fines was negligible (5.6% dry of optimum, designated 5.6%DRY in the acronym). One test was conducted on A2SCPI10 at a water content 2.6% wet of optimum, designated 2.6% wet.

Moisture Condition of Soil During Loading: Loaded as-compacted to the maximum load and then soaked with water (LACS) or loaded to the maximum load after soaking the soil with water at a small seating load (LS).

Maximum Load: The maximum total vertical stress to which the specimen was loaded, in units of tons per square foot (tsf), is shown as the last digit in the acronym (except for the repeat tests – see below).

Repeat Tests: A few tests were repeated for the same nominal conditions that were used in previous tests. For those tests, "-R" is added to the end of the acronym.

For example, the acronym **FDGW-90M-Opt-LACS8** means the soil was free-draining, well-graded gravel, it was compacted to 90% of the Modified Proctor maximum dry unit weight at a water content equal to the Modified Proctor optimum water content, it was loaded in the as-compacted condition to a load of 8 tsf and allowed to come to equilibrium before the specimen was soaked with water and the corresponding wetting-induced deformations were measured. All tests were stress-controlled and 20 of the tests were loaded to total vertical stresses of ¼, ½, 1, 2, 4 and 8 tsf, with time provided at each load for the specimen to come to equilibrium before the next load was applied. In seven tests, the specimens were loaded to total vertical stresses of ¼, ½, 1, and 2 tsf in the as-compacted condition, and then were soaked with water.

Table 5.2 Completed Large-scale Consolidometer Tests

Soil Type	Relative Compaction (%)	Compaction Water Content	Loading/Wetting Sequence	Acronym
A1aSW	90M	5.6% Dry of Opt.	Loaded as-compacted to 2 tsf then soaked	A1aSW-90M-5.6%DRY-LACS2
A1aSW	90M	5.6% Dry of Opt.	Loaded as-compacted to 2 tsf then soaked	A1aSW-90M-5.6%DRY-LACS2-R
A1aSW	90M	5.6% Dry of Opt.	Loaded as-compacted to 8 tsf then soaked	A1aSW-90M-5.6%DRY-LACS8
A1aSW	90M	5.6% Dry of Opt.	Loaded as-compacted to 8 tsf then soaked	A1aSW-90M-5.6%DRY-LACS8-R
A1aSW	90M	5.6% Dry of Opt.	Soaked at small seating stress then loaded to 8 tsf	A1aSW-90M-5.6%Dry-LS8
A1aSW	90M	5.6% Dry of Opt.	Soaked at small seating stress then loaded to 8 tsf	A1aSW-90M-5.6%Dry-LS8-R
A1aSW	90M	Optimum	Loaded as-compacted to 2 tsf then soaked	A1aSW-90M-OPT-LACS2
A1aSW	90M	Optimum	Loaded as-compacted to 8 tsf then soaked	A1aSW-90M-OPT-LACS8
A1aSW	90M	Optimum	Soaked at small seating stress then loaded to 8 tsf	A1aSW-90M-OPT-LS8
A1aSW	96M	Optimum	Loaded as-compacted to 8 tsf then soaked	A1aSW-96M-OPT-LACS8
A1aSW	96M	Optimum	Soaked at small seating stress then loaded to 8 tsf	A1aSW-96M-OPT-LS8
A2SCPI10	96S	2.6% Wet of Opt.	Loaded as-compacted to 8 tsf then soaked	A2SCPI10-96S-2.6%Wet-LACS8
A2SCPI10	96S	Optimum	Loaded as-compacted to 2 tsf then soaked	A2SCPI10-96S-OPT-LACS2
A2SCPI10	96S	Optimum	Loaded as-compacted to 8 tsf then soaked	A2SCPI10-96S-OPT-LACS8
A2SCPI10	96S	Optimum	Soaked at small seating stress then loaded to 8 tsf	A2SCPI10-96S-OPT-LS8
FDGW	90M	Dry	Loaded as-compacted to 2 tsf then soaked	FDGW-90M-DRY-LACS2
FDGW	90M	Dry	Loaded as-compacted to 8 tsf then soaked	FDGW-90M-DRY-LACS8
FDGW	90M	Dry	Soaked at small seating stress then loaded to 8 tsf	FDGW-90M-DRY-LS8
FDGW	90M	Optimum	Loaded as-compacted to 8 tsf then soaked	FDGW-90M-OPT-LACS8
FDGW	90M	Optimum	Soaked at small seating stress then loaded to 8 tsf	FDGW-90M-OPT-LS8
FDGW	96M	Dry	Loaded as-compacted to 2 tsf then soaked	FDGW-96M-DRY-LACS2
FDGW	96M	Dry	Loaded as-compacted to 2 tsf then soaked	FDGW-96M-DRY-LACS2-R
FDGW	96M	Dry	Loaded as-compacted to 8 tsf then soaked	FDGW-96M-DRY-LACS8
FDGW	96M	Dry	Loaded as-compacted to 8 tsf then soaked	FDGW-96M-DRY-LACS8-R
FDGW	96M	Dry	Soaked at small seating stress then loaded to 8 tsf	FDGW-96M-DRY-LS8
FDGW	96M	Optimum	Loaded as-compacted to 8 tsf then soaked	FDGW-96M-OPT-LACS8
FDGW	96M	Optimum	Soaked at small seating stress then loaded to 8 tsf	FDGW-96M-OPT-LS8

The results from these tests will be presented graphically and analyzed in the following section. The following rules were followed when preparing the graphs, so colors and symbols are consistent among all graphs, except in instances where it was not possible to do so:

Colors: **Red** = 90% relative compaction, **Blue** = 96% relative compaction

Symbols:

Open circles (○) are for LACS8 tests on specimens compacted at optimum water content.

Filled circles (●) are for LS8 tests on specimens compacted at optimum water content.

Open squares (□) are for LACS8 tests on specimens compacted dry.

Filled squares (■) are for LS8 tests on specimens compacted dry.

Open diamonds (◊) are for LACS2 tests on specimens compacted dry.

Filled diamonds (♦) are for LACS2 tests on specimens compacted at optimum water content.

Line Type: All lines are solid, except when comparisons are made between the different types of soils, in which case the A1aSW specimens are represented by solid lines, and the FDGW specimens are represented by dashed lines.

5.8 Results and Analysis of Large-scale Consolidometer Tests

5.8.1 Strain-Stress Characteristics during Loading

5.8.1.1 Effect of Moisture Condition

5.8.1.1.1 As-compacted vs. Soaked

The effect of moisture condition during loading will be analyzed in this subsection. Graphs are presented in Figure 5.19 through Figure 5.26 showing comparisons between the LACS8 and LS8 tests conducted on nominally identical specimens. Nominally identical means that they were the same type of soil, compacted at the same water content to the same relative compaction using the same method of compaction. The only nominal difference is the LAC specimens were at the as-compacted water content during the loading sequence (prior to the wetting sequence at the end of the test), while the LS specimens were soaked with water at a small seating load prior to loading.

In five out of the seven cases for granular soils, the loading-induced strain was lower for the LAC tests than for the LS tests, which is to be expected because of the higher water content during loading for the LS tests. In one case (Figure 5.21), the results are nearly identical for the LAC and LS tests. In one case (Figure 5.23), the LS specimen is slightly less compressible than the LAC specimen. In general, higher water content usually means greater loading-induced compressibility, although in granular soils the difference is usually significantly smaller than for cohesive soils. In five out of the six cases where the LAC specimen was less compressible, the differences in loading-induced strain for the two types of tests are relatively small, with the exception of FDGW compacted to 90% Relative Compaction in the Air-Dry Condition (Figure 2), where the differences are more significant compared to the other cases. It makes sense that the differences are larger for the case shown in Figure 5.19 for two reasons: (a) The porosity is higher for a lower dry density (lower relative compaction), which means the difference in water content will be greater between as-compacted and soaked, and (b) there is less water in the as-compacted specimen when dry than at optimum water content.

The one comparison available for A2SCPI10 is shown in Figure 5.26. The soaked specimen was significantly more compressible than the as-compacted specimen. For example, the strains at stresses of 2 and 8 tsf were 34% and 31% higher for the soaked specimen than for the as-compacted, with an average of 43% for the seven stress levels. The higher compressibility for the soaked specimen is due to the higher water content. It is well-known that the addition of water to a cohesive soil will make it softer and more compressible, all other factors being the same.

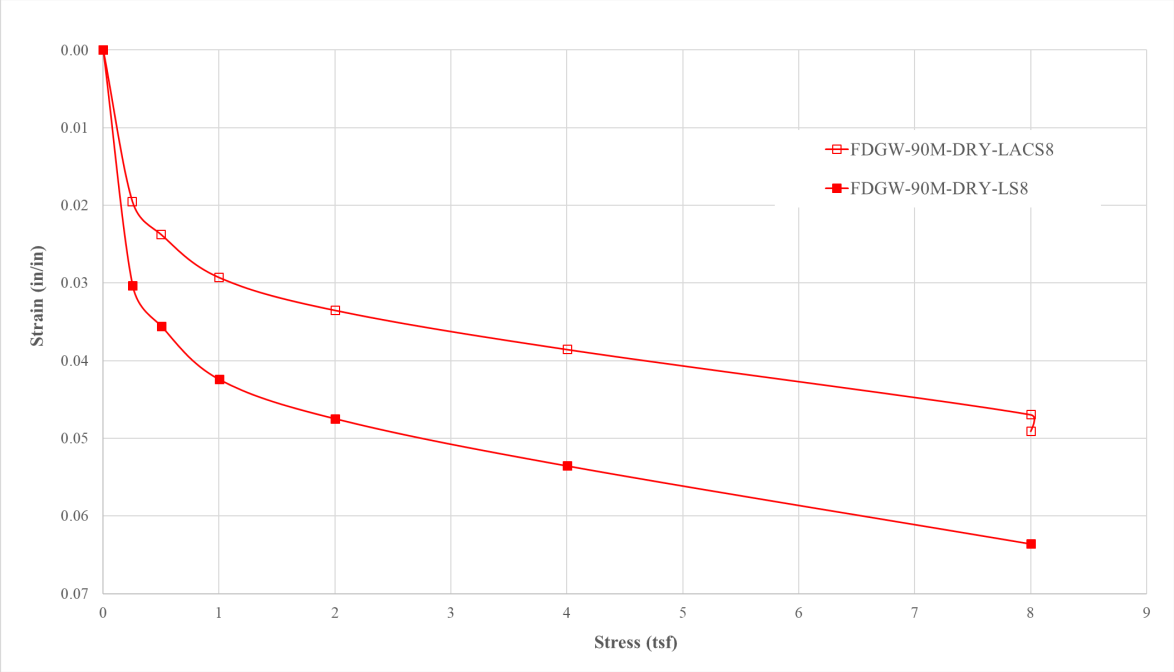

Figure 5.19 Effect of Moisture Condition during Loading on the Strain vs. Stress Results for Specimens of FDGW Compacted to 90% Relative Compaction in the Air-dry Condition

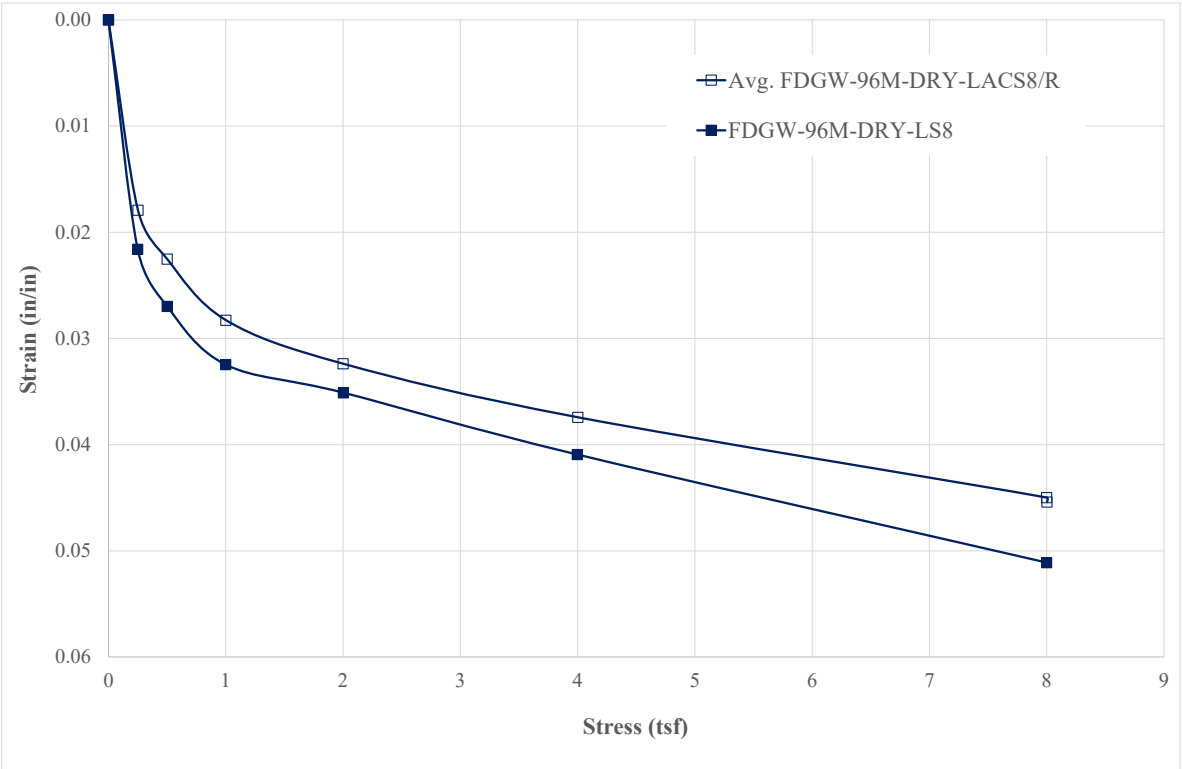

Figure 5.20 Effect of Moisture Condition during Loading on Strain vs. Stress Results for Specimens of FDGW Compacted to 96% Relative Compaction in the Air-dry Condition

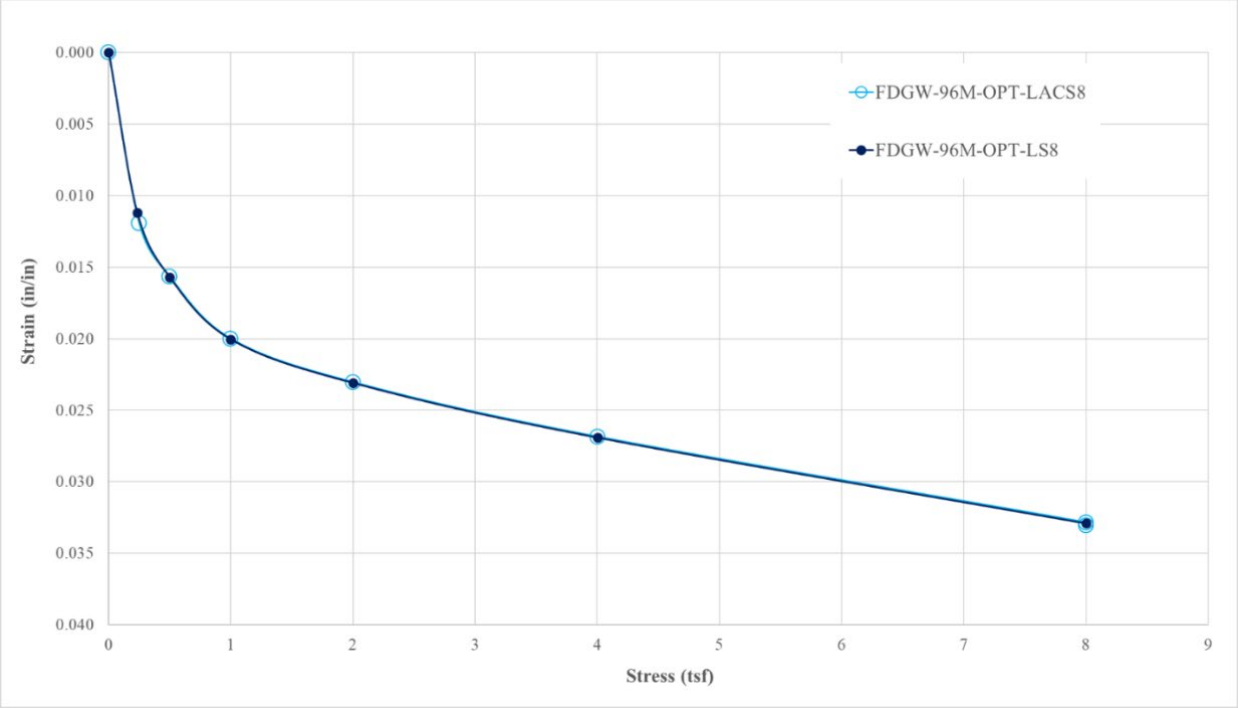

Figure 5.21 Effect of Moisture Condition during Loading on Strain vs. Stress Results for Specimens of FDGW Compacted to 96% Relative Compaction at Optimum Water Content

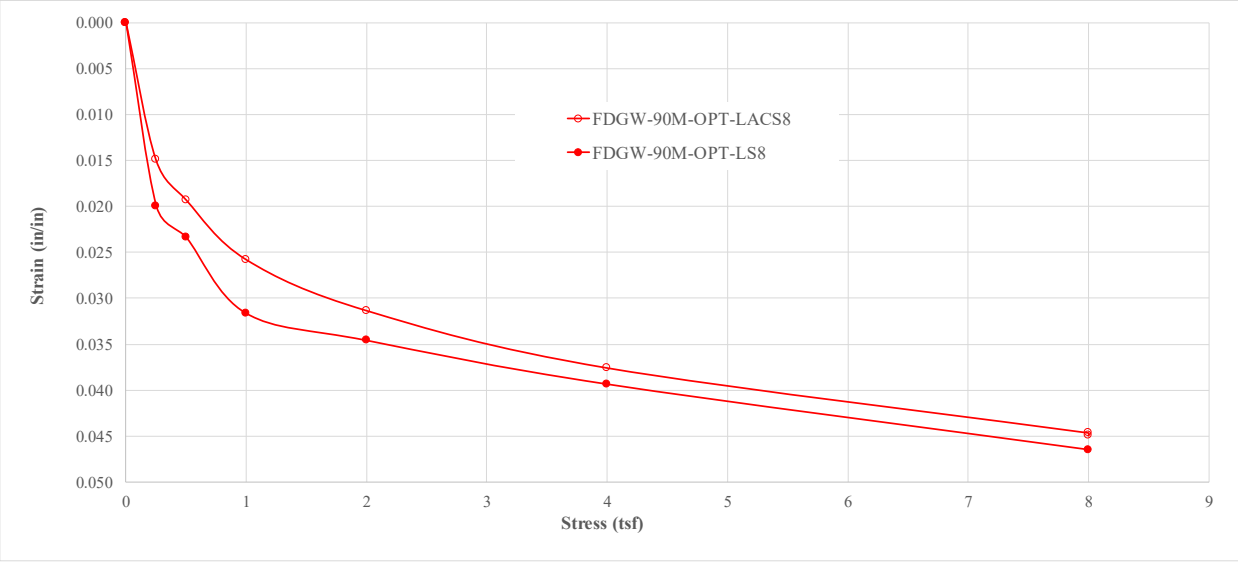

Figure 5.22 Effect of Moisture Condition during Loading on Strain vs. Stress Results for Specimens of FDGW Compacted to 90% Relative Compaction at Optimum Water Content

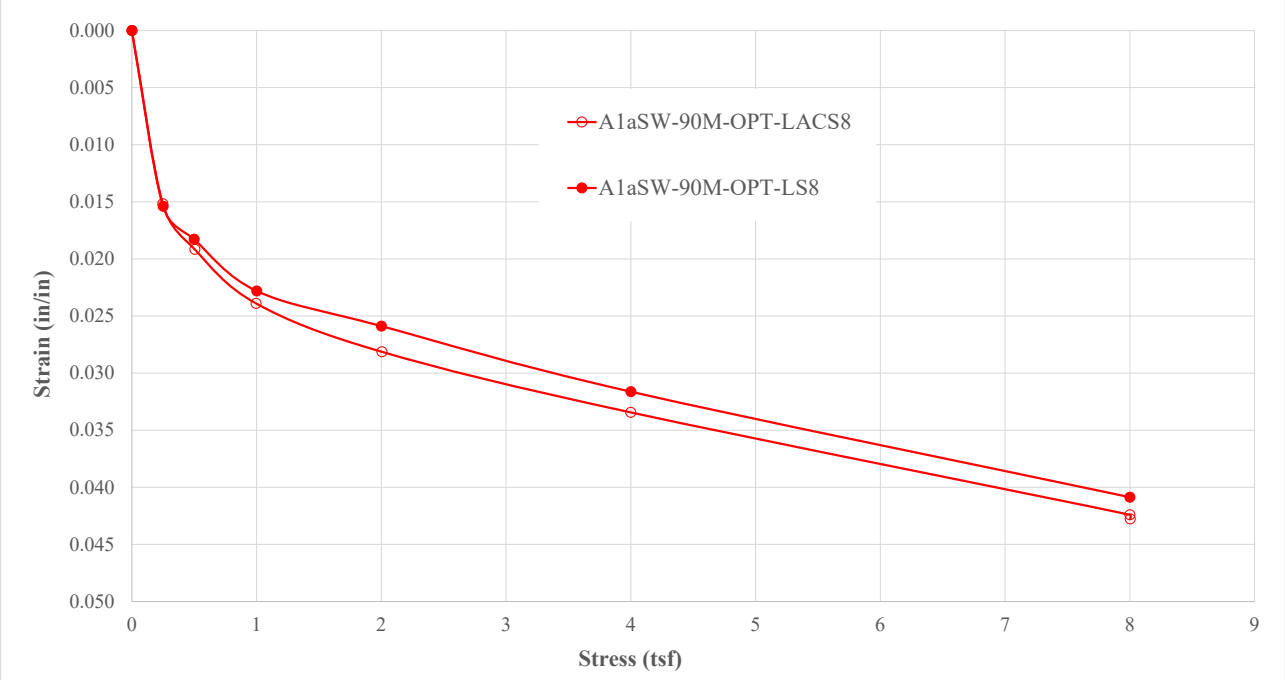

Figure 5.23 Effect of Moisture Condition during Loading on Strain vs. Stress Results for Specimens of A1aSW Compacted to 90% Relative Compaction at Optimum Water Content

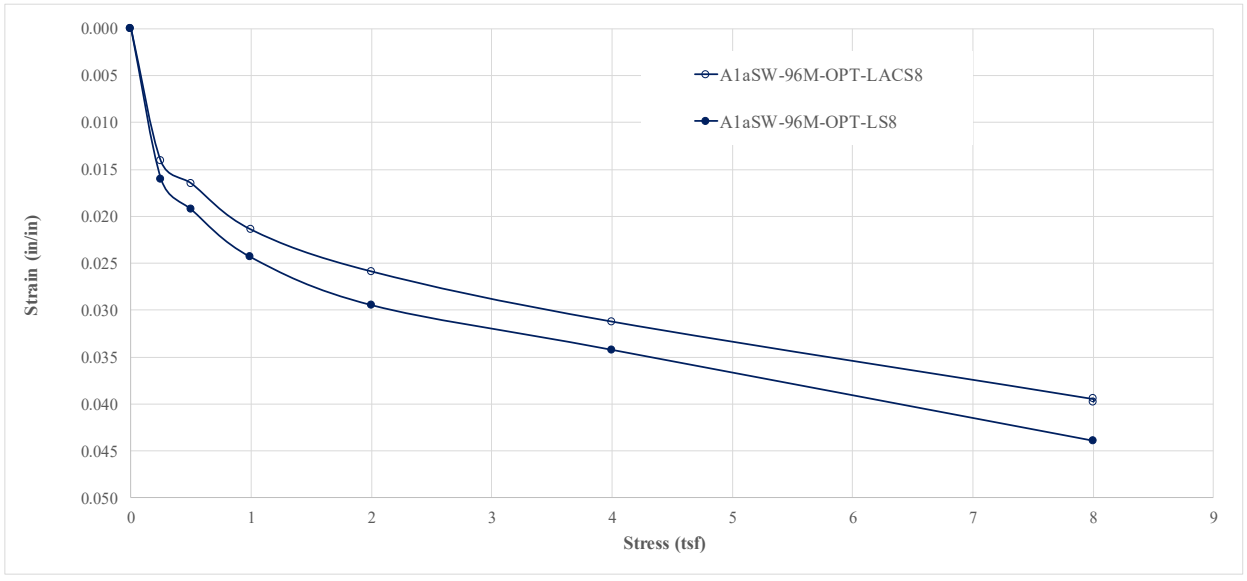

Figure 5.24 Effect of Moisture Condition during Loading on Strain vs. Stress Results for Specimens of A1aSW Compacted to 96% Relative Compaction at Optimum Water Content

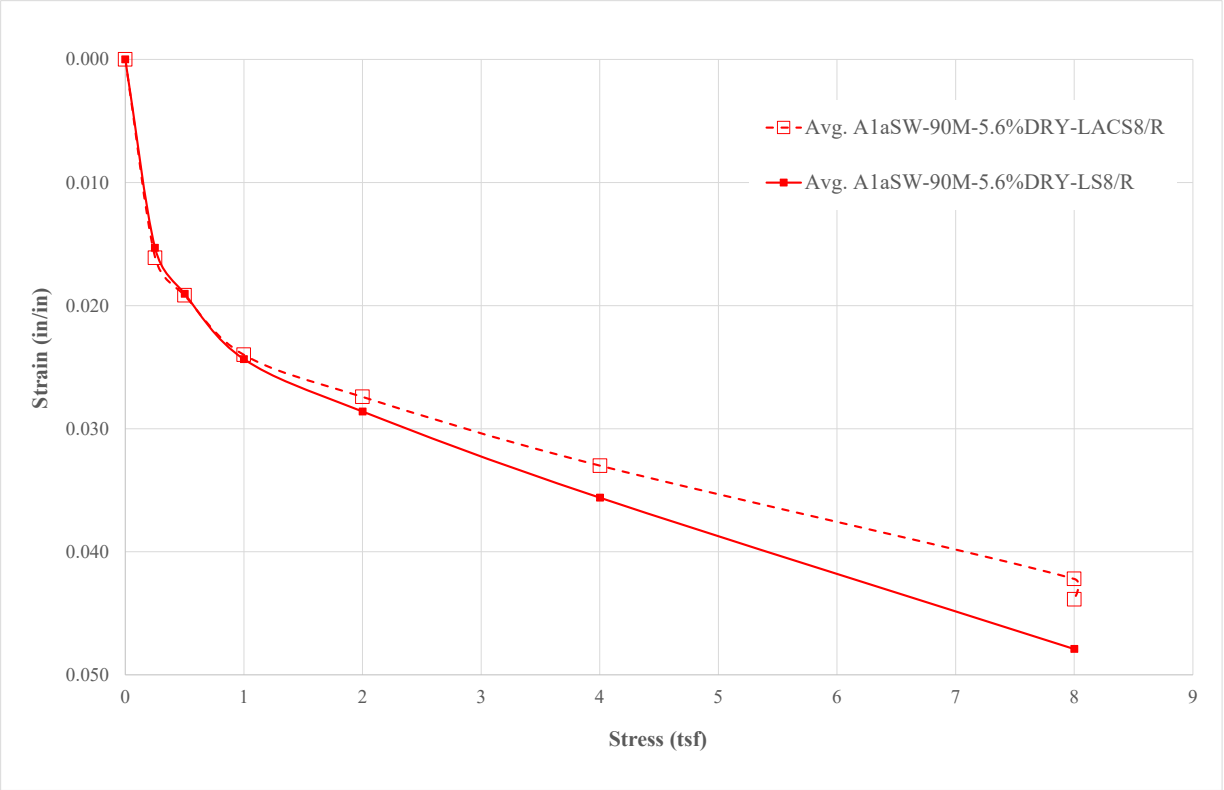

Figure 5.25 Effect of Moisture Condition during Loading on Strain vs. Stress Results for Specimens of A1aSW Compacted to 90% Relative Compaction at a Water Content 5.6% Dry of Optimum

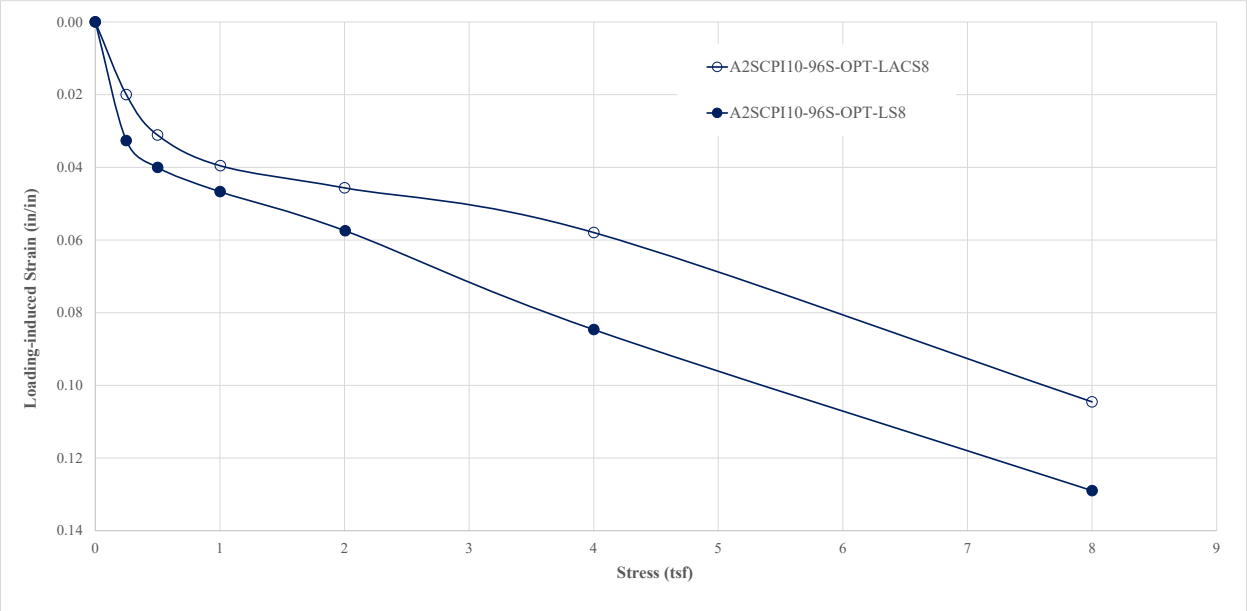

Figure 5.26 Effect of Moisture Condition during Loading on Strain vs. Stress Results for Specimens of A2SCPI10 Compacted to 96% Relative Compaction at Optimum Water Content

5.8.1.1.2 Compaction Water Content

Six comparisons showing the effect of compaction water content on the loading-induced strain-stress characteristics are provided in Figure 5.27 through Figure 5.32. The first three comparisons are for LACS8 specimens, and the last three comparisons are for LS8 specimens. In five of the six cases, the specimens compacted dry were more compressible than the specimens compacted at optimum water content. For the A1aSW specimens compacted to 90% relative compaction and loaded as-compacted (Figure 5.29), the results are nearly the same. The differences in strain at stresses of 2 tsf and 8 tsf for all six cases are summarized in Table 5.3. The differences for the A1aSW (less than 19%) were smaller than for the FDGW (5 to 55%).

For the LACS tests, the soil and dry unit weight are nominally the same, so the differences in strain-stress behavior must be related to differences in water content, differences in fabric (the way the particles are arranged), or both. The lower water content (and therefore greater matric suction) for the dry specimens should result in greater effective stress and therefore less compressibility, but the matric suction in most granular soils is relatively small and would likely have only a minor effect. However, this effect becomes greater as the size of the particles decreases, which partially explains why the differences for the A1aSW specimens were less than for the FDGW. Compaction of dry granular soils using vibration probably results in finer particles settling to the bottom of each compacted lift, resulting in a partial loss of well-gradedness for the soil and probably an increase in compressibility of the soil. This separation of particles would probably be greater for the A1aSW soil due to the smaller size particles. Overall, the difference in compressibility for any situation depends on the relative magnitude of the two phenomena — decrease in compressibilty due to lower water content and increase in compressibility due to separation of particles.

For the LS tests, both the dry-compacted and optimum-compacted specimens would be nearly saturated during the loading, so the water content would be essentially the same. Therefore, differences in strain-stress behavior must be due to differences in fabric, with the compressibility of the dry-compacted specimens increasing due to separation of particles.

The first and third authors have recent personal experience with the differences in strain-stress behavior of granular soil for dry-compacted and wet-compacted soils. While observing compaction of the Untreated Base Course (UTBC) for a roadway project, a water truck was not available, but the operator of the compaction roller compacted the UTBC while it was dry. Other nearby sections had been compacted wetter, which were notably stiffer than the ones compacted dry. A consultant performing plate load tests, where the UTBC had been compacted dry, commented on the significant difference in the subgrade modulus for that location compacted to another location on the same roadway several miles away. The consultant, who was surprised by differences in subgrade modulus at the two locations, asked the Superintendent of the project if the same material was used for the UTBC at both locations, and the Superintendent stated that the materials were the same.

One comparison is available for the one cohesive soil (A2SCPI10) tested in the Large-scale Consolidometer. Both specimens were compacted to 96% relative compaction based on Standard Proctor maximum dry unit weight, with one specimen compacted at optimum water content and the other specimen compacted 2.6% wet of optimum. The strain-stress results are shown in Figure 5.33 and the values of loading-induced strain at stresses of 2 and 8 tsf are summarized in Table 5.4. For this cohesive material, the results are the opposite of what occurred in the nonplastic granular materials — the wetter specimen compressed 50% more at 2 tsf and 76% more at 8 tsf than did the drier specimen. This result is expected for cohesive soils loading in the as-compacted condition, since increased water content is known to produce softer and, hence, more compressible behavior in cohesive soils when all other factors are the same.

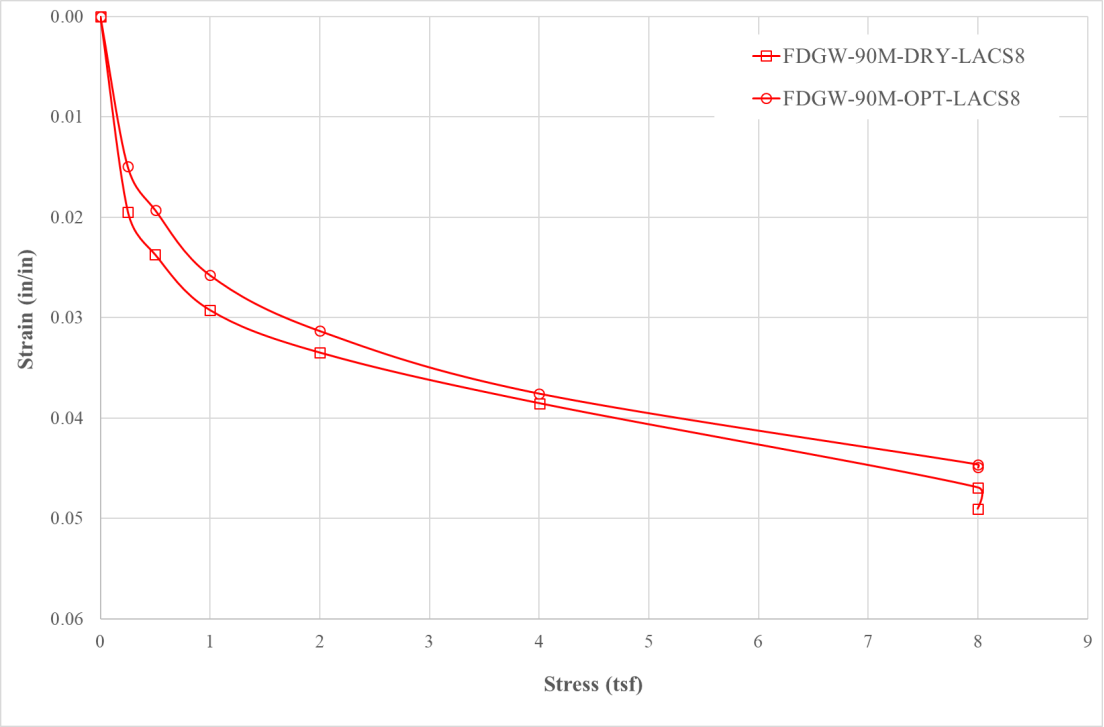

Figure 5.27 Effect of Compaction Water Content on Loading-induced Strain vs. Stress Results for Specimens of FDGW Compacted to 90% Relative Compaction and Loaded As-compacted to 8 tsf

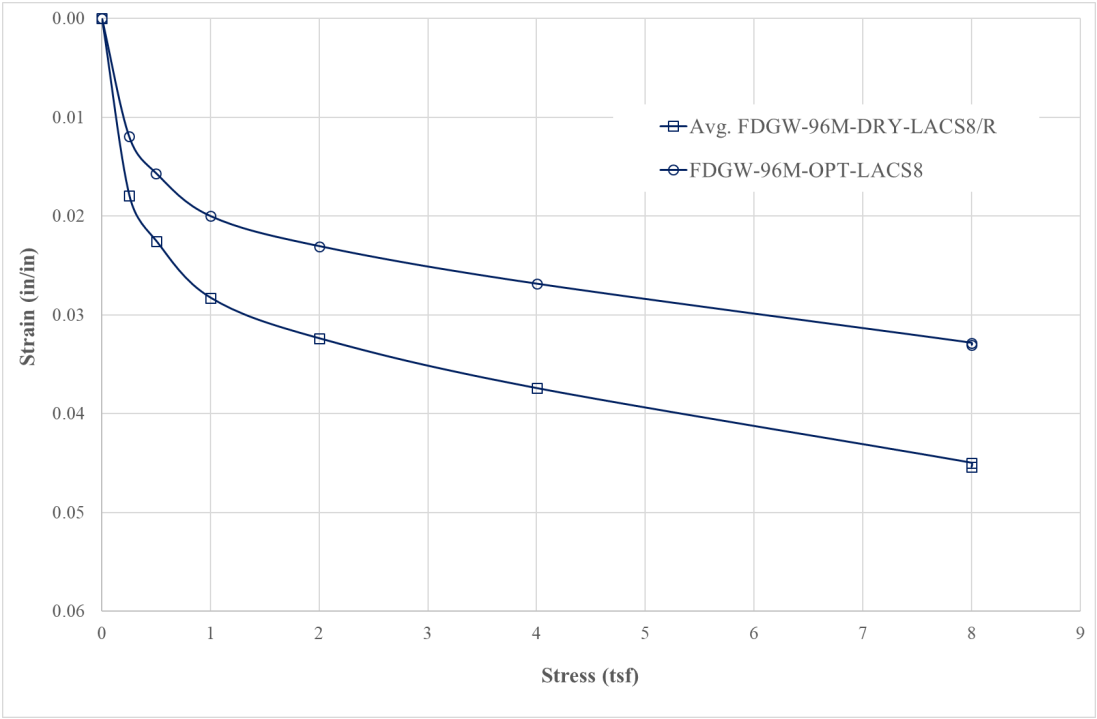

Figure 5.28 Effect of Compaction Water Content on Loading-induced Strain vs. Stress Results for Specimens of FDGW Compacted to 96% Relative Compaction and Loaded As-compacted to 8 tsf

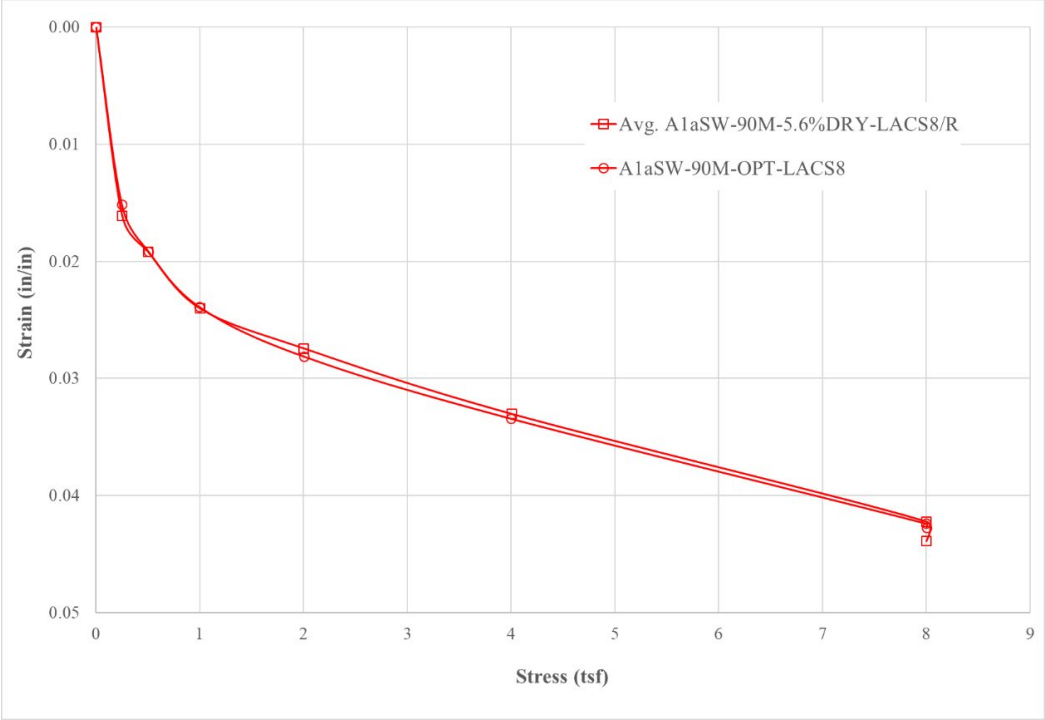

Figure 5.29 Effect of Compaction Water Content on Loading-induced Strain vs. Stress Results for Specimens of A1aSW Compacted to 90% Relative Compaction and Loaded As-compacted to 8 tsf

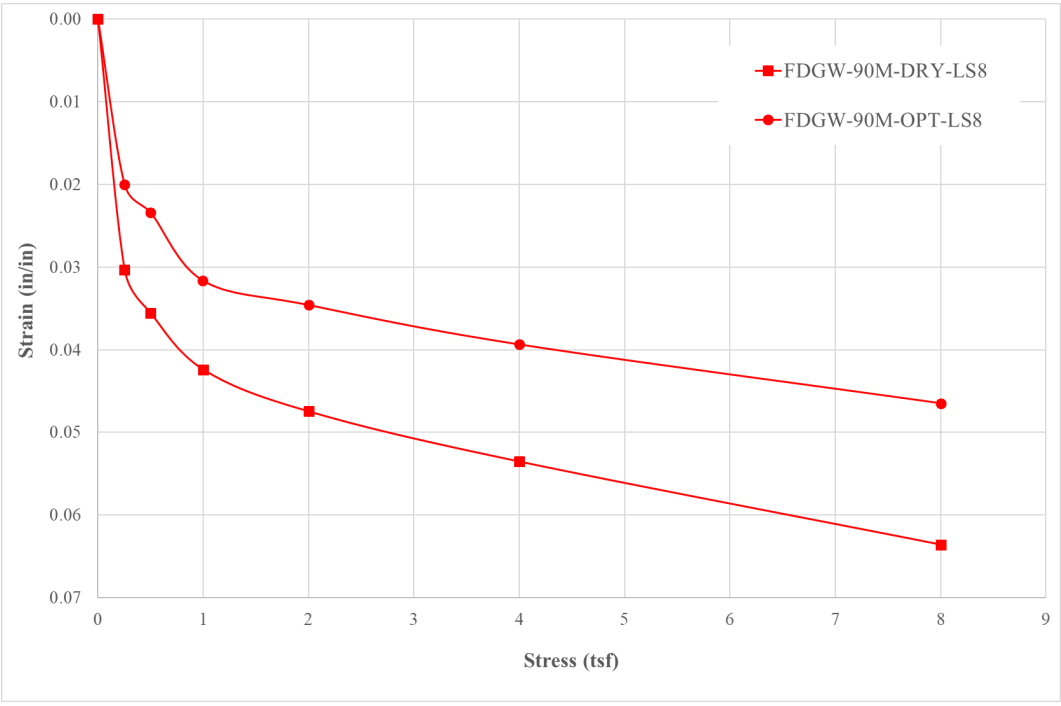

Figure 5.30 Effect of Compaction Water Content on Loading-induced Strain vs. Stress Results for Specimens of FDGW Compacted to 90% Relative Compaction and Loaded Soaked to 8 tsf

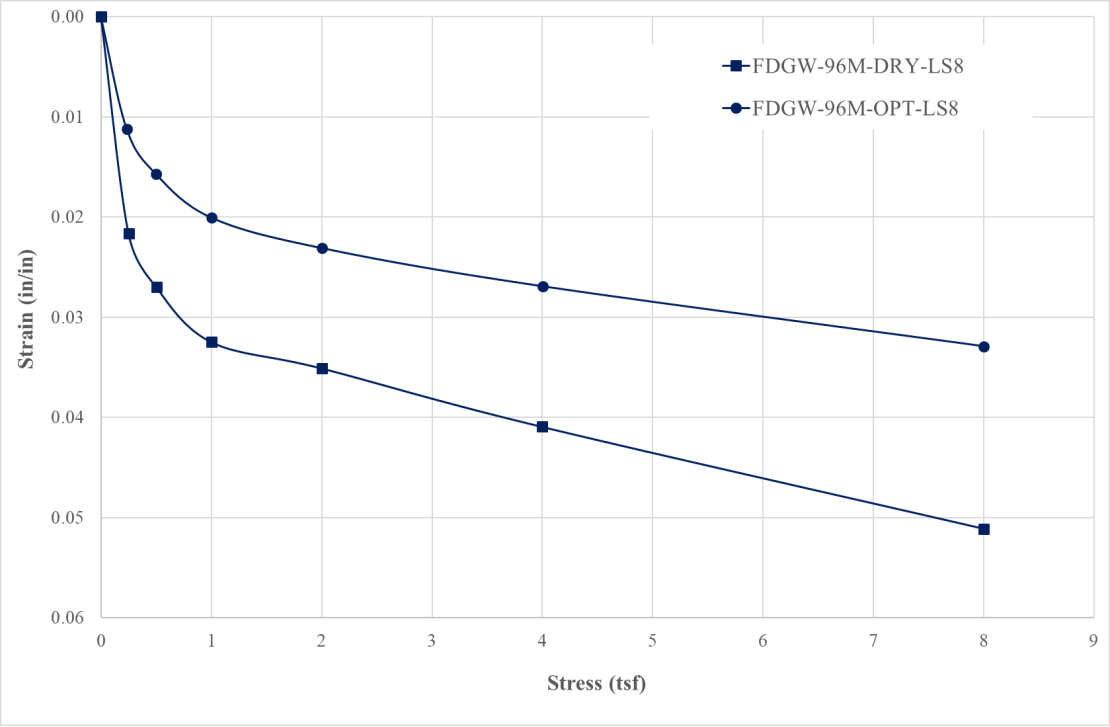

Figure 5.31 Effect of Compaction Water Content on Loading-induced Strain vs. Stress Results for Specimens of FDGW Compacted to 96% Relative Compaction and Loaded Soaked to 8 tsf

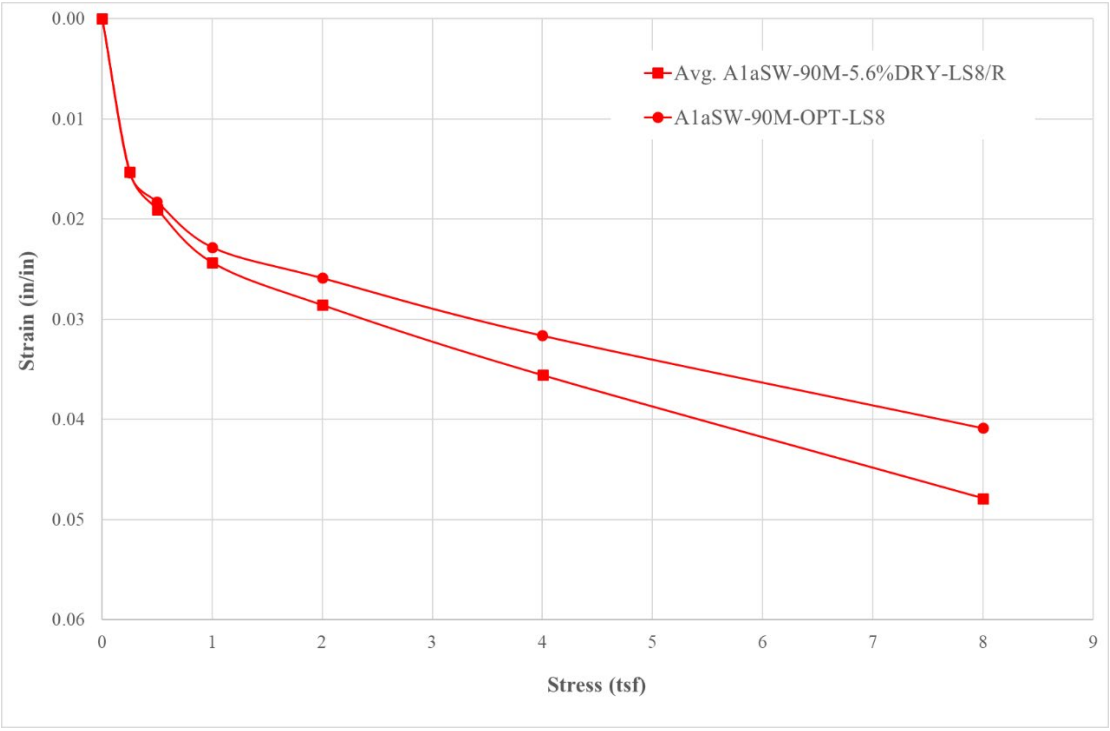

Figure 5.32 Effect of Compaction Water Content on Loading-induced Strain vs. Stress Results for Specimens of A1aSW Compacted to 90% Relative Compaction and Loaded Soaked to 8 tsf

Table 5.3 Effect of Compaction Water Content on Loading-induced Strains at Stresses of 2 tsf and 8 tsf for Six Comparisons on Nonplastic A-1 Soils from LSC Tests

Comparison	Strain at Stress of 2 tsf			Strain at Stress of 8 tsf		
	Dry	Opt	Dry/Opt	Dry	Opt	Dry/Opt
A1aSW-90M-LACS8	0.0275	0.0282	0.973	0.0424	0.0425	0.998
A1aSW-90M-LS8	0.0287	0.0260	1.10	0.0489	0.0411	1.19
FDGW-90M-LACS8	0.0335	0.0314	1.07	0.0471	0.0448	1.05
FDGW-90M-LS8	0.0476	0.0347	1.37	0.0639	0.0468	1.37
FDGW-96M-LACS8	0.0324	0.0231	1.40	0.0452	0.0330	1.37
FDGW-96M-LS8	0.0352	0.0231	1.52	0.0515	0.0331	1.55

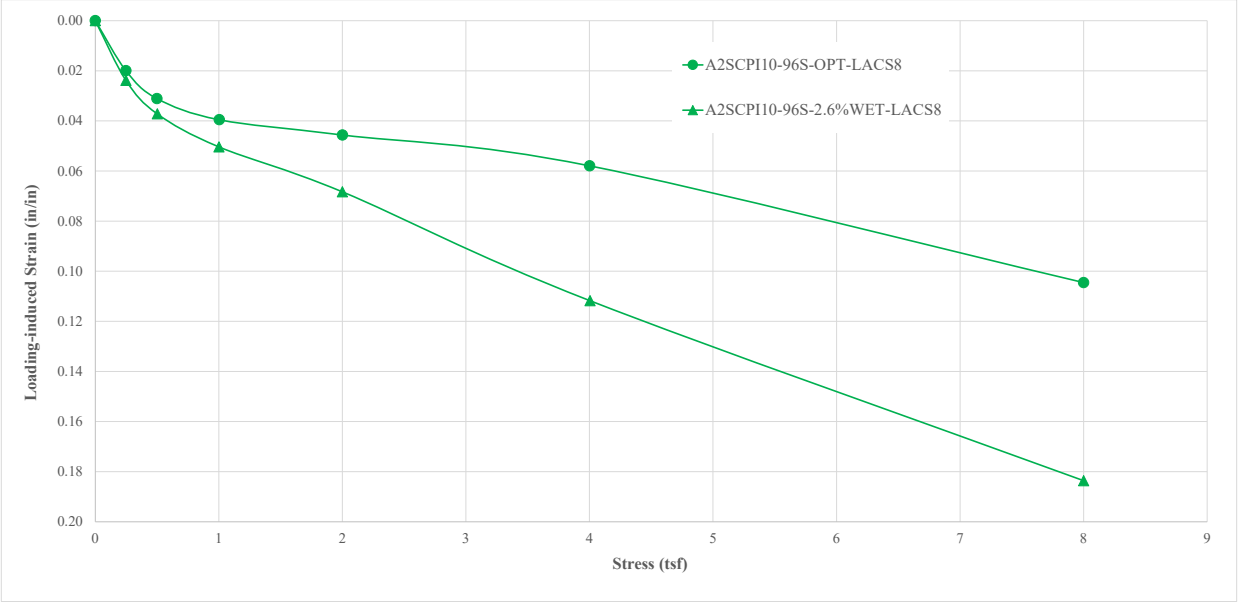

Figure 5.33 Effect of Compaction Water Content on Loading-induced Strain vs. Stress Results for Specimens of A2SCPI10 Compacted to 96% Relative Compaction and Loaded As-compacted to 8 tsf

Table 5.4 Effect of Compaction Water Content on Loading-induced Strains at Stresses of 2 tsf and 8 tsf for Specimens of A2SCPI10

Comparison	Strain at Stress of 2 tsf			Strain at Stress of 8 tsf		
	Opt	Wet	Wet/Opt	Opt	Wet	Wet/Opt
A2SCPI10-96S-LACS8	0.0456	0.0683	1.50	0.1045	0.184	1.76

5.8.1.2 Effect of Relative Compaction

Six comparisons of the effect of relative compaction on the strain vs. stress characteristics of the two granular soils are provided in Figure 5.34 through Figure 5.39. (No comparisons are available for the A2SCPI10.) Three of the comparisons are for specimens loaded in the as-compacted condition, and three are for specimens tested in the soaked condition. The differences are small in three cases (Figure 5.34, Figure 5.38, and Figure 5.39), and the differences are moderate to significant in the other three cases. Overall, the differences are greater for the FDGW specimens than for the A1aSW specimens.

In all but one case, these results are consistent with *a priori* expectations where the denser specimens were less compressible. The one exception is the case shown in Figure 5.39, where the differences are small, but the specimen compacted to 90% relative compaction was found to be slightly less compressible than the specimen compacted to 96% relative compaction. One possible explanation for this unexpected result is that the small difference could be within the range of variation in strain-stress characteristics due to differences in material properties and compacted density that are a natural part of any testing program on soil. A second possible explanation is that more particles were crushed during compaction and testing for 96% relative compaction than for 90% relative compaction. Data supporting this possibility are provided in Table 5.5 and Figure 5.40, which show the grain-size data for the coarse-grained portion of the A1aSW soil prior to testing and after testing. (Hydrometer analyses were not performed on the post-testing soil, so data is also not show for the pre-testing soil.) The data for the post-testing soil was obtained after all the tests had been completed on the A1aSW. Another factor supporting this possibility is that at optimum water content, the energy required to obtain 90% relative compaction was moderate, but an enormous amount of energy was required to obtain 96% relative compaction. When the soil was air-dry, compacting to 90% relative compaction required significant energy, and it was impossible to get 96% relative compaction with the compaction equipment used for these large-scale tests. It is not possible to determine from available data what portion of the particle crushing occurred during compaction and what portion occurred during loading/wetting, but it seems likely most of it occurred during compaction due to the dynamic energy applied during compaction versus the static energy applied during loading/wetting.

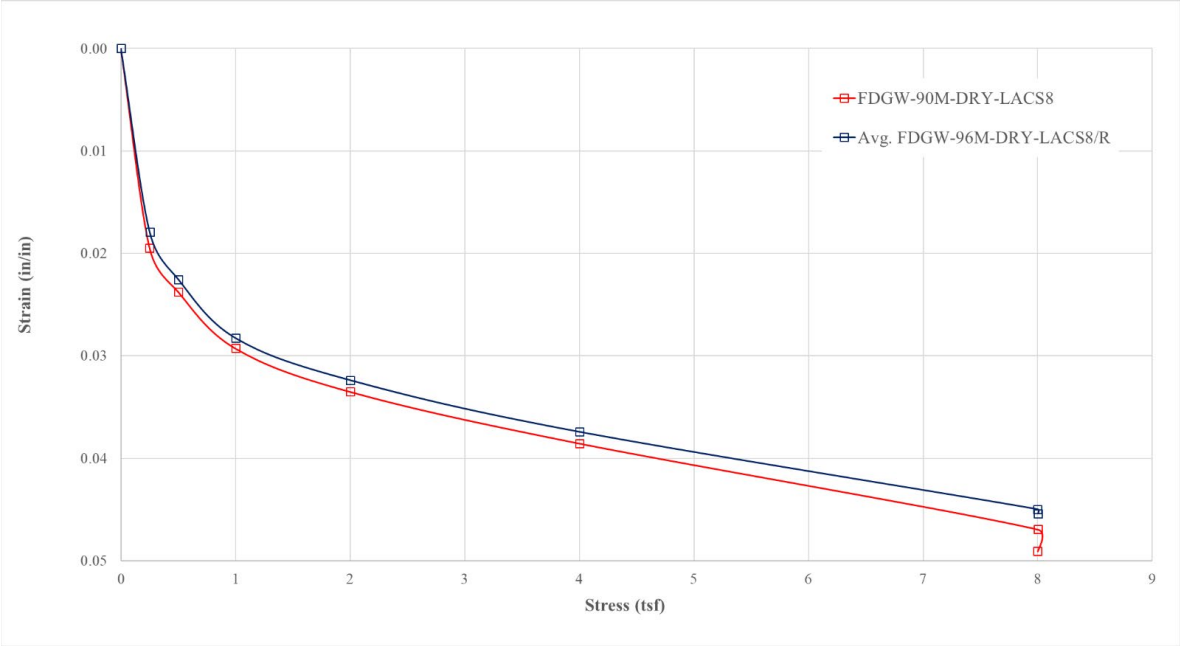

Figure 5.34 Effect of Relative Compaction during Loading in the As-compacted Condition on Strain vs. Stress Results for Specimens of FDGW Compacted Air-dry

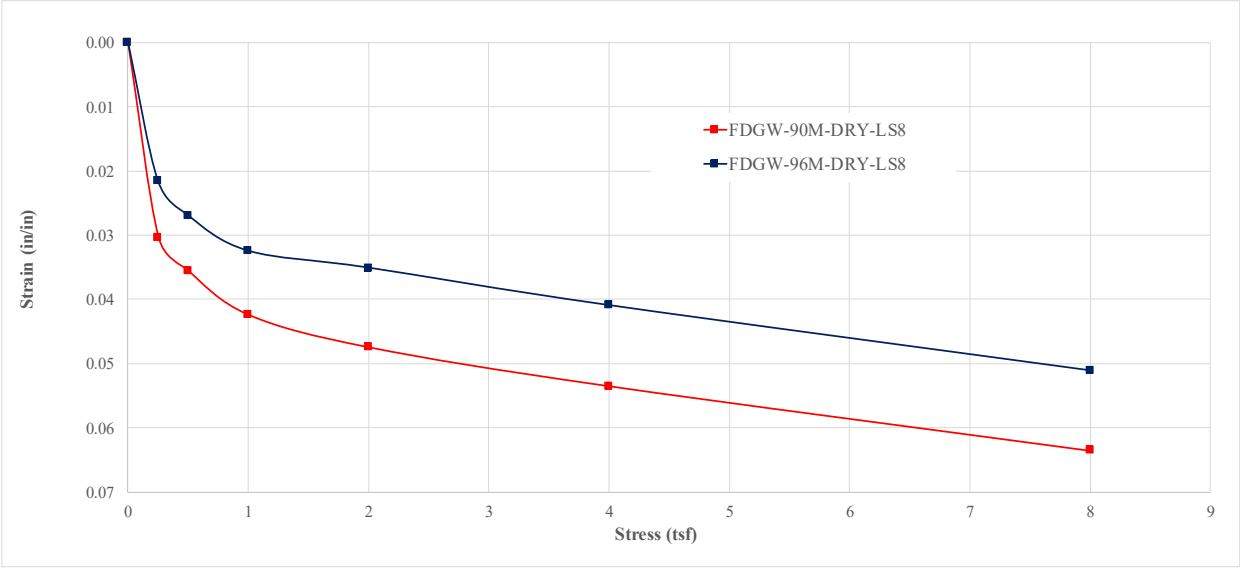

Figure 5.35 Effect of Relative Compaction during Loading in the Soaked Condition on Strain vs. Stress Results for Specimens of FDGW Compacted Air-dry

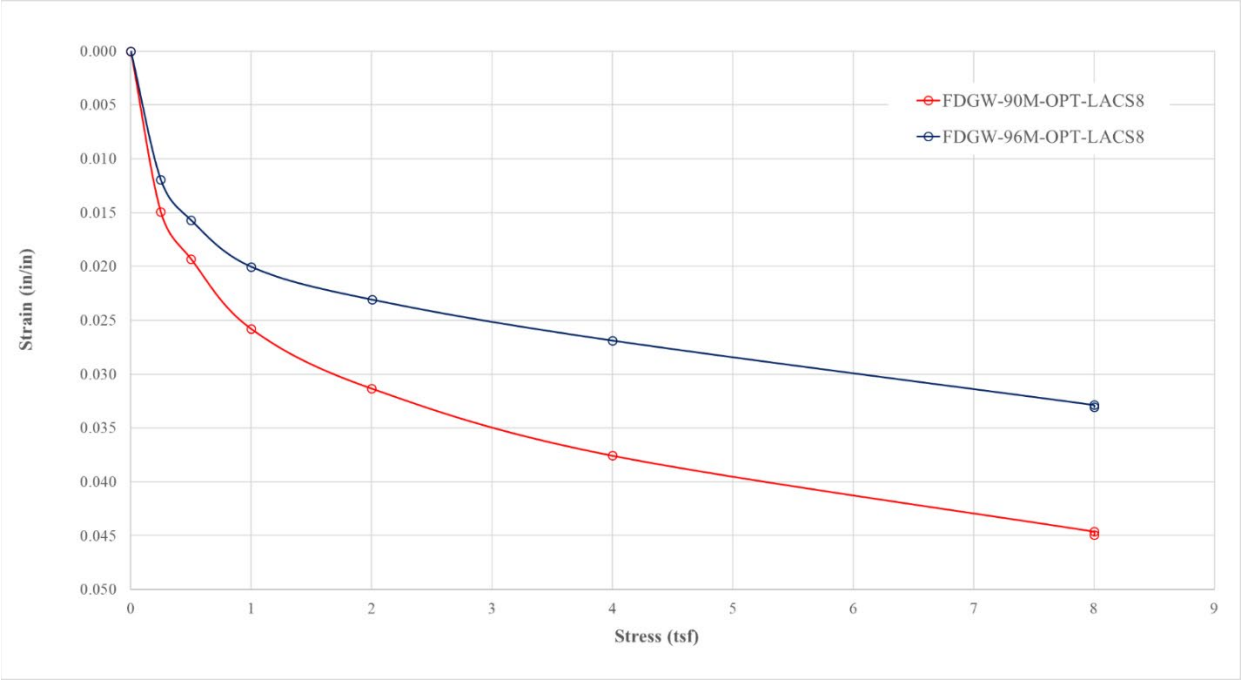

Figure 5.36 Effect of Relative Compaction during Loading in the As-compacted Condition on Strain vs. Stress Results for Specimens of FDGW Compacted at Optimum Water Content

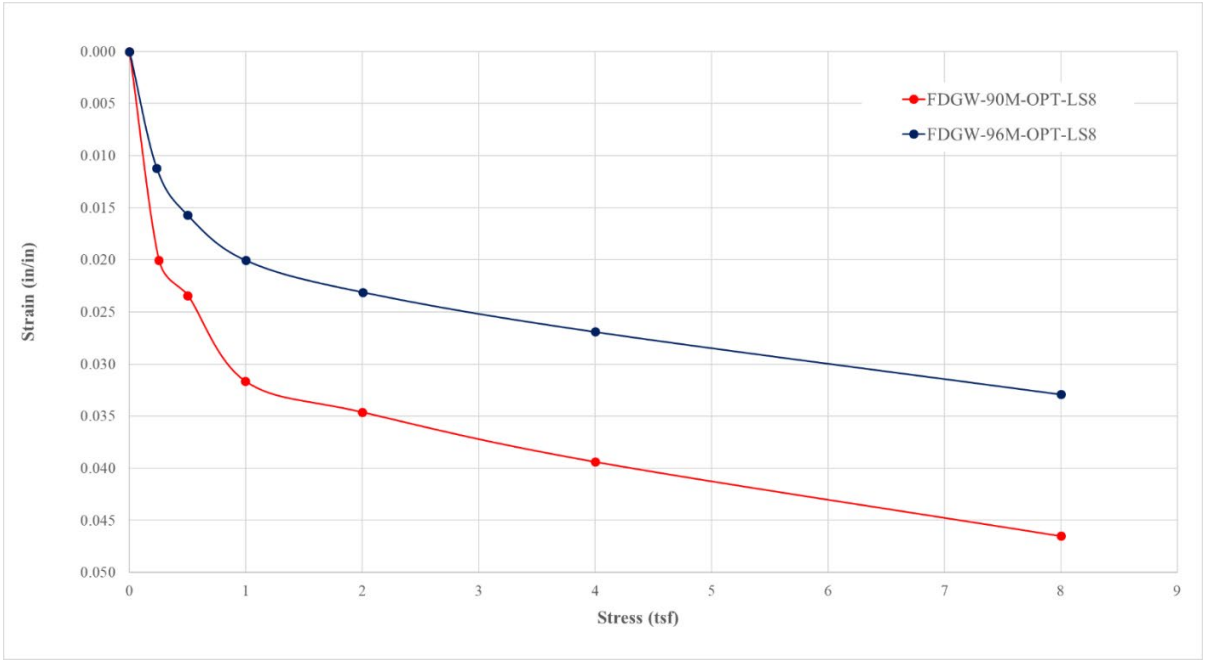

Figure 5.37 Effect of Relative Compaction during Loading in the Soaked Condition on Strain vs. Stress Results for Specimens of FDGW Compacted at Optimum Water Content

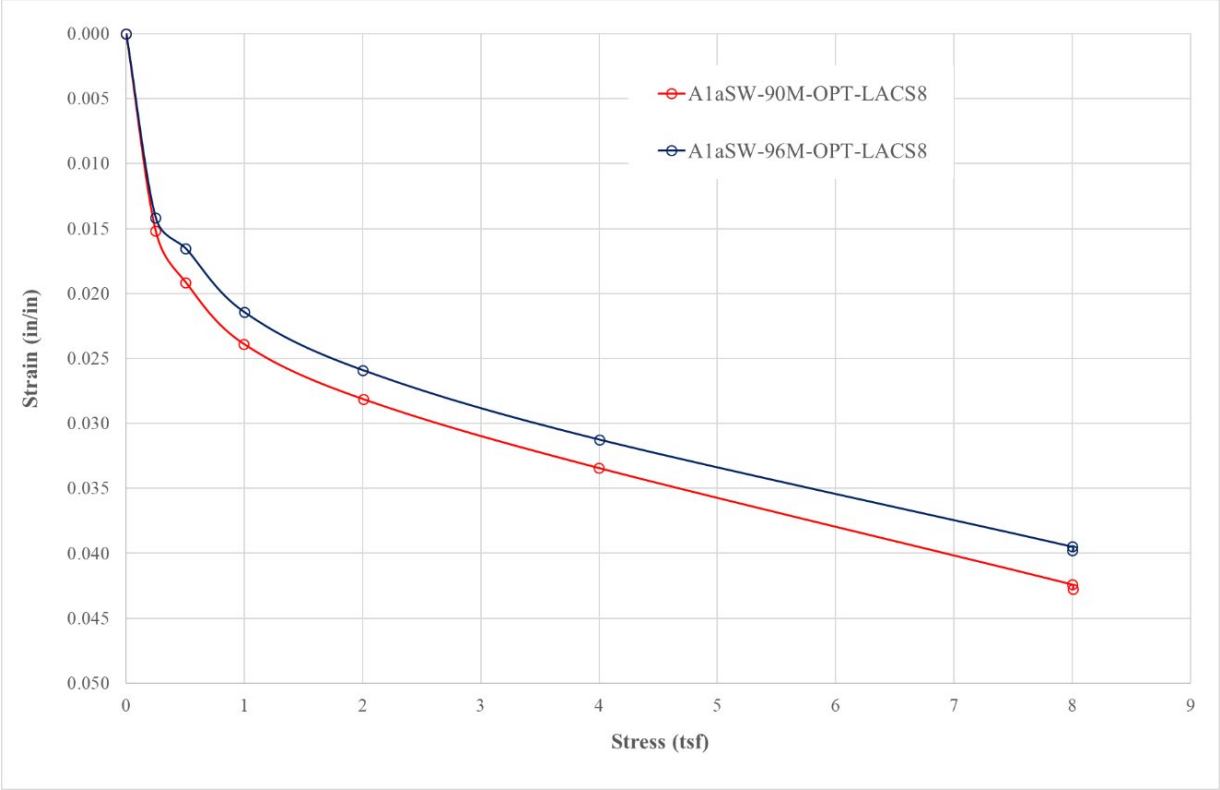

Figure 5.38 Effect of Relative Compaction during Loading in the As-compacted Condition on Strain vs. Stress Results for Specimens of A1aSW Compacted at Optimum Water Content

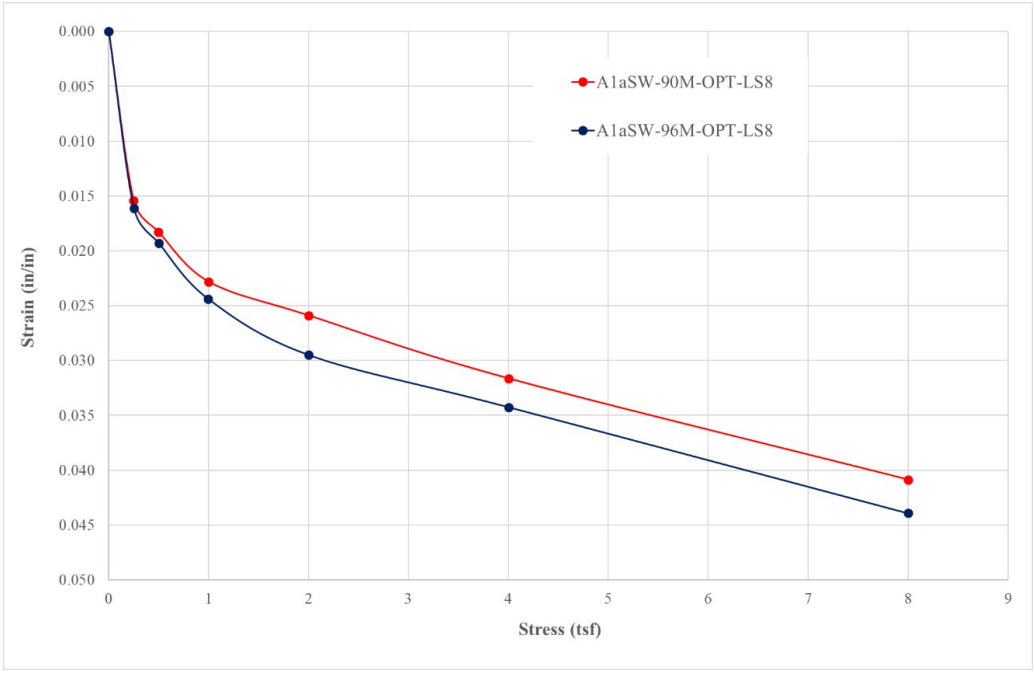

Figure 5.39 Effect of Relative Compaction during Loading in the Soaked Condition on Strain vs. Stress Results for Specimens of A1aSW Compacted at Optimum Water Content

Table 5.5 Grain-size Distribution Data for A1aSW Prior to and After Testing

Particle Size (mm)	Sieve No.	A1aSW % Finer	
		Pre-testing	Post-testing
19.05	3/4 in.	100	100
12.70	1/2 in.	99.8	100
9.5	3/8 in.	98.0	100
4.75	No. 4	85.6	86.3
2.36	No. 8	72.0	74.0
2.00	No. 10	69.0	72.7
0.85	No. 20	50.7	57.9
0.60	No. 30	42.4	---
0.425	No. 40	35.1	47.1
0.25	No. 60	22.9	37.3
0.15	No. 100	13.4	28.7
0.075	No. 200	5.7	10.8

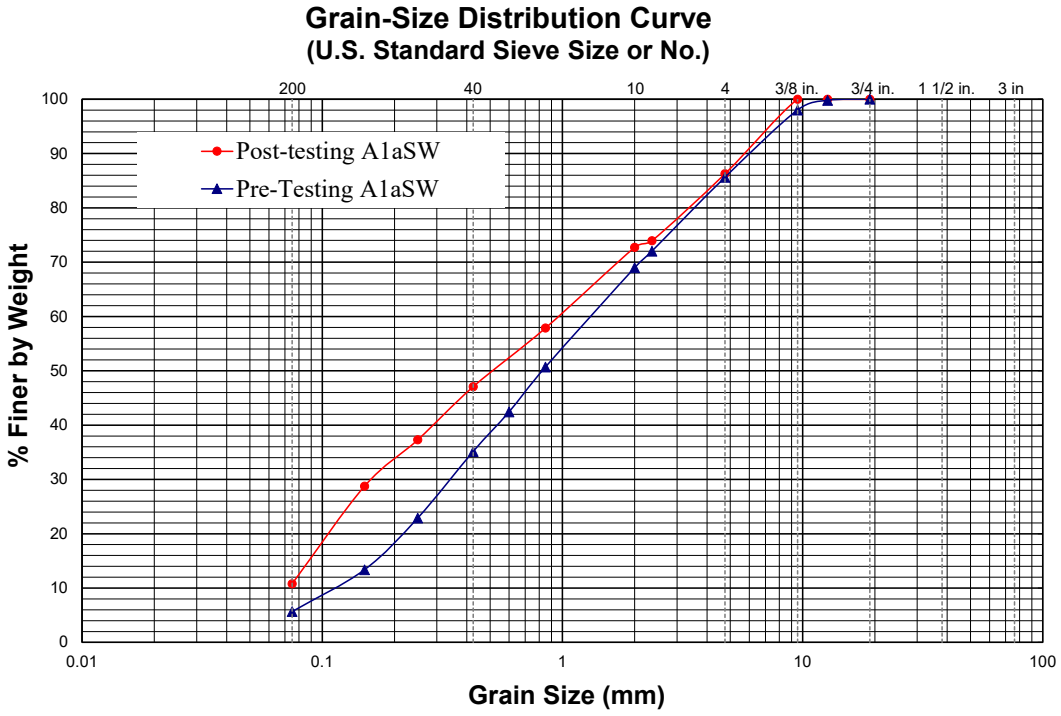

Figure 5.40 Grain-size Distribution Curves for A1aSW Prior to and After Testing

5.8.1.3 Effect of Soil Type

Six comparisons showing the effect of soil type on the strain-stress characteristics are provided in Figure 5.41 through Figure 5.46 for A1aSW and FDGW, with the differences ranging from small to large The A1aSW soil was less compressible than the FDGW soil at all stress levels in three of the six cases (Figure 5.42, Figure 5.45, and Figure 5.46). The compressibility of both soils was essentially the same for the two soils compacted to a relative compaction of 90% at optimum water content and loaded in the as-compacted condition to stresses less than ½ tsf (Figure 5.41), but at stresses greater than ½ tsf, the differences are small, with the A1aSW less compressible than the FDGW. The FDGW was less compressible than the A1aSW for both the as-compacted and soaked tests when the specimens were compacted at optimum water content to 96% relative compaction (Figure 5.43and Figure 5.44). As noted previously, the A1aSW could not be compacted to 96% when compacted in the dry condition (at a water content 5.6% dry of optimum). Therefore, no comparison is available for 96% relative compaction compacted in the dry condition.

In all four cases where the A1aSW was less compressible than the FDGW, the relative compaction was 90%. For the two cases where the FDGW was less compressible than the A1aSW, the relative compaction was 96%. As noted previously, the A1aSW could not be compacted to 96%, when compacted in the dry condition (at a water content 5.6% dry of optimum). Therefore, no comparison is available for 96% relative compaction compacted in the dry condition. Based on the results presented in this section and all other results, it seems that the A1aSW achieves close to its maximum stiffness at a relative compaction significantly less than 96% and possibly very close to 90%. That is, the additional stiffness achieved is small when the relative compaction of the A1aSW is increased from 90% to 96%. Another factor supporting this conclusion is the large difference in dry unit weight for the two soils: 128 pcf for the A1aSW and 143 pcf for the FDGW.

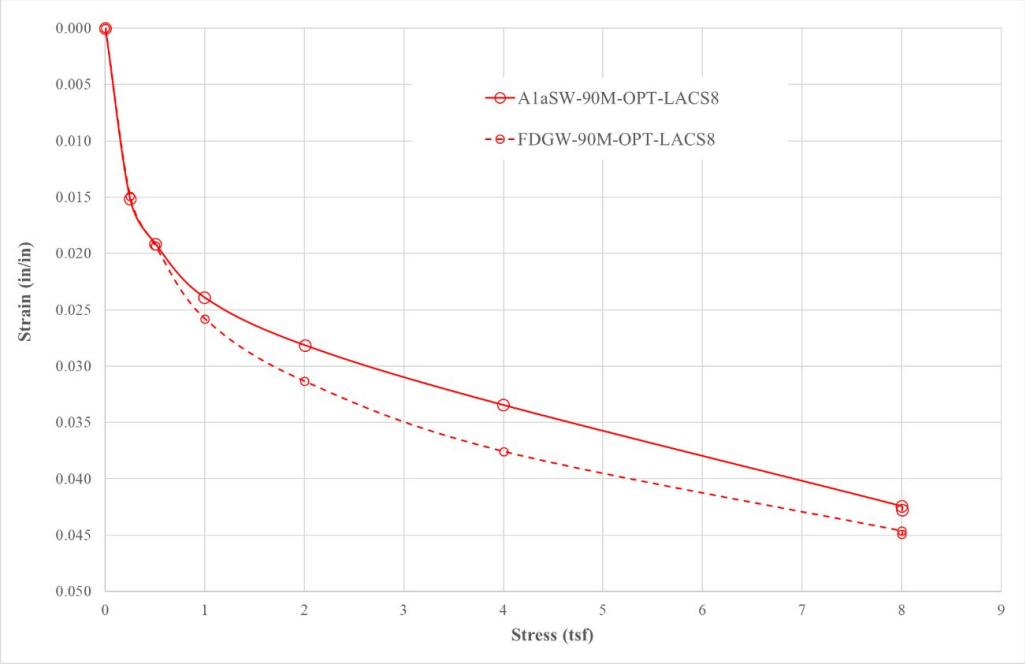

Figure 5.41 Comparison of the Strain vs. Stress Characteristics A1aSW and FDGW Compacted to a Relative Compaction of 90% at Optimum Water Content and Loaded in the As-compacted Condition

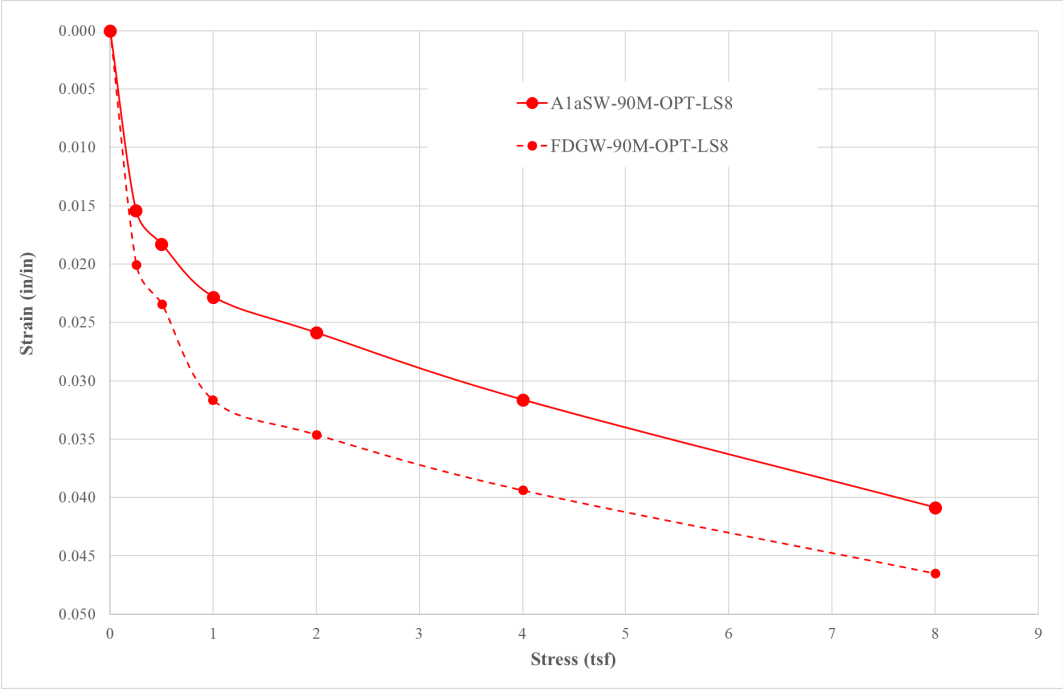

Figure 5.42 Comparison of the Strain vs. Stress Characteristics for A1aSW and FDGW Compacted to a Relative Compaction of 90% at Optimum Water Content and Loaded in the Soaked Condition

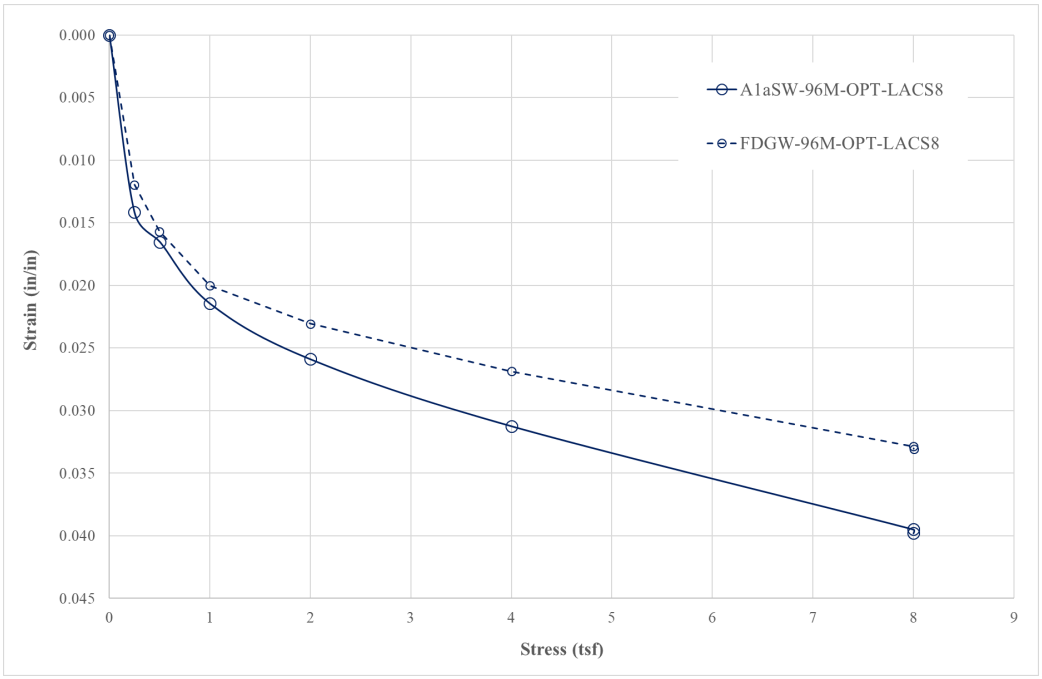

Figure 5.43 Comparison of the Strain vs. Stress Characteristics for A1aSW and FDGW Compacted to a Relative Compaction of 96% at Optimum Water Content and Loaded in the As-Compacted Condition

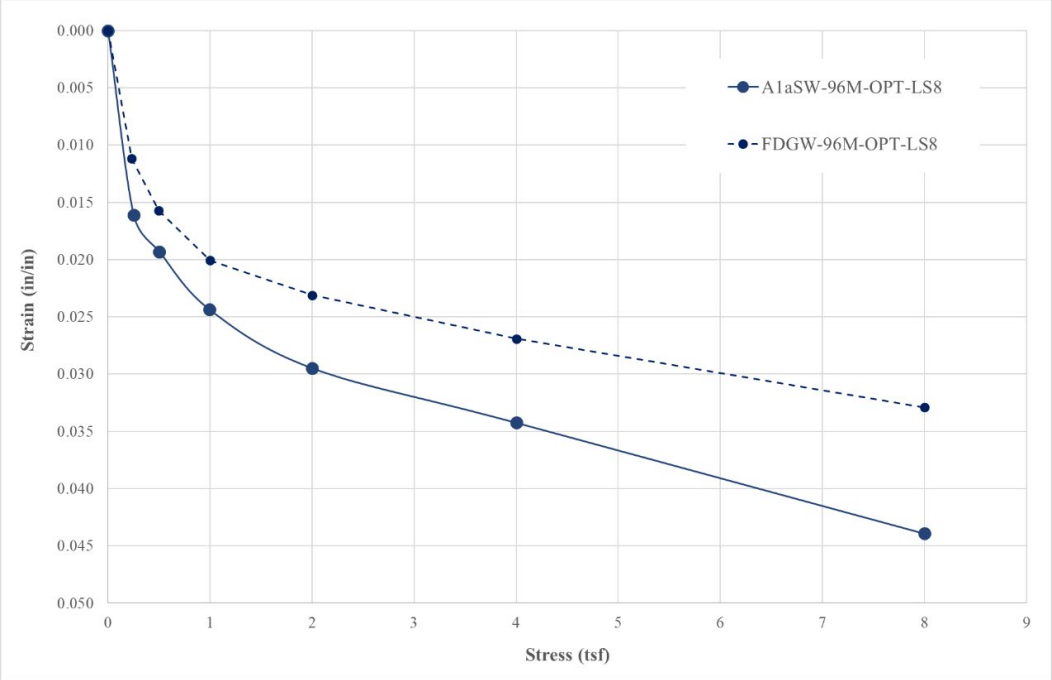

Figure 5.44 Comparison of the Strain vs. Stress Characteristics for A1aSW and FDGW Compacted to a Relative Compaction of 96% at Optimum Water Content and Loaded in the Soaked Condition

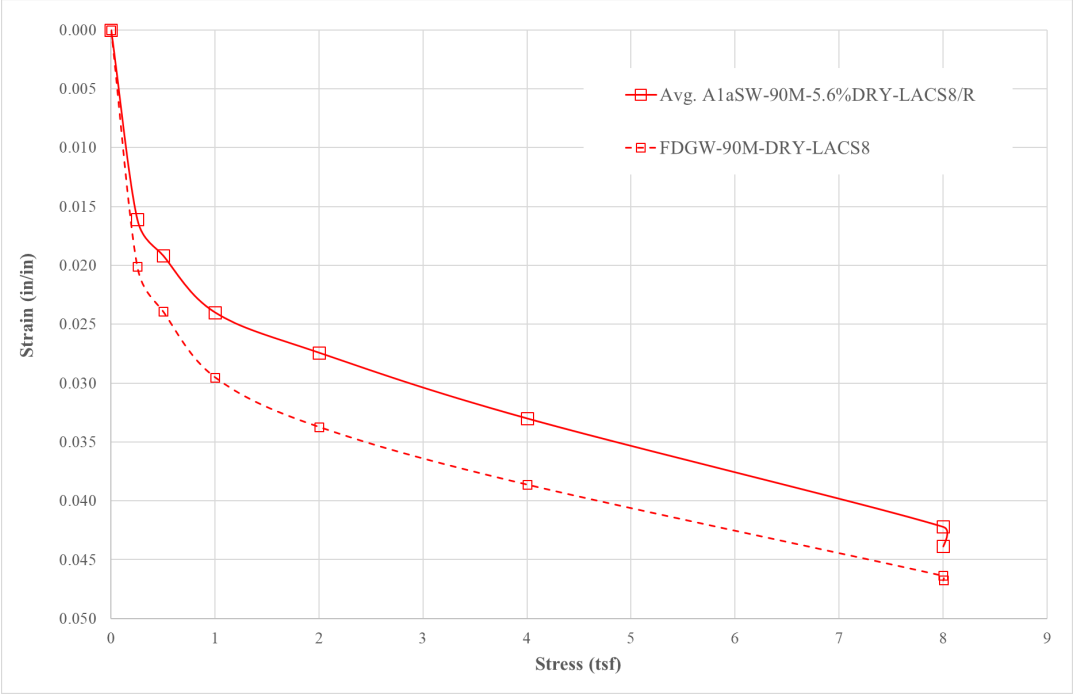

Figure 5.45 Comparison of the Strain vs. Stress Characteristics for A1aSW and FDGW Compacted Dry to a Relative Compaction of 90% and Loaded in the As-Compacted Condition

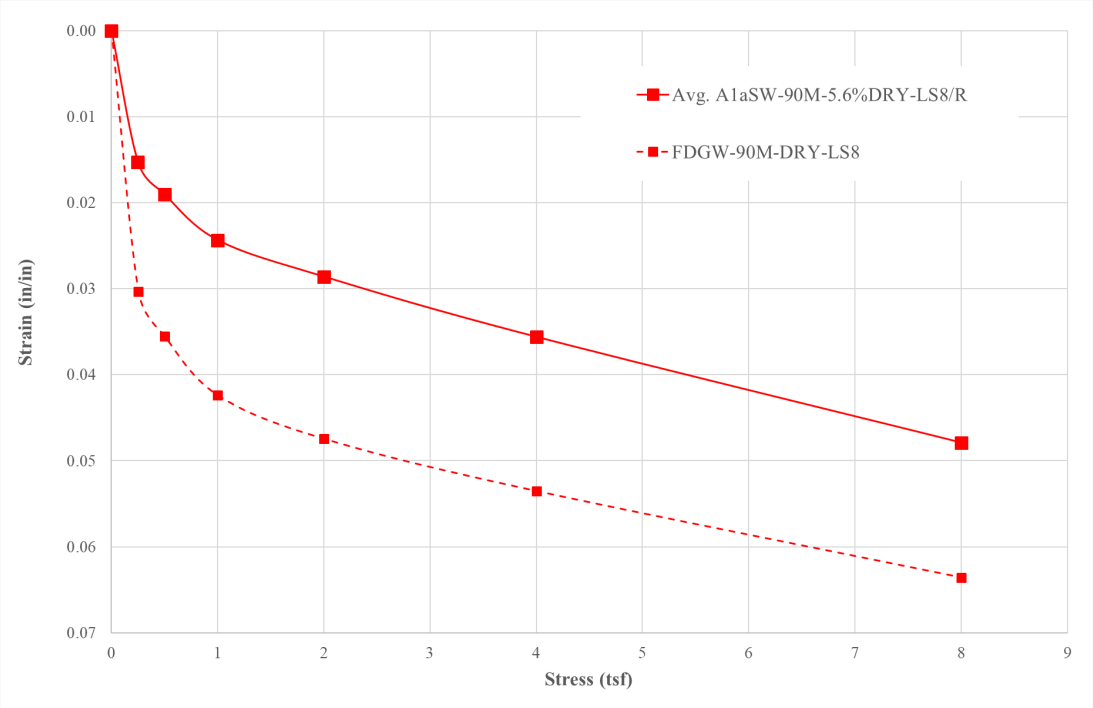

Figure 5.46 Comparison of the Strain vs. Stress Characteristics for A1aSW and FDGW Compacted Dry to a Relative Compaction of 90% and Loaded in the Soaked Condition

Since the A2SCPI10 specimens were compacted to a relative compaction of 96% based on Standard Proctor maximum dry unit weight, while the A1aSW and FDGW specimens were compacted to relative compactions of 90% or 96% based on Modified Proctor maximum dry unit weight, comparisons between the soils are difficult. However, to provide some insight into the differences in strain-stress characteristics, comparisons are made in Figure 5.47 and Figure 5.48 for the three soils, for the A2SCPI10 specimens at 96% of Standard Proctor, and the two granular soils at 90% of Modified Proctor. The A2SCPI10 specimen at 96% of Standard Proctor should be reasonably close to 90% of Modified Proctor, at least for the purposes of this comparison. For both the as-compacted and soaked conditions, the A2SCPI10 is significantly more compressible than the A1aSW and FDGW. For the as-compacted condition, the strains for the A2SCPI10 were 73% more than for the A1aSW and 63% more than for the FDGW on average for the six stress levels. For the soaked condition, the strains for the A2SCPI10 were, on average, 139% more than for the A1aSW and 89% more than for the FDGW.

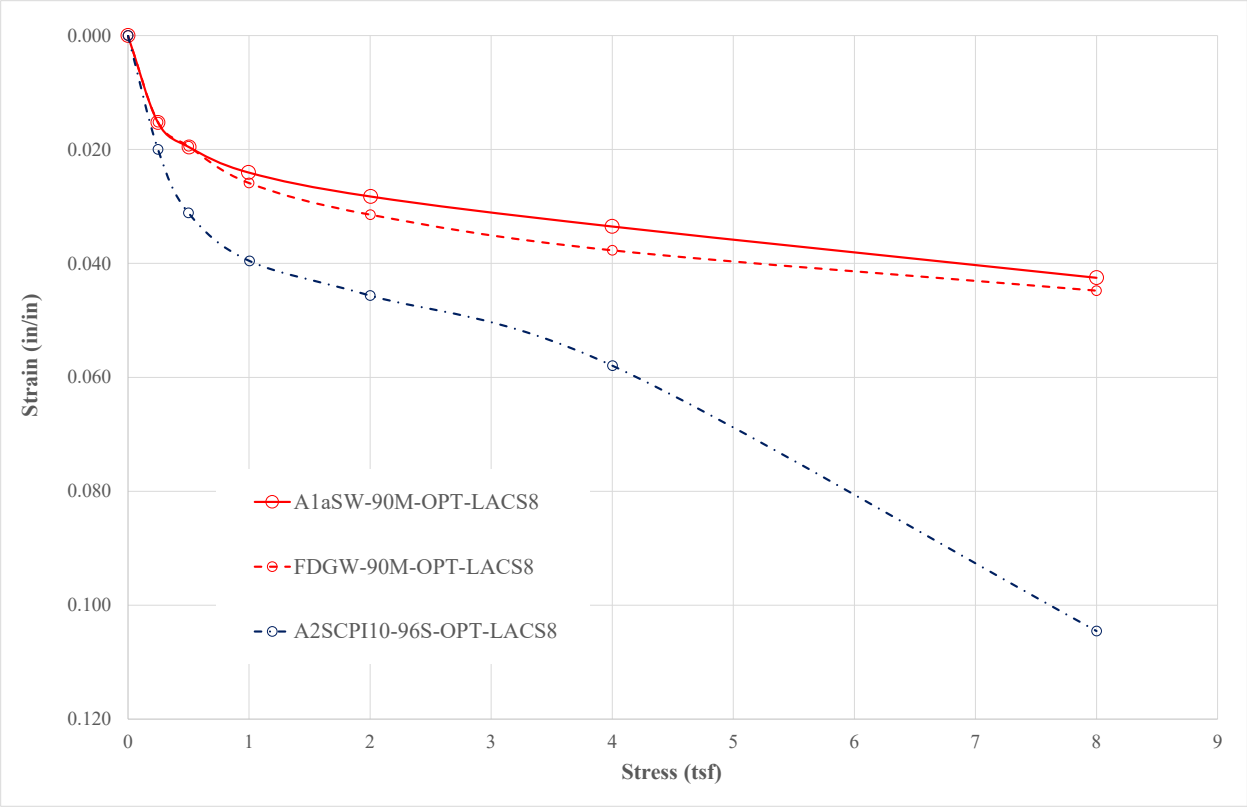

Figure 5.47 Comparison of the Strain vs. Stress Characteristics for A1aSW and FDGW Compacted at Optimum Water Content to a Relative Compaction of 90% Modified Proctor and A2SCPI10 Compacted at Optimum Water Content to a Relative Compaction of 96% Standard Proctor, with All Specimens Loadedin the As-compacted Condition

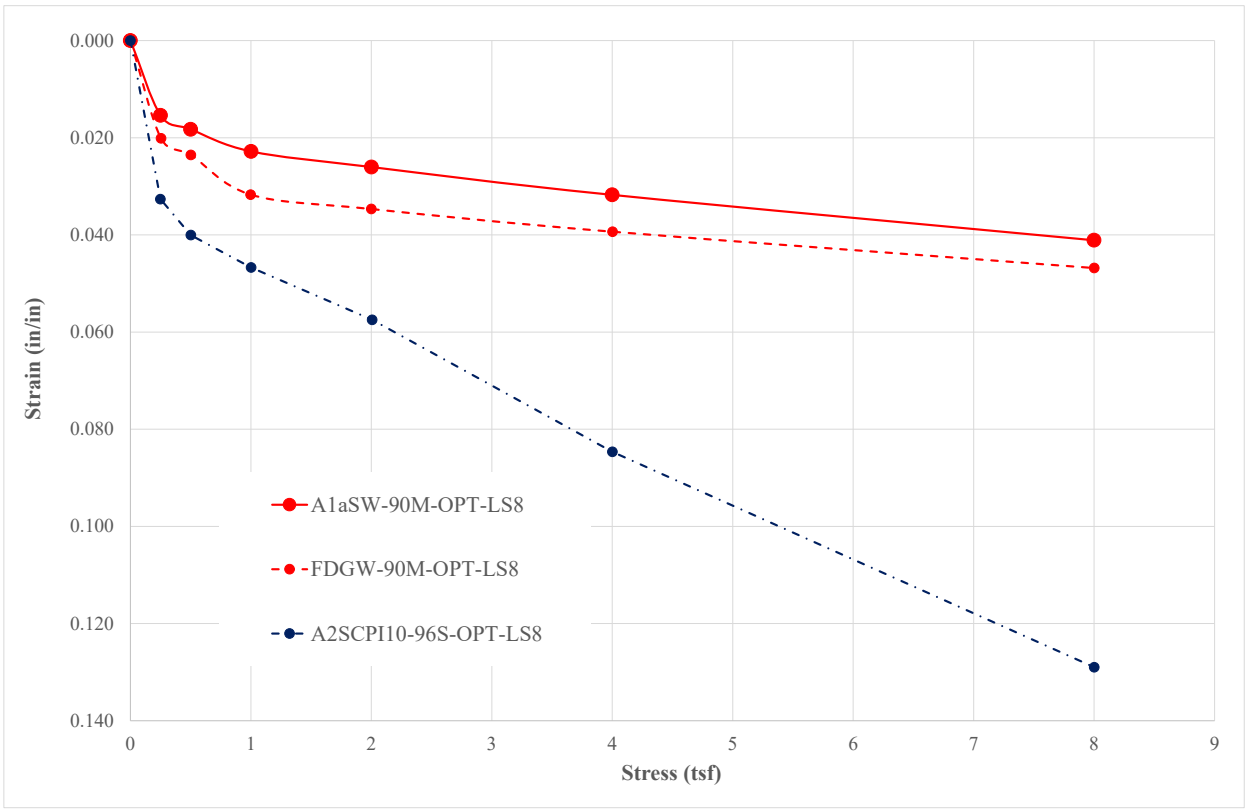

Figure 5.48 Comparison of the Strain vs. Stress Characteristics for A1aSW and FDGW Compacted at Optimum Water Content to a Relative Compaction of 90% Modified Proctor and A2SCPI10 Compacted at Optimum Water Content to a Relative Compaction of 96% Standard Proctor, with All Specimens Loaded in the Soaked Condition

5.8.1.4 Comparison of Standard and Large-Scale Consolidometer Results

Unfortunately, there are no direct comparisons available for Standard Consolidometer (SC) and Large-Scale Consolidometer (LSC) tests for the same soils compacted and tested under all the same conditions. There were three LSC tests conducted on the A2SCPI10 soil and 10 SC tests conducted on the same soil [A-2(SC, PI=10)], but there were no tests using both the SC and LSC, where all compaction and testing conditions were the same. The FDGW was tested using the LSC but not the SC, because 83% of the particles are larger than the #4 sieve, and, therefore, it could not be tested in the SC. The A1aSW soil tested in the LSC was similar to the A-1-a(SW) soil tested in the SC but included the material larger than the #4 sieve, which comprised 14% of the total material in the A1aSW. The grain-size distribution curves and the modified Proctor curves for the A1aSW and the A-1-a(SW) were previously compared in Figure 5.2 and Figure 5.3, respectively. However, since 86% of the material was the same, it would be reasonable to expect that the loading-induced strain-stress behavior would be reasonably similar for the same compaction and loading conditions.

Results for the A1aSW and A-1-a(SW) soils are compared in Figure 5.49 for the conditions most relevant of all the test results for these two soils: Optimum compaction water content for both and relative compaction of 95% for A-1-a(SW) and 96% for A1aSW. Both soaked and as-compacted loading conditions are given in Figure 5.49. Analysis of the results clearly show that for both the soaked and as-compacted specimens, the A1aSW soil tested in the LSC was significantly more compressible than the A-1-a(SW) soil tested in the SC. For example, at a stress of 8 tsf, the strain for the soaked A1aSW

specimen was 3.3 times the strain for the soaked A-1-a(SW) specimen, and the strain for the as-compacted A1aSW specimen was 4.2 times the strain for the as-compacted A-1-a(SW) specimen. Clearly these exceptionally large differences cannot be attributed solely to the small differences in grain-size distribution of the two soils and the 1% difference in relative compaction, especially since the A-1-a(SW) soil was compacted to a slightly lower relative compaction, which would make it less compressible than if it had been compacted to 96% relative compaction. Most of the difference in the stress-strain characteristics is related to the difference in size of the two specimens and corresponding differences in boundary effects.

In laboratory tests, one-dimensional strain is simulated by confining the soil within a metal ring or pipe, so all macroscopic strain for the specimen occurs in the axial (vertical) direction only. The effect of the boundary restraint can be analyzed by considering what happens in a centrically loaded, rigid circular footing of diameter B bearing at a depth of D below a horizontal ground surface and homogeneous soil layer, as illustrated in Figure 5.50. Application of centric vertical load, Q, to the top of the footing creates an average bearing (contract) stress, $q_{b,avg}$, along the bottom of the footing that strains the soil beneath it, resulting in a uniform settlement. Directly beneath the footing, the strains are one-dimensional (vertical) within a central portion of the bearing soil and two-dimensional (primarily radial but some vertical) beneath the edges of the footing, with a transition zone between the two regions. For true one-dimensional compression to occur for these conditions, the footing would need to be infinitely wide. Therefore, as the width of the footing increases with all other factors remaining the same (D, $q_{b,avg}$, soil properties), the closer the conditions approximate true one-dimensional compression because the width of the one-dimensional compression zone increases, while the widths of the distortion and transition zones remain approximately the same.

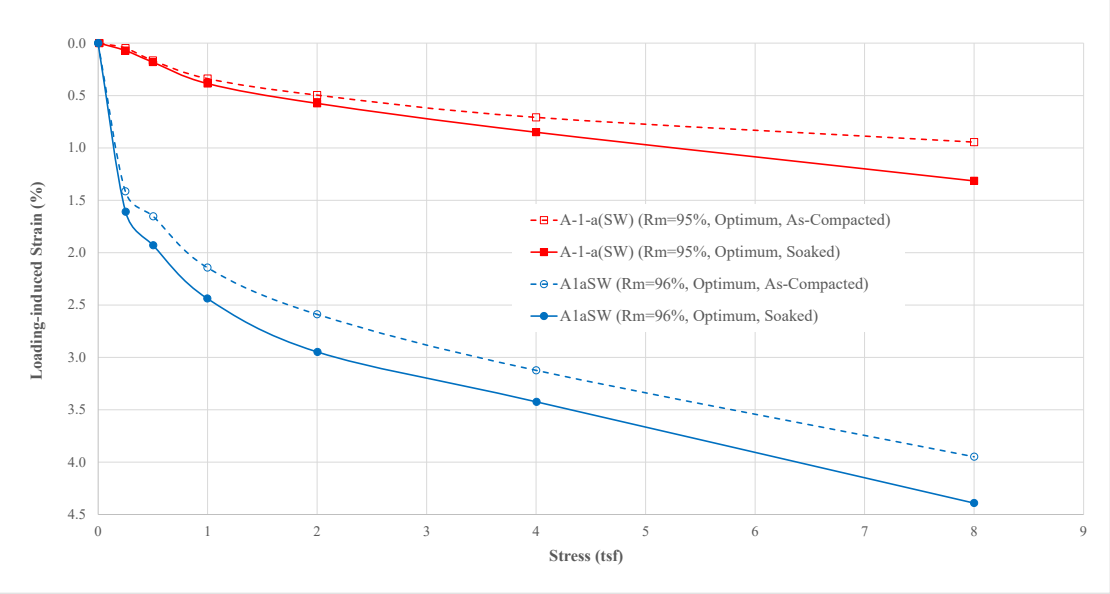

Figure 5.49 Comparison of Loading-Induced Strain vs. Stress Characteristics for A1aSW Specimens Compacted at Optimum Water Content to 96% Relative Compaction and Tested in the Large-scale Consolidometer and A-1-a(SW) Specimens Compacted at Optimum Water Content to 95% Relative Compaction and Tested in the Standard Consolidometer

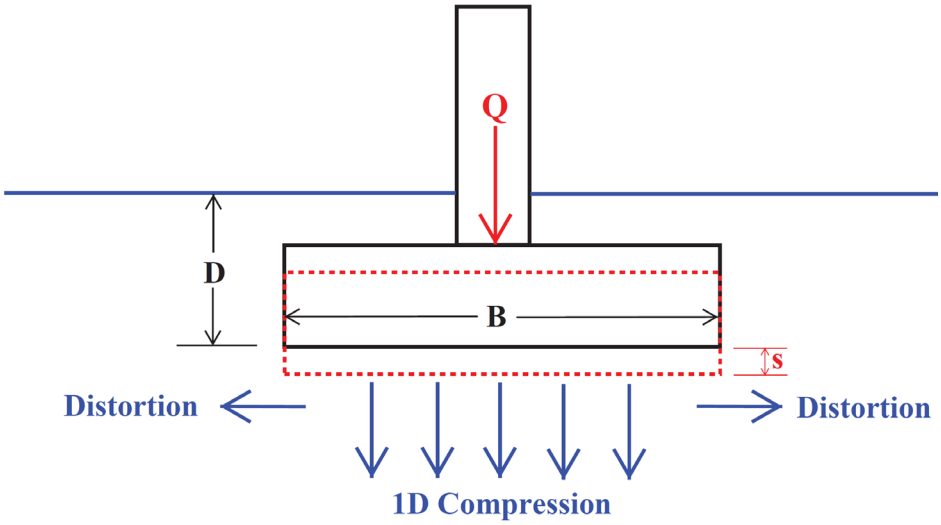

Figure 5.50 One-dimensional Compression and Distortion of Soil Directly Underneath Embedded Rigid Circular Footing

In laboratory one-dimensional compression tests, where the soil specimen is typically confined within a metal ring or pipe, the strain condition is categorized as confined or constrained compression because the ring or pipe prevents any significant radial strain (distortion) from occurring during compaction and loading. (The ring or pipe will expand slightly in the radial direction because it is not infinitely rigid.) Because of this radial constraint during compaction and loading, the radial stresses during compaction and loading will increase. The more the specimen is compacted or loaded, the higher the resulting radial stresses near the interface of the specimen and the ring or pipe. As the specimen is loaded in compression, upward shearing stresses are generated on the inside of the ring or pipe, which inhibit the compression of the specimen near the edges of the specimen due to the higher radial (confining) stresses that stiffen the soil compared to the central region where the radial stresses are lower. Using the analogy presented in Figure 5.50 as a guideline, it is reasonable to expect the width of the constrained and transition zones are approximately the same regardless of the diameter of the specimen being tested in the laboratory (assuming that the specimen is of reasonable width). If this assumption is correct, then it would be expected that the smaller specimens tested in the SC would be much stiffer than the larger specimens tested in the LSC. For example, if it is assumed that the width of the constrained plus transition zone is ½ inch, the volume of the central one-dimensional compression zone would comprise 36% of the total volume of the specimen for the SC tests and 83% of the total volume of the specimen for the LSC tests, as determined from the following calculations:

Parameter	Specimen Type	
	SC	LSC
Diameter of Specimen (in.)	2.500	11.527
Area of Specimen (in^2)	4.909	104,4
Diameter of Central 1D Compression Zone (in.)	1.500	10.527
Area of Central 1D Compression Zone (in^2)	1.767	87.04
Area of Central 1D Compression Zone/Area of Specimen (%)	36	83

Although the real conditions within the two types of specimens are certainly more complicated than this simplified analogy, and the width of the constrained and transition zones are not known, this discussion does provide a reasonable explanation as to why the LSC specimens are much more compressible than the LC specimens under reasonably similar conditions. The results also emphasize the importance of doing tests on specimens that are sufficiently wide to produce reasonably reliable strain-stress data.

The most direct comparison for the A1aSW and A-1-a(SW) soils is presented in Figure 5.51, where both soils were compacted at optimum water content to 90% relative compaction. Similar to the soils compacted to 95 and 96% relative compaction, the A1aSW is significantly more compressible than the A-1-a(SW) primarily because of the difference in size of the specimens, as noted previously. However, it is also important to note at this lower value of relative compaction of 90%, the A-1-a(SW) has considerably more sensitivity to soaking prior to loading, compared to the as-compacted condition, than the A1aSW.

A final comparison for these two soils is provided in Figure 5.52 where the soils were compacted dry of optimum to 90% relative compaction. However, this is the least direct comparison for these two soils because the A1aSW was compacted 5.6% dry of optimum, while the A-1-a(SW) was compacted 2.0% dry of optimum. As for the other two comparisons, the A1aSW was substantially more compressible than the A-1-a(SW) for the reasons noted previously. Also, the sensitivity of the A-1-a(SW) to soaking prior to loading was much more substantial than for the A1aSW, which provides some confirmation that this characteristic seems to occur at 90% relative compaction but not at 96%. However, it is not known whether this difference in strain-stress behavior is difference in grain-size distribution, differences in boundary conditions due to the large difference in size of the specimens, or both.

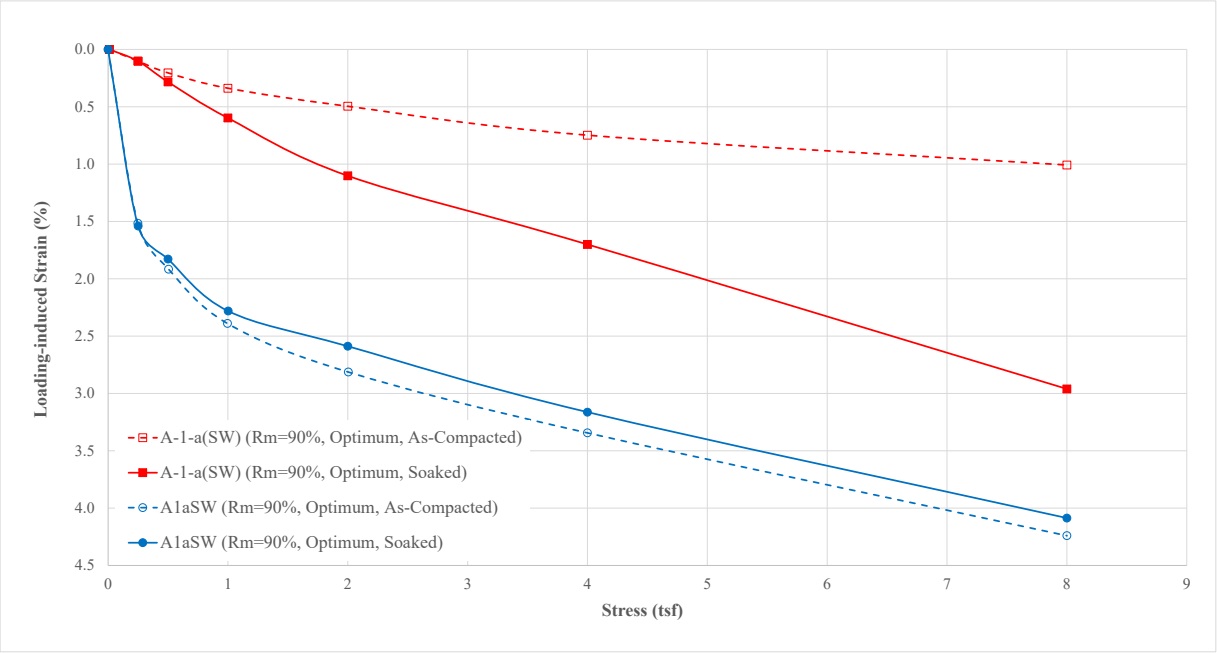

Figure 5.51 Comparison of Loading-induced Strain vs. Stress Characteristics for A1aSW and A-1-a(SW) Specimens Compacted at Optimum Water Content to 90% Relative Compaction

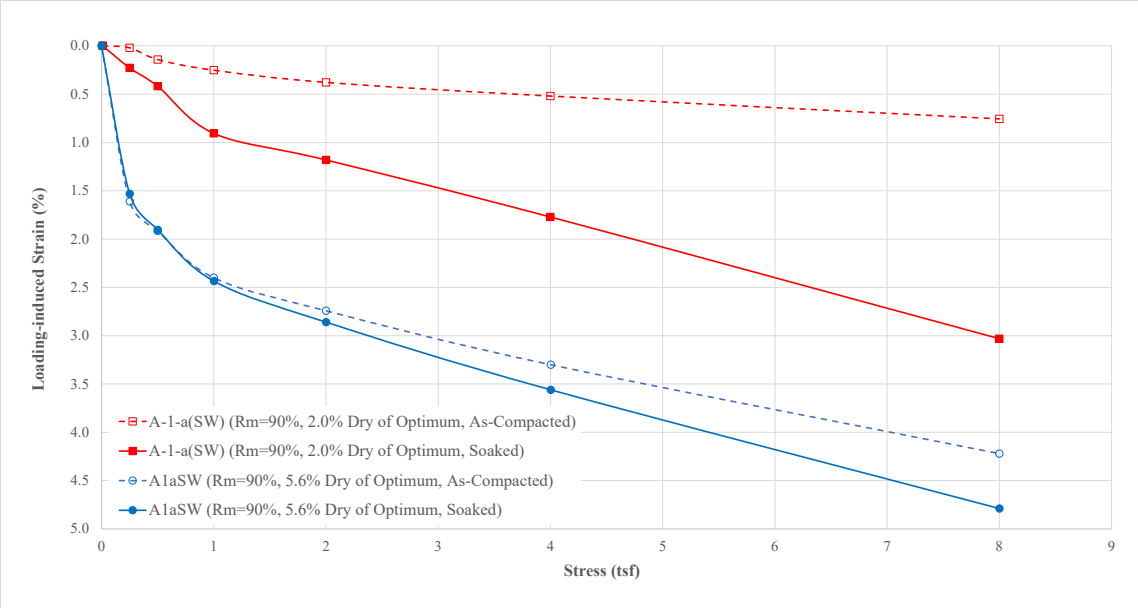

Figure 5.52 Comparison of Loading-induced Strain vs. Stress Characteristics for A1aSW and A-1-a(SW) Specimens Compacted Dry of Optimum Water Content to 90% Relative Compaction

Both SC and LSC tests were conducted on the same A-2 soil with a PI of 10. Unfortunately, no comparisons can be made in which all nominal parameters were the same. However, two close comparisons can be made for specimens compacted to 96% Standard Proctor relative compaction, where the SC specimens were compacted at a water content 2% dry of optimum and the LSC specimens were compacted at optimum water content. The loading-induced results for the four tests, from which the two comparisons can be made, are given in Figure 5.53. Although they are the same soil, the as-compacted water contents relative to optimum were, unfortunately, different, but the results still provide some information relative to the differences in testing for a cohesive soil using the SC and LSC apparatuses. It is important to note the two soaked specimens each swelled a small amount under the seating load when they were soaked, so the results shown in Figure 5.53 for those two tests have been adjusted to show the strains produced by the loading only.

Comparing the results for the A2SCPI10 specimen compacted at optimum water content and loaded as-compacted with those for the A-2(SC, PI=10) specimen compacted 2.0% dry of optimum and also loaded as-compacted, the strain for the A2SCPI10 specimen at each of the six stress levels varied from 32 to 5.7 times the strain for the A-2(SC,PI=10). Although some of the difference can be attributed to the difference in compaction water content, with the drier A-2(SC, PI=10) specimen would be expected to be less compressible than the wetter A2SCPI10 specimen, it is unlikely that these large differences could be attributed solely to the difference in compaction water content, especially since the soil is only slightly to perhaps moderately cohesive. Therefore, the primary cause of the large difference was probably the difference in the size of the specimens. Similar comparisons and conclusions can be drawn from the results of the SC and LSC specimens soaked prior to loading, but the differences are smaller than for the as-compacted condition - the strain for the A2SCPI10 soaked specimen at each of the six stress levels varied from 14 to 1.6 times the strain for the soaked A-2(SC, PI=10) specimen.

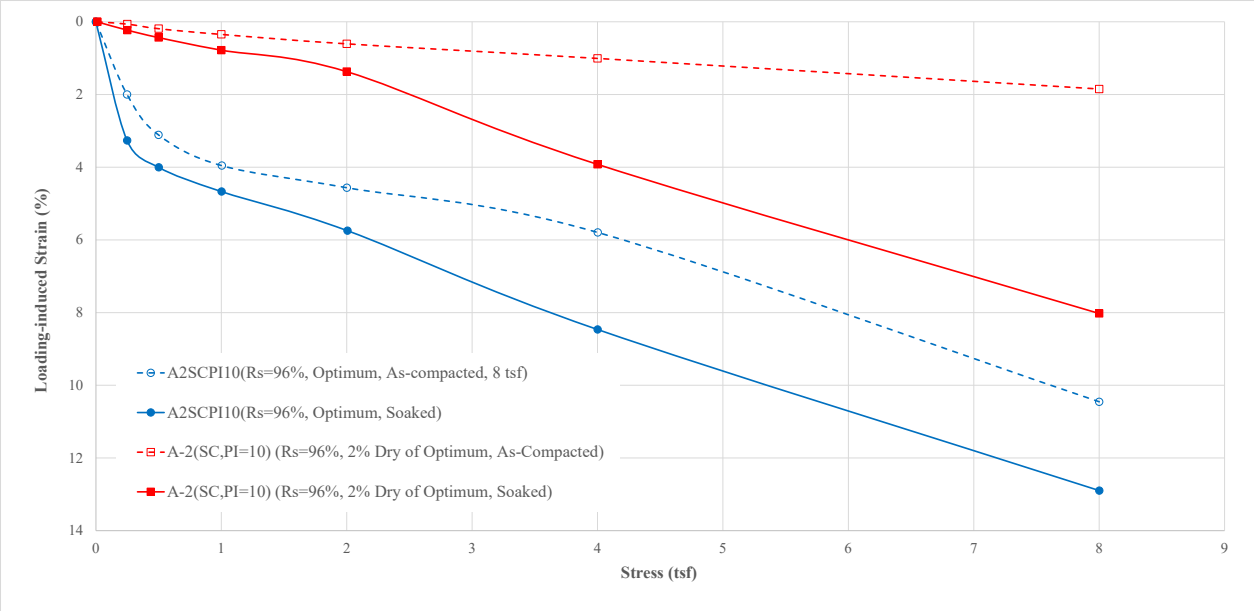

Figure 5.53 Comparison of Loading-induced Strain vs. Stress Characteristics for A2SCPI10 and A-2(SC,PI=10) Specimens Compacted to 96% Relative Compaction

5.8.2 Wetting-Induced Strains

At the end of LSC tests where the A1aSW and FDGW specimens were loaded in the as-compacted condition, the specimen was allowed to come to equilibrium at the highest level of stress, then water was added, and the wetting-induced strains were measured. Some of the tests were loaded to a maximum stress level of 8 tsf, and some were loaded to a maximum stress level of 2 tsf. The loading and wetting strain-stress results for all tests are summarized in Table 5.6.

Table 5.6 Wetting-induced Strains from LSC Tests where A1aSW and FDGW Specimens were Wetted at Constant Total Vertical Stress

Test Acronym	Vertical Stress during Wetting (tsf)	Wetting-Induced Strain (in./in.)	Wetting-Induced Strain (%)
A1aSW-90M-5.6%DRY-LACS2R	2	0.000872	0.0872
A1aSW-90M-5.6%DRY-LACS8R	8	0.00408	0.4083
A1aSW-90M-OPT-LACS2	2	0.000328	0.0328
A1aSW-90M-OPT-LACS8	8	0.000377	0.0377
A1aSW-96M-OPT-LACS8	8	0.000122	0.0122
A2SCPI10-96S-2.6%WET-LACS8	8	0.00772	0.7716
A2SCPI10-96S-OPT-LACS2	2	0.000977	0.0977
A2SCPI10-96S-OPT-LACS8	8	0.0237	2.37
FDGW-90M-DRY-LACS2	2	0.000716	0.0716
FDGW-90M-DRY-LACS8	8	0.00254	0.254
FDGW-90M-OPT-LACS8	8	0.000170	0.0170
FDGW-96M-DRY-LACS2R	2	0.000392	0.0392
FDGW-96M-DRY-LACS8/R	8	0.000773	0.0773
FDGW-96M-OPT-LACS8	8	0.000121	0.0121

Four trends are apparent from data provided in Table 5.6, with three of the trends illustrated graphically in Figure 5.54. The four trends are as follows, which apply when all other factors are nominally the same:

1. Looser soils collapse more than denser soils. Four direct comparisons that are summarized in Table 5.7 below. The reduction in collapse varies from 29% to 70% as the relative compaction increases from 90 to 96%. In the one direct comparison between the two soils (OPT-LACS8), the reduction for A1aSW is 68% compared to 29% for FDGW. For this one comparison, the reduction is substantially greater for A1aSW than for FDGW.

Table 5.7 Influence of Relative Compaction on Wetting-induced Strains from LSC Tests

Condition	Wetting-Induced Strain (in./in.)		Ratio of Wetting-Induced Strains
	90M	96M	96M/90M
A1aSW-OPT-LACS8	0.000377	0.000122	0.32
FDGW-DRY-LACS2	0.000716	0.000392	0.55
FDGW-DRY-LACS8	0.00254	0.000773	0.30
FDGW-OPT-LACS8	0.000170	0.000121	0.71

2. Collapse typically increases with increasing total vertical stress at the time of wetting. The word "typically" is used for some soils, particularly cohesive soils, because the densification that occurs under large loads can sometimes result in a decrease in collapse compared to lower values of stress. This phenomenon can be simply explained as follows: If the total vertical stress is increased to the level that all of the particles crush until there is no longer any void space (all solid material), collapse could not occur because there is no void space to allow either additional densification or the infiltration of water into the soil. However, for soils as dense and stiff as the ones tested here, the densification under load was small and the typical trend would be expected to occur, as illustrated in these results. The four direct comparisons are summarized in Table 5.8 below and shown graphically in Figure 5.54 and Figure 5.55.

   Comparing the results for the two granular soils, the increase in collapse going from a total vertical stress of 2 tsf to a total vertical stress of 8 tsf ranges from 15 to 368% for A1aSW, and from 97 to 255% for FDGW. There is only one semi-direct comparison for the two granular soils – 90% relative compaction and dry compaction water content, for which the A1aSW increased by 368% and the FDGW increased by 255%. The only comparison available for the cohesive material A2SCPI10 shows a staggering 2,328% increase in collapse for a stress increase from 2 to 8 tsf. For the one reasonably comparable comparison between a granular and cohesive soil, A1aSW-90M-OPT and A2SCPI10-96S-OPT, the increase in collapse over the same range of stresses was substantially greater for the cohesive soil (2,328%) than for the granular soil (15%).

Table 5.8 Influence of Stress on Wetting-Induced Strains from LSC Tests

Condition	Wetting-Induced Strain (in./in.)		Ratio of Wetting-Induced Strains
	2 tsf	8 tsf	8 tsf /2 tsf
A1aSW-90M-5.6%DRY-LACS	0.000872	0.00408	4.68
A1aSW-90M-OPT-LACS	0.000328	0.000377	1.15
A2SCPI10-96S-OPT-LACS	0.000977	0.0237	24.28
FDGW-90M-DRY-LACS	0.000716	0.00254	3.55
FDGW-96M-DRY-LACS	0.000392	0.000773	1.97

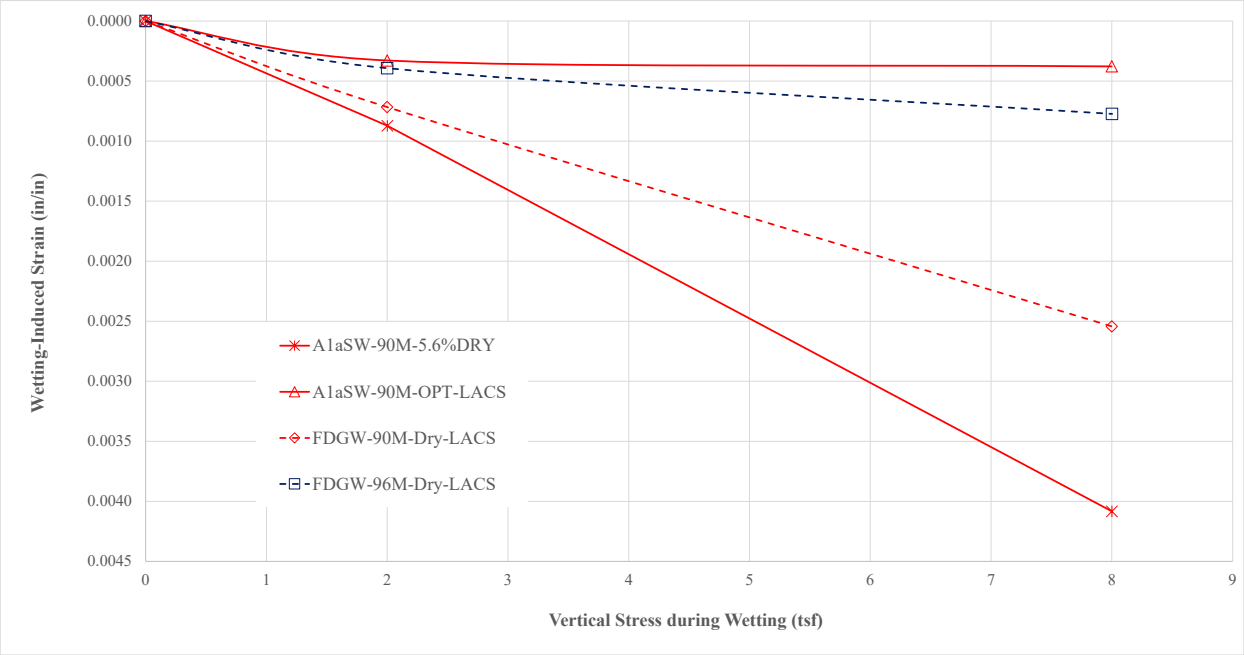

Figure 5.54 Influence of Total Vertical Stress on Wetting-Induced Strain for A1aSW and FDGW

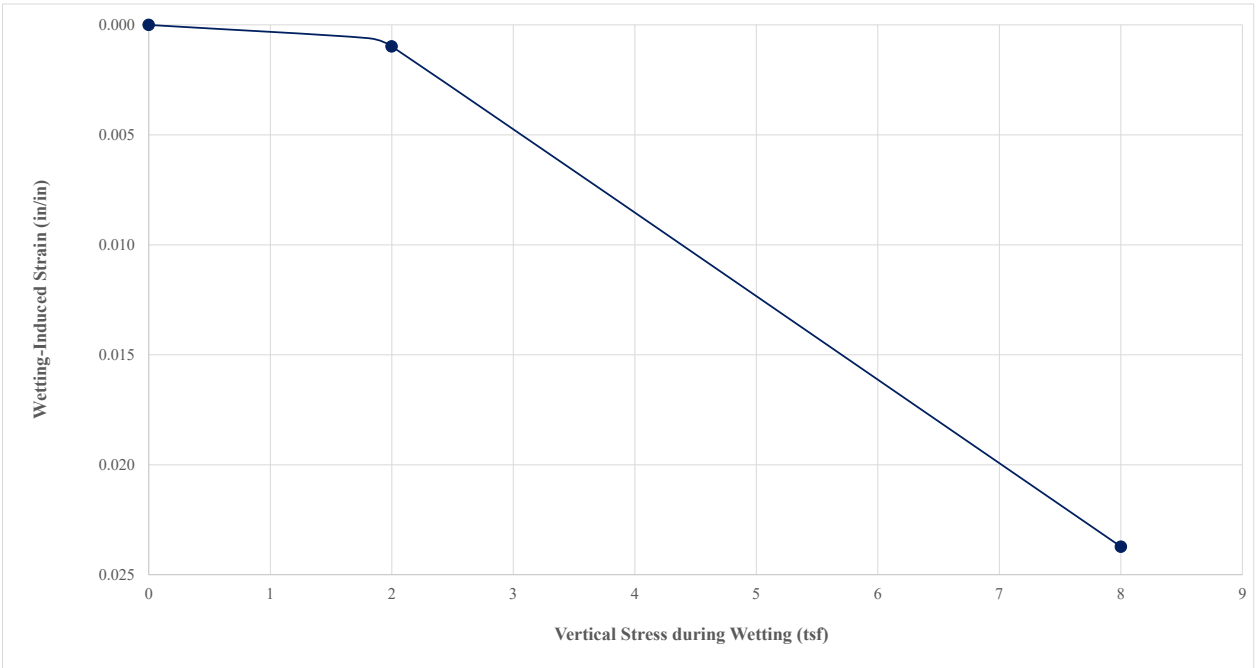

Figure 5.55 Influence of Total Vertical Stress on Wetting-Induced Strain for A2SCPI10

3. The drier the soil is at the time of wetting (in the laboratory tests, when the specimen is soaked at constant vertical stress), the more it will collapse (all other factors being the same). This trend can be illustrated by comparing the values of wetting-induced strain for LACS tests by comparing specimens of the same soil compacted to the same dry density but at different water contents (dry of optimum, at

optimum, wet of optimum). Five sets of data that meet these criteria are summarized in Table 5.9 below. In all four cases, the wetting-induced strain (collapse) is significantly less for the specimens compacted and loaded at optimum water content than those compacted and loaded dry. For the three comparisons of granular soils at a relative compaction of 90%, the collapse for the optimum specimen ranged from 7 to 38% of the collapse for the dry specimen. For the one comparison for a granular at a relative compaction at 96%, the collapse for the optimum specimen was 51% of that for the dry specimen. For the one comparison for a cohesive soil at a relative compaction at 96%, the collapse for the optimum specimen was 33% of that for the dry specimen. Since wetting-induced collapse occurs when the soil gets wetter, it makes sense that the drier soil will collapse more because it can take on more water during the wetting sequence. However, the moisture condition that determines how much collapse will occur in a soil is degree of saturation, rather than water content, because degree of saturation dictates how much additional water can be taken in by the soil. This correlation has been shown previously by Lawton (1986), among others, and was confirmed by the statistical regression analyses conducted on the results of the standard consolidometer tests in this research, as described in Section 4.4 of this report. The FDGW specimen compacted at optimum water content to 96% relative compaction collapsed 16% of the value for the comparable dry specimen, whereas at a relative compaction of 90%, the ratio was 6.7%. This difference is primarily attributable to the lower degree of saturation for the specimen compacted to 90% relative compaction, since the water contents are the same and after soaking the degree of saturation would be close to 100% for both specimens. It should also be noted the degree of saturation changes during loading as a specimen compresses, even though the water content is the same. So the magnitude of collapse is related to the degree of saturation at the time of wetting, at which time, the degree of saturation is somewhat higher than the as-compacted value and depends on the magnitude of the densification that occurs during loading.

Table 5.9 Influence of Compaction Water Content on Wetting-induced Strains from LSC Tests

Condition	Wetting-Induced Strain (in./in.)			Ratio of Wetting-Induced Strains	Ratio of Wetting-Induced Strains
	DRY	OPT	WET	OPT/DRY	WET/OPT
A1aSW-90M-LACS2	0.000872	0.0003280	---	0.38	---
A1aSW-90M-LACS8	0.004083	0.0003774	---	0.092	---
A2SCPI10-96S-LACS8	---	0.0237244	0.0077157	---	0.33
FDGW-90M-LACS8	0.00254	0.000170	---	0.067	---
FDGW-96M-LACS8	0.000773	0.000121	---	0.16	---

4. For the four cases where a direct comparison is available, AlaSW collapsed more than FDGW in three of the four cases, and the collapse was essentially the same in one case. The results are compared in Table 5.10 below. The relative compaction was 90% for the three cases where A1aSW collapsed more than FDGW, and the relative compaction was 96% for the one case where the collapse was the same for both soils. Since only four comparisons are available, no definite conclusion can be made regarding which soil is more susceptible to wetting-induced collapse. However, these limited results indicate that the A1aSW is 22 to 122% more collapsible at 90% relative compaction, and there is little difference for the two soils at 96% relative compaction.

Table 5.10 Comparison of Wetting-induced Strains from LSC Tests for FDGW and A1aSW

Condition	Wetting-Induced Strain (in./in.)		Ratio of Wetting-Induced Strains
	FDGW	A1aSW	A1aSW/FDGW
90M-DRY/5.6%DRY-LACS2	0.000716	0.000872	1.22
90M-DRY/5.6%DRY-LACS8	0.00254	0.004083	1.61
90M-OPT-LACS8	0.000170	0.000377	2.22
96M-OPT-LACS8	0.000121	0.000122	1.01

5.9 Settlement Estimates for a 30-foot Tall Embankment

5.9.1 Overview of Settlement Calculations

Based on the experimental results from the large-scale consolidometer tests, estimates of both loading-induced and wetting-induced settlement were calculated for a 30-foot tall embankment, which is a reasonable approximation of a "typical" maximum height of the approach embankment for major bridges in Utah. A surcharge of 300 psf was used as a rough estimate to represent the dead loads from materials constructed on the surface of the fill (approach slab, pavement, etc.). The general equation for settlement, *S*, is:

$$S = \int_{z=0}^{z=H} \varepsilon_v \cdot dz \qquad (5.1)$$

where ε_v is the vertical strain, z is the depth below the top of the layer for which settlement is being calculated, and H is the height of the layer.

In cases where an equation is not available for vertical strain as a function of vertical stress, but values are known at certain depths within the layer, the layer can be subdivided into sublayers and Eq. (5.1) can be approximated by the following summation:

$$S \cong \sum_{i=1}^{i=n} \varepsilon_{v,avg} \cdot \Delta z \qquad (5.2)$$

where n is the number of sublayers into which the layer is subdivided, $\varepsilon_{v,avg}$ is the average value of vertical strain within each sublayer, and Δz is the thickness of each sublayer.

5.9.2 Loading-Induced Settlement

An attempt was made to fit each set of loading-induced strain vs. stress data with a valid regression line, but no reasonable fit could be obtained for the data using the standard types of regression available in the spreadsheet software being used. Therefore, to be consistent, the loading-induced settlement was calculated using Eq. 5.2, with the results shown in Table 5.11 for FDGW-96M-OPT-LS8 as an example. The loading-induced settlement for all tests loaded to 8 tsf, and one test on the A2SCPI10 loaded to 2 tsf are summarized in Table 5.12. The results in Table 5.12 are re-ordered in Table 5.13, from smallest to largest settlement. Sample calculations for the second depth increment for FDGW-96M-OPT-LS8 are as follows:

$\gamma_{dmax} := 142.0\text{pcf}$ $\quad w_{opt} := 6.6\%$ $\quad R_m := 96\%$ $\quad G_s := 2.66$

$\gamma_d := R_m \cdot \gamma_{dmax} = 136.32\text{pcf}$

Assume: $\gamma_w := 62.4\text{pcf}$

Assuming that the specimen is completed saturated after soaking, the following equation for the saturated unit weight of the soil can be derived from fundamental phase relations:

$$\gamma_{sat} := \gamma_d \cdot \left(1 + \frac{\gamma_w}{\gamma_d} - \frac{1}{G_s}\right) = 147.47\text{pcf}$$

Stress at start of second loading increment: $\sigma_{vi} := 0.233191703517344\,tsf$

$\sigma_{vi} = 466.38\,psf$

Stress at end of second loading increment: $\sigma_{vf} := 0.499330604814391\,tsf$

$\sigma_{vf} = 998.7\,psf$

Strain at the start of second loading increment: $\varepsilon_{vLi} := 0.0125009690507082\,\frac{in}{in}$

Strain at the start of second loading increment: $\varepsilon_{vLf} := 0.0158040640177301\,\frac{in}{in}$

Average strain for this loading increment:

$$\varepsilon_{vL.avg} := \frac{1}{2}\cdot\left(\varepsilon_{vLi} + \varepsilon_{vLf}\right) = 0.0141525\cdot\frac{in}{in}$$

Now find the depth below the ground surface, z, corresponding to stresses at the start and end of the loading increment:

$$z_i := \frac{\sigma_{vi} - 300psf}{\gamma_{sat}} = 1.1282\,ft$$

$$z_f := \frac{\sigma_{vf} - 300psf}{\gamma_{sat}} = 4.7376\,ft$$

Depth increment: $\Delta z := z_f - z_i = 3.6094\,ft$ $\Delta z = 43.312\cdot in$

Now calculate settlement increment for this depth increment:

$\Delta S_L := \varepsilon_{vL.avg}\cdot\Delta z = 0.051081\,ft$ $\Delta S_L = 0.61298\cdot in$

The calculated values of loading-induced settlement in TTable 5.12 and Table 5.13 vary from about 7 to 18 inches Although these values may seem high, they are significantly smaller than for lesser quality embankment materials. For the two granular (cohesionless) soils (A1aSW and FDGW), these settlements are generally inconsequential to the bump-at-the-bridge problem because the settlements will occur quickly during construction owing to the high permeability of these two materials. In the laboratory, the loads were applied quickly (typically less than 10 seconds) and the granular specimens came to equilibrium under each load in about 15 to 30 minutes. In the field, the construction of a bridge approach embankment typically occurs over several weeks or months and sometimes longer and, therefore, the load is applied much slower and there is much more time for the material to come to equilibrium. However, for the cohesive soil (A2SCPI=10), the settlements are generally larger than for the two granular soils (with

only one exception), and the settlements will occur over a much longer period of time, owing to the time-dependency of settlement in cohesive soils. Comparing the settlements of the two granular soils, the settlements for all the A1aSW specimens are less than the FDGW specimens, except for the two FDGW specimens compacted to 96% relative compaction at optimum water content.

Table 5.11 Calculation of Loading-Induced Settlement for FDGW-96M-OPT-LS8 in a Spreadsheet

Vertical Stress σ_v (tsf)	Vertical Stress σ_v (psf)	Vertical Strain ε_{vL} (in./in.)	Depth z (ft)	Depth Increment No.	Depth Increment Δz (ft)	Avg. Vert. Strain $\varepsilon_{vL,avg}$ (in./in.)	Settlement Increment ΔS_L (in.)
0	0	0	0				
0.233	466	0.01250	1.128	1	1.128	0.00625	0.0846
0.499	999	0.01580	4.738	2	3.609	0.01415	0.6130
1.001	2001	0.02009	11.535	3	6.797	0.01795	1.4640
2.003	4006	0.02314	25.133	4	13.598	0.02162	3.5277
2.362	4724	0.02387	30.000	5	4.867	0.02351	1.3728
4.001	8003	0.02718	52.232	Total Settlement, $S_L = \Sigma\Delta S_L =$			7.0621

Table 5.12 Calculated Loading-induced Settlement of the Embankment for all LSC Test Data

Condition	Loading-Induced Settlement S_L (in.)
A1aSW-90M-5.6%DRY-LACS8/R	8.06
A1aSW-90M-5.6%DRY-LS8/R	8.44
A1aSW-90M-OPT-LACS8	8.23
A1aSW-90M-OPT-LS8	7.86
A1aSW-96M-OPT-LACS8	7.52
A1aSW-96M-OPT-LS8	8.90
A2SCPI10-96S-2.6%Wet-LACS8	17.7
A2SCPI10-96S-OPT-LACS8	13.2
A2SCPI10-96S-OPT-LS8	16.6
FDGW-90M-DRY-LACS8	10.0
FDGW-90M-DRY-LS8	14.8
FDGW-90M-OPT-LACS8	9.05
FDGW-90M-OPT-LS8	10.7
FDGW-96M-DRY-LACS8/R	9.77
FDGW-96M-DRY-LS8	11.1
FDGW-96M-OPT-LACS8	7.01
FDGW-96M-OPT-LS8	7.06

Table 5.13 Calculated Loading-induced Settlement of the Embankment for all LSC Test Data Re-ordered from Smallest to Largest Settlement

Condition	Loading-Induced Settlement S_L (in.)
FDGW-96M-OPT-LACS8	7.01
FDGW-96M-OPT-LS8	7.06
A1aSW-96M-OPT-LACS8	7.52
A1aSW-90M-OPT-LS8	7.86
A1aSW-90M-5.6%DRY-LACS8/R	8.06
A1aSW-90M-OPT-LACS8	8.23
A1aSW-90M-5.6%DRY-LS8/R	8.44
A1aSW-96M-OPT-LS8	8.90
FDGW-90M-OPT-LACS8	9.05
FDGW-96M-DRY-LACS8/R	9.77
FDGW-90M-DRY-LACS8	10.0
FDGW-90M-OPT-LS8	10.7
FDGW-96M-DRY-LS8	11.1
A2SCPI10-96S-OPT-LACS8	13.2
FDGW-90M-DRY-LS8	14.8
A2SCPI10-96S-OPT-LS8	16.6
A2SCPI10-96S-2.6%Wet-LACS8	17.7

5.9.3 Wetting-Induced Settlement

For the embankment height of 30-ft, the maximum total vertical stress — which occurs at the bottom of the embankment — for the soils and conditions tested varies from about 1.9 to 2.3 tsf (3800 to 4600 psf). Most tests on the as-compacted specimens were wetted at 8 tsf, which is significantly higher than the maximum value for the embankment. Because the relationship between wetting-induced strain and total vertical stress for otherwise identical conditions is not linear, it is difficult to calculate the wetting-induced settlement for these cases. There were five conditions for which the specimens were soaked at more than one value of total vertical stress, and, in all five cases, the soaking occurred at stresses of 2 and 8 tsf. The results for these five cases are summarized in Table 5.14 and are shown graphically in Figure 5.56 and Figure 5.57. The same graphs are plotted in Figure 5.58 and Figure 5.59 with best-fit second-order polynomials for each condition. With only two data points, it is impossible to know the true trend. Although the fit is not necessary statistically reliable because of only two data points (other than the origin), and the smooth curve is probably a more realistic fit to the data, the polynomial can be used to provide a reasonable estimate of the magnitude of the wetting-induced settlement, since the range of stresses fall within the zone where the two curves are close. Wetting-induced settlement for each of the cases was calculated using Eq. 5.1. The regression equations for wetting-induced vertical strain, ε_{vw}, shown in Figure 5.58 and Figure 5.59 are a function of total vertical stress, σ_v in units of tsf.

Table 5.14 Values of Wetting-induced Strain for Five Conditions where LACS Tests were Soaked at Total Vertical Stresses of 2 and 8 tsf)

Condition	Wetting-Induced Strain (in./in.)		Ratio of Wetting-Induced Strains
	2 tsf	8 tsf	8 tsf /2 tsf
A1aSW-90M-5.6%DRY-LACS	0.000872	0.00408	4.68
A1aSW-90M-OPT-LACS	0.000328	0.000377	1.15
A2SCPI10-96S-OPT-LACS	0.000977	0.0237	24.28
FDGW-90M-DRY-LACS	0.000716	0.00254	3.55
FDGW-96M-DRY-LACS	0.000392	0.000773	1.97

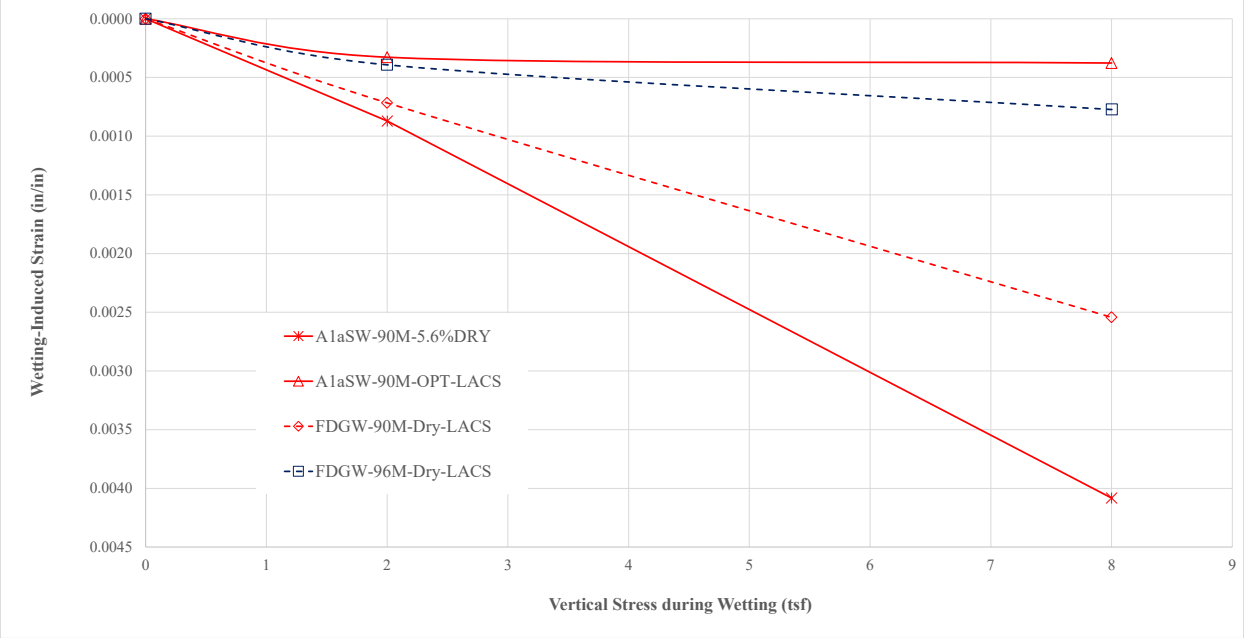

Figure 5.56 Wetting-induced Strain vs. Total Vertical Stress for Four Conditions where LACS Tests on A1aSW and FDGW were Soaked at Total Vertical Stresses of 2 and 8 tsf

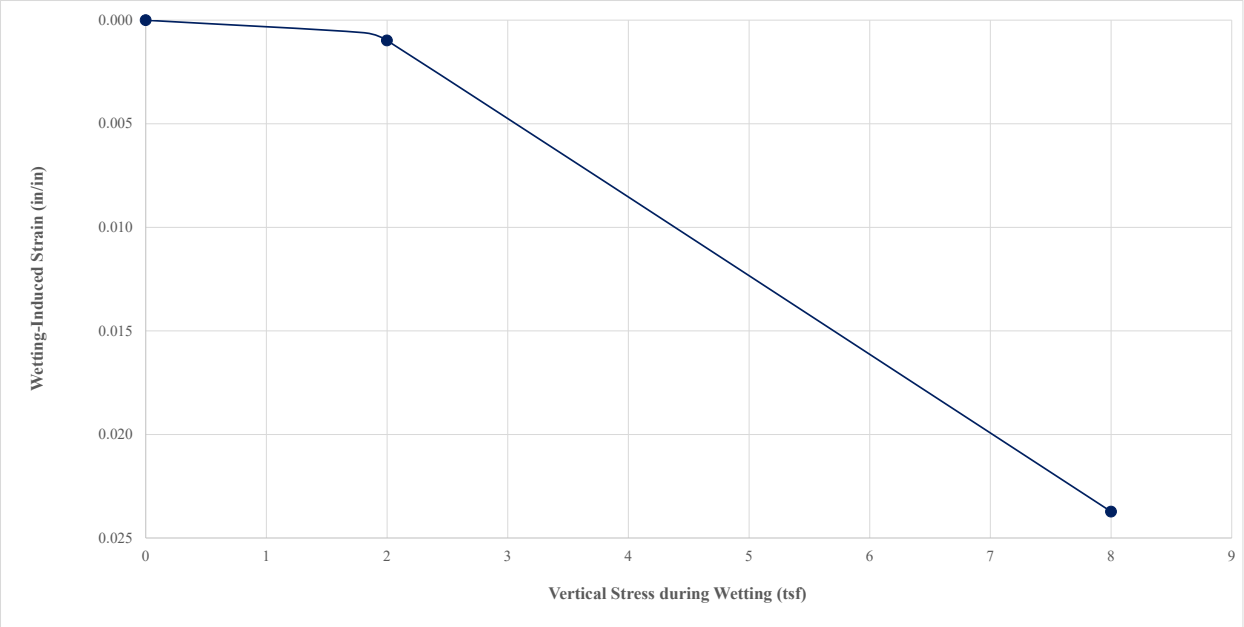

Figure 5.57 Wetting-induced Strain vs. Total Vertical Stress for One Condition where LACS Tests on A2SCPI10 were Soaked at Total Vertical Stresses of 2 and 8 tsf

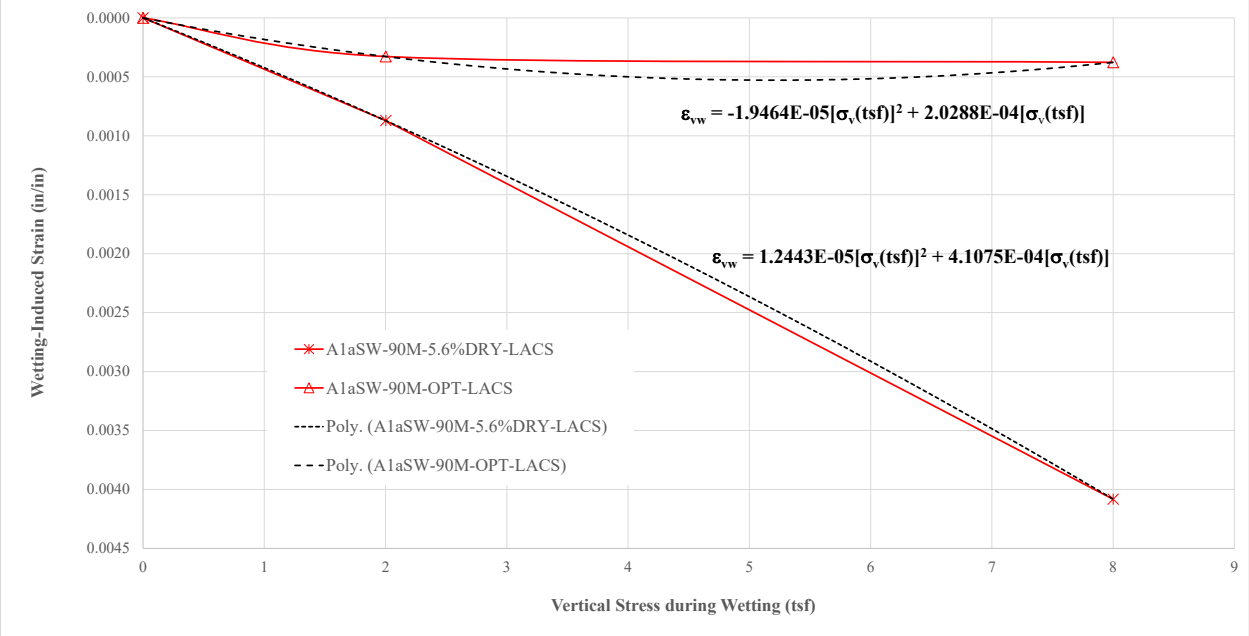

Figure 5.58 Best-fit Polynomial Regression of Wetting-induced Strain vs. Total Vertical Stress for Specimens of A1aSW Soaked at Total Vertical Stresses of 2 and 8 tsf

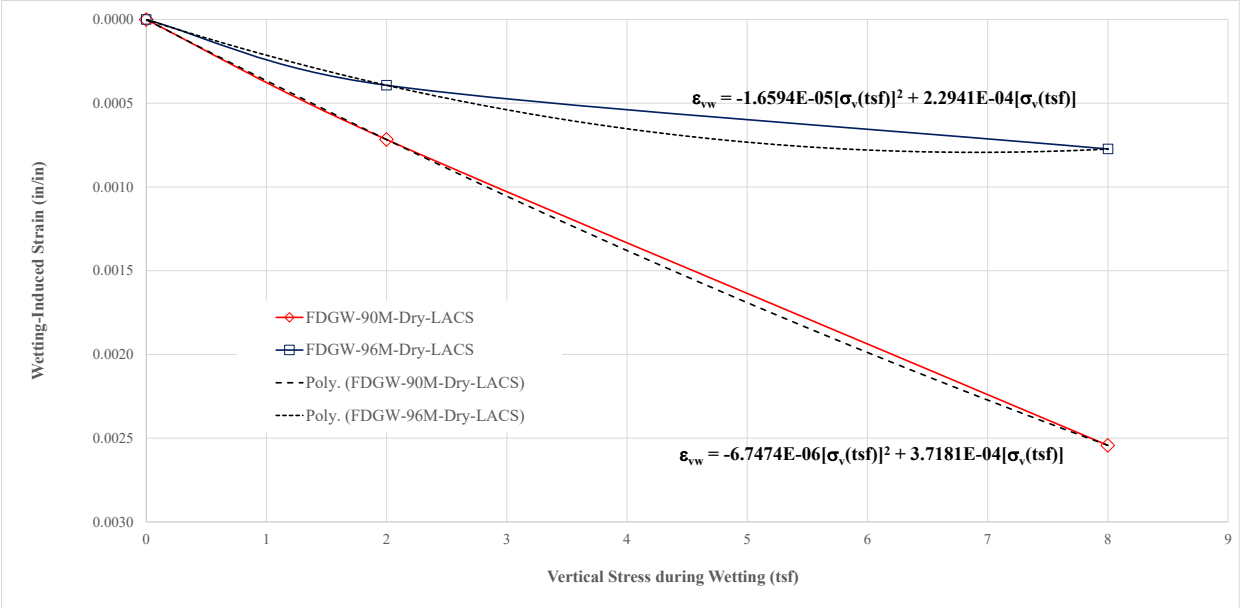

Figure 5.59 Best-fit Polynomial Regression of Wetting-Induced Strain vs. Total Vertical Stress for Specimens of FDGW Soaked at Total Vertical Stresses of 2 and 8 tsf

The wetting-induced settlement for each case was calculated in MathCad using the regression equations of $\varepsilon_{vw} = f(\sigma_v)$, with the calculations for FDGW-90M-DRY-LACS provided below as an example:

$\gamma_{dmax} := 142.0pcf \qquad w_{dry} := 0\% \qquad RC := 90\%$

Total unit weight of the as-compacted soil: $\gamma := RC \cdot \gamma_{dmax} \cdot (1 + w_{dry}) = 127.8 \cdot pcf$

$\sigma_v(z) := \gamma \cdot z + 300psf$

$$\varepsilon_{vw}(z) := -6.7474 \cdot 10^{-6} \cdot \left(\frac{\sigma_v(z)}{1tsf}\right)^2 + 3.7181 \cdot 10^{-4} \cdot \frac{\sigma_v(z)}{1tsf}$$

$$S_w := \int_0^{360in} \varepsilon_{vw}(z)\, dz = 0.145 \cdot in$$

For A2SCPI10, the wetting-induced settlement was calculated assuming straight lines between data points. The values wetting-induced settlement for all five conditions are summarized in Table 5.15.

Table 5.15 Calculated Values of Wetting-induced Settlement for Five Conditions where LACS Tests were Soaked at Total Vertical Stresses of 2 and 8 tsf

Condition	Wetting-Induced Settlement S_w (in.)
A1aSW-90M-5.6%DRY-LACS	0.160
A1aSW-90M-OPT-LACS	0.0691
A2SCPI10-96S-OPT-LACS	0.177
FDGW-90M-DRY-LACS	0.145
FDGW-96M-DRY-LACS	0.0866

These calculations are for the worst-case scenario, where the embankment becomes completely soaked at some point within the service life throughout the entire depth of the embankment where it comes into the bridge. Note that the soaking does not need to occur at every depth simultaneously for these calculations to apply. The calculated wetting-induced settlement for dry FDGW at 96% relative compaction is only 60% of the settlement for dry FDGW at 90% relative compaction. The calculated wetting-induced settlement for A1aSW compacted to 90% relative compaction at optimum water content (8.4%) is 43% of the settlement for the same soil and relative compaction but compacted at a water content of 2.8% (5.6% dry of optimum). Note that the settlement for A2SCPI10 compacted to 96% relative compaction at optimum water content was 2.6 times that of A1aSW compacted to 90% relative compaction at optimum water content. In addition, the A2SCPI10 would be expected to settle substantially more if compacted at water contents only a few percent dry of optimum.

These four values of settlement for the two granular soils (A1aSW and FDGW) are small (only about 1/14 to 1/6 of an inch) for a wide range of water contents. Therefore, it appears likely that if either of these two soils are used in the approach embankments for bridges and constructed properly, the wetting-induced settlement of the embankment itself should not contribute significantly to the bump at the bridge.

5.10 Summary

Details regarding the design and construction of the Large-Scale Consolidometer (LSC), the materials tested, preparation and compaction of the materials, and results and analyses of the 27 loading-wetting tests conducted using the LSC are described in this chapter. The main conclusions determined from analysis of the results from these tests are summarized as follows:

- In most cases, the loading-induced strains were smaller for nominally identical specimens loaded as-compacted than loaded after soaking. The differences were small for the two granular soils tested and significantly larger for the one cohesive soil tested.
- In most cases, the loading-induced strains were smaller for granular specimens compacted dry of optimum water content than those compacted at optimum water content to the same relative compaction and loaded in the same condition (as-compacted or soaked). The loading-induced strain for a cohesive specimen compacted at optimum water content and loaded as-compacted was smaller than for a specimen compacted wet of optimum water content to the same relative compaction and also loaded as-compacted.
- In general, granular specimens compacted to a greater relative compaction strained less under loading than specimens compacted to a lesser relative compaction, all other factors being the same.
- Six comparisons were made regarding the effect of soil type on the loading-induced strain-stress characteristics of the two granular soils. At a relative compaction of 90%, the A1aSW was less

compressible than the FDGW. At a relative compaction of 96%, the FDGW was less compressible than the A1aSW.

- The A2SCPI10 material was significantly more compressible at 96% Standard Proctor relative compaction than the A1aSW and FDGW were at 90% Modified Proctor relative compaction. This was for specimens loaded both as-compacted and soaked. The differences were greater for specimens loaded soaked than those loaded as-compacted.
- Unfortunately, no comparisons could be made for tests conducted in the Standard Consolidometer (SC) and those conducted in the Large-Scale Consolidometer for all materials and conditions being nominally identical. However, reasonably close comparisons showed the strains in LSC tests were several times greater than the strains in the SC tests. These large differences are likely attributable to the differences in boundary constraints related to the different sizes of the specimens. (See discussion on pp. 118–119 and Figure 5.50) These results illustrate the importance of testing compacted fill materials using specimens as large as possible.
- Four trends were found with respect to wetting-induced strains — all other factors being the same:
  1. Looser granular soils collapsed more than denser soils. (No comparisons were available for the cohesive soil.
  2. Collapse increases with increasing total vertical stress at the time of wetting. Comparing the results for vertical stresses of 2 and 8 tsf, the difference in collapse for the cohesive soil was much greater for the cohesive soil than for the two granular soils.
  3. The drier the soil is at the time of wetting, the more it will collapse.
  4. For the four cases where direct comparisons are available, A1aSW collapsed more than FDGW in three of the four cases, and the collapse was essentially the same in one case.
- Estimates of loading-induced settlement resulting from strains within a 30-foot tall bridge approach embankment ranged from about 7– 18 inches. The estimated settlements for the A2SCPI10 were larger than for A1aSW and FDGW. For the two granular soils, these settlements would generally be expected to be inconsequential to the bump-at-the-bridge problem because the settlements will occur quickly during construction owing to their high permeability. For the cohesive soil, however, the settlements will occur over a much longer period of time, owing to the time-dependency of settlement in cohesive soils. Therefore, use of cohesive materials, even with low plasticity indices, could result in substantial loading-induced settlements resulting from strains within the embankment material itself.
- Estimates of wetting-induced settlement resulting from strains within a 30-foot tall bridge approach embankment ranged from about 1/14 to 1/6 in. The estimated settlements for the A2SCPI10 were larger than for A1aSW and FDGW. In addition, the wetting-induced settlement was only calculated for the A2SCPI10 compacted at or wet of optimum. If the A2SCPI10 were compacted dry of optimum, the collapse would be expected to be substantially more. Based on the results, it is concluded that if either of the two granular soils were used in the approach embankments for bridges and constructed properly, the wetting-induced settlement from strains within the embankment itself should not contribute significantly to the bump-at-the-bridge problem.

6. ANALYSIS OF CURRENT UDOT SPECIFICATIONS

6.1 Overview

The results from this research and other research on fill materials has shown that the most important characteristics for limiting both the loading and wetting-induced settlements of the fill material itself are as follows:

- Granular (cohesionless).
- Dense.
- Clean (only a small amount of fines).
- Nonplastic with little or no clay particles, particularly colloidal-sized particles (smaller than about 0.001 mm).
- Coarse-grained particles are either angular or subangular in shape.
- Well-graded.
- Mineralogy is such that the particles are hard, durable under load, and insoluble in water.
- No deleterious or degradable materials are present in the fill material, such as petroleum, chemicals, organics, sulfates (particularly gypsum), twigs or branches, non-soil construction debris, etc.

In this chapter, the current UDOT specifications for Bridge Embankment Material will be analyzed in terms of the results of this research, and recommendations for changes to the specifications will be made.

6.2 Discussion and Recommendations Regarding Current Requirements

The following discussions and recommendations are based on the UDOT *2022 Standard Specifications for Road and Bridge Construction* and are organized by topic.

6.2.1 Plasticity

The current specification for bridge embankment material (Section 02056, Part 2.2.E) requires the Plasticity Index (PI) for the fraction passing No. 40 sieve be 6 or less (to meet the requirement for an *A-1* soil). As a general example of how plastic a soil can be with a PI or 6 or less, the soil in Figure 6.1 is a sample of Untreated Base Course from SR-10 near Emery, Utah, that classified as *A-1-a* with a PI of 4. This sample was not obtained as part of this research project, but the photograph is presented to illustrate the potential plasticity of A-1 materials with a maximum allowable PI of 6. The sample was air-dry at the time of the photograph and was extremely hard and brittle but was soft and deformable when wet. This type of material is potentially susceptible to relatively large values of wetting-induced collapse, especially under high loads near the bottom of a tall embankment where wetting can easily occur. It also is potentially susceptible to swelling near the top of the embankment and to time-dependent loading-induced settlements. Therefore, it is strongly recommended that the plasticity requirement be changed to nonplastic.

A soil found to be nonplastic according to the standard tests for determining the liquid limit and plastic limit of a soil (AASHTO T 89 and T 90, ASTM D4318) does not guarantee the soil is truly nonplastic from the standpoint of engineering behavior. The primary deficiency of these tests is the use of the material passing the #40 sieve. For soils with a high percentage of material passing the #40 sieve and retained on or above the #200 sieve, the plasticity of the fines can be masked by the coarse-grained material. Most clay particles are smaller than 0.002 mm, and these clay particles are the primary cause of plasticity in a soil, so it is also recommended that a maximum percentage of this value be specified.

Colloidal-sized particles (smaller than 0.001 mm) are generally highly plastic and even small amounts in a soil can cause severe problems from both swelling and collapsed. Based on these considerations, it is recommended that at least one, but preferably both, of the following options be specified to ensure the soil is truly nonplastic:

Option 1. The criteria in AASHTO T 89 and T90 shall be used to determine if the soil is nonplastic, but the tests shall be performed using the material passing the #200 sieve rather than the #40 sieve.

Option 2. (a) % Finer than 0.002 mm ≤ 2.0, and (b) no particles finer than 0.001 mm.

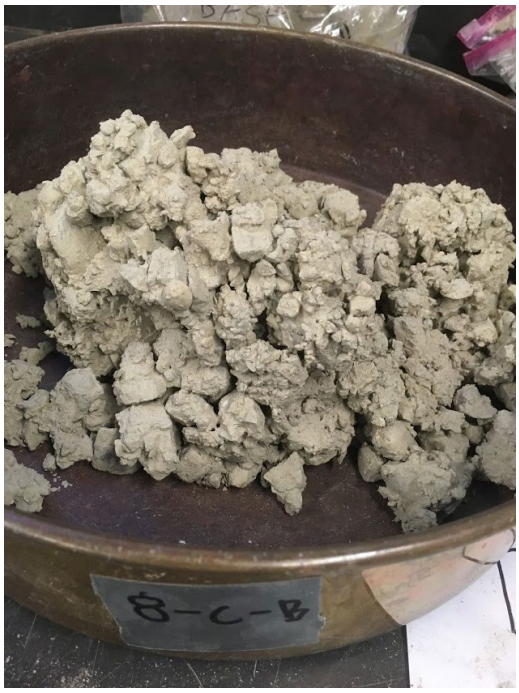

Figure 6.1 Photograph of a Sample of Untreated Base Course Material from SR-10 Near Emery, Utah

6.2.2 Maximum Particle Size and Oversize Particles

The current specifications limit the maximum particle size to three inches. This maximum size is reasonable, but it should be clearly stated in the specifications that no oversize particles shall be permitted.

6.2.3 Gradation

6.2.3.1 Introduction

A-1 materials are currently specified for *Embankment for Bridge* (Section 02056, Part 2.2.E). The required particle size distribution for A-1 soils is as follows:

% Passing No. 40 Sieve: 50 maximum (≤ 50)

% Passing No. 200 Sieve: 25 maximum (≤ 25)

Based on the results of the large-scale consolidometer tests conducted in this research project, it appears both the FDGW and A1aSW materials would work well for bridge approach embankments, and those materials meet the specifications for A-1, as summarized in Table 6.1.

Table 6.1 Comparison of A1aSW and FDGW Properties with A-1 Requirements

Material	% Passing No. 40 Sieve	% Passing No. 200 Sieve	Plasticity Index (%)
A-1	≤ 50	≤ 25	≤ 6
A1aSW	35	6	Non-plastic
FDGW	11	7	Non-plastic

It is important to note that the FDGW soil also meets the stricter requirements for an A-1-a soil, but the A1aSW does not meet either of the two requirements for A-1-a, as shown in Table 6.2.

Table 6.2 Comparison of A1aSW and FDGW Properties with A-1-a Requirements

Material	% Passing No. 10 Sieve	% Passing No. 40 Sieve	% Passing No. 200 Sieve	Plasticity Index (%)
A-1-a	≤ 50	≤ 30	≤ 15	≤ 6
A1aSW	69	35	6	Non-plastic
FDGW	13	11	7	Non-plastic

Furthermore, it is important to recognize that both soils had only small amounts of fines, were nonplastic, and reasonably well-graded from the standpoint of engineering behavior.

6.2.3.2 Amount of Fines

The current specifications allow up to 25% fines (material passing #200 sieve). In this section, the difference in strain-stress characteristics for the A-1 nonplastic soils with varying amounts of fines are analyzed. The loading-induced strain-stress characteristics will be discussed first, followed by the wetting-induced strain-stress characteristics.

The only comparisons available for nonplastic soils with varying fines content are from the tests conducted in the standard consolidometer (SC). The three nonplastic *A-1* soils from the *SC* tests and their nominal percent fines content, maximum dry unit weight, and optimum water content are summarized as follows (see Table 3.1, Table 3.2, and Figure 3.3 for additional details):

A-1-a(SW), 5% fines, γ_{dmax} = 129 pcf, w_{opt} = 10.1%
A-1-a(SM), 15% fines, γ_{dmax} = 128 pcf, w_{opt} = 10.0%
A-1-b(SM), 25% fines, γ_{dmax} = 123 pcf, w_{opt} = 12.0%

Figures can be found in Appendix B for all double-consolidometer tests conducted on these three soils for each set of compaction conditions (relative compaction and water content). The graphs for A-1-a(SW) are in Figures B.1 through B.3, for A-1-a(SM) in Figures B.8 through B.11, and for A-1-b(SM) in Figures B.16 through B.19. A review of these figures shows that for all three materials, the difference in loading-induced strains between specimens loaded as compacted, and those loaded soaked increases significantly with decreasing relative compaction, decreasing compaction water content, and increasing vertical stress. In many cases, the differences are significant, indicating high sensitivity to water.

Comparisons of the loading-induced strains for the three nonplastic *A-1* soils loaded as-compacted, 95% relative compaction, and 2% dry of optimum water content are shown in Figure 6.2. A similar graph is provided in Figure 6.3 for the same conditions except the compaction water content was at optimum. In Figure 6.4, comparisons are made for loaded as-compacted, 90 to 92% relative compaction, and 2% dry of optimum water content. In Figure 6.5, comparisons are made for loaded as-compacted, 90 to 92% relative compaction, and optimum water content. Values of loading-induced strain at a stress of 2 tsf are summarized in Table 6.3 to provide a basis for numerical comparison. At a compaction water 2% dry of optimum, the loading-induced strain at all stresses increased with increasing fines content. For compaction at optimum water content except, the strain for the specimens with 25% fines was greater than the specimens with 5% and 15% fines, but there was little difference between the specimens with 5% and 15% fines.

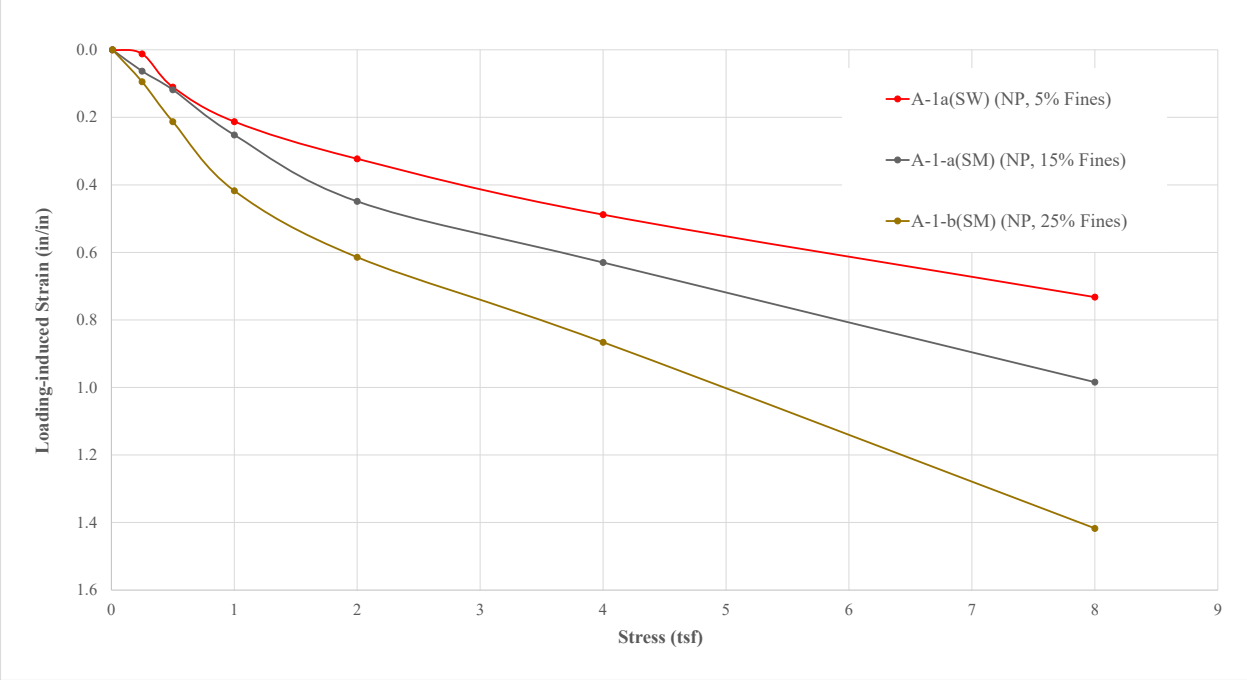

Figure 6.2 Comparison of Loading-induced Strain-stress Characteristics for Nonplastic A-1 Materials Tested in the Standard Consolidometer, Compacted to 95% Relative Compaction at a Water Content 2% Dry of Optimum, and Loaded As-compacted

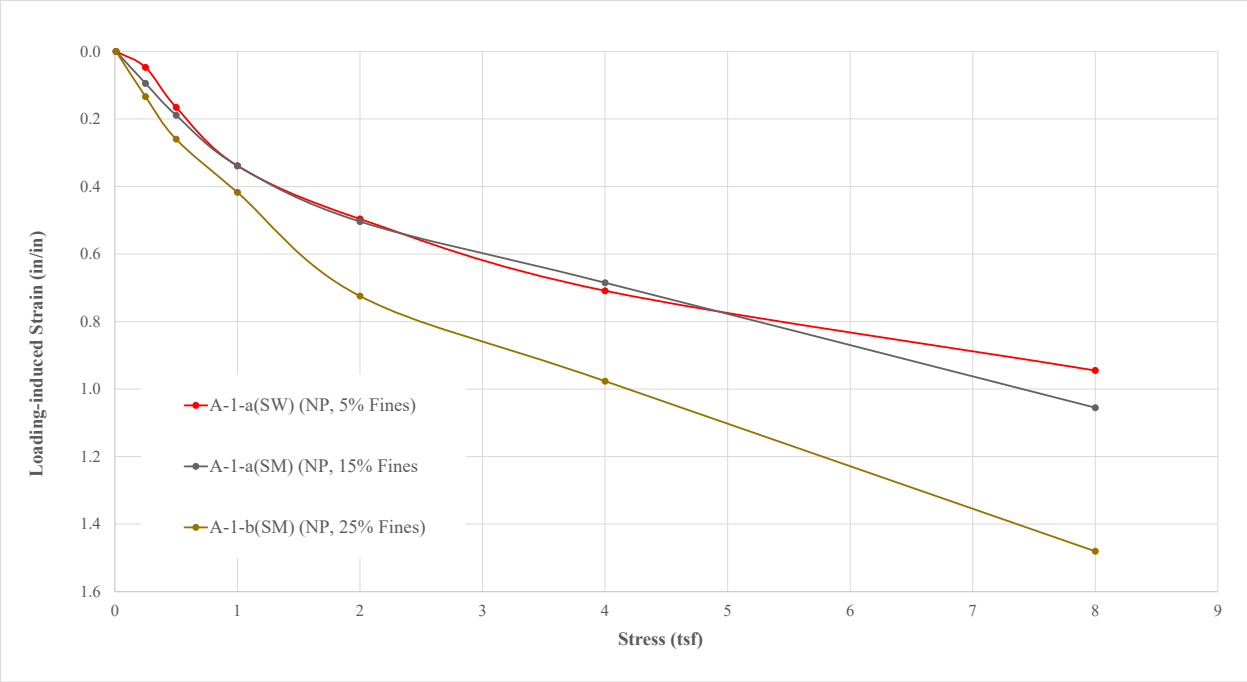

Figure 6.3 Comparison of Loading-induced Strain-stress Characteristics for Nonplastic A-1 Materials Tested in the Standard Consolidometer, Compacted to 95% Relative Compaction at Optimum Water Content, and Loaded As-compacted

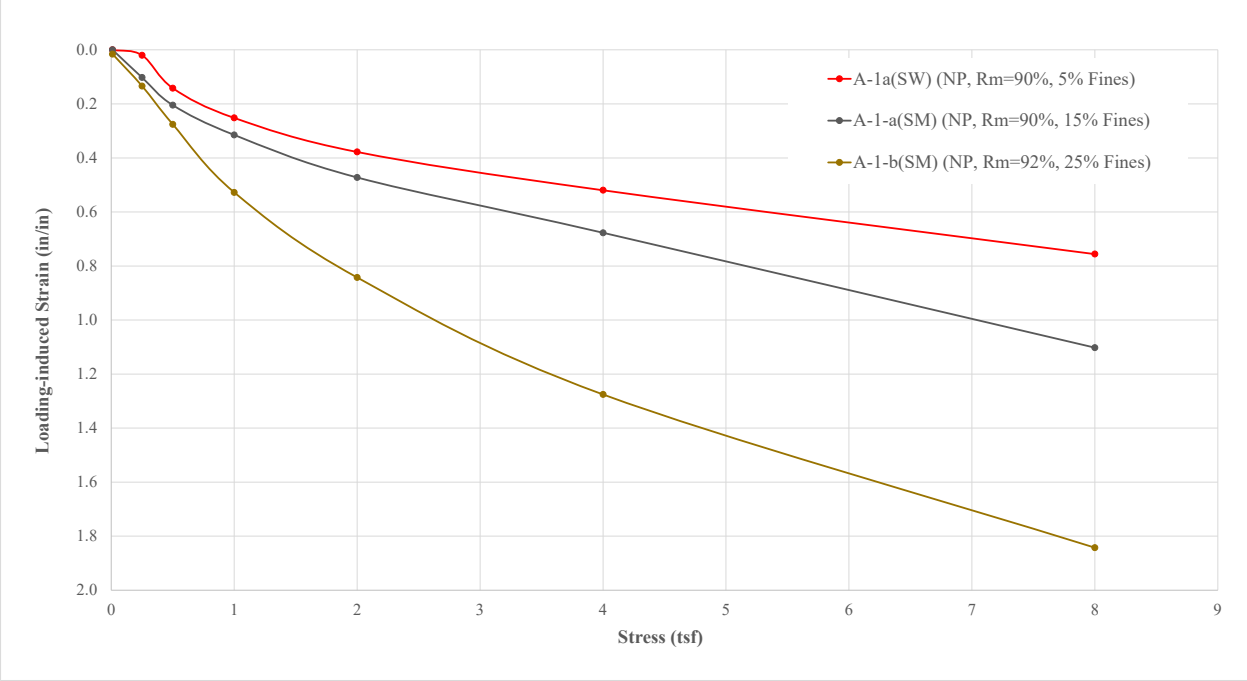

Figure 6.4 Comparison of Loading-induced Strain-stress Characteristics for Nonplastic A-1 Materials Tested in the Standard Consolidometer, Compacted to 90% or 92% Relative Compaction at a Water Content 2% Dry of Optimum, and Loaded As-compacted

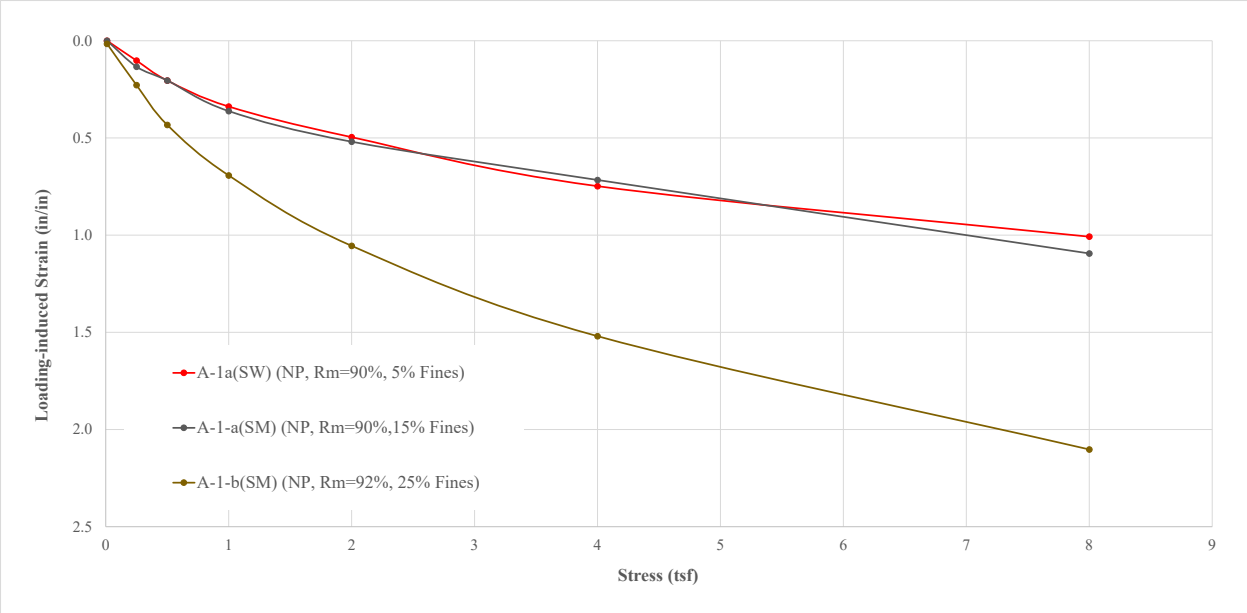

Figure 6.5 Comparison of Loading-induced Strain-stress Characteristics for Nonplastic A-1 Materials Tested in the Standard Consolidometer, Compacted to 90% or 92% Relative Compaction at Optimum Water Content, and Loaded As-compacted

Table 6.3 Comparison of Loading-induced Strain at a Stress of 2 tsf for the Nine Standard Consolidometer Tests on As-compacted Specimens Shown in Figure 6.2 through Figure 6.5

Soil	Fines (%)	Relative Compaction (%)	Water Content	Loaded Condition	Strain at Stress of 2 tsf (%)	Difference* (%)	Reference Figure
A-1-a(SW)	5	95	2% Dry	As-compacted	0.323	---	6.2
A-1-a(SM)	15	95	2% Dry	As-compacted	0.449	39	6.2
A-1-b(SM)	25	95	2% Dry	As-compacted	0.614	90	6.2
A-1-a(SW)	5	95	Optimum	As-compacted	0.496	---	6.3
A-1-a(SM)	15	95	Optimum	As-compacted	0.504	2	6.3
A-1-b(SM)	25	95	Optimum	As-compacted	0.724	46	6.3
A-1-a(SW)	5	90	2% Dry	As-compacted	0.378	---	6.4
A-1-a(SM)	15	90	2% Dry	As-compacted	0.472	25	6.4
A-1-b(SM)	25	92	2% Dry	As-compacted	0.843	123	6.4
A-1-a(SW)	5	90	Optimum	As-compacted	0.496	---	6.5
A-1-a(SM)	15	90	Optimum	As-compacted	0.520	5	6.5
A-1-b(SM)	25	92	Optimum	As-compacted	1.055	113	6.5

Similar comparisons are made in Figure 6.6 through Figure 6.9 for the same conditions, except the specimens were soaked at a small-seating load prior to loading. Numerical comparisons of loading-induced strain for these nine soaked tests are summarized in Table 6.4 at a stress level of 2 tsf. For the specimens compacted to 95% relative at a water content 2% dry of optimum (Figure 6.6), the A-1-a(SW) was the least compressible and the A-1-a(SM) the most compressible, with the exception that the A-1-a(SM) and A-1-b(SM) had essentially the same compressibility up to a stress of ½ tsf. At stresses of 1 tsf and above, the A-1-b(SM) was only slightly more compressible than the A-1-a(SW). For the specimens compacted to 95% relative at optimum water content (Figure 6.7), the A-1-b(SM) was the most compressible at all stress levels, the A-1-a(SW) was the least compressible up to a stress of about ¾ tsf, and the A-1-a(SM) was least compressible at higher stresses. However, the differences between A-1-a(SW) and A-1-a(SM) is small at all stress levels. For the specimens compacted to 90 or 92% relative compaction at a water content 2% dry of optimum (Figure 6.8), the compressibility of the A-1-a(SW) and the A-1-b(SM) was about the same at all stress levels, keeping in mind that the A-1-b(SM) was compacted to 92% compared to 90% for the A-1-a(SW). The A-1-a(SM) was most compressible at all stress levels. For the specimens compacted to 90 or 92% relative compaction at optimum water content (Figure 6.9), the A-1-a(SW) and A-1-a(SM) had nearly the same compressibility at all stress levels, while the A-1-b(SM) was about twice as compressible as the other two materials at all stress levels.

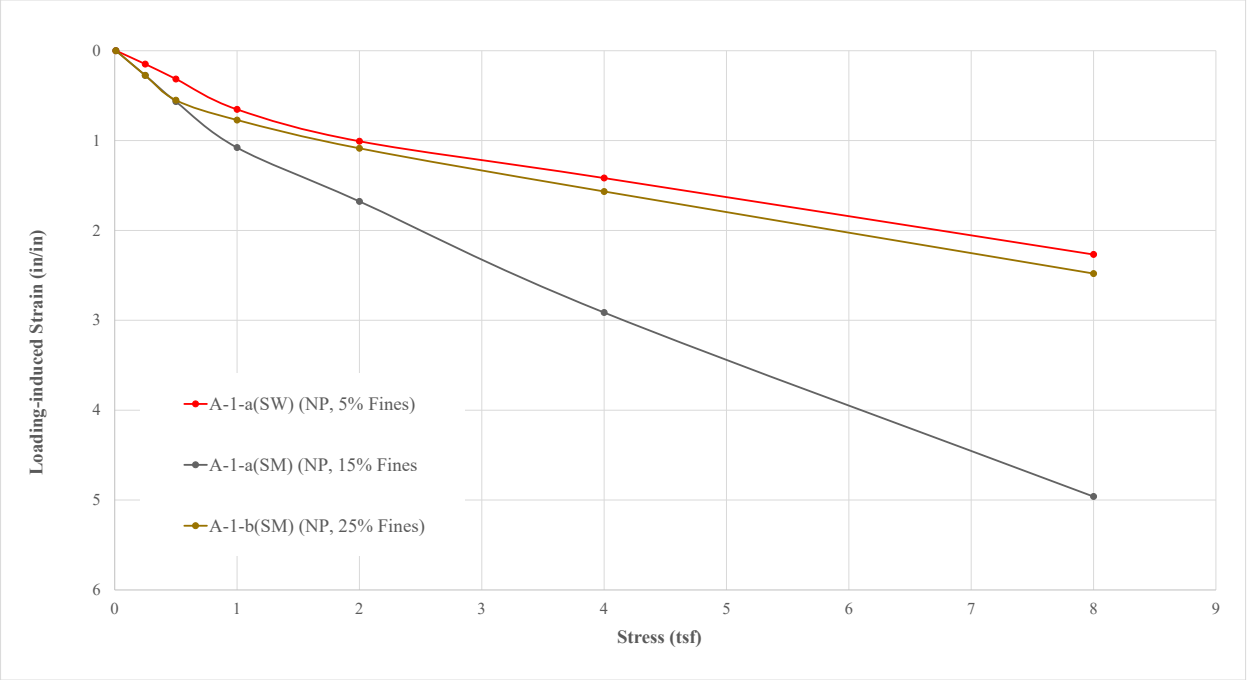

Figure 6.6 Comparison of Loading-induced Strain-stress Characteristics for Nonplastic A-1 Materials Tested in the Standard Consolidometer, Compacted to 95% Relative Compaction at a Water Content 2% Dry of Optimum, and Loaded Soaked

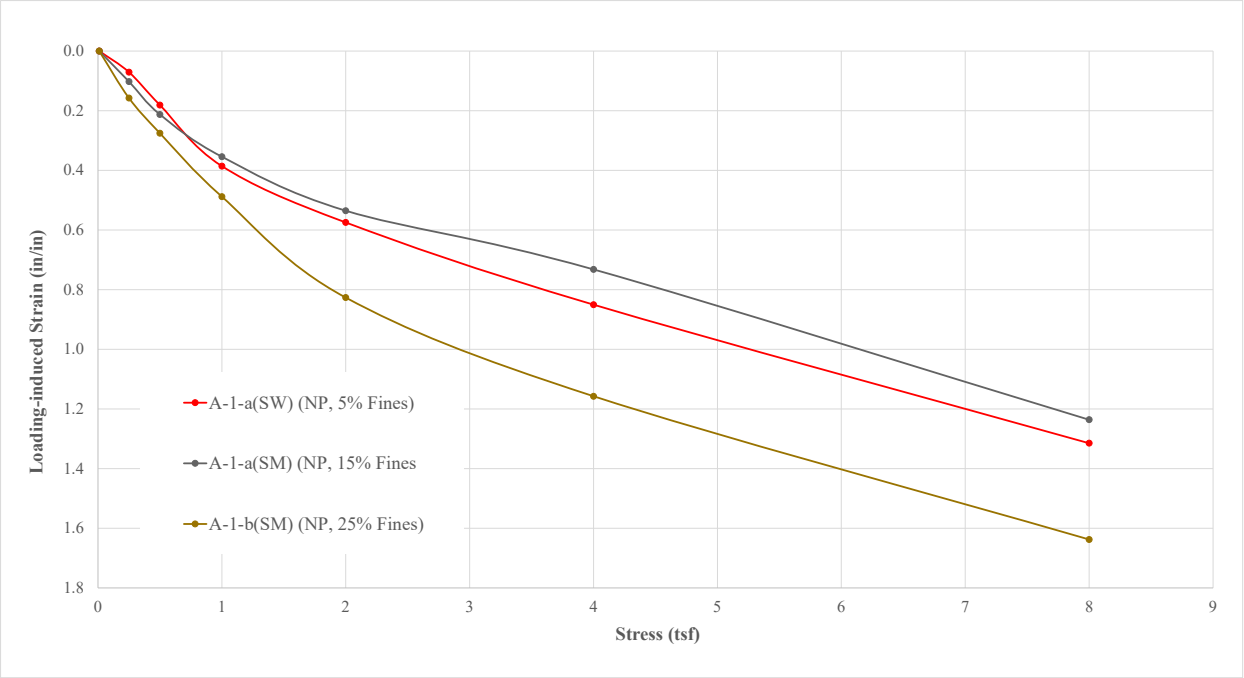

Figure 6.7 Comparison of Loading-induced Strain-stress Characteristics for Nonplastic A-1 Materials Tested in the Standard Consolidometer, Compacted to 95% Relative Compaction at Optimum Water Content, and Loaded Soaked

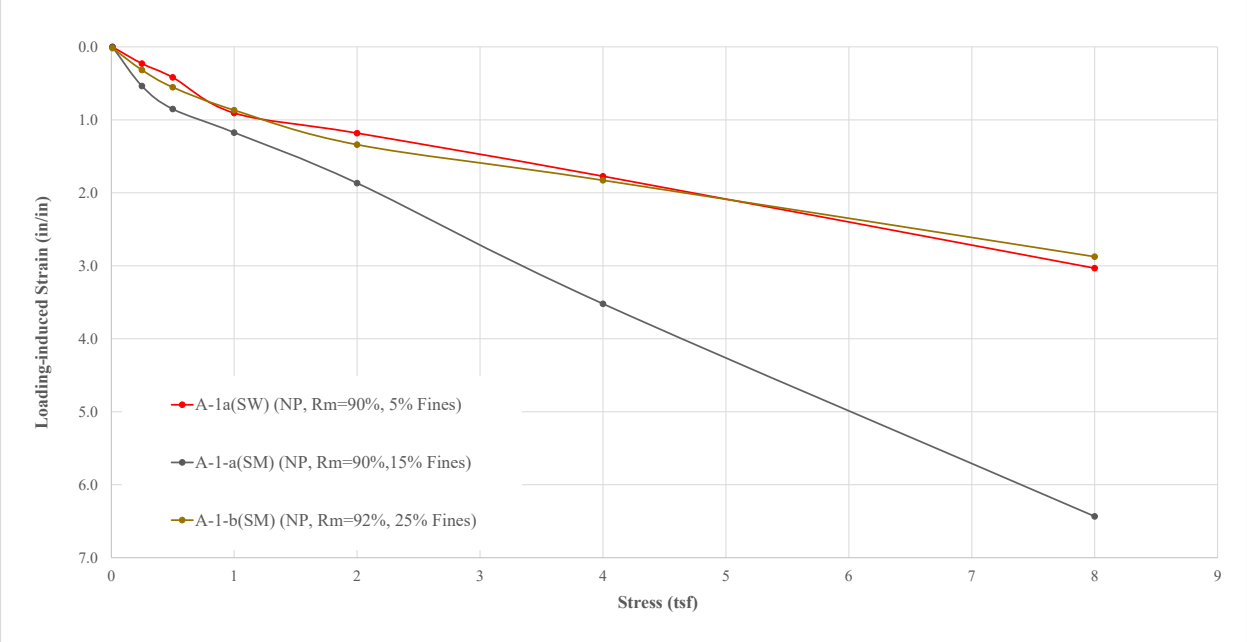

Figure 6.8 Comparison of Loading-induced Strain-stress Characteristics for Nonplastic A-1 Materials Tested in the Standard Consolidometer, Compacted to 90% or 92% Relative Compaction at a Water Content 2% Dry of Optimum, and Loaded Soaked

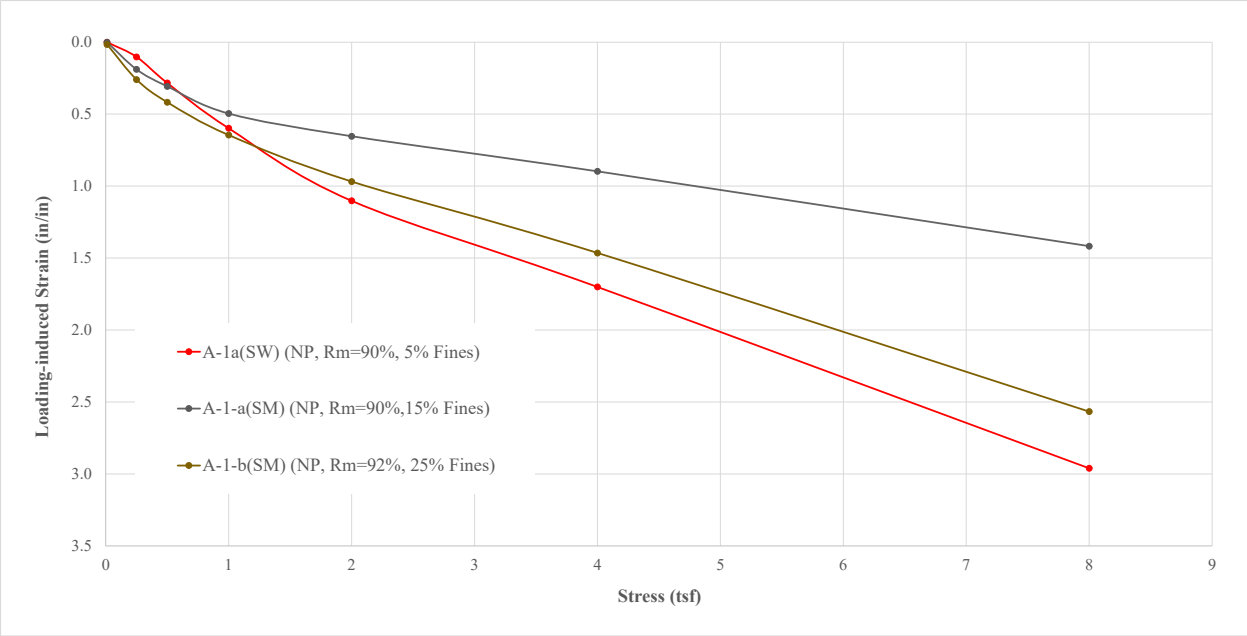

Figure 6.9 Comparison of Loading-induced Strain-stress Characteristics for Nonplastic A-1 Materials Tested in the Standard Consolidometer, Compacted to 90% or 92% Relative Compaction at Optimum Water Content, and Loaded As-compacted

Table 6.4 Comparison of Loading-induced Strain at a Stress of 2 tsf for the Nine Standard onsolidometer Tests on Soaked Specimens Shown in Figure 6.6 through Figure 6.9

Soil	Fines (%)	Relative Compaction (%)	Water Content	Loaded Condition	Strain at Stress of 2 tsf (%)	Difference* (%)	Reference Figure
A-1-a(SW)	5	95	2% Dry	Soaked	1.008	---	6.6
A-1-a(SM)	15	95	2% Dry	Soaked	1.677	66	6.6
A-1-b(SM)	25	95	2% Dry	Soaked	1.087	8	6.6
A-1-a(SW)	5	95	Optimum	Soaked	0.575	---	6.7
A-1-a(SM)	15	95	Optimum	Soaked	0.535	-7	6.7
A-1-b(SM)	25	95	Optimum	Soaked	0.827	44	6.7
A-1-a(SW)	5	90	2% Dry	Soaked	1.181	---	6.8
A-1-a(SM)	15	90	2% Dry	Soaked	1.866	58	6.8
A-1-b(SM)	25	92	2% Dry	Soaked	1.339	13	6.8
A-1-a(SW)	5	90	Optimum	Soaked	1.102	---	6.9
A-1-a(SM)	15	90	Optimum	Soaked	0.654	-41	6.9
A-1-b(SM)	25	92	Optimum	Soaked	0.969	-12	6.9

*Percent difference using the value for A-1-a(SW) as the base

Wetting-induced collapse is also a potential problem, even for *A-1* nonplastic soils. Unfortunately, in this research, no tests that directly measured wetting-induced strain were conducted on nonplastic *A-1* materials that had more than 7% fines. The only wetting-induced tests on nonplastic soil conducted in this research were (a) LSC tests conducted on specimens of FDGW and A1aSW, which contained 7.0% and 5.9% fines, respectively; and two SC tests, one on an A-1-a(SW) specimen containing 5% fines and one on an A-3(SM) specimen containing 25% fines. Therefore, the only comparison that can be made for the influence of fines on wetting-induced collapse using data from tests on this research was to compare the results from these two SC tests. The specimens in both tests were compacted at a water content 2% dry of optimum and wetted at a stress of 8 tsf. The A-1-a(SW) specimen was compacted at 90% relative compaction, while the A-3(SM) specimen was compacted to 93% relative compaction. The results of wetting-induced strain vs. time for both tests are plotted in Figure 6.10. The final values of wetting-induced strain were 3.26% for the A-1-a(SW) specimen and 12.2% for the A-3(SM) specimen. The time required for the wetting-induced strains to end was about 30 minutes for the A-1-a(SW) specimen and about 1,000 minutes for the A-3(SM) specimen. Therefore, the A-3(SM) specimen with 25% fines collapsed 3.7 times that of the A-1-a(SW) specimen, even though it was compacted to 3% greater relative compaction. The time to the end of collapse was about 33 times greater for the A-3(SM) specimen than for the A-1-a(SW) specimen.

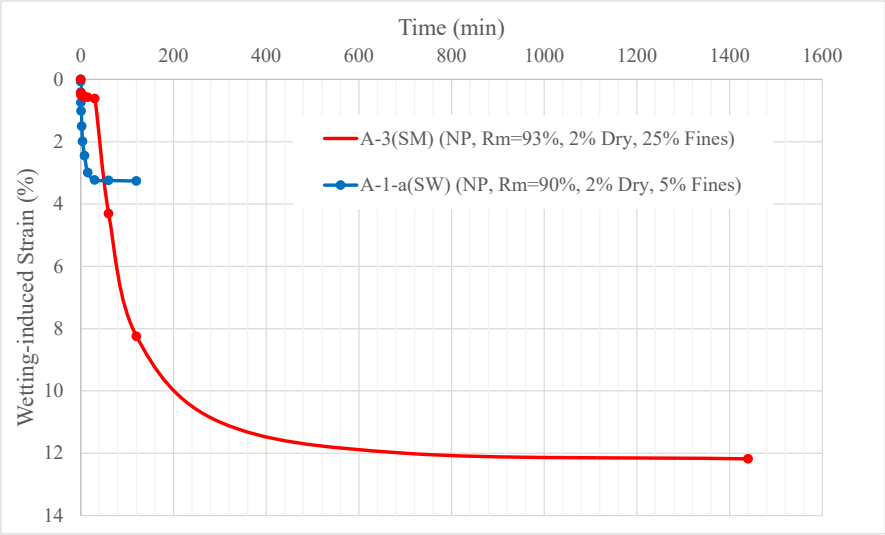

Figure 6.10 Comparison of Wetting-iInduced Strain vs. Time for an A-1-a(SW) Specimen Compacted to 90% Relative Compaction and an A-3(SM) Specimen Compacted to 93% Relative Compaction. Both Specimens were Compacted 2% Dry of Optimum and Wetted at a Stress of 8 tsf.

A search was undertaken for external references that contain information helpful in determining if nonplastic A-1 soils with up to 25% fines could have large-enough wetting-induced strains that they might contribute to the bump-at-the-bridge problem. Two papers were found that have some information on this topic, but, unfortunately, are of limited use. Alwail et al. (1992) reported results from standard consolidometer tests conducted on compacted soils with low cohesion. Noorany and Houston (1995) on both granular and cohesive soils tested in standard and large-scale consolidometers for collapse and swell potential.

Alwail et al. (1992) studied two manufactured and compacted groups of soils consisting of poorly-graded sand and silt. The sands were commercially available Ottawa sands, and the silts were natural deposited and obtained from two different sites. Double consolidometer tests were conducted to a total vertical stress of 16.7 tsf on specimens containing mixtures of sand and silt in various proportions, and collapse potential was estimated from the results of these tests. No results from soaked-after-loading (single consolidometer tests) were reported. All specimens were compacted to 90% Modified Proctor relative compaction using static compaction; however, the water content during compaction was not reported. Silt in the Group 1 soils was nonplastic with 3.0% clay-sized particles and mixed with sand with percentages of silt of 25, 35, 45, and 55. The silt in the Group 2 soils had a PI = 5 and 8.8% clay-sized particles and was mixed with sand in percentages of silt of 10, 20, and 30. Results of maximum collapse, defined as the maximum predicted collapse for any stress level, are plotted as a function of the percentage of silt for both groups of soil in Figure 6.11. For both groups of soils, the maximum collapse increased with increasing percentage of silt. The values of maximum collapse are significantly larger for the Group 2 soils (2.7 to 4.5%) than for the Group 1 soils (0.2 to 0.6%). The differences in the collapse potential for the two groups of soils were attributed to amount of clay that was present as a temporary binder and the shape of the silt grains, which were rounded to subrounded for the Group 1 silt and angular and flaky for the Group 2 silt.

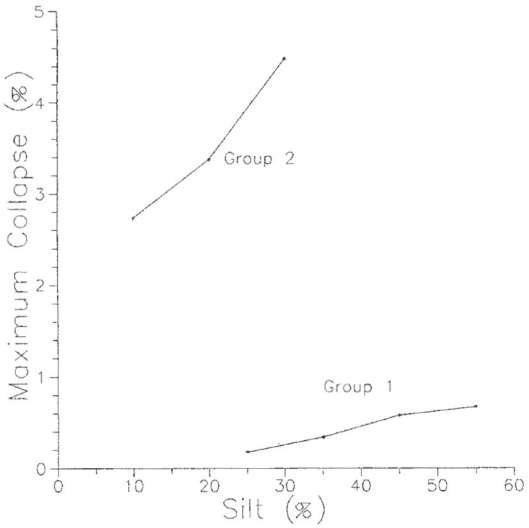

Figure 6.11 Maximum Collapse as a Function of Percent Silt from Double-oedometer Tests on Group 1 and Group 2 Soils (from Alwail et al. 1992)

Noorany and Houston (1995) conducted soaked-after-loading wetting tests in a large-scale consolidometer on seven clays, four silts, and three silty sands. The silts had PI = 4 and, therefore, were somewhat plastic. All three silty sands were nonplastic, but none met the requirements for *A-1* material. The percentage passing the #200 sieve for these three soils varied from 16 to 23%, and the percentage passing the #40 sieve varied from 57 to 73%. The grain-size distribution curves for the three soils are provided in Figure 6.12. The specimens were compacted to 90% of Modified Proctor relative compaction based on tests conducted on the material passing the #4 sieve, with the results corrected for the oversize material (larger than the #4 sieve). The water content during compaction was 2% dry of the optimum water content from the material passing the #4 sieve. At a total vertical stress of 1.04 tsf, the wetting-induced collapse strains varied from 0.1 to 0.3%. (Note: The results were only reported to one significant figure.) Assuming these values of strain at 1.04 tsf are approximately average for a 30-foot-tall embankment, a rough estimate of the wetting-induced settlement for full wetting throughout the embankment is 0.4 to 1.0 in. Although comparison with the results from the LSC tests conducted in this

project is difficult because of significant differences in stress at wetting and water content relative to optimum, it is likely the collapse potential for the soils tested by Noorany and Houston would be significantly larger than for the two granular soils tested for this project under comparable conditions. However, because the three soils tested by Noorany and Houston are not well-graded (in fact, two of them are gap-graded), it is difficult to know how much of the difference in collapse potential is due to differences in gradation and how much is due to the differences in percentage of fines.

In summary, it is apparent from the results from the SC tests conducted in this research that increasing the amount of fines results in greater loading-induced settlement and wetting-induced settlement for nonplastic granular soils loaded and wetting in the as-compacted condition. In addition, the rate at which the settlement occurs is also increased. External references also appear to confirm these findings, but the data is not conclusive. Interestingly, results from the SC tests on soaked specimens do not show a clear trend with respect to the amount of fines. However, most embankments will be constructed in the as-compacted condition, so this condition is the major consideration. Considering the results from this research and information found in other references, it is recommended that specifications be changed to limit the amount of fines to a maximum of 10%.

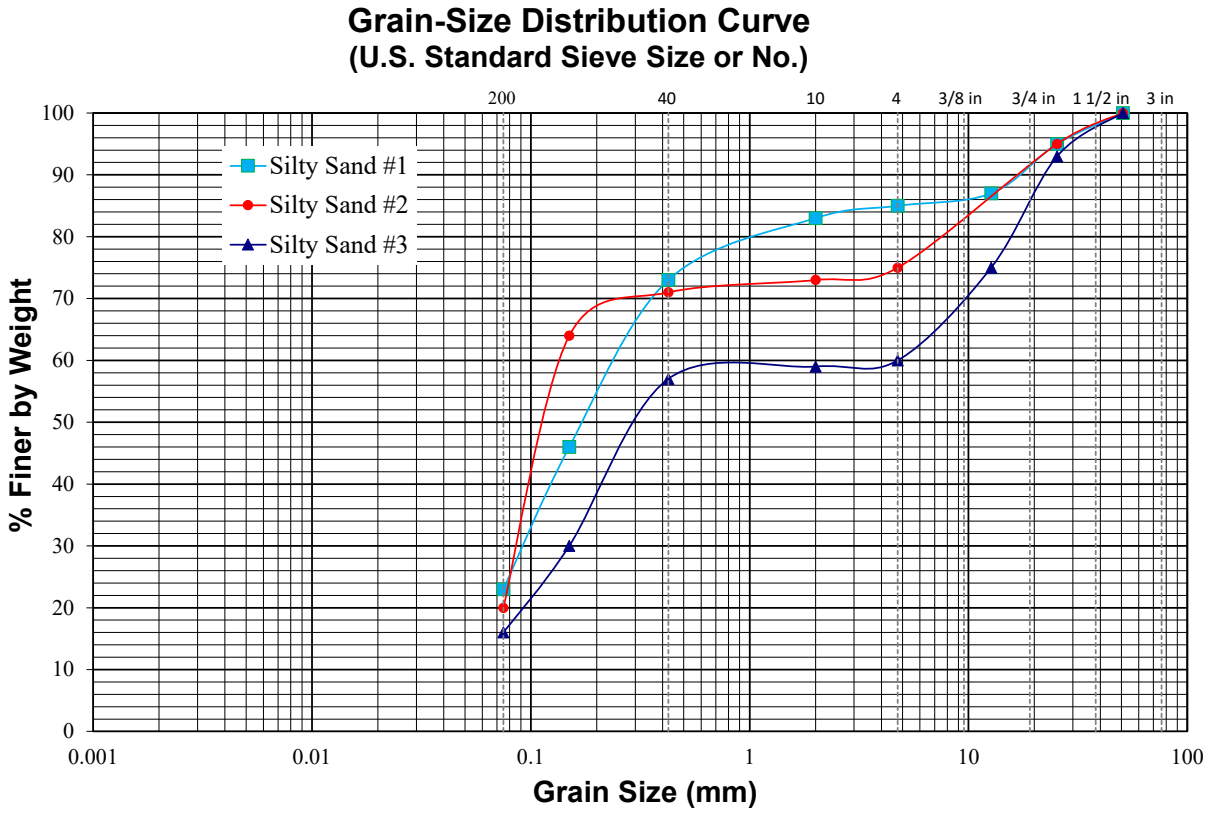

Figure 6.12 Grain-size Distribution Curves for Three Silty Sands Tested in a Large Consolidometer (Data from Noorany and Houston, 1995)

6.2.3.3 Well-graded

It is imperative that the material used for bridge approach embankments be well-graded. The definition of a well-graded material given in the UDOT standard specifications, Section 02056, Part 1.4A, is:

Material having an even distribution of different particle sizes. This even distribution of particles of different sizes results in a dense mass upon compaction.

This definition is a good general one but is too vague and cannot be easily enforced because of the lack of a metric to determine if the material has *an even distribution of different particle sizes*. For example, how even is *even*? How does one measure quantitatively the evenness of the grain-size distribution? One possible interpretation is the grain-size distribution relationship should be linear when plotted in the traditional manner of *% Finer* on the vertical axis using a linear axis vs. the logarithm to the base 10 of *Grain Size* on the horizontal axis. For a soil with grain sizes ranging between 0.1 and 10 mm, a linear grain-size distribution would have half the particles ranging in size from 0.1 to 1 mm, and the other half from 1 to 10 mm, in order of magnitude (10 times) larger.

There is no method provided in the AASHTO classification system (AASHTO M145) to determine if a soil is well-graded. However, the standard states that the typical A-1 material is a "well-graded mixture of stone fragments or gravel, coarse sand, fine sand, and a nonplastic or febbly-plastic soil binder." The method given in the Unified Soil Classification System (USCS, ASTM D2487) is based on values of the coefficient of uniformity and the coefficient of curvature, C_u and C_c, defined as follows:

$$C_u = \frac{D_{60}}{D_{10}} \quad \text{and} \quad C_c = \frac{D_{30}^2}{D_{10} \cdot D_{60}}$$

The following criteria must be met for a soil to be classified as well-graded, according to the USCS:

More gravel than sand: $C_u \geq 4.0$ and $1.0 \leq C_c \leq 3.0$

More sand than gravel or equal amounts: $C_u \geq 6.0$ and $1.0 \leq C_c \leq 3.0$

To provide further insight into the well-graded characteristics a soil needs as fill material to be resistant to both loading and wetting-induced strains, the grain-size distribution curves for five soils deemed to have these characteristics are plotted in Figure 6.13. Three of the five soils are from this research [A-1-a(SW), A1aSW, FDGW] and two are from an ongoing roadway project used for the Granular Borrow (GB) and Untreated Base Course (UTBC) in the section of the roadway where the first and third authors installed instrumentation within these materials. All five soils are nonplastic. Both of these roadway materials were stiff and strong when compacted properly, as evidenced by the effort required to dig into these materials and from Dynamic Cone Penetrometer and Plate Load tests conducted on these materials. All five of these soils are nonplastic. Also shown on the figure are the three points representing the current upper and lower limits for Bridge Approach Embankment material and two curves representing theoretically perfectly well-graded materials, where the grain-size distribution relationship would be a straight line when plotted with horizontal axis on a linear scale, rather than the traditional logarithmic scale.

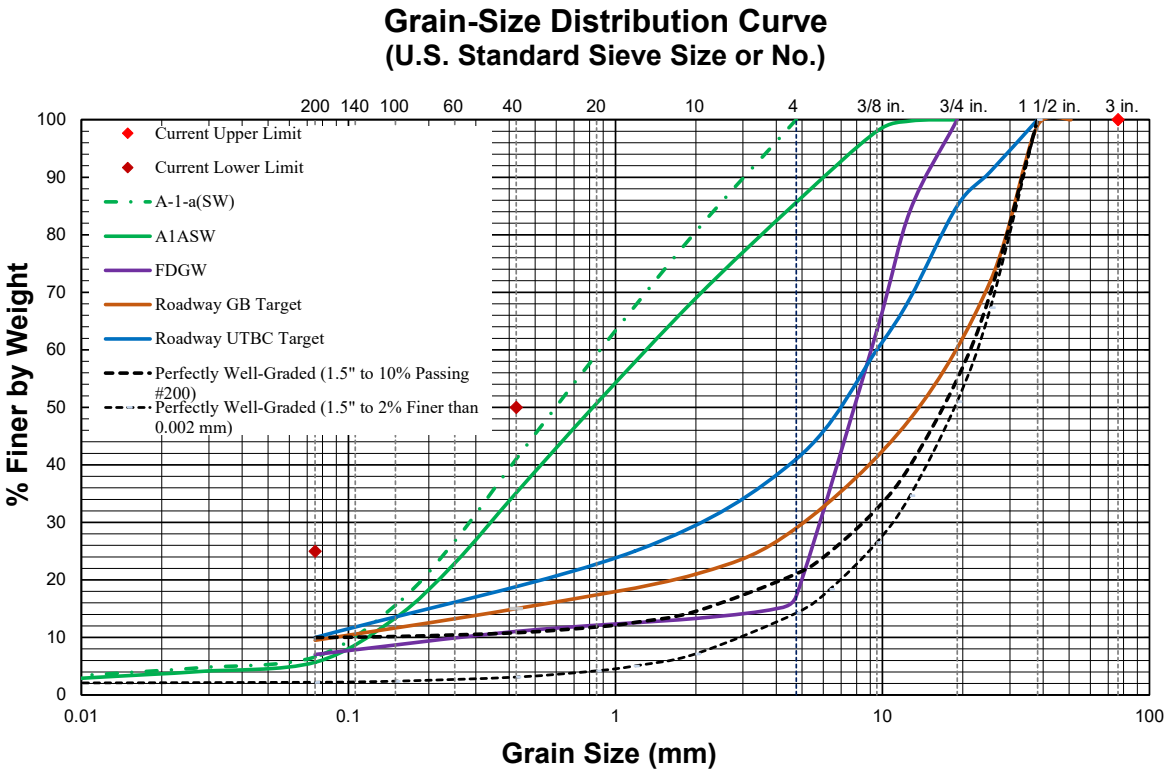

Figure 6.13 Comparison of Grain-size Distribution Curves for Five Nonplastic Granular Soils, Current Specifications for Bridge Approach Embankment, and Two Perfectly Well-graded Soils

The curves for four of the five real soils shown in Figure 6.13 are concave downward for the larger-sized particles, transitioning to concave upward for the smaller-sized particles. The only exception is the curve for Roadway GB, which is entirely concave upward. Almost all introductory geotechnical engineering textbooks and references books show a well-graded soil as having a grain-size distribution curve that is concave downward for the larger-sized particles, transitioning to concave upward for the smaller-sized particles. For example, the figure from the introductory textbook by Holtz, Kovacs, and Sheahan (2011) illustrating the general shape of a well-graded soil is shown in Figure 6.14.

Of the two curves for perfectly well-graded soils, the upper one on Figure 6.13 (thicker black line with longer dashes), was drawn to show the perfect gradation for a soil with all material passing the 1½-inch sieve and 10% fines (passing #200 sieve). This curve would be the perfect gradation for the coarse-grained portion of the Roadway UTBC, and both curves have a similar shape, thus indicating that a curve with a strong concave upward shape in the coarse-grained region is closer to being perfectly well-graded than one with a concave downward shape in that region. However, the curve is nearly horizontal as it approaches the size of the #200 sieve and indicates 9.82% colloids (≤ 0.001 mm) would be required to maintain the perfect shape. This large percentage of colloids would clearly be unacceptable as a material for a bridge approach embankment, as discussed previously. The lower perfect curve is for all material passing the 1½ -inch sieve transitioning to 0 percent finer than 0.001 mm (no colloids). However, these criteria result in 0.19% fines, which would essentially be the same as requiring no fines. Therefore, it is clear that specifying a perfect grain-size distribution would not necessarily result in a material appropriate for a bridge approach embankment.

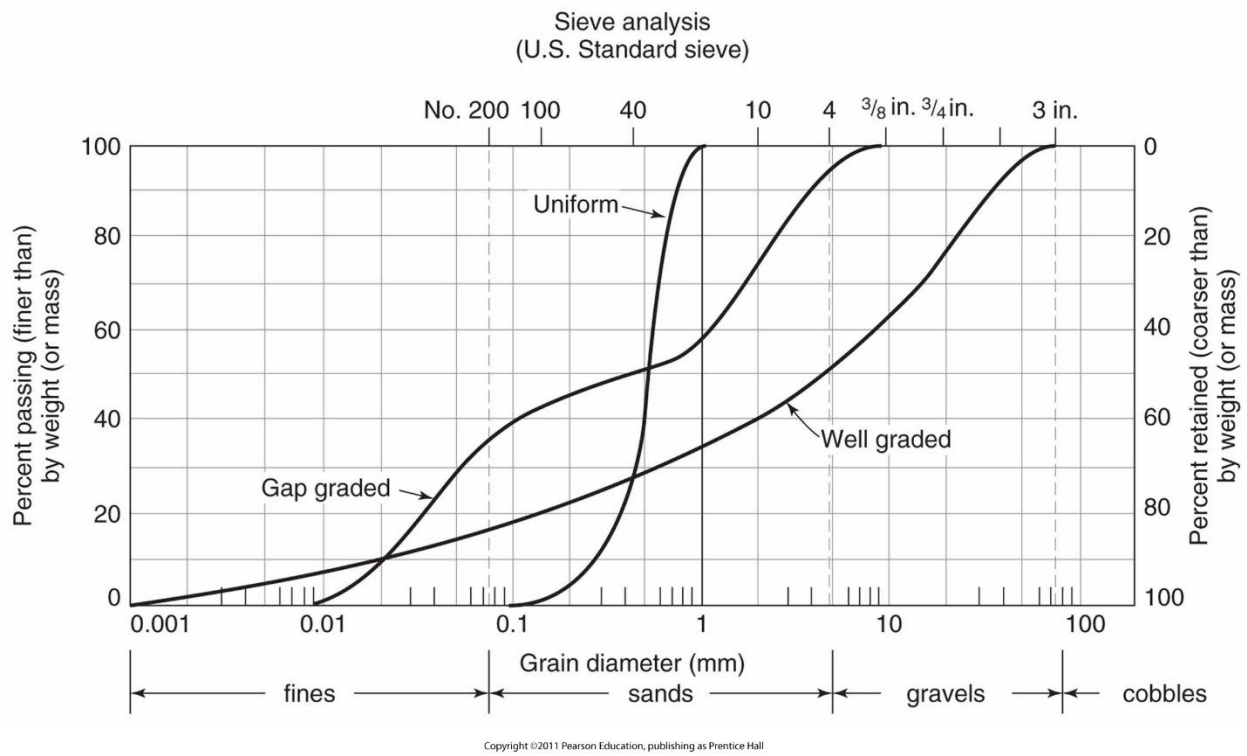

Figure 6.14 Figure Illustrating the Shape of Well-graded, Poorly-graded, and Gap-graded Grain-size Distribution Curves (from Holtz, Kovacs, and Sheahan 2011)

Values of percent sand, percent gravel, D_{10}, D_{30}, D_{60}, C_c, and C_u, are presented in Table 6.5 for the five real soils, the two perfectly well-graded soils shown in Figure 6.13, and a well-graded soil from an introductory textbook for geotechnical engineering. Of the eight soils, only the well-graded soil from the textbook would be classified as well-graded, according to the USCS. All eight soils meet the criterion based on C_u, but only the textbook soil meets the criterion for C_c. Note the shape of the textbook soil is slightly concave upward throughout the region from D_{10} to D_{60}, where the determination of well-graded vs. poorly graded is done using the USCS and the value of C_c is near the center of the range needed to be well-graded.

Table 6.5 Determination of Gradation According to the Unified Soil Classification System for Eight Soils

Soil	USCS % Sand	USCS %Gravel	D_{10} (mm)	D_{30} (mm)	D_{60} (mm)	C_u	$C_u \geq 4.0$ or 6.0?	C_c	$1.0 \leq C_c \leq 3.0$?	USCS Well-graded?	D_{90} (mm)	D_{90} / D_{10}
A-1-a(SW)	93	0	0.11	0.28	0.88	8	YES	0.81	NO	NO	3.0	27
A1aSW	80	14	0.13	0.34	1.3	10	YES	0.68	NO	NO	6.0	46
FDGW	10	83	0.25	7.9	14	56	YES	18	NO	NO	14	56
Roadway GB	19	71	0.084	5.0	19.1	227	YES	16	NO	NO	33	393
Roadway UTBC	31	59	0.075	2.10	9.53	127	YES	6.2	NO	NO	24	320
Perfectly Well-Graded - 10% Passing #200	11	79	0.075	17.0	42.4	565	YES	91	NO	NO	33.88	452
Perfectly Well-Graded - 2% Finer than 0.002 mm	12	88	3.811	8.53	21.2	6	YES	1	NO	NO	34.29	9
HKS 2011 Well-Graded	34	49	0.020	0.57	8.4	420	YES	1.9	YES	YES	35	1750

A detailed analysis of these criteria for this research project showed the criteria for C_u were reasonable, but the criterion for C_c was too strict because C_c is sensitive to small changes in gradation. Furthermore, both criteria are based on a limited range of particle sizes representing only half of the material (from D_{10} to D_{60}). Values of D_{90} and D_{90}/D_{10} are also shown in Table 6.5 for the eight soils. The values of D_{90}/D_{10} for the first five soils in Table 6.5 range from 27 to 393. Use of D_{90}/D_{10} as a coefficient of uniformity is preferred over D_{60}/D_{10} because it represents 80% of the material, rather than the 50% represented by D_{60}/D_{10}.

Potential segregation of the granular borrow material during processing, transport, and compaction is related to the grain-size distribution and water content of the material. Consideration of the grain-size distribution will be provided here, and consideration of the water content will be discussed in Section 6.2.6. Segregation has been defined in different ways in literature, with the following definition provided by FEMA (2011): "The tendency of particles of the same size in a given mass of aggregate to gather together whenever the material is being loaded, transported, or otherwise disturbed." A significant amount of research has been conducted on this topic relative to the use of granular soils as filters, particularly for earthen dams. A good review of proposed requirements for mitigating segregation is provided by Rönnqvist et al. (2020). However, it is important to note the main criteria for filter design (retention of base particles and free flow of the water through the filter without build-up of excess pore water pressures) are substantially different than for approach embankments for bridges (adequate stiffness under loading and wetting).

With respect to grain-size distribution, the potential for segregation increases with increasing range in particle sizes. Several grain-size criteria have been proposed to mitigate the problem of segregation. USDA (1994) and FEMA (2011) recommended the guidelines for D_{90} based on D_{10} given in Table 6.6. Sherard et al. (1984) suggested limiting the material greater than the No. 4 sieve (4.75 mm) to no more than 60% and the maximum particle size to 2 inches. Ripley (1984, 1986) advocated limiting the material greater than the No. 4 sieve to no more than 40%, the maximum particle size to ¾ inch, and D_{100}/D_{10} to a maximum of six inches. Milligan (1999, 2003) showed a graphical boundary in grain-size distribution space delineating materials that will not segregate when wetted and those that will (Figure 6.15).

It is clear from the discussions above that the requirements for preventing or substantially mitigating segregation of the borrow materials during processing, transport, and compaction based strictly on grain-size distribution are in contrast to those for limiting loading and wetting-induced settlements. Because the general consensus within the literature is that segregation can be significantly controlled through moisture control (see Section 6.2.6), the recommendations provided below regarding modifications to the grain-size requirements are based on limiting loading and wetting-induced settlements.

Table 6.6 Segregation Criteria for D_{90} Based on D_{10} (from USDA 1994)

If D_{10} is :	Then maximum D_{90} is:
(mm)	(mm)
< 0.5	20
0.5 – 1.0	25
1.0 – 2.0	30
2.0 – 5.0	40
5.0 – 10	50
> 10	60

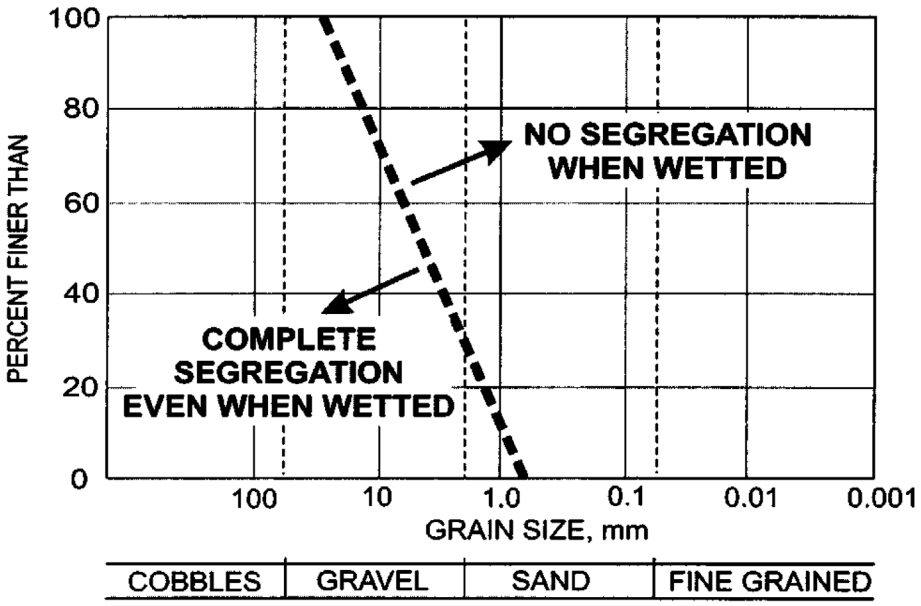

Figure 6.15 Proposed Grain-size Distribution Boundary Separating Materials that Will Not Segregate When Wetted and Those that Will Segregate (from Milligan 2003)

It is recommended that the following changes be made to the specifications to ensure that the material used for bridge approach embankments is well-graded based on engineering behavior:

- The definition of a well-graded material given in Section 02056, Part 1.4A be modified as follows (changes shown in red):

Well-graded material — Material having an even distribution of different particle sizes with no gaps in size. This even distribution of particles of different sizes results in a dense mass upon compaction. When the grain-size data is plotted in the traditional manner of % Finer by Dry Weight on a linear scale vs. Grain Size (Diameter) on a logarithmic scale (logarithm to the base 10), the best-fit curve drawn through the data points shall be continuous and smooth without any abrupt changes. Several examples of acceptable grain-size distribution curves are shown in Figure 6.16.

- Add the following specification: The ratio D_{90}/D_{10} shall be at least 25, where D_{90} is the particle diameter for which 90% of the material is finer by dry weight, and D_{10} is the particle diameter for which 10% of the material is finer by dry weight.

6.2.4 Relative Compaction

Current relative compaction requirement for *Embankment for Bridge* (Section 02056, Part 3.1.F.1.a) is an average value of 96% based on Modified Proctor (AASHTO T 180) with no single determination lower than 92%. It is recommended that these requirements be kept with one additional requirement: *A maximum of 20% of the tested material shall have a value less than 94%.*

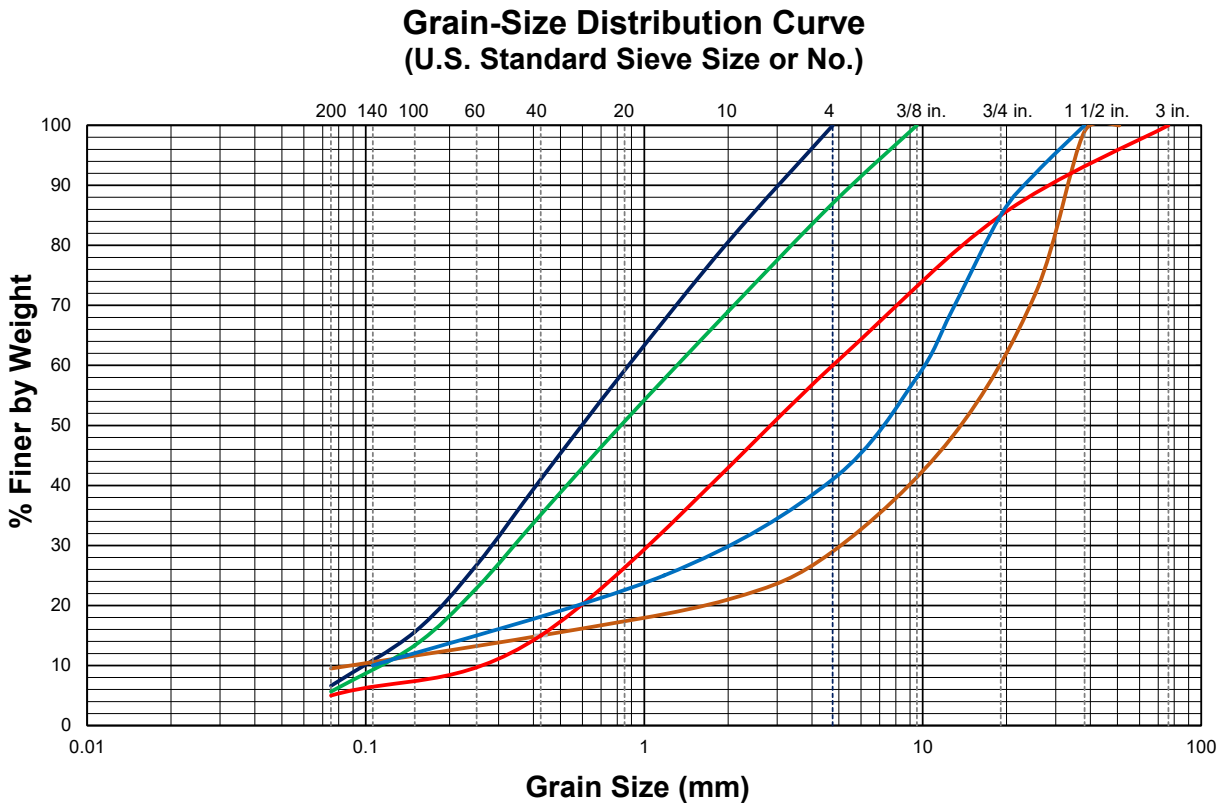

Figure 6.16 Examples of Acceptable Grain-Size Distribution Curves

Historically and currently, other methods have been used to ensure that compacted granular fill has the desired engineering properties. The most common methods include Plate Load Test (ASTM D1195, D1196), Dynamic Cone Penetrometer (ASTM D7380), Cone Penetration Test (CPT, ASTM D5778), Standard Penetration Test (SPT, ASTM D1586), and California Bearing Ratio (CBR, ASTM D4429). Of these methods, only plate-load and CBR tests provide direct measurement of strength and stiffness. However, the CBR test would not provide evaluation to the full depth of a 9- or 10-inch lift that would result from the maximum loose lift thickness of 12 inches. The plate-load test has the following advantages over typical Proctor-type specification and testing:

- The stiffness and strength of the compacted soil are evaluated directly.
- No laboratory testing is required.
- The test is suitable for a wide range of soil types and maximum particle sizes.

According to Hausmann (1990), once it is established as a routine test, it can be conducted rapidly at low cost. There are at least two companies that now have automated equipment to do rapid, cyclic plate-load tests. In addition, the test can be done manually using standard equipment some geotechnical and/or materials testing companies have readily available. Hausmann also indicated it was not uncommon in Europe at that time to have compaction specified in terms of the second loading modulus (first reload modulus) determined from the plate-load test. The specification for modulus can be in terms of either the Modulus of Subgrade Reaction, k_s (commonly known as the Subgrade Modulus) or the Modulus of Elasticity, E (commonly known as Young's Modulus), as calculated from the following equations:

$$k_s = \frac{q_b}{S} \quad (6.1)$$

$$E_0 = \frac{q_b \cdot B \cdot I_s \cdot I_z \cdot I_r \cdot I_e \cdot (1-\nu^2)}{S_{center}} \quad (6.2)$$

where E_0 is the Young's modulus at the bearing level, q_b is the average bearing pressure applied by the plate to the ground, S is the settlement for a specified range in stress (for example, 0 to 100 psi), S_{center} is the settlement at the center of the plate, B is the width of the plate, I_s accounts for the shape of the plate, I_z accounts for the change in modulus with depth, I_r accounts for the rigidity of the plate, I_e accounts for embedment of the plate below the ground surface, and ν is Poisson's ratio for the soil. Mayne and Poulos (1999) provide details to determine the influence factors for circular foundations. When plate-load tests are used for compaction control, usually a rigid circular plate (or series of plates) is used ($I_r = \pi/4$), the plate bears on the ground surface (no embedment, $I_e = 1$), and the modulus of the soil is assumed to be constant within the zone of influence ($I_z = 1$). For these conditions, Eq. 6.2 reduces to:

$$E = \frac{q_b \cdot d}{S} \cdot \frac{\pi}{4} \cdot (1 - \nu^2) \quad (6.3)$$

where d is the diameter of the loading plate. Eq. 6.3 is the well-known equation for a perfectly rigid circular foundation subjected to a centric, vertical load bearing on the surface of an elastic half-space, which has been rearranged to solve for E.

k_s and E each have advantages and disadvantages for use in compaction control. The equation for k_s is simpler and both parameters can be determined directly from measurements during the test. However, k_s varies as a function of the size of the plate. This variation could be avoided if the specifications require the use of one size plate. If E is used, ν must either be estimated or some type of testing performed to determine its value. Unfortunately, the value of ν varies depending on the stress level and the boundary conditions of the soil during loading, so performing tests to obtain reliable values of ν are difficult and expensive. ν can also be estimated from information provided in the open literature, but the values given in different references can vary significantly. Mayne and Poulos stated that values of ν for all soil types under drained loading vary between 0.1 and 0.2, significantly less than the range of values from 0.25 to 0.45 that are typically reported in the literature. Hausmann provided typical minimum required values of E as about 2500 ksf for a surface course, 1250 ksf for a base course, and 950 ksf for a subgrade. The diameter or width of the plate should be approximately equal to the thickness of the fill over which k_s or E is being determined.

It is recommended that UDOT consider using a type of test that directly measures the stiffness of the soil, such as the plate-load test, as a replacement for the Proctor-type tests for quality control and assurance of bridge approach embankments. This change would not be easy and would likely take several years or more for the transition since the Proctor-type tests have been used as the standard for many decades within the construction industry in the United States. One possible way to determine the viability of this change would be to require a certain number of plate-load or similar tests on every lift (or every other lift) for each new bridge approach embankment that is constructed. A database could be developed in which dry unit weights and relative compaction are compared with k_s and E determined from the plate-load or similar tests. Other parameters that could be included in the database include grain-size distribution data (which could be used to calculate parameters such as percent fines, percent sand, percent gravel, D_{10}, D_{30}, D_{60}, D_{90}), characteristics of the coarse-grained particles (shape, elongation, mineralogy) and some type of qualitative or quantitative measure of the performance of the bridge approach embankment. This information could be used to determine appropriate values of either k_s or E and, potentially, make changes to the specifications regarding some of the other parameters.

6.2.5 Characteristics of Particles

Currently, there are no requirements in Section 02056 regarding the characteristics of the particles (aggregates). It is recommended that the following requirements provided in Part 2.1 of Section 02721 [Untreated Base Course (UTBC)], which have been modified slightly, be adopted by direct inclusion in Section 02056:

All bridge embankment material shall be hard, tough, durable, nonplastic, and sound mineral particles that are insoluble in water and free of organic matter and contamination from chemical or petroleum products, with a dry rodded unit weight of 75 pcf or greater (AASHTO T 19), and an aggregate wear of 50% or less (AASHTO T 96). In addition, at least 50% of the coarse grained material (retained on the #200 sieve) shall be (a) naturally angular or subangular in shape, as shown in Figure 6.17, (b) crushed with at least two fractured faces, or (c) a combination of *a* and *b*.

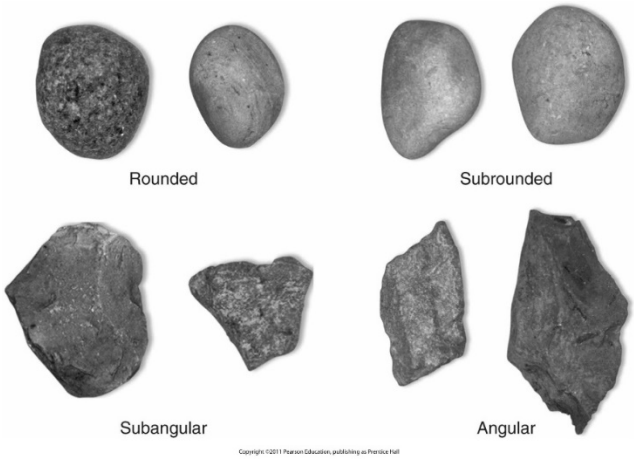

Figure 6.17 Typical Shapes of Coarse-grained Bulky Particles (from Holtz, Kovacs, and Sheahan 2011)

6.2.6 Moisture Condition During Processing, Transport, and Compaction

Prior research on the segregation of granular soils has shown some granular materials are susceptible to segregation, regardless of moisture content, while others are susceptible when dry but not when wet. In general, segregation is almost unavoidable in dry cohesionless coarse-grained materials; segregation is almost completely inhibited in soils containing a significant amount of sand; and water has little influence on the segregation behavior of gravels (Milligan 2003).

Milligan (1999) provided a "very approximate gradation limit" separating materials that will not segregate when wetted from those for which complete segregation will occur even when wetted. A graph showing Milligan's gradation limit has been provided previously in Figure 6.15. Sutherland (2002) proposed a range of gradations for materials that are highly susceptible to segregation. Milligan's and Sutherland's gradation limits are shown in Figure 6.18, with the proposed acceptable grain-size distribution curves provided previously in Figure 6.16. All acceptable curves either fall entirely outside the range for materials that are highly susceptible to segregation or with only small parts falling within the range, suggesting all these acceptable materials would probably not be highly susceptible to segregation. The two soils with steep curves within the coarser material (blue and orange) fall primarily on the coarser side of Milligan's line, suggesting they would probably segregate in the field even if wetted, but that the degree of segregation would not likely be significant. Curves for the remaining three materials fall either

completely on the finer side of the Milligan line (blue and green) or mostly on the finer side (red), indicating segregation could be controlled in these materials by keeping them wetted.

Rönnqvist et al. (2020) performed research on a sand-gravel material sourced from crushed rock to determine the moisture condition necessary to limit segregation in a material with a grain-size distribution that falls entirely on the finer side of the Milligan line. The susceptibility of this material to segregation was evaluated using an inclined plane sloping onto a horizontal surface at the angle of repose for the material prepared at seven different water contents. From these tests, they concluded acceptable resistance to segregation for this material was achieved at a water content of 30% of Modified Proctor optimum water content and there was practically no segregation when the water content was near optimum.

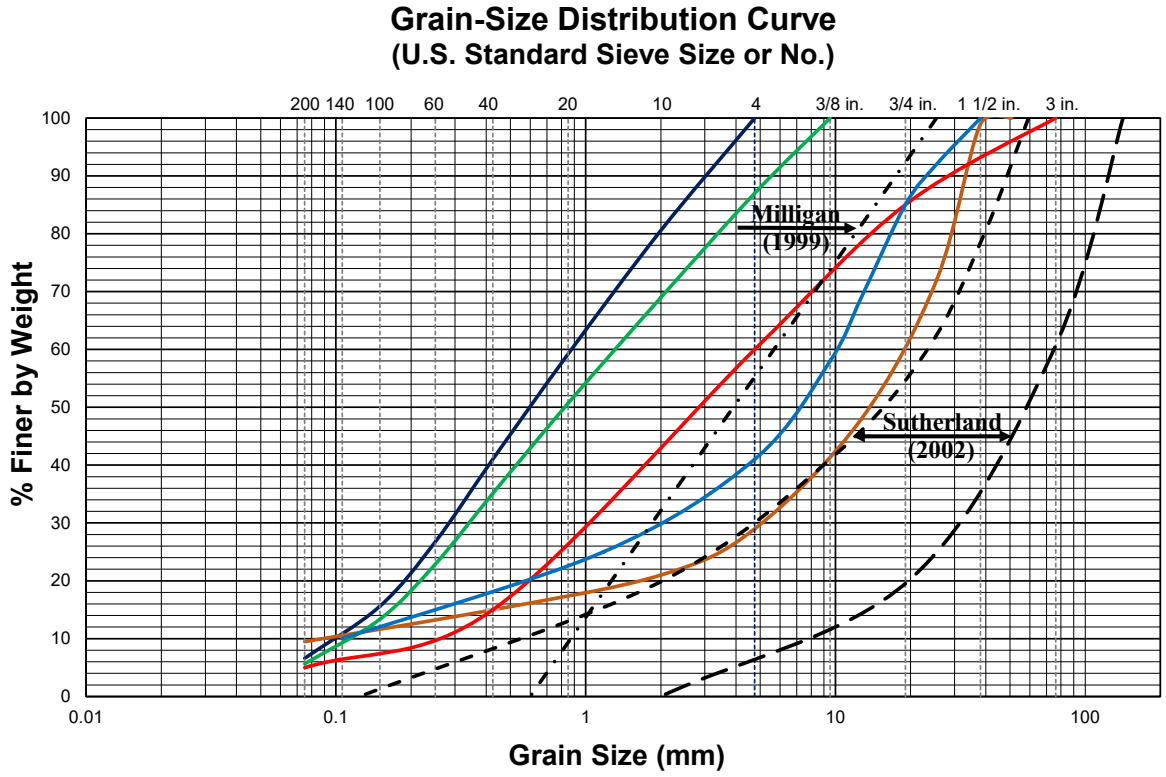

Figure 6.18 Comparison of Acceptable Grain-size Distribution Curves with Gradation Limits Proposed by Milligan (1999) and Sutherland (2002)

The current specification simply states that appropriate moisture for compaction be maintained during processing (Section 02056, Part 3.1.F.1.a.2). It is recommended that the following sentence be added to this specification to minimize the amount of segregation that will occur prior to and during compaction:

In particular, it is imperative that the on-site stockpiled material and material during hauling, spreading, and compaction be kept at a sufficient moisture content to prevent separation and segregation of the different-sized particles.

6.2.7 Maximum Lift (Layer) Thickness

The current maximum allowable loose lift thickness of 1 foot (Section 02056, Part 3.5C) is appropriate and should be retained.

6.2.8 Compaction During Freezing or Snowy Conditions

Part 3.1.B of Section 02056 addresses the issue of placing embankment material during freezing or snowy conditions, which is allowed, except that embankment cannot be constructed on frozen or snow-covered areas. Furthermore, the use of frozen borrow material is prohibited.

The problems associated with allowing compaction during freezing weather are three-fold:

1. Achieving a density of 96% of Modified Proctor maximum dry unit weight is a moderately difficult task under good conditions. As shown in Figure 6.19, at temperatures below freezing, less densification is achieved with the same amount of compactive effort (energy per volume of material). Therefore, more effort is required to achieve the required average relative compaction of 96%, increasing the likelihood of large contiguous zones of material below the average value, even if the overall average of the embankment is 96%.
2. All borrow material will have some water in it, especially during cold weather. The inevitable result is that clumps of borrow material will freeze together, resulting in inhomogeneous embankment material that may not have the desired engineering properties. This result is why the specifications state frozen material should not be delivered or used. Therefore, it does not make sense to allow compaction during freezing weather.
3. The interior portions of a large fill constructed during freezing weather may take many months or years to thaw. Since water decreases in volume when it thaws (changes from solid to liquid), the result will likely be some settlement of those frozen zones when they thaw, especially if the borrow material had a high water content at the time of compaction. Furthermore, the thawing results in higher water content and, therefore, somewhat greater compressibility of the material, which may also result in settlement.

Based on these considerations, it is strongly recommended that compaction of bridge embankment materials not be allowed in air temperatures less than 34°F. Compaction during snowy conditions where the temperatures are 34°F or higher should be fine, as long as the snow does not accumulate. Hence, the current specification of prohibiting compaction in snow-covered areas is acceptable if it is clarified that compaction must stop if it is snowing and the snow starts accumulating on the surface of the embankment.

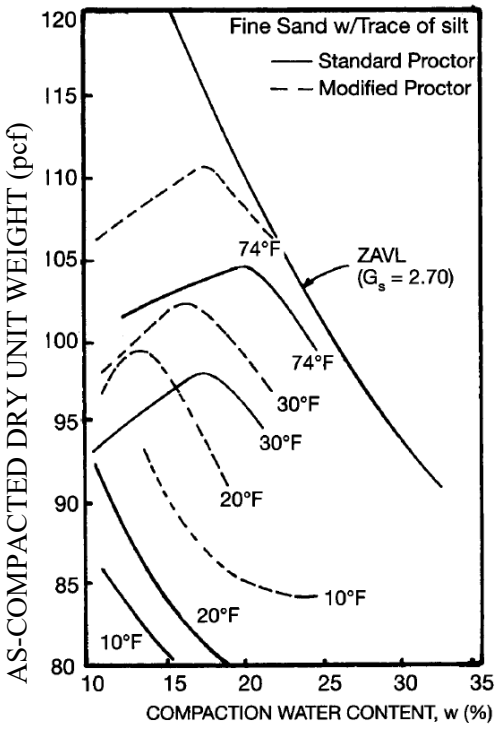

Figure 6.19 Influence of Temperature on the Moisture-density Relationships of a Sand with a Trace of Silt (from Waidelich 1990 as cited in Lawton 2001)

6.3 Summary

A review of the current UDOT specifications relevant to Embankment for Bridge materials was undertaken based on the results found from the Standard Consolidometer and the Large-scale Consolidometer tests and external references found in the open literature. Recommended changes to the specifications are summarized as follows:

- *Plasticity.* The current specifications allow a Plasticity Index (PI) up to a value of 6 based on the material passing the #40 sieve. It is recommended that the soil be required to be nonplastic using the following criteria:

The criteria in AASHTO T 89 and T90 shall be used to determine if the soil is nonplastic, but the tests shall be performed using the material passing the #200 sieve rather than the #40 sieve.

The percent finer than 0.002 mm $\leq$ 2.0 and no particles finer than 0.001 mm.

- *Gradation.* It is recommended that the following changes to the requirements for gradation be implemented:

The amount of fines (passing the #200 sieve) shall be limited to a maximum of 10%.

The definition of a well-graded material given in Section 02056, Part 1.4A be modified as follows (changes shown in red):

Well-graded material — material having an even distribution of different particle sizes with no gaps in size. This even distribution of particles of different sizes results in a dense mass upon compaction. When the grain-size data is plotted in the traditional manner of % Finer by Dry Weight on a linear scale vs.

Grain Size (Diameter) on a logarithmic scale (logarithm to the base 10), the best-fit curve drawn through the data points shall be continuous and smooth without any abrupt changes. Several examples of acceptable grain-size distribution curves are shown in the figure below.

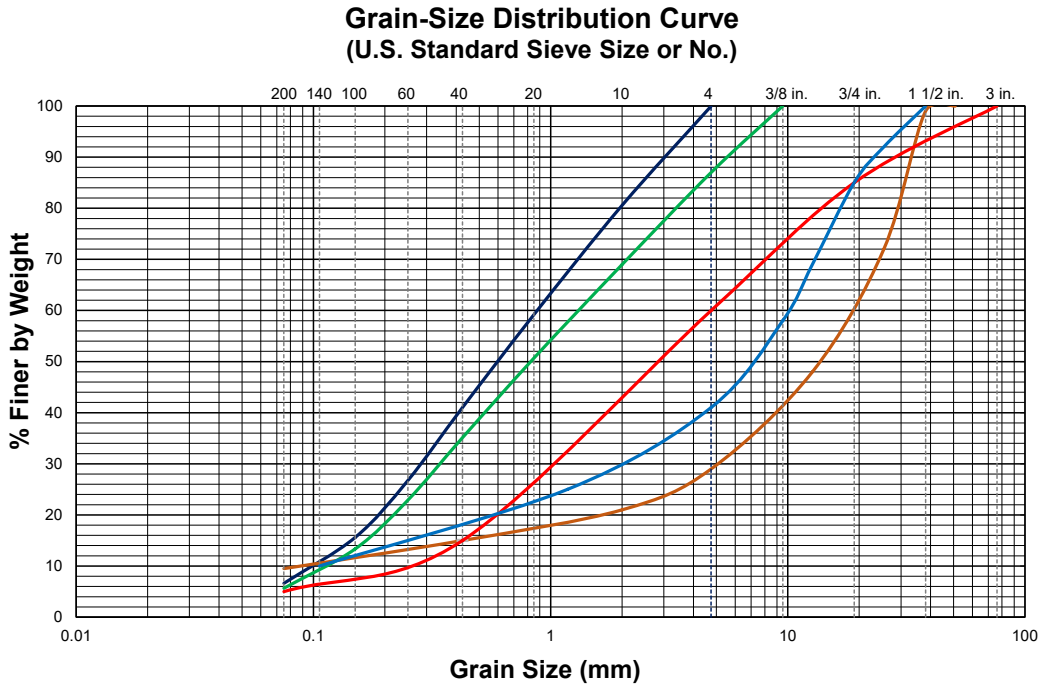

The following specification should be added: The ratio D_{90} / D_{10} shall be at least 25, where D_{90} is the particle diameter for which 90% of the material is finer by dry weight, and D_{10} is the particle diameter for which 10% of the material is finer by dry weight.

- *Relative Compaction*. The current relative compaction requirement for Embankment for Bridge (Section 02056, Part 3.1.F.1.a) is an average value of 96% based on Modified Proctor (AASHTO T 180) with no single determination lower than 92%. It is recommended that these requirements be kept with one additional requirement: A maximum of 20% of the tested material shall have a value less than 94%.
- *Characteristics of Particles.* There are currently no requirements in Section 02056 regarding the characteristics of the particles (aggregates). It is recommended that the following requirements provided in Part 2.1 of Section 02721 [Untreated Base Course (UTBC)], which have been modified slightly, be adopted by direct inclusion in Section 02056:

All bridge embankment material shall be hard, tough, durable, nonplastic, and sound mineral particles that are insoluble in water and free of organic matter and contamination from chemical or petroleum products, with a dry rodded unit weight of 75 pcf or greater (AASHTO T 19), and an aggregate wear of 50% or less (AASHTO T 96). In addition, at least 50% of the coarse grained material (retained on the #200 sieve) shall be (a) naturally angular or subangular in shape, as shown in Figure 6.20, (b) crushed with at least two fractured faces, or (c) a combination of *a* and *b*.

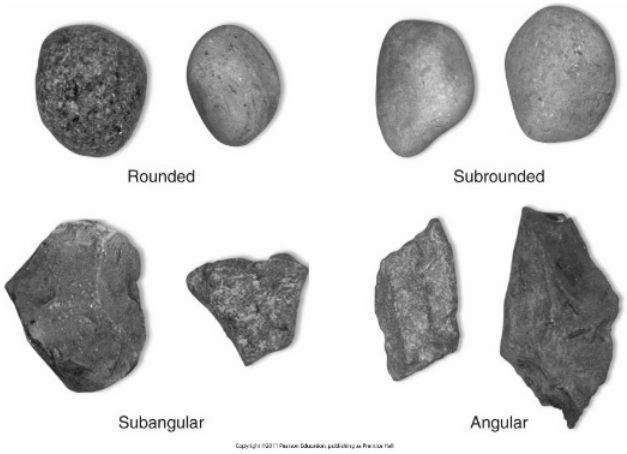

Figure 6.20 Photograph of Rounded, Subrounded, Subangular, and Angular Particles (from Holtz, Kovacs, and Sheahan 2011)

- *Moisture Condition During Processing, Transport, and Compaction.* The current specification simply states that appropriate moisture for compaction be maintained during processing (Section 02056, Part 3.1.F.1.a.2). It is recommended that the following sentence be added to this specification:

In particular, it is imperative that the on-site stockpiled material and the material during hauling, spreading, and compaction be kept at a sufficient moisture content to prevent separation and segregation of the different-sized particles.

- *Compaction During Freezing or Snowy Conditions.* Part 3.1.B of Section 02056 addresses the issue of placing embankment material during freezing or snowy conditions, which is allowed except embankment cannot be constructed on frozen or snow-covered areas. Furthermore, the use of frozen borrow material is prohibited. It is strongly recommended that compaction of bridge embankment materials not be allowed in air temperatures less than 34°F. Compaction during snowy conditions, where the temperatures are 34°F or higher, should be fine as long as the snow does not accumulate. Hence, the current specification of prohibiting compaction in snow-covered areas is acceptable if it is clarified that compaction must stop if it is snowing and the snow starts accumulating on the surface of the embankment.

One final recommendation is that UDOT should consider replacing the specifications for relative compaction based on Proctor-type tests with resilient modulus measured in the field using cyclic plate-load tests. The plate-load test has the following advantages over typical Proctor-type specification and testing:

- The stiffness and strength of the compacted soil are evaluated directly.
- No laboratory testing is required.
- The test is suitable for a wide range of soil types and maximum particle sizes.

7. CONCLUSIONS AND RECOMMENDATIONS

7.1 Summary

The primary objectives of this research project are:

1. Determine the loading-wetting stress-strain properties of selected types of embankment materials under varying conditions of density, load, and moisture in the laboratory.
2. Based on the results of the loading/wetting laboratory tests, identify potential problems for each type of embankment material in terms of contributing to settlement that may exacerbate the "bump at the end of the bridge" problem. The potential problems include long-term settlements from both loading (self-weight and loads from pavement system) and wetting (swell and collapse).
3. Based on the problems that have been identified, recommend changes to the UDOT specifications for embankment materials used in bridge approaches.

These objectives were achieved by conducting loading and wetting tests on specimens of 10 different soils tested in both standard consolidometers and a large-scale consolidometer. Findings from these tests, and recommendations for changes to current specifications for bridge approach embankment materials and recommendations for future research are provided in this chapter.

7.2 Findings

7.2.1 Tests in Standard Consolidometers

The following results and conclusions were drawn from the single- and double-consolidometer tests conducted on nine different soils on various grades of soil commonly used for the construction of roadway embankments.

1. For A-1 soils, the collapse potential increased with an increase in the magnitude of overburden stress. However, for other soil types, at low initial dry unit weights the collapse potential increases with increasing overburden stress up to a critical maximum value and beyond that, the collapse potential decreases with an increase in the overburden stress.
2. The magnitude of collapse depends on the soil gradation. For well-graded soils, the collapse potential is significantly less compared to the poorly graded soils. This may be because the interlocking between the particles is greater in well-graded soils.
3. For granular soils, at moisture-density conditions much drier than the line of optimums, the collapse potential depends primarily on the initial dry unit weight rather than the initial moisture condition. For all soil types, at a given initial moisture condition, collapse potential increases with a decrease in the initial dry unit weight.
4. At a given initial dry unit weight, the collapse potential of the soil decreases with an increase in the initial moisture conditions before soaking.
5. For soils containing plastic fines, at low overburden stress, significant increase in the volume (swell) is observed upon soaking with soil type A-4 (CL) having the most expansive nature. At given initial moisture conditions, the swelling potential of the soil increases with an increase in the initial dry unit weight of the soil.
6. For a given soil type and water content, the magnitude of the loading-induced strain increases with increasing overburden pressure.
7. The magnitude of loading-induced strain in as-compacted specimens is most in poorly graded soils, such as A-4 (CL), and reduces significantly in well-graded soils, like A-1-a (SP or SW). This

indicates that, as the uniformity in the gradation of soils increases, loading-induced strain in soils before soaking increases.

8. As the initial moisture conditions in as-compacted specimens increases, magnitude of loading-induced strain in soils increases at any given initial dry unit weight. This is more evident in soft soils like A-4 (CL).
9. The magnitude of loading-induced strain increases as the initial dry unit weight decreases at any given initial moisture condition and overburden pressure.
10. In general, at the same magnitude of overburden stress and similar initial dry unit weight and moisture conditions, the soaked specimens have a higher magnitude of loading-induced strain than the as-compacted specimens. However, in highly expansive soils, it was observed that the as-compacted specimens compressed more than the soaked specimens at low magnitudes of overburden stress.
11. For soils compacted according to Modified Proctor Test (A-1 soils) at the same conditions of initial dry unit weight and moisture conditions relative to the optimum moisture content, the loading-induced strain in soaked specimens is greatest in A-1-b (SC-SM) soil. There is a slight difference in the loading-induced strain between A-1-a (SC-SM) and A-1-a (SM) soils. The significant increase in the loading-induced strain observed in A-1-b soils is attributed to the greater fraction of finer particles in A-1-b soils with 100% of material passing through No. 10 sieve.
12. For soils compacted according to Modified Proctor Test (A-1 soils) at the same conditions of initial dry unit weight and moisture conditions relative to the optimum moisture content, the loading-induced strain in as-compacted specimens is greatest in A-1-b (SM) soil, which is the most poorly graded soil among the A-1 soils and contains non-plastic fines. There is a slight difference in the loading-induced strain between A-1-a (SC-SM), A-1-a (SM) and A-1-b (SC-SM) soils. This result indicates the cohesiveness between particles in soils containing plastic fines helps resist loading-induced stresses before the soil gets saturated.
13. For soils other than A-1 grades, soaked specimens at the same conditions of initial dry unit weight and moisture conditions relative to the optimum moisture content show a slight difference in the loading-induced strains between A-2 (SC) PI>>11 and A-3 (SP-SM) soils. The possible explanation for this is since the soil used for testing A-2 (SC) PI>>11 is highly expansive when saturated, it compensates the effects caused due to the loading-induced stress. Although, significant loading-induced strain is observed in the soil A-2 (SC) with PI=10 as it does not contain enough expansive material to counteract the effects of the loading-induced stress.
14. For soils other than A-1 grades, as-compacted specimens at the same conditions of initial dry unit weight and moisture conditions relative to the optimum moisture content, there is a significant difference induced strains at the same magnitude of overburden stress.

7.2.2 Tests in Large-Scale Consolidometer

The main conclusions determined from analysis of results from these tests are summarized as follows:

1. In most cases, the loading-induced strains were smaller for nominally identical specimens loaded as-compacted than loaded after soaking. Differences were small for the two granular soils tested and significantly larger for the one cohesive soil tested.
2. In most cases, the loading-induced strains were smaller for granular specimens compacted dry of optimum water content than those compacted at optimum water content to the same relative compaction and loaded in the same condition (as-compacted or soaked). The loading-induced strain for a cohesive specimen compacted at optimum water content and loaded as-compacted was smaller than for a specimen compacted wet of optimum water content to the same relative compaction and also loaded as-compacted.
3. In general, granular specimens compacted to a greater relative compaction strained less under loading than specimens compacted to a lesser relative compaction, all other factors being the same.

4. Six comparisons were made regarding the effect of soil type on the loading-induced strain-stress characteristics of the two granular soils. At a relative compaction of 90%, the A1aSW was less compressible than the FDGW. At a relative compaction of 96%, the FDGW was less compressible than the A1aSW.
5. The A2SCPI10 material was significantly more compressible at 96% Standard Proctor relative compaction than the A1aSW and FDGW were at 90% Modified Proctor relative compaction, for specimens loaded both as-compacted and soaked. The differences were greater for specimens loaded soaked than those loaded as-compacted.
6. Unfortunately, no comparisons could be made for tests conducted in the Standard Consolidometer (SC) and those conducted in the Large-scale Consolidometer for all materials and conditions being nominally identical. However, reasonably close comparisons showed the strains in LSC tests were several times greater than the strains in the SC tests. These large differences are likely attributable to the differences in boundary constraints related to the different sizes of the specimens. These results illustrate the importance of testing compacted fill materials using specimens as large as possible.
7. Four trends were found with respect to wetting-induced strains, all other factors being the same: (a) Looser granular soils collapsed more than denser soils. (No comparisons were available for the cohesive soil.) (b) Collapse increases with increasing total vertical stress at the time of wetting. Comparing the results for vertical stresses of 2 and 8 tsf, the difference in collapse for the cohesive soil was much greater for the cohesive soil than for the two granular soils. (c) The drier the soil is at the time of wetting, the more it will collapse. (d) For the four cases where direct comparisons are available, A1aSW collapsed more than FDGW in three of the four cases, and the collapse was essentially the same in one case.
8. Estimates of loading-induced settlement resulting from strains within a 30-foot tall bridge approach embankment ranged from about 7 to 18 inches. The estimated settlements for the A2SCPI10 were larger than for A1aSW and FDGW. For the two granular soils, these settlements would generally be expected to be inconsequential to the bump-at-the-bridge problem because the settlements will occur quickly during construction, owing to their high permeability. However, for the cohesive soil, the settlements will occur over a much longer period of time, owing to the time-dependency of settlement in cohesive soils. Therefore, use of cohesive materials, even with low plasticity indices, could result in substantial loading-induced settlements resulting from strains within the embankment material itself.
9. Estimates of wetting-induced settlement resulting from strains within a 30-foot tall bridge approach embankment ranged from about 1/14 to 1/6 inch. The estimated settlements for the A2SCPI10 were larger than for A1aSW and FDGW. In addition, the wetting-induced settlement was only calculated for the A2SCPI10 compacted at or wet of optimum. If the A2SCPI10 were compacted dry of optimum, the collapse would be expected to be substantially more. Based on the results, it is concluded that if either of the two granular soils were used in the approach embankments for bridges and constructed properly, the wetting-induced settlement from strains within the embankment itself should not contribute significantly to the bump-at-the-bridge problem.

7.3 Recommendations

7.3.1 Changes to Current Specifications

Recommended changes to the current UDOT specifications relevant to Embankment for Bridge materials are summarized below. These recommendations are based on the research performed for this project and other projects by the first author, and experience and knowledge of the first author.

- The current specifications allow a Plasticity Index (PI) up to a value of 6 based on the material passing the #40 sieve. It is recommended that the soil be required to be nonplastic using the following criteria:

The criteria in AASHTO T 89 and T90 shall be used to determine if the soil is nonplastic, but the tests shall be performed using the material passing the #200 sieve rather than the #40 sieve.

The percent finer than 0.002 mm ≤ 2.0 and no particles finer than 0.001 mm.

- *Gradation.* t is recommended that the following changes to the requirements for gradation be implemented:

The amount of fines (passing the #200 sieve) shall be limited to a maximum of 10%.

The definition of a well-graded material given in Section 02056, Part 1.4A be modified as follows (changes shown in red):

Well-graded material — material having an even distribution of different particle sizes with no gaps in size. This even distribution of particles of different sizes results in a dense mass upon compaction. When the grain-size data is plotted in the traditional manner of % Finer by Dry Weight on a linear scale vs. Grain Size (Diameter) on a logarithmic scale (logarithm to the base 10), the best-fit curve drawn through the data points shall be continuous and smooth without any abrupt changes. Several examples of acceptable grain-size distribution curves are shown in the figure below.

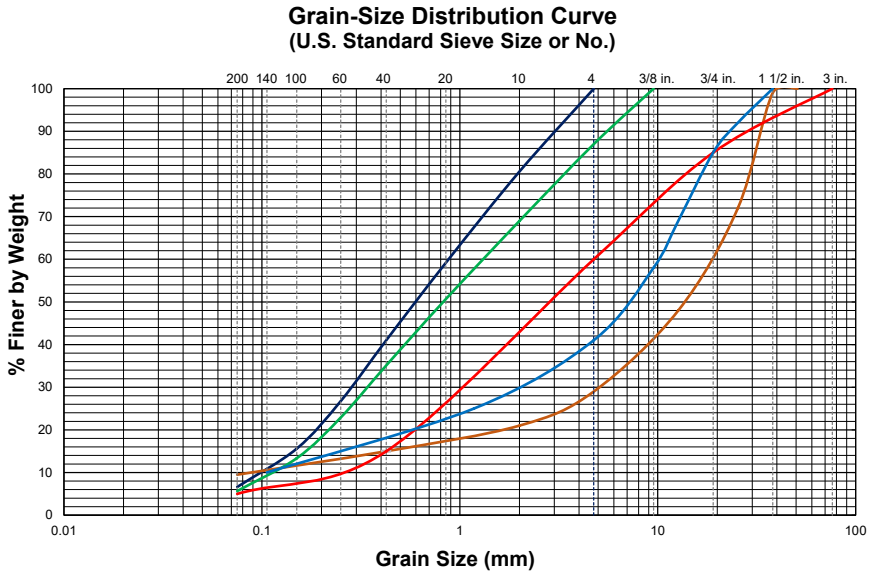

The following specification should be added: The ratio D_{90} / D_{10} shall be at least 25, where D_{90} is the particle diameter for which 90% of the material is finer by dry weight, and D_{10} is the particle diameter for which 10% of the material is finer by dry weight.

- *Relative Compaction*. The current relative compaction requirement for Embankment for Bridge (Section 02056, Part 3.1.F.1.a) is an average value of 96% based on Modified Proctor (AASHTO T 180) with no single determination lower than 92%. It is recommended these requirements be kept with one additional requirement: A maximum of 20% of the tested material shall have a value less than 94%.
- *Characteristics of Particles.* Currently, there are no requirements in Section 02056 regarding the characteristics of the particles (aggregates). It is recommended that the following requirements provided in Part 2.1 of Section 02721 [Untreated Base Course (UTBC)], which have been modified slightly, be adopted by direct inclusion in Section 02056:

All bridge embankment material shall be hard, tough, durable, nonplastic, and sound mineral particles that are insoluble in water and free of organic matter and contamination from chemical or petroleum products, with a dry rodded unit weight of 75 pcf or greater (AASHTO T 19), and an aggregate wear of 50% or less (AASHTO T 96). In addition, at least 50% of the coarse-grained material (retained on the #200 sieve) shall be (a) naturally angular or subangular in shape, as shown in the figure below, (b) crushed with at least two fractured faces, or (c) a combination of *a* and *b*.

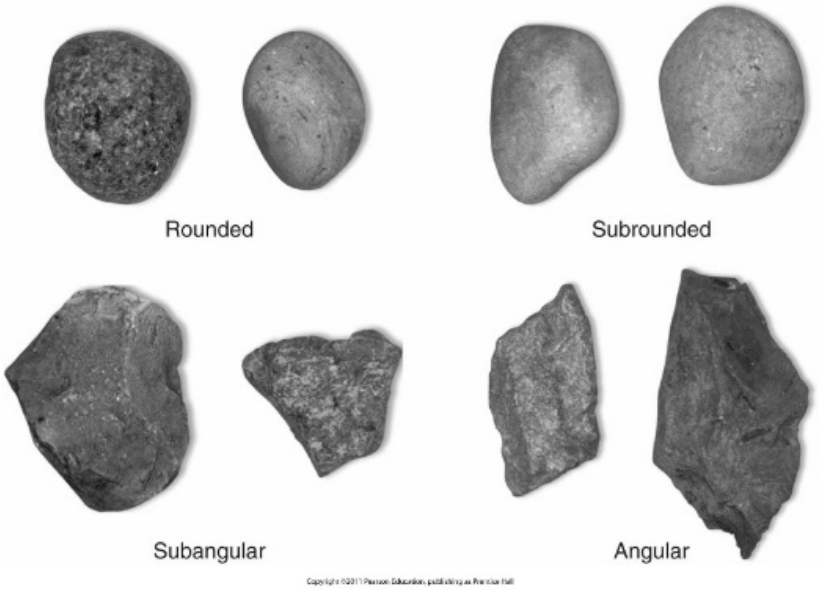

- *Moisture Condition During Processing, Transport, and Compaction.* The current specification simply states that appropriate moisture for compaction be maintained during processing (Section 02056, Part 3.1.F.1.a.2). It is recommended that the following sentence be added to this specification:

In particular, it is imperative that the on-site stockpiled material and the material during hauling, spreading, and compaction be kept at a sufficient moisture content to prevent separation and segregation of the different-sized particles.

- *Compaction During Freezing or Snowy Conditions.* Part 3.1.B of Section 02056 addresses the issue of placing embankment material during freezing or snowy conditions, which is allowed, except that embankment cannot be constructed on frozen or snow-covered areas. Furthermore, the use of frozen borrow material is prohibited. It is strongly recommended that compaction of bridge embankment materials not be allowed in air temperatures less than 34°F. Compaction during snowy conditions where the temperatures are 34°F or higher should be fine as long as the snow does not accumulate. Hence, the current specification of prohibiting compaction in snow-covered areas is acceptable if it is clarified that compaction must stop if it is snowing and the snow starts accumulating on the surface of the embankment.

One final recommendation is that UDOT should consider a long-term goal of replacing the specifications for relative compaction based on Proctor-type tests with resilient or subgrade modulus measured in the field using cyclic plate-load tests. The plate-load test has the following advantages over typical Proctor-type specification and testing:

- The stiffness and strength of the compacted soil are evaluated directly.
- No laboratory testing is required.
- The test is suitable for a wide range of soil types and maximum particle sizes.

This change would not be easy and would likely take several years or more for the transition, since the Proctor-type tests have been used as the standard for many decades within the construction industry in the United States. One possible way to determine the viability of this change would be to require a certain number of plate-load or similar tests on every lift (or every other lift) for each new bridge approach embankment that is constructed. A database could be developed in which dry unit weights and relative compaction are compared with subgrade modulus or Young's modulus determined or back calculated from plate-load or similar tests. Other parameters that could be included in the database include grain-size distribution data (which could be used to calculate parameters such as percent fines, percent sand, percent gravel, D_{10}, D_{30}, D_{60}, D_{90}), characteristics of the coarse-grained particles (shape, elongation, mineralogy) and some type of qualitative or quantitative measure of the performance of the bridge approach embankment. This information could be used to determine appropriate values of modulus and potentially make changes to the specifications regarding some of the other parameters.

7.3.2 Future Research

Comparisons of loading-induced strain for similar tests conducted in the Standard Consolidiometer (SC) and the Large-Scale Consolidometer (LC) showed that the materials were significantly more compressible when larger-diameter specimens (LC) were tested than when smaller-diameter specimens were tested. Typically, the loading-induced strains at each level of total vertical stress for similar soils and similar compactive parameters where several orders of magnitude are greater. Unfortunately, there were no direct comparisons available where the soils and compactive parameters were all the same for both the SC and LSC tests. Furthermore, no comparisons were available for wetting-induced strains. Therefore, additional SC and LSC testing should be undertaken where the soils and compactive parameters are nominally identical, which will allow direct comparisons of both loading and wetting-induced strains. In addition, it is recommended that even larger diameter tests be conducted to determine what diameter is needed to get results not affected by the problems at the boundary conditions that were identified in Section 5.8.1.4 of this report. The University of Utah currently has the ability to test specimens 36-inch diameter in size. This equipment has previously been used in research supported by the Materials and Pavements Division of UDOT.

Other index and compactive parameters that have not been studied sufficiently for granular soils include the elongation and angularity of the particles, and what constitutes a well-graded soil. Therefore, it is recommended that additional testing be undertaken on granular soils with the same mineralogy but different elongation and the angularity of the particles. It is clear from the research conducted in this study that the definition of a well-graded soil in the Unified Soil Classification System does not adequately differentiate between well-graded and poorly-graded for fill materials with respect to their stress-strain characteristics under load and wetting. Further research is clearly needed on this topic.

It is also recommended that cyclic plate-load tests be conducted on bridge approach embankments as they are being constructed and to start compiling a data base of resilient modulus (or perhaps subgrade modulus after a certain number of cycles) vs. factors, such as the moisture condition and relative compaction (water content and dry unit weight) typically specified and determined as part of the Quality Control and Quality Assurance. Doing so would enable UDOT to determine (a) what values of relative compaction are needed to ensure adequate performance of the embankment, (b) if the current specifications for relative compaction adequate, (c) if the use of the Proctor-type tests ensures adequate performance, and (d) if cyclic plate-load tests would be a better method to ensure adequate performance.

The most important recommendation for future research is that one or more actual bridge approach embankments be instrumented and monitored to determine how much settlement is occurring near the ends of the bridges because of strains within the embankment material, and how much settlement is occurring due to strains within the underlying subgrade (native) material. In addition, instrumentation and monitoring could be conducted on both embankments of a new bridge in which one of the embankments is built according to the current specifications, and the other embankment is constructed according to the updated specifications (if any of the proposed changes are adopted). It is anticipated that the cost of the instrumentation could be built into the project itself, but that the monitoring of the project would need to be funded by the Research Division. It would also be important to ensure, through appropriate Quality Control (QC) and Quality Assurance (QA), all embankments that are monitored be constructed strictly according to the specifications. It would be important the QC and QA be done by independent companies or institutions not associated with the project.

8. REFERENCES

AASHTO Standard M 145. "Classification of Soils and Soil-Aggregate Mixtures for Highway Construction Purposes." American Association of State Highway and Transportation Officials, Washington, D.C.

AASHTO Standard T 19. "Bulk Density ("Unit Weight") and Voids in Aggregate." American Association of State Highway and Transportation Officials, Washington, D.C.

AASHTO Standard T 96. "Resistance to Degradation of Small-Size Coarse Aggregate by Abrasion and Impact in the Los Angeles Machine." American Association of State Highway and Transportation Officials, Washington, D.C.

AASHTO Standard T 180. "Moisture-Density Relations of Soils Using a 4.54-kg (10-lb) Rammer and a 457-mm (18-in.) Drop." American Association of State Highway and Transportation Officials, Washington, D.C.

Alwail, T. A., Ho, C. L., and Fragaszy, R. J. (1992). "Collapse Mechanisms of Low Cohesion Compacted Soils." *Bulletin of the Association of Engineering Geologists*, Vol. 29, No. 4, pp. 345-353.

Ashour, M., Abbas, A., Altahrany, A., & Alaaeldin, A. (2020). Modelling the Behavior of Inundated Collapsible Soils. *Engineering Reports*, *2*(4), e12156. https://doi.org/10.1002/eng2.12156

ASTM Standard D1195. "Repetitive Static Plate Tests of Soils and Flexible Pavement Components for Use in Evaluation and Design of Airport and Highway Pavements." ASTM International, West Conshohocken, PA.

ASTM Standard D1196. "Nonrepetitive Static Plate Tests of Soils and Flexible Pavement Components for Use in Evaluation and Design of Airport and Highway Pavements." ASTM International, West Conshohocken, PA.

ASTM Standard D1586. "Standard Penetration Test (SPT) and Split-Barrel Sampling of Soils." ASTM International, West Conshohocken, PA.

ASTM Standard D2487. "Classification of Soils for Engineering Purposes (Unified Soil Classification System)." ASTM International, West Conshohocken, PA.

ASTM Standard D4429. "CBR (California Bearing Ratio) of Soils in Place." ASTM International, West Conshohocken, PA.

ASTM Standard D5778. "Electronic Friction Cone and Piezocone Penetration Testing of Soils." ASTM International, West Conshohocken, PA.

ASTM Standard D7380. "Soil Compaction Determination at Shallow Depths Using 2.3-kg (5-lbm) Dynamic Cone Penetrometer." ASTM International, West Conshohocken, PA.

Basma, A. A., & Tuncer, E. R. (1992). Evaluation and Control of Collapsible Soils. *Journal of Geotechnical Engineering*, *118*(10), 1491–1504. https://doi.org/10.1061/(ASCE)0733-9410(1992)118:10(1491)

Booth, A. R. (1977). *Collapse Settlement in Compacted Soils*. https://researchspace.csir.co.za/dspace/handle/10204/1248

Briaud, J.-L. (1997). Settlement of Bridge Approaches: (The Bump at the End of the Bridge). Washington, DC: National Academy Press.

Cerato, A. B., Miller, G. A., & Hajjat, J. A. (2009). Influence of Clod Size and Structure on Wetting-Induced Volume Change of Compacted Soil. *Journal of Geotechnical and Geoenvironmental Engineering*, *135*(11), 1620–1628. https://doi.org/10.1061/(ASCE)GT.1943-5606.0000146

FEMA (2011). *Filters for Embankment Dams – Best Practices for Design and Construction*. Federal Emergency Management Agency, Washington, D.C., October, 332 pp.

Habibagahi, G. (2004). Prediction of Collapse Potential for Compacted Soils Using Artificial Neural Networks. *Scientia Iranica*, *11*(1). http://scientiairanica.sharif.edu/article_2515.html

Holtz, R.D., Kovacs, W.D. and Sheahan, T.C. (2011). *An Introduction to Geotechnical Engineering*, 2nd Edition, Pearson, Upper Saddle River, New Jersey, p. 171.

Hausmann, M. R. (1990). *Engineering Principles of Ground Modification*. McGraw-Hill, New York, pp. 93-94 and 125-126.

Johnson, A.W. and Sallberg, J.R. (1960). "Factors that Influence Field Compaction of Soils." *Bulletin 272*, Highway Research Board, Washington, D.C., 206 pp.

Lawton, E.C. (1986). *Wetting-Induced Collapse in Compacted Soil*. PhD Dissertation, Washington State University. [ProQuest Dissertations Publishing]. http://search.proquest.com/docview/303547482/?pq-origsite=primo

Lawton, E.C. (2001). "Soil Improvement and Stabilization – Nongrouting Techniques." Part 6A in *Practical Foundation Engineering Handbook*, 2nd edition, McGraw-Hill, New York, pp. 6.3-6.340.

Learn Something. (2015, May 8). *Multiple Regression Explained with Excel*. https://www.youtube.com/watch?v=jGd2cj4K4Ww&ab_channel=LearnSomething

Lim, Y. Y., & Miller, G. A. (2004). Wetting-Induced Compression of Compacted Oklahoma Soils. *Journal of Geotechnical and Geoenvironmental Engineering*, *130*(10), 1014–1023. https://doi.org/10.1061/(ASCE)1090-0241(2004)130:10(1014)

Mayne, P. W., and Poulos, H. G. (1999). "Approximate Displacement Influence Factors for Elastic Shallow Foundations." *Journal of Geotechnical and Geoenvironmental Engineering*, 125(6), 453-460.

Milligan, V. (1999). "An Historical Perspective of the Development of the Embankment Dam." *2nd Annual Conference of the Canadian Dam Association*, Edmunton, Alberta, Canada.

Milligan, V. (2003). "Some Uncertainties in Embankment Dam Engineering." *Journal of Geotechnical and Geoenvironmental Engineering*, 129(9), 785-797.

Noorany, I., and Houston, S. (1995). "Effect of Oversize Particles on Swell and Compression of Compacted Unsaturated Soils." *Geotechnical Special Publication No. 56*, M. D. Evans and R. J. Fragaszy, editors, American Society of Civil Engineers, pp. 107-121.

Qian, Z., Lu, X.-L., Yang, W.-Z., & Cui, Q. (2014). Behaviour of Micropiles in Collapsible Loess under Tension or Compression Load. *Geomechanics and Engineering*, *7*, 477–493. https://doi.org/10.12989/gae.2014.7.5.477

Ripley, C.F. (1984). "Discussion of: Progress in Rockfill Dams." *Journal of Geotechnical Engineering*, 114(2), 236-240.

Ripley, C.F. (1986). "Internal Stability of Granular Filters: Discussion." *Canadian Geotechnical Journal*, 23, 255-258.

Rönnqvist, H., et al. (2020). "The Segregation of a Sand-Gravel Dam Filter of Crushed Rock and the Influence of Water Content." *Material Science & Engineering*, 4(6), 152-156.

Sample Splitter. (n.d.). GlobalGilson.Com. Retrieved November 22, 2020, from https://www.globalgilson.com/gilson-universal-sample-splitters

Sasitharan, S., Robertson, P., Sego, D., & Morgenstern, N. (1993). Collapse Behavior of Sand. *Canadian Geotechnical Journal,* 30, 569–577. https://doi.org/10.1139/t93-049

Selig, E.T. and Yoo, T.S. (1977). "Fundamentals of Vibratory Roller Behavior." *Proceedings of the Ninth International Conference on Soil Mechanics and Foundation Engineering*, Tokyo, Japan, Vol. 2, pp. 375-380.

Sherard, J.L., Dunnigan, L.P., and Talbot, J.R. (1984). "Filters for Silts and Clays." *Journal of Geotechnical Engineering*, 110(6), 701-718.

Sridharan, A., & Gurtug, Y. (2004). Swelling Behaviour of Compacted Fine-Grained Soils. *Engineering Geology*, *72*(1), 9–18. https://doi.org/10.1016/S0013-7952(03)00161-3

Testing Screen. (n.d.). GlobalGilson.Com. Retrieved November 22, 2020, from https://www.globalgilson.com/gilson-testing-screen

USDA (1994). "Gradation Design of Sand and Gravel Filters". *Part 633, Chapter 26 in National Engineering Handbook*, U.S. Department of Agriculture, Natural Resources Conservation Service, Washington, D.C..

Vibrating Table. (n.d.). GlobalGilson.Com. Retrieved November 23, 2020, from https://www.globalgilson.com/relative-density-vibrating-table

Waidelich, W.C. (1990). "Earthwork Construction." Chapter 4 in Guide to Earthwork Construction, *State of the Art Report 8*, Transportation Research Board, Washington, D.C., pp. 25-48.

APPENDIX A: MOISTURE–DENSITY CURVES FROM PROCTOR TESTS

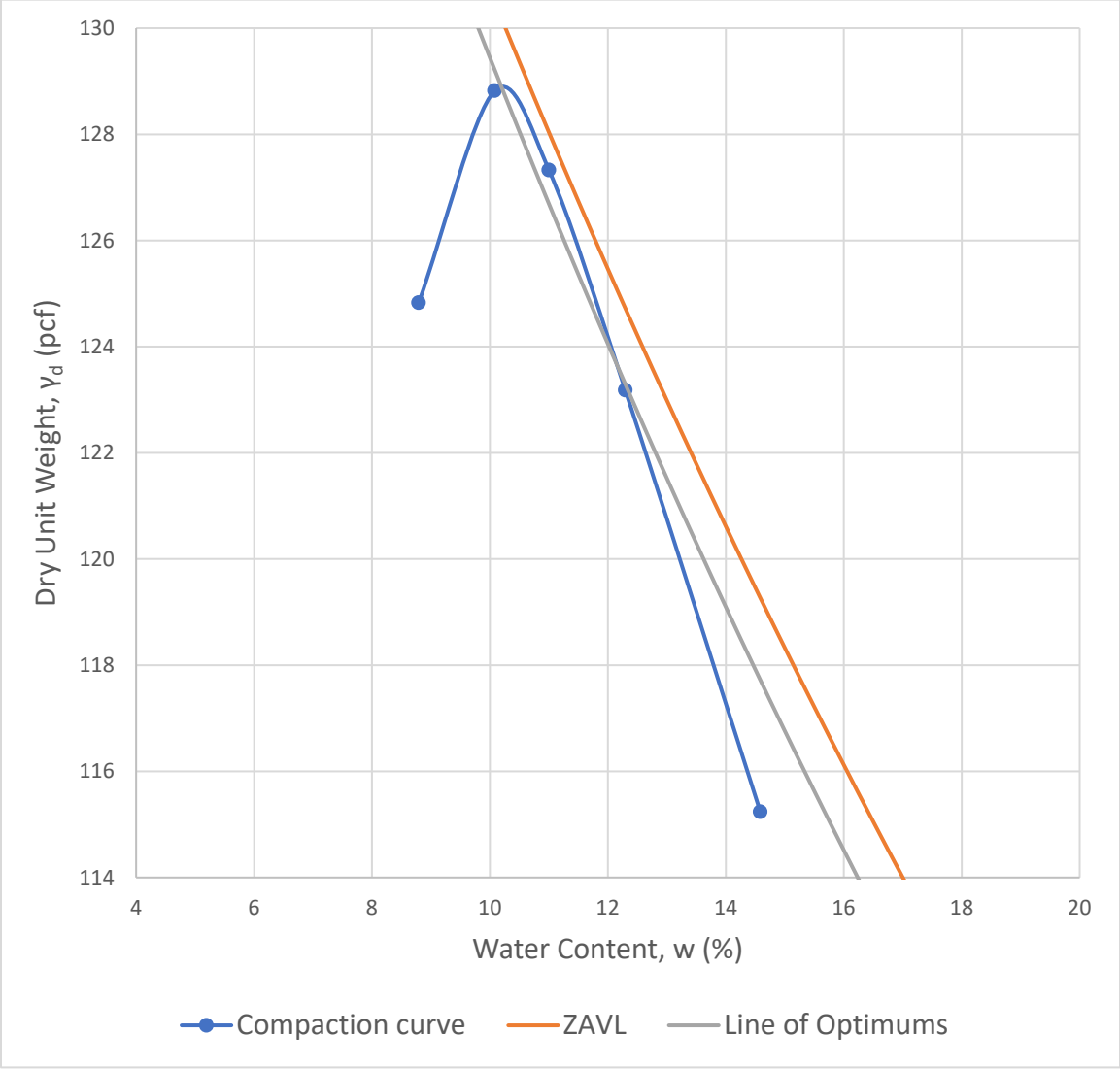

Figure A.1: Compaction Curve for A-1-a (SP or SW) Soil.

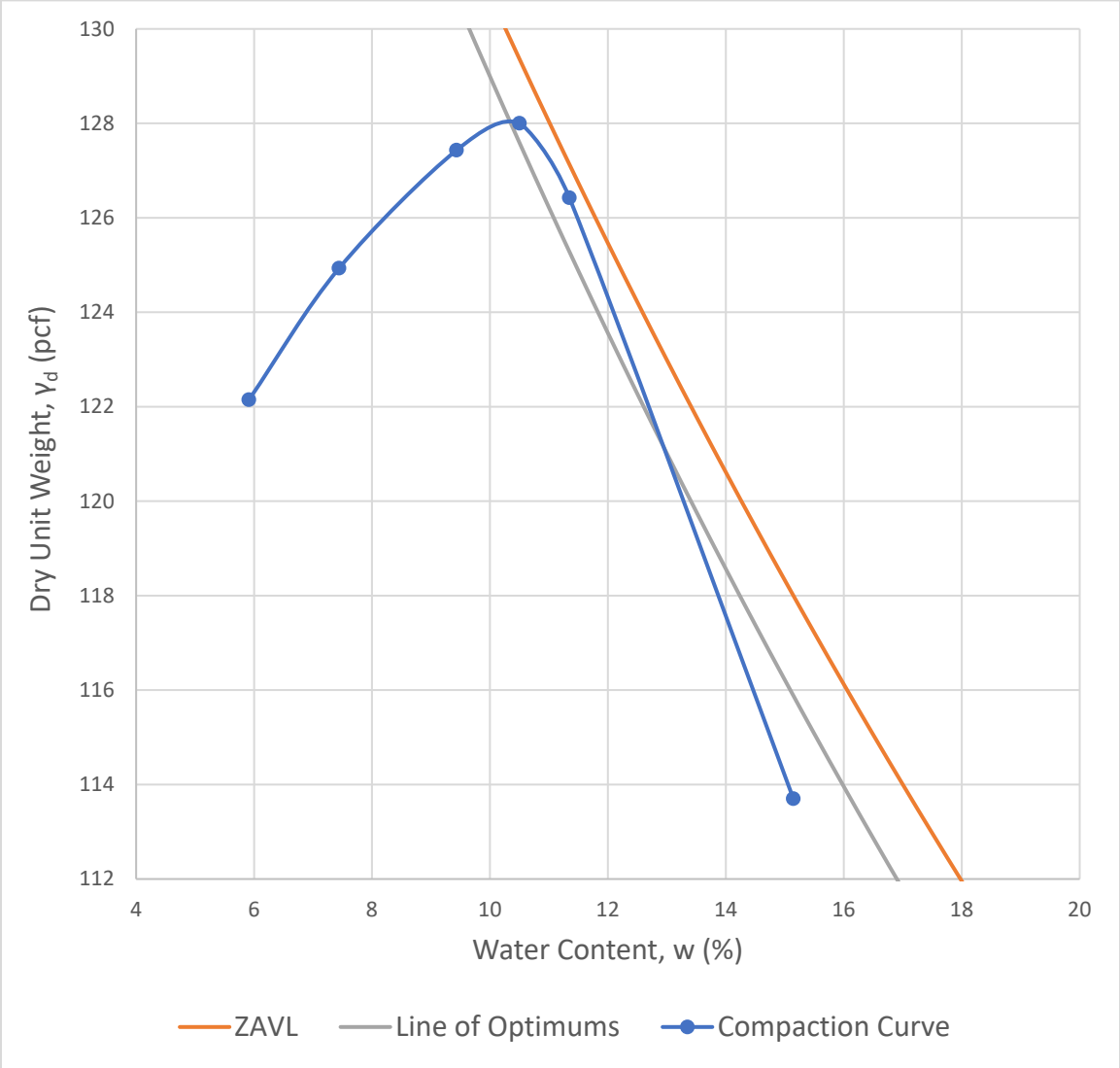

Figure A.2: Compaction Curve for A-1-a (SM) Soil.

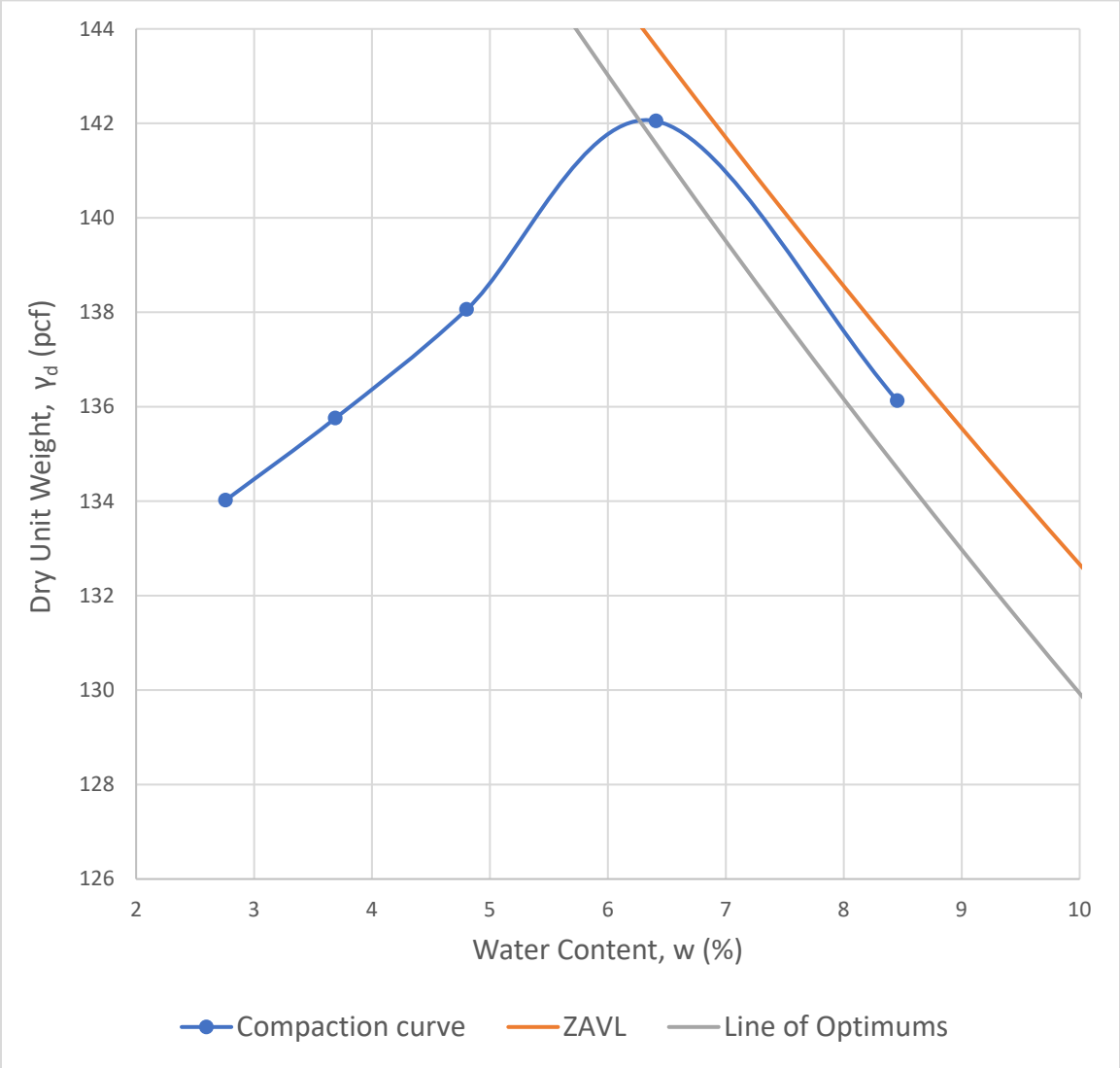

Figure A.3: Compaction Curve for A-1-a (SC-SM) Soil.

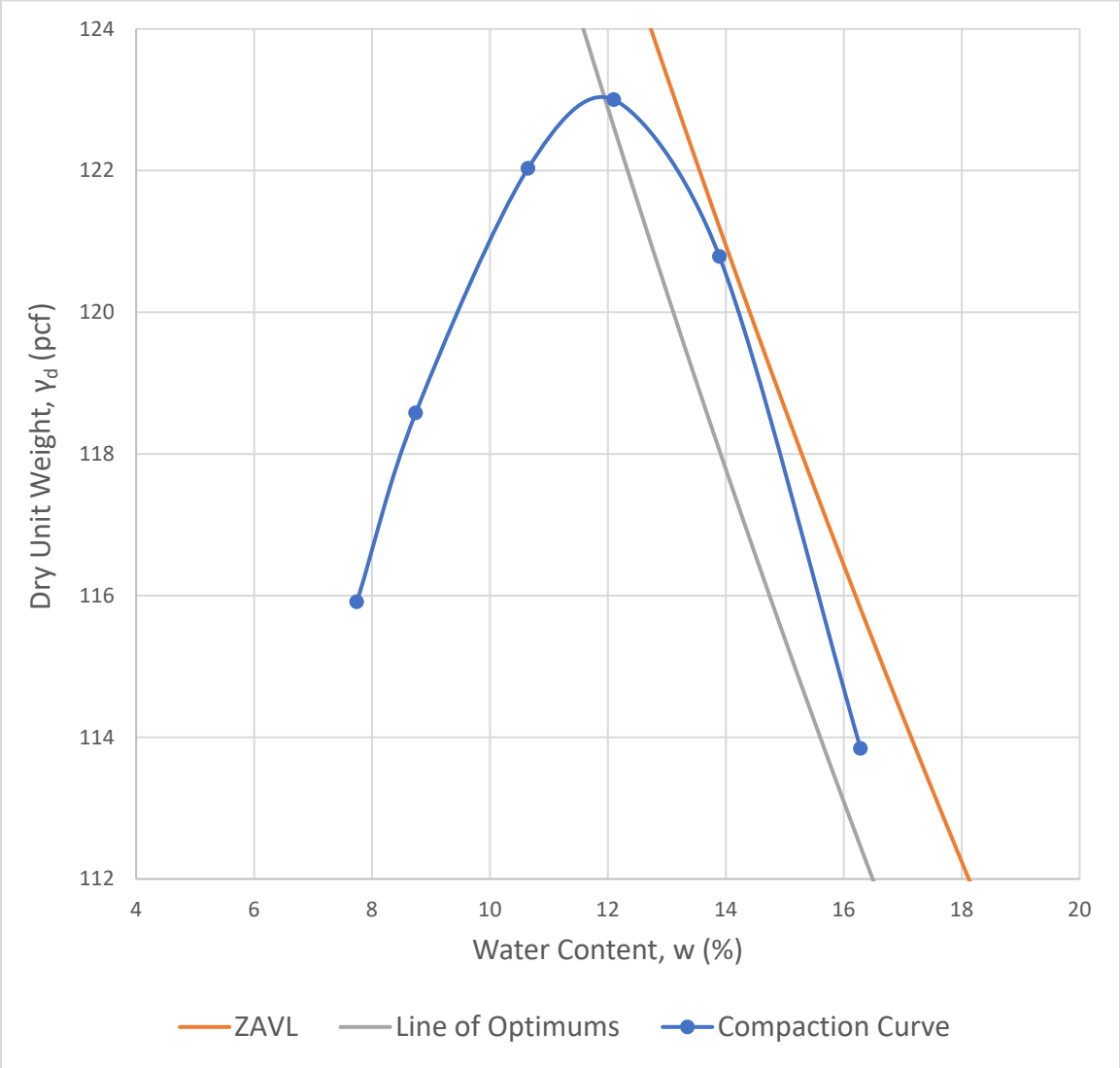

Figure A.4: Compaction Curve for A-1-b (SM) Soil.

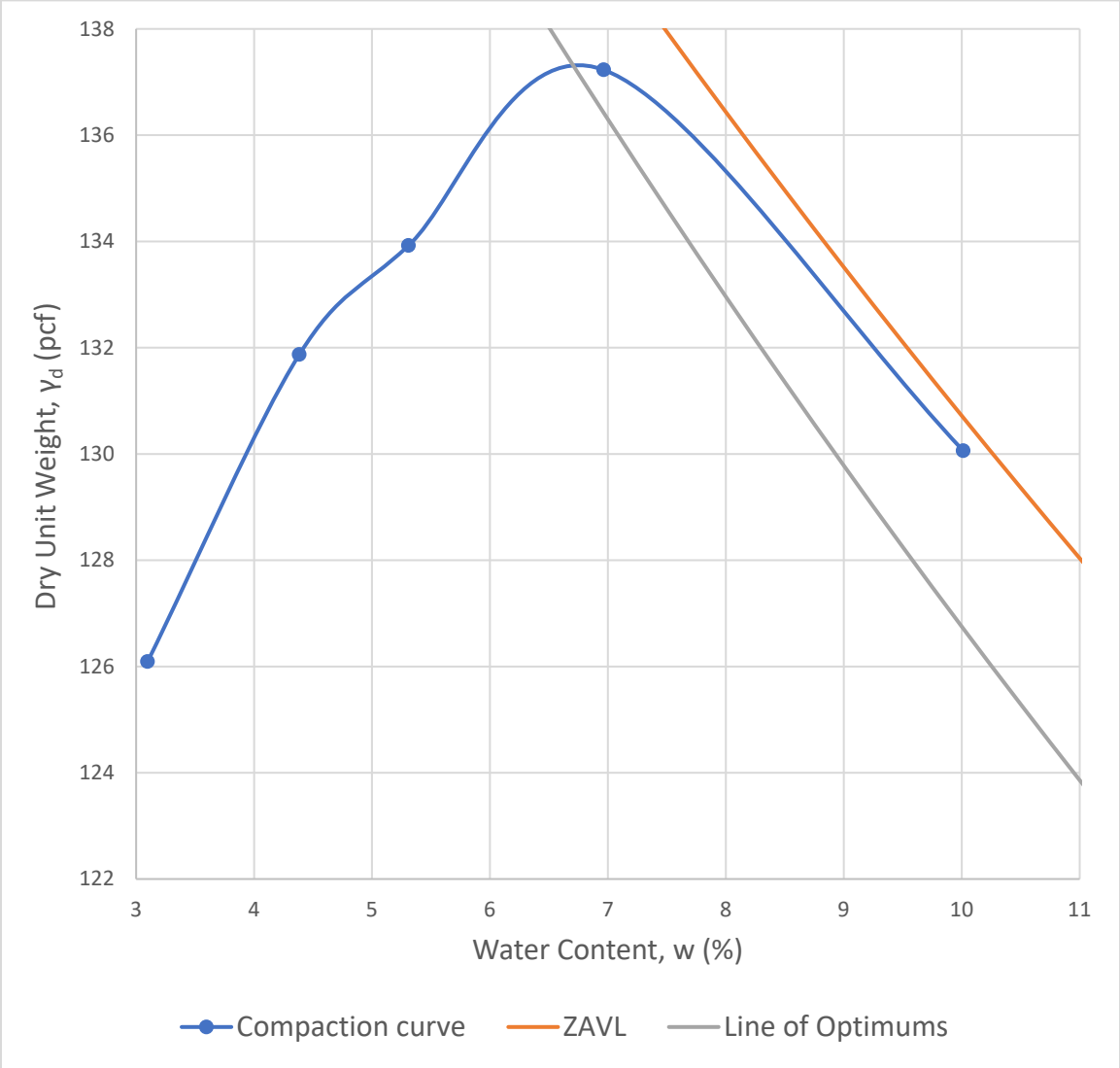

Figure A.5: Compaction Curve for A-1-b (SC-SM) Soil.

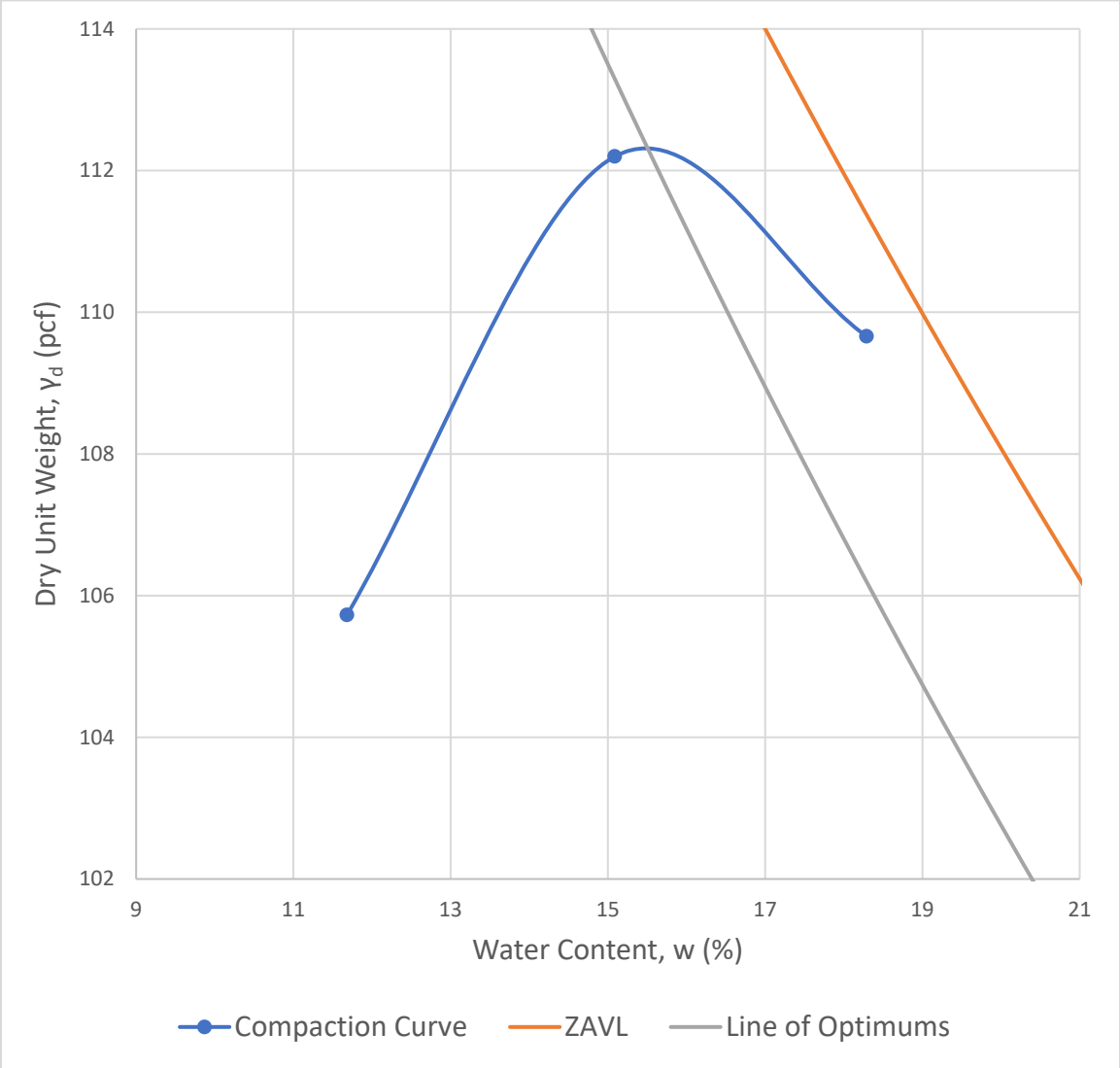

Figure A.6: Compaction Curve for A-2 (SC) With PI=10 Soil.

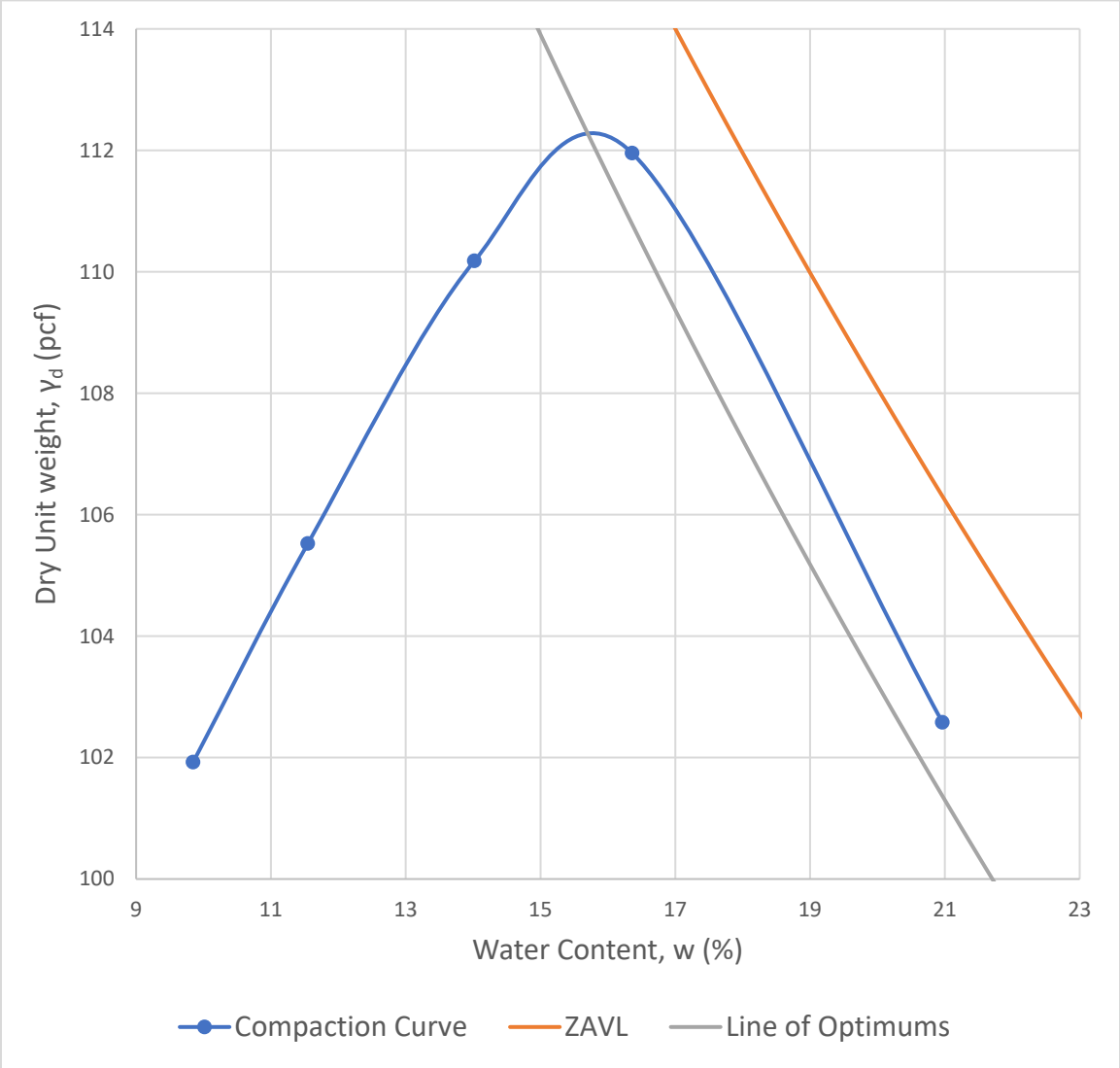

Figure A.7: Compaction Curve for A-3 (SP-SM) Soil.

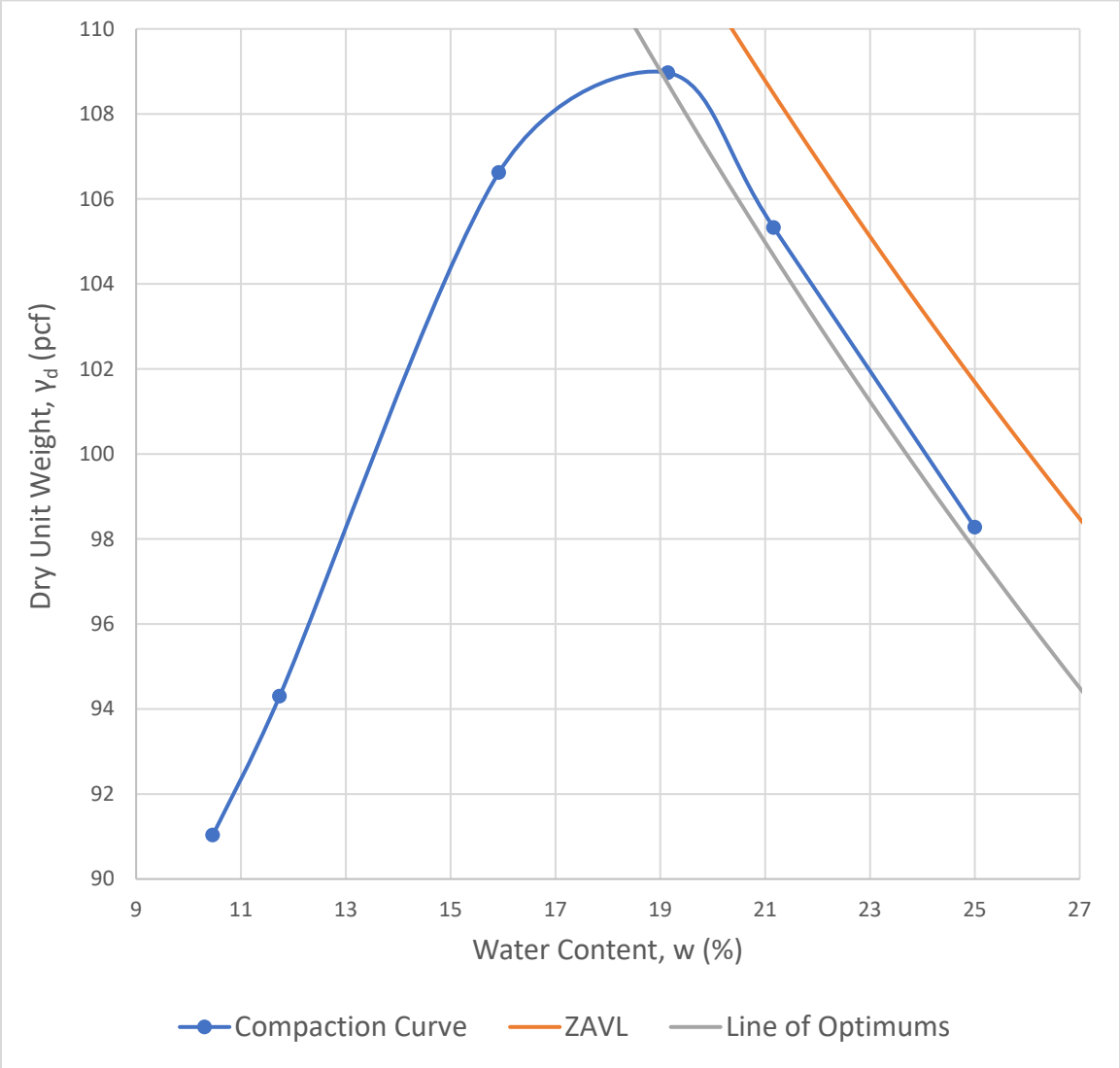

Figure A.8: Compaction Curve for A-2 (SC) With PI>>11 Soil.

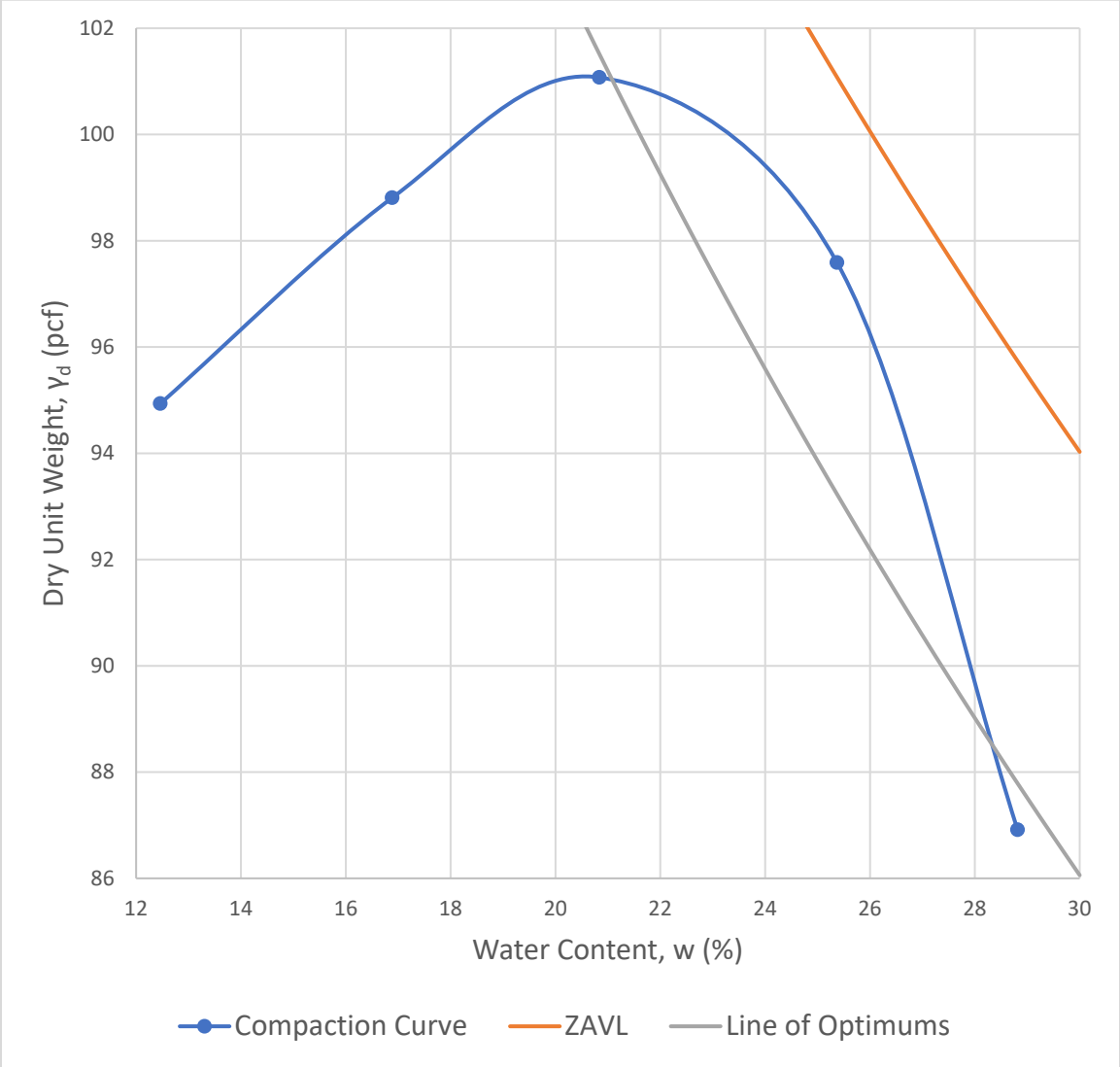

Figure A.9: Compaction Curve for A-4 (CL) Soil.

APPENDIX B: DOUBLE CONSOLIDOMETER TEST RESULTS

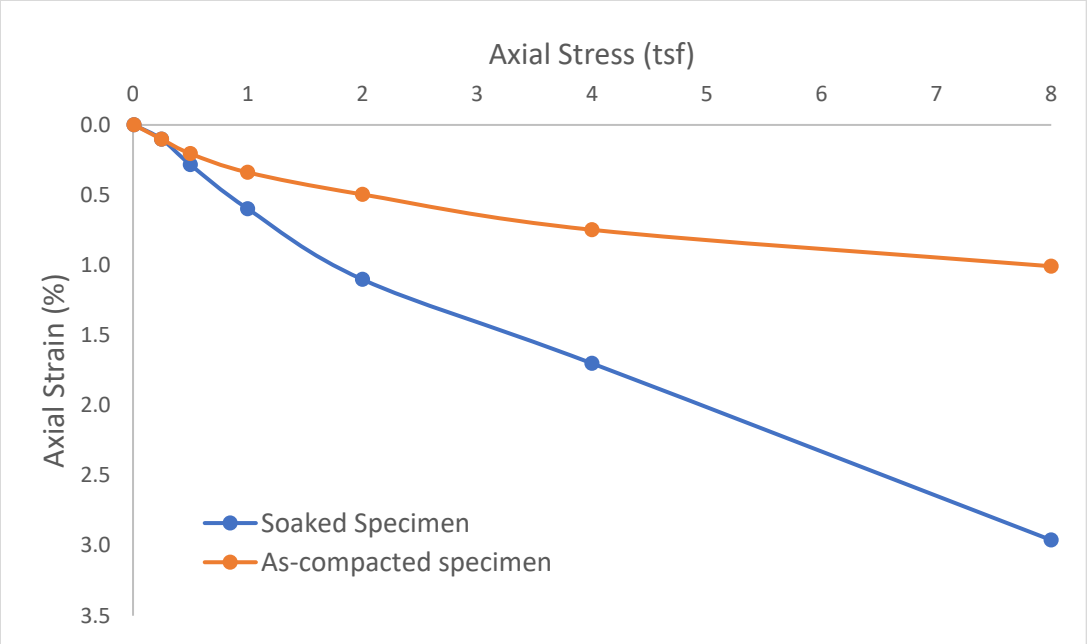

Figure B.1: Comparison of Stress-strain Characteristics Between Soaked and As-compacted Specimens for A-1-a (SP or SW) Soil at R_m = 90%, w = 10.1%

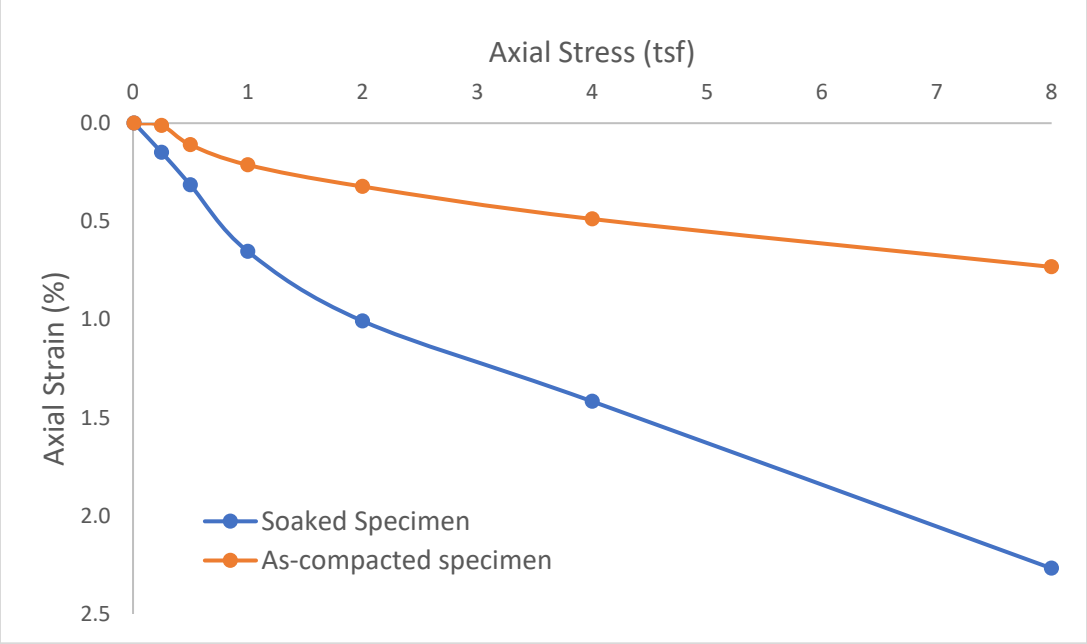

Figure B.2: Comparison of Stress-strain Characteristics Between Soaked and As-compacted Specimens for A-1-a (SP or SW) Soil at R_m = 95%, w = 8.1%

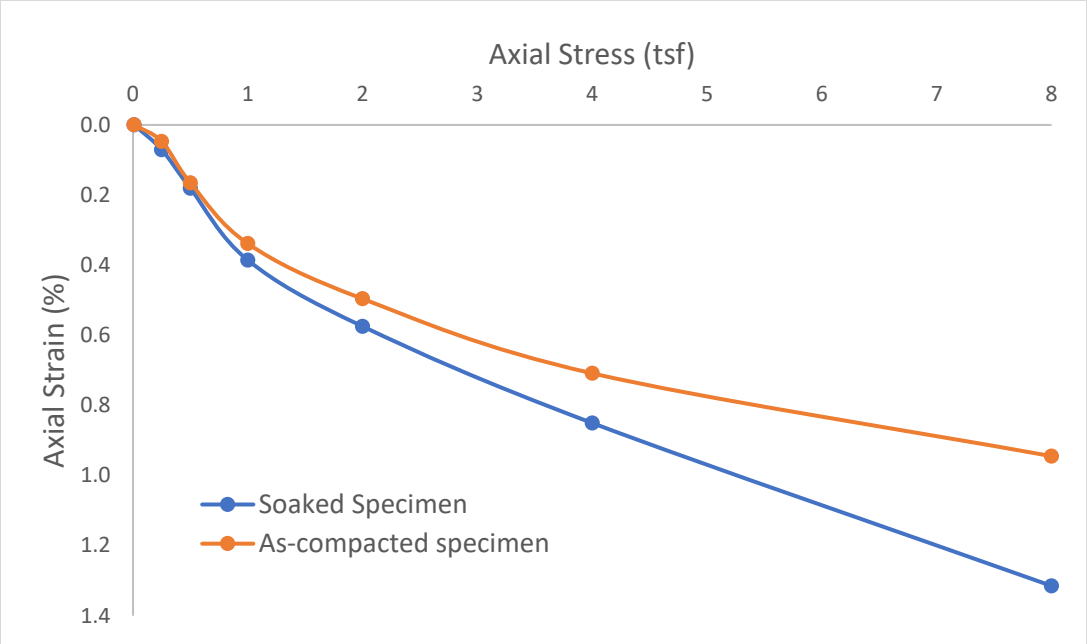

Figure B.3: Comparison of Stress-strain Characteristics Between Soaked and As-compacted Specimens for A-1-a (SP or SW) Soil at R_m = 95%, w = 10.1%

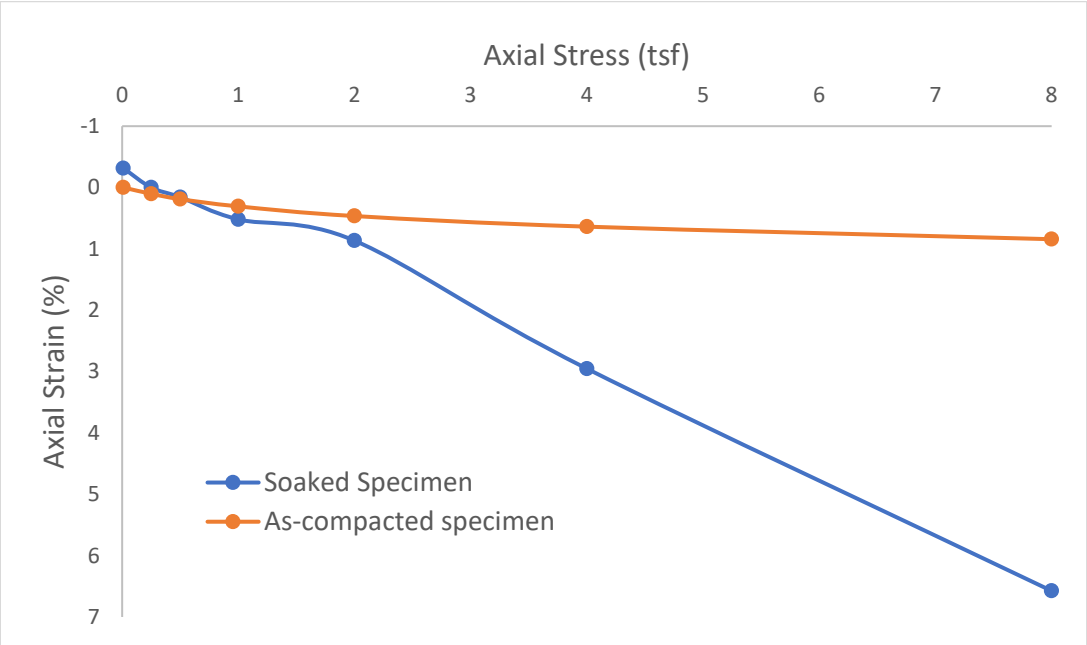

Figure B.4: Comparison of Stress-strain Characteristics Between Soaked and As-compacted Specimens for A-1-a (SC-SM) Soil at R_m = 90%, w = 4.3%

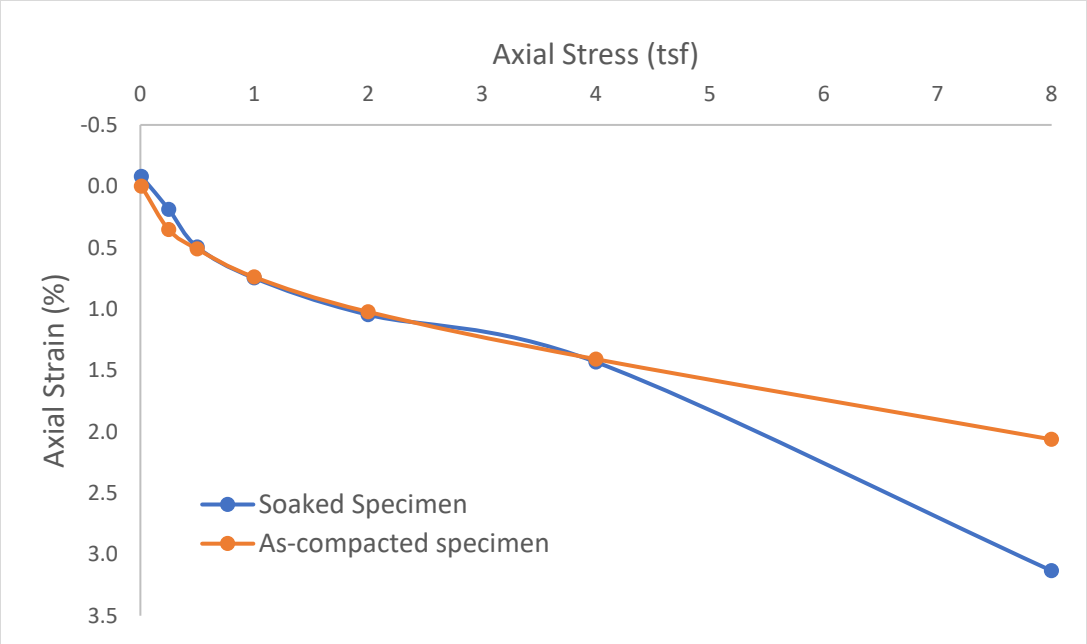

Figure B.5: Comparison of Stress-strain Characteristics Between Soaked and As-compacted Specimens for A-1-a (SC-SM) Soil at R_m = 90%, w = 6.3%

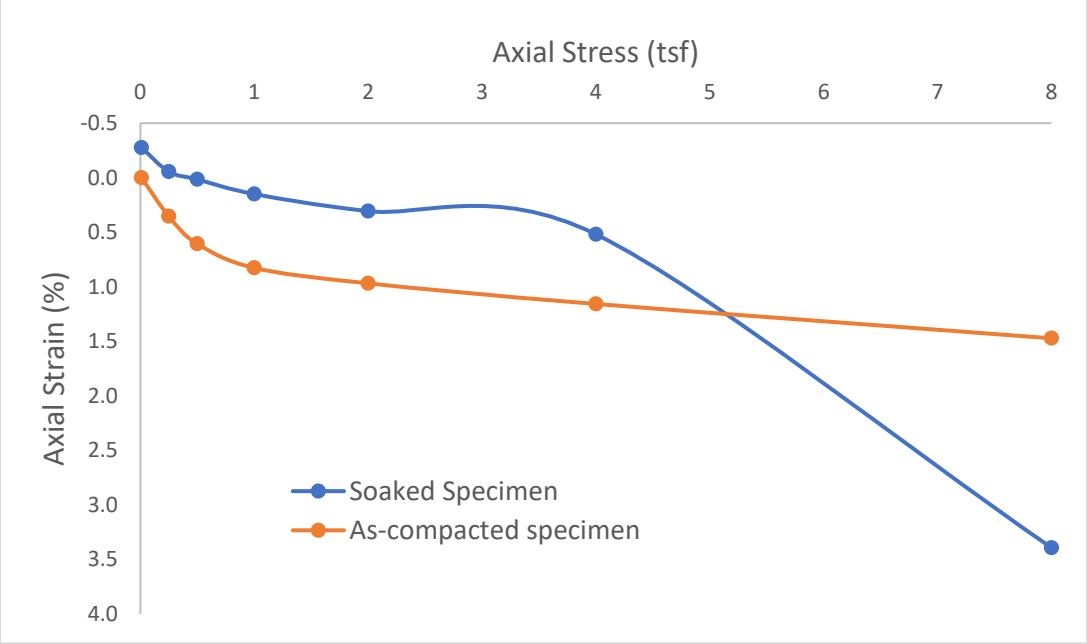

Figure B.6: Comparison of Stress-strain Characteristics Between Soaked and As-compacted Specimens for A-1-a (SC-SM) Soil at R_m = 95%, w = 4.3%

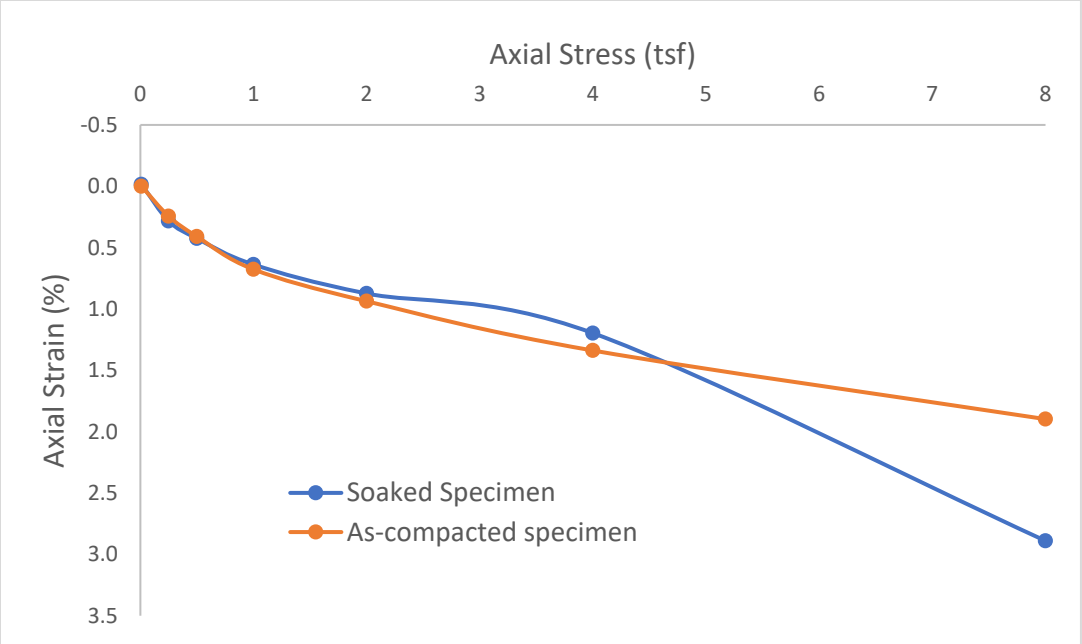

Figure B.7: Comparison of Stress-strain Characteristics Between Soaked and As-compacted Specimens for A-1-a (SC-SM) Soil at R_m = 95%, w = 6.3%

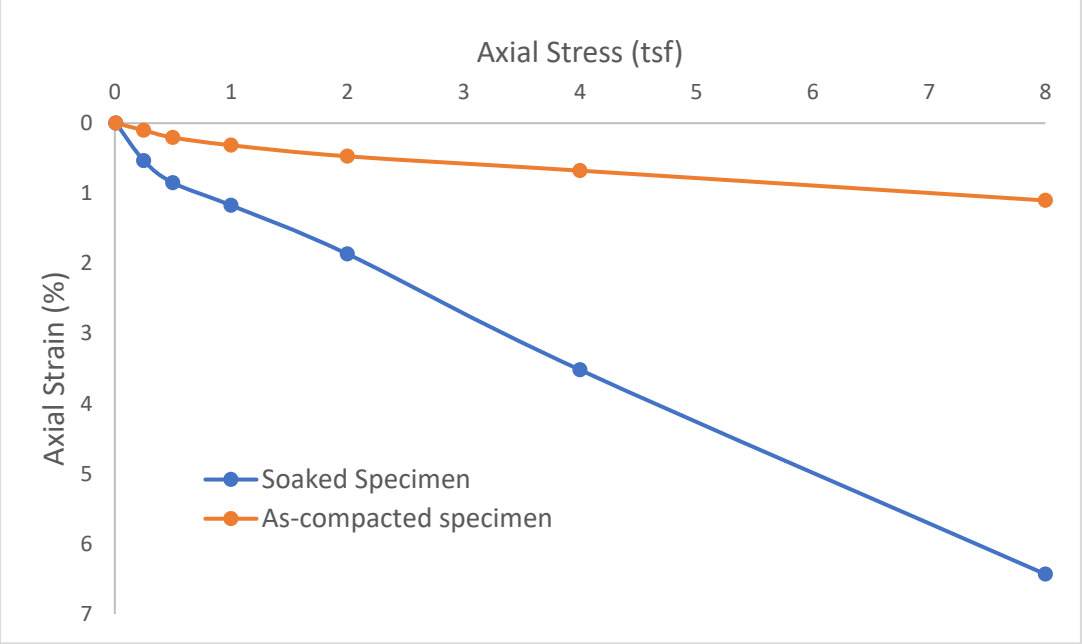

Figure B.8: Comparison of Stress-strain Characteristics Between Soaked and As-compacted Specimens for A-1-a (SM) Soil at R_m = 90%, w = 8%

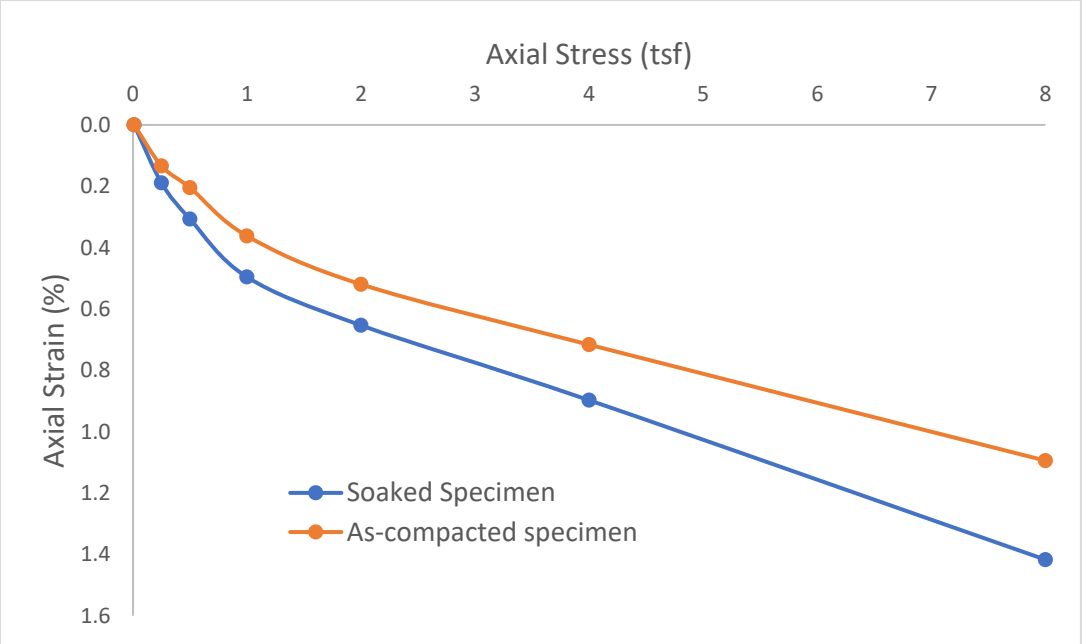

Figure B.9: Comparison of Stress-strain Characteristics Between Soaked and As-compacted Specimens for A-1-a (SM) Soil at R_m = 90%, w = 10%

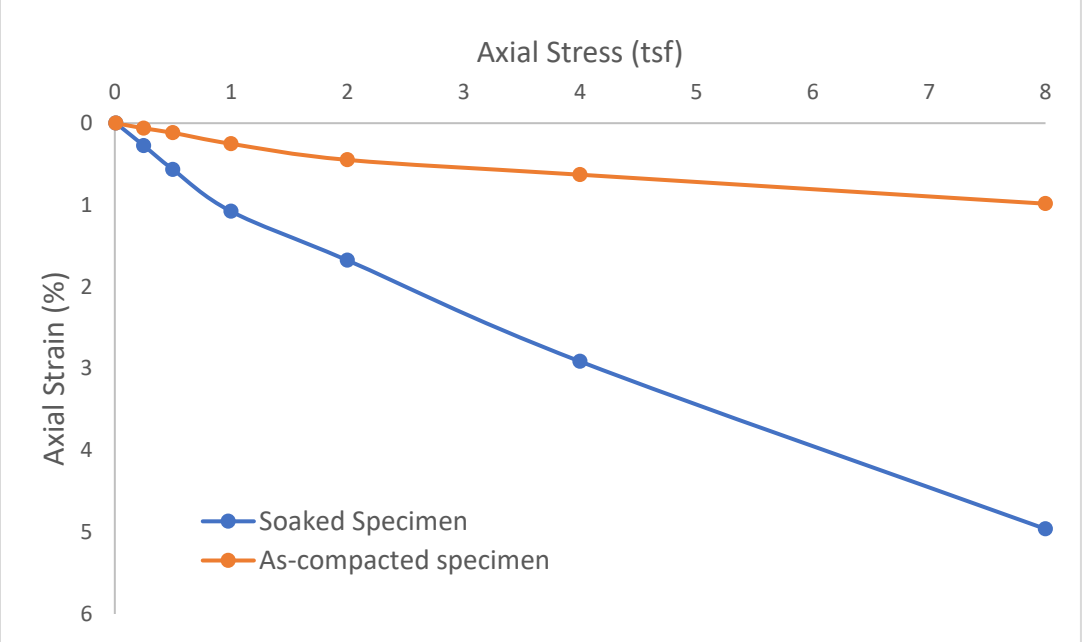

Figure B.10: Comparison of Stress-strain Characteristics Between Soaked and As-compacted Specimens for A-1-a (SM) Soil at R_m = 95% , w = 8%

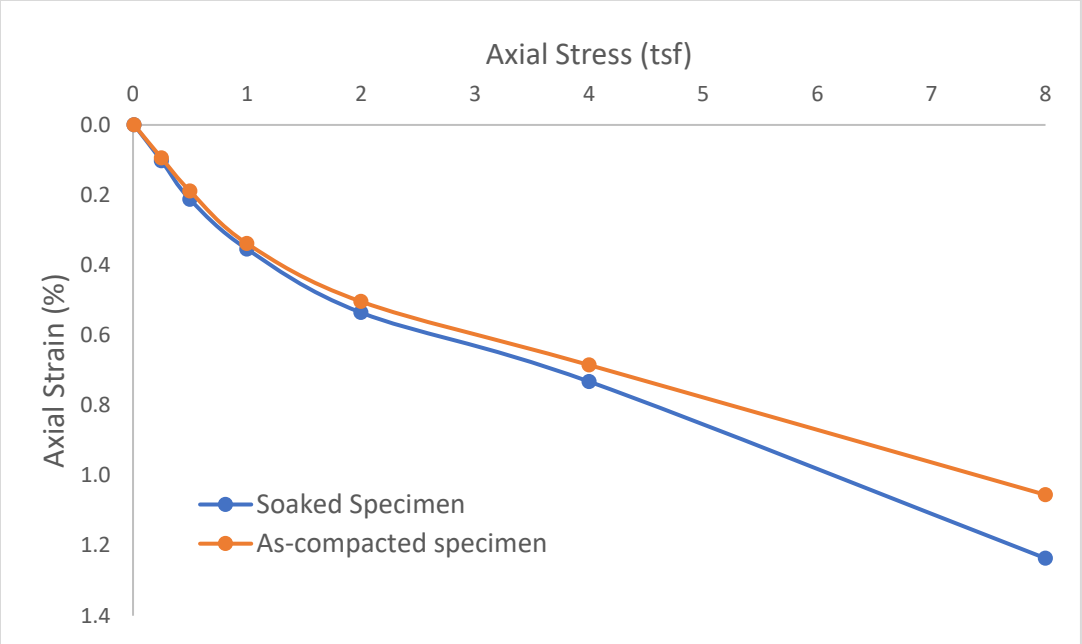

Figure B.11: Comparison of Stress-strain Characteristics Between Soaked and As-compacted Specimens for A-1-a (SM) Soil at R_m = 95%, w = 10%

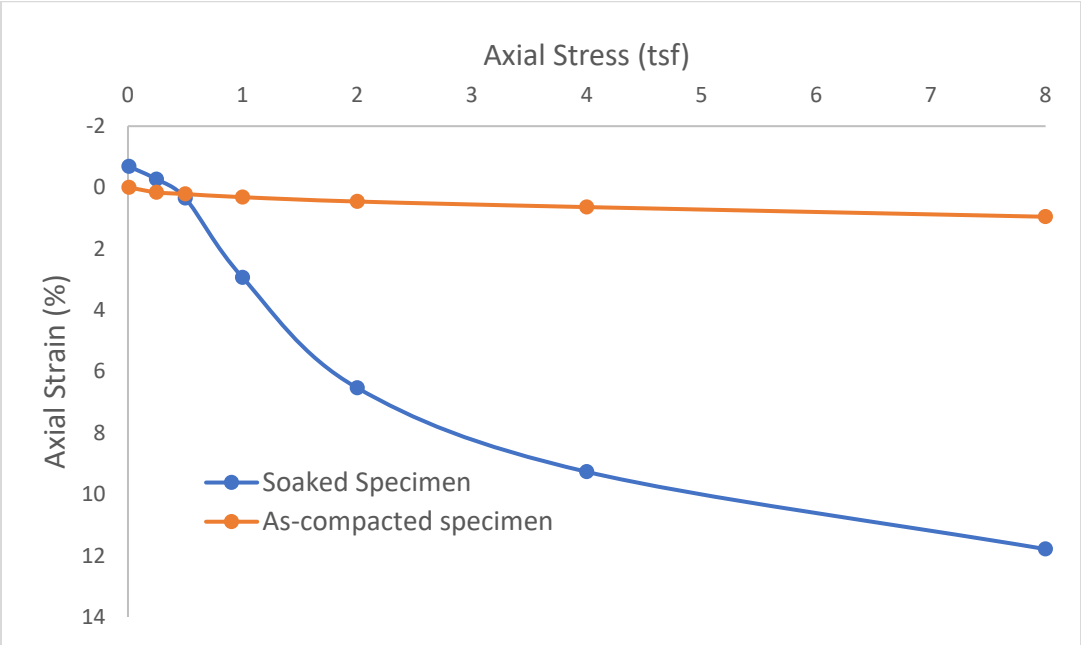

Figure B.12: Comparison of Stress-strain Characteristics Between Soaked and As-compacted Specimens for A-1-b (SC-SM) Soil at R_m = 90%, w = 4.7%

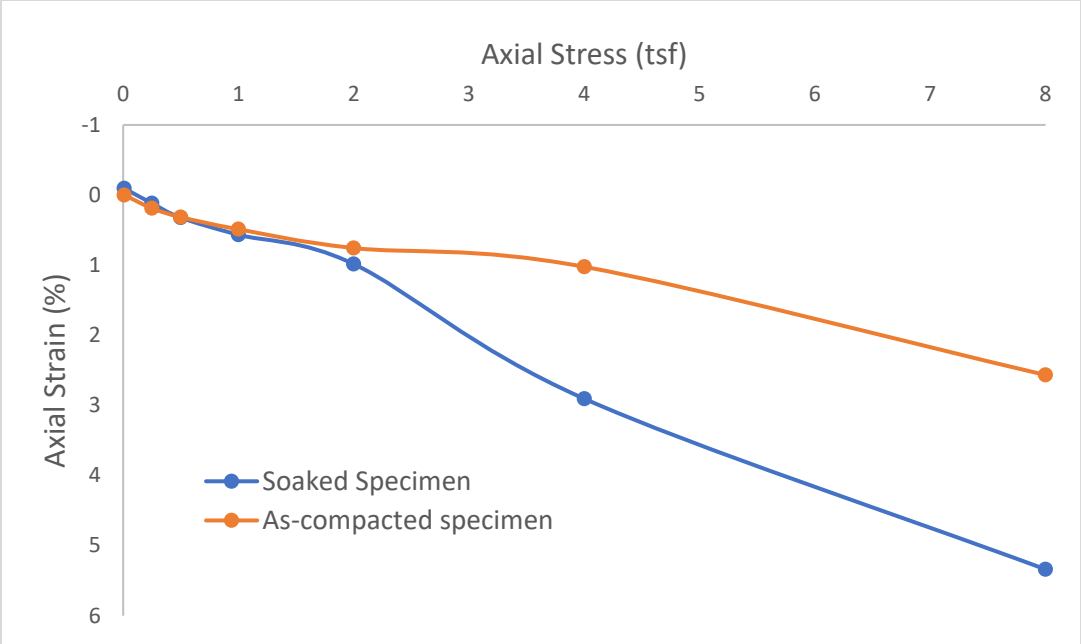

Figure B.13: Comparison of Stress-strain Characteristics Between Soaked and As-compacted Specimens for A-1-b (SC-SM) Soil at R_m = 90%, w = 6.7%

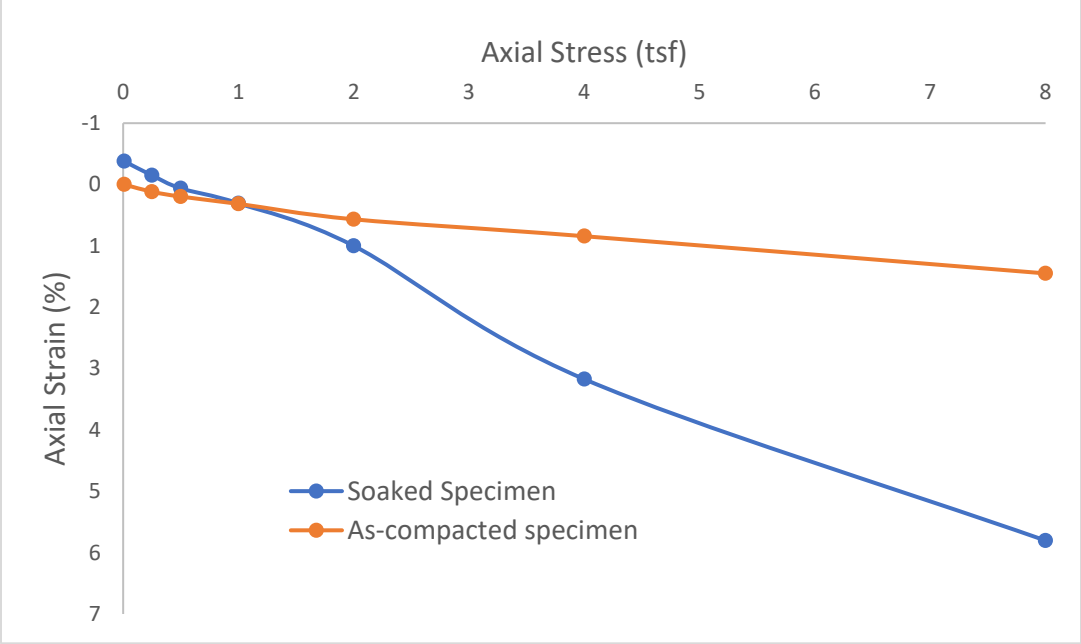

Figure B.14: Comparison of Stress-strain Characteristics Between Soaked and As-compacted Specimens for A-1-b (SC-SM) Soil at R_m = 95%, w = 4.7%

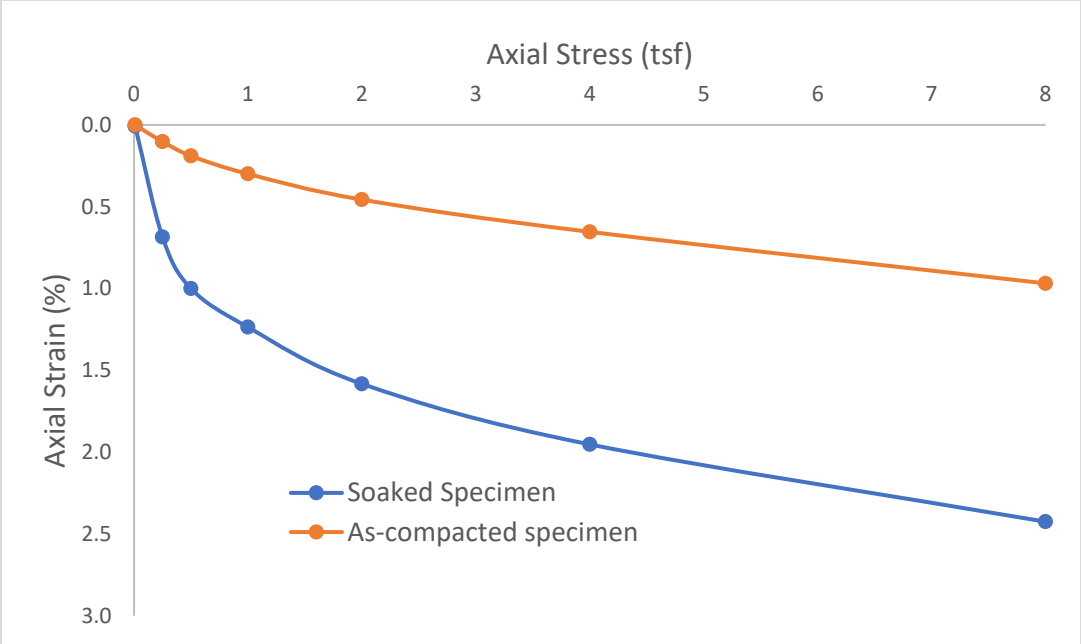

Figure B.15: Comparison of Stress-strain Characteristics Between Soaked and As-compacted Specimens for A-1-b (SC-SM) Soil at R_m = 95%, w = 6.7%

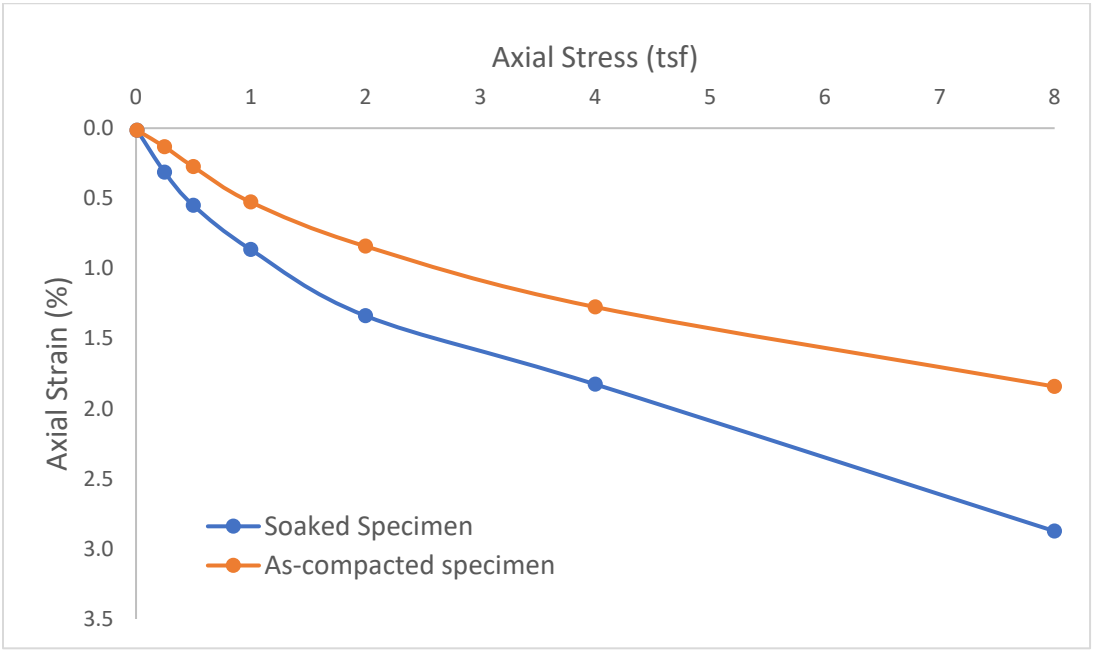

Figure B.16: Comparison of Stress-strain Characteristics Between Soaked and As-compacted Specimens for A-1-b (SM) Soil at R_m = 92%, w = 10%

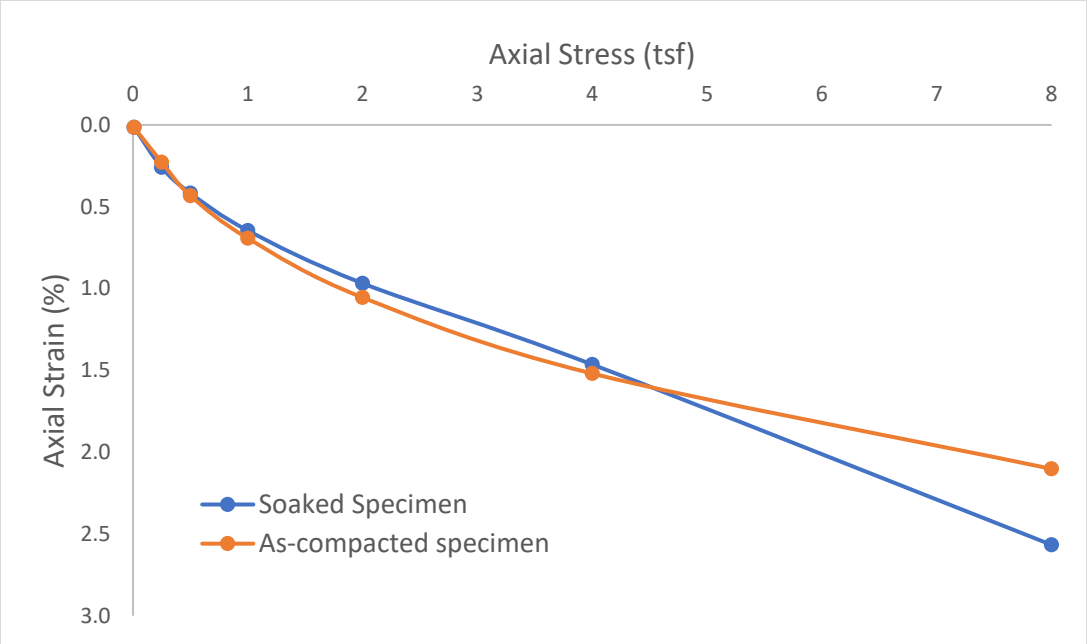

Figure B.17: Comparison of Stress-sStrain Characteristics Between Soaked and As-compacted Specimens for A-1-b (SM) Soil at R_m = 92%, w = 12%

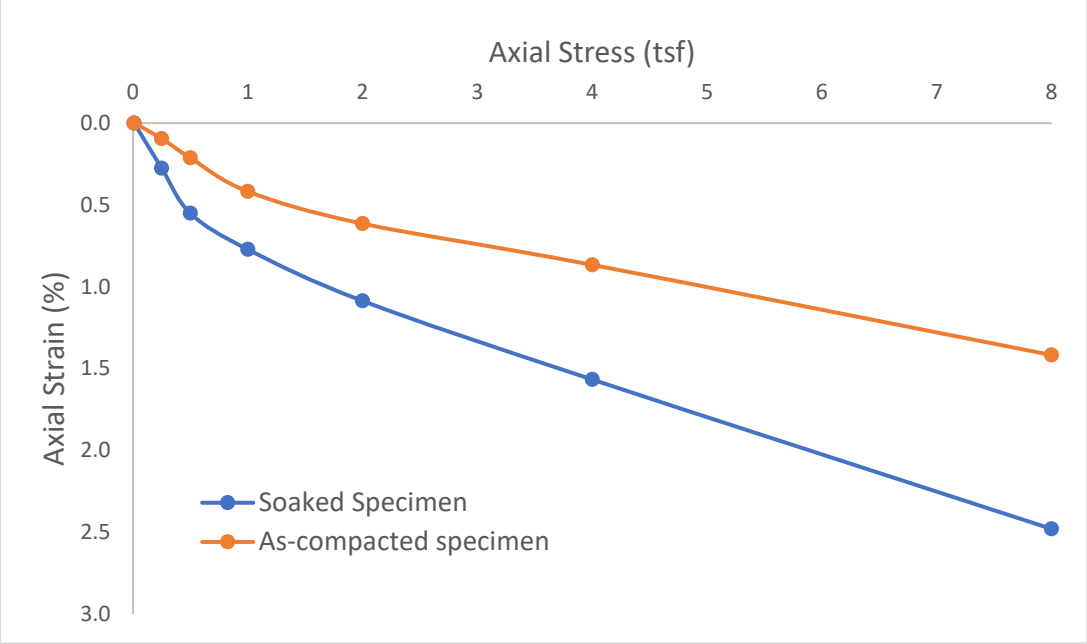

Figure B.18: Comparison of Stress-strain Characteristics Between Soaked and As-compacted Specimens for A-1-b (SM) Soil at R_m = 95%, w = 10%

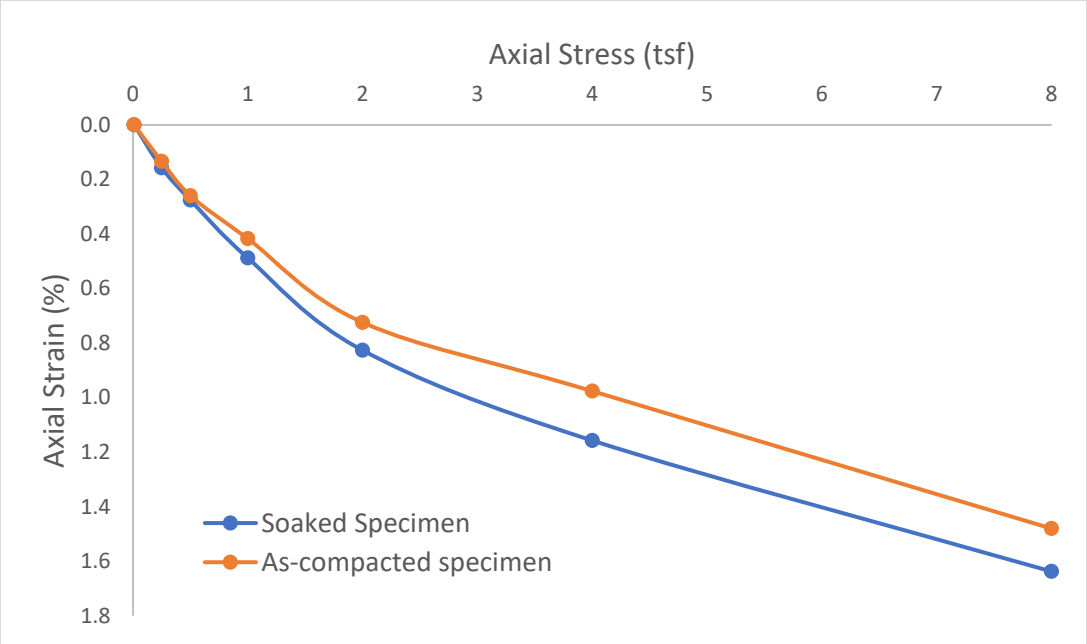

Figure B.19: Comparison of Stress-strain Characteristics Between Soaked and As-compacted Specimens for A-1-b (SM) Soil at R_m = 95%, w = 12%

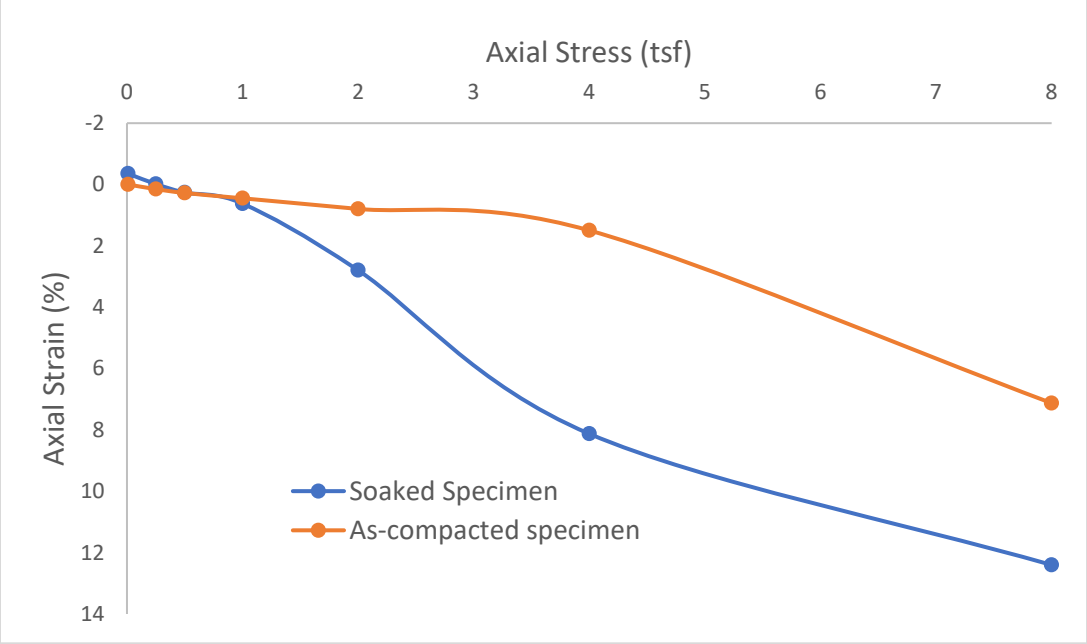

Figure B.20: Comparison of Stress-strain Characteristics Between Soaked and As-compacted Specimens for A-2 (SC) PI=10 Soil at R_s = 92%, w = 13.5%

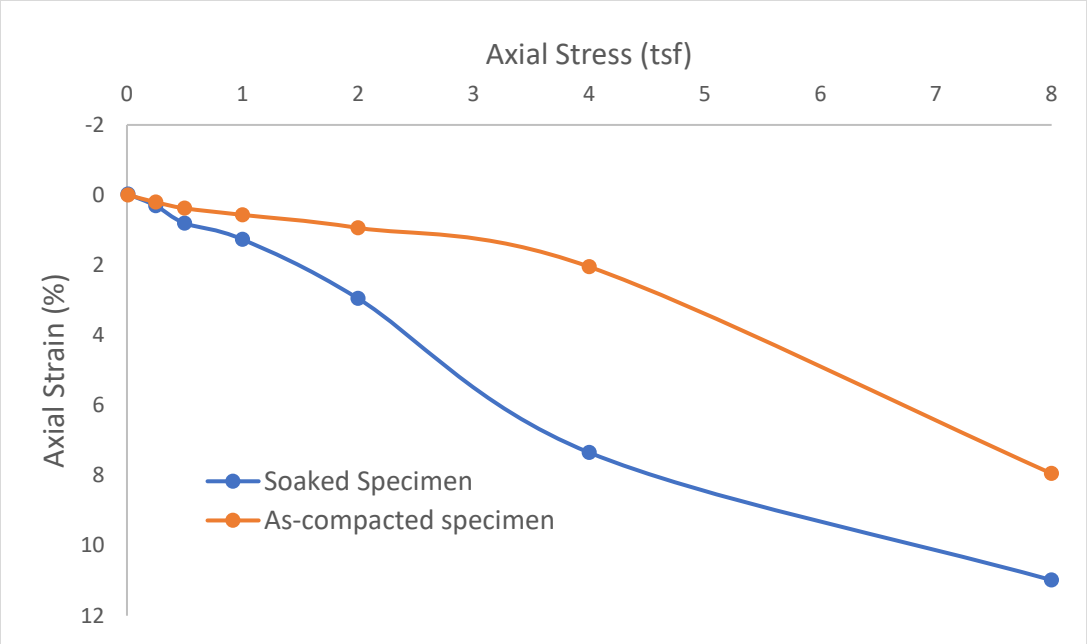

Figure B.21: Comparison of Stress-strain Characteristics Between Soaked and As-compacted Specimens for A-2 (SC) PI=10 Soil at R_s = 92%, w = 15.5%

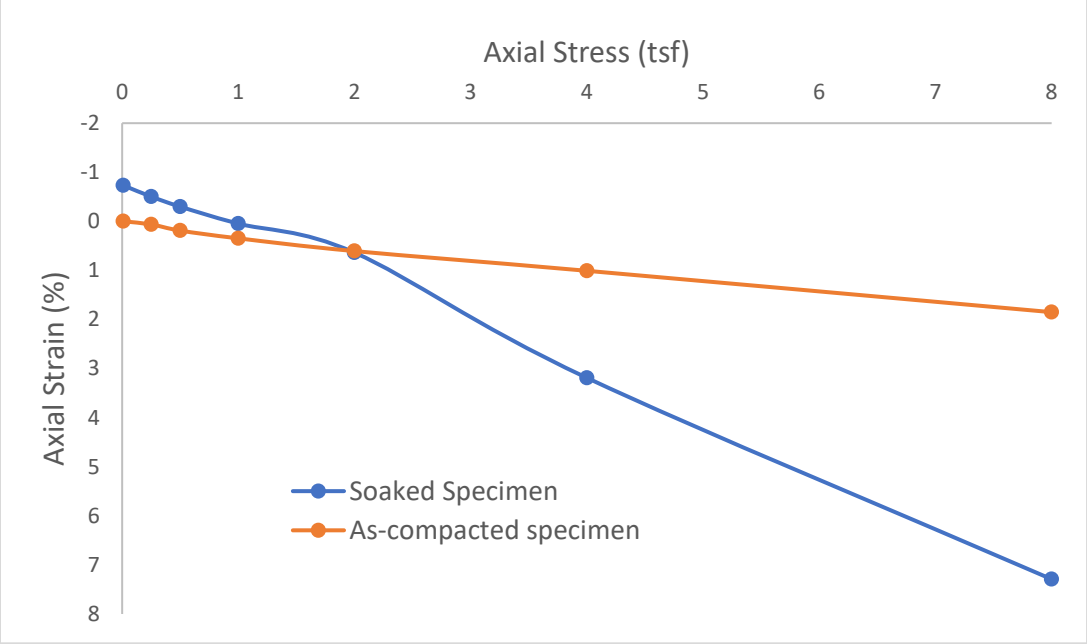

Figure B.22: Comparison of Stress-strain Characteristics Between Soaked and As-compacted Specimens for A-2 (SC) PI=10 Soil at R_s = 96%, w = 13.5%

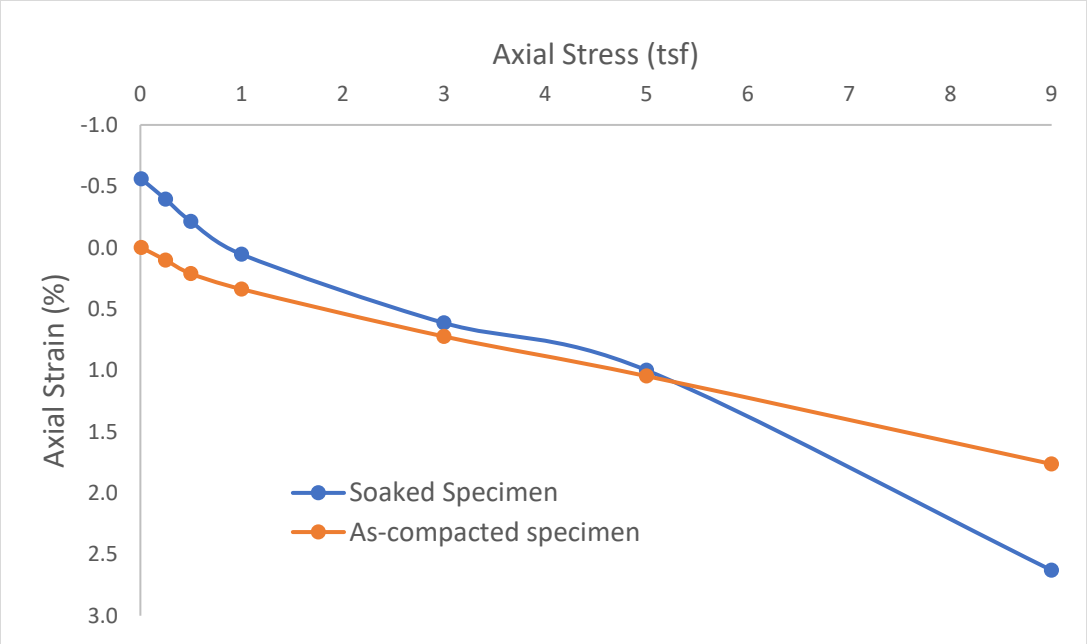

Figure B.23: Comparison of Stress-strain Characteristics Between Soaked and As-compacted Specimens for A-2 (SC) PI=10 Soil at R_s = 100%, w = 13.5%

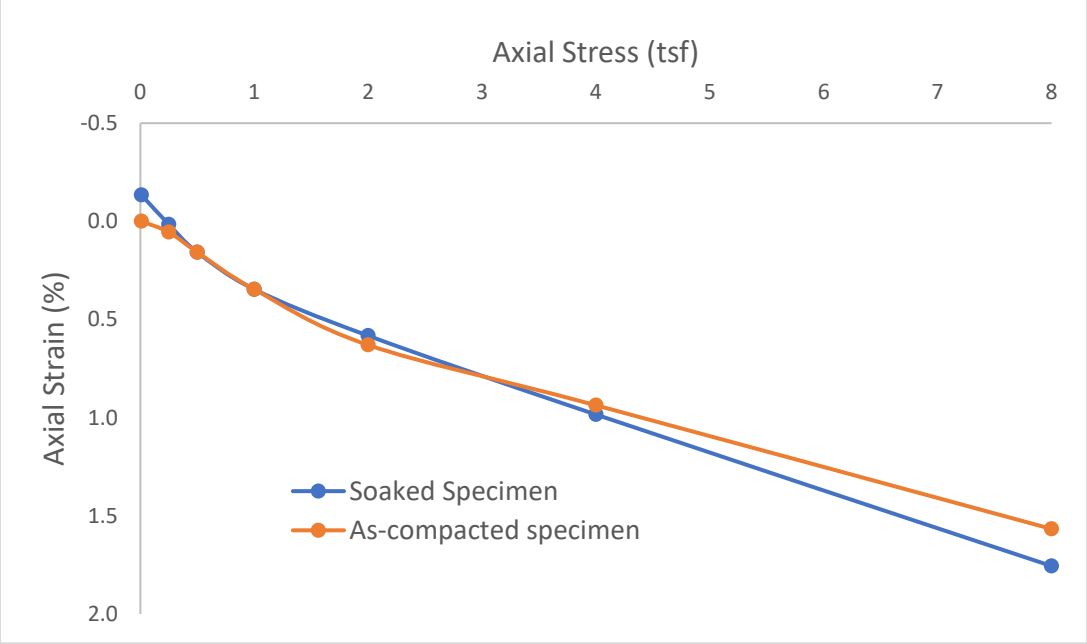

Figure B.24: Comparison of Stress-strain Characteristics Between Soaked and As-compacted Specimens for A-2 (SC) PI=10 Soil at R_s = 100%, w = 15.5%

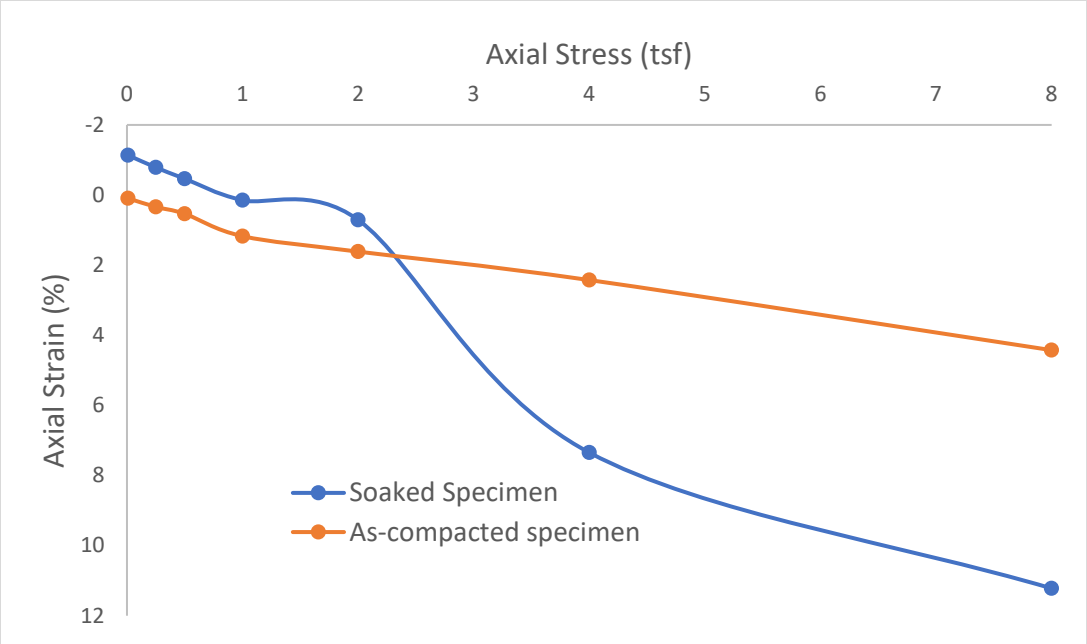

Figure B.25: Comparison of Stress-strain Characteristics Between Soaked and As-compacted Specimens for A-2 (SC) PI>>11 Soil at R_s = 96%, w = 17%

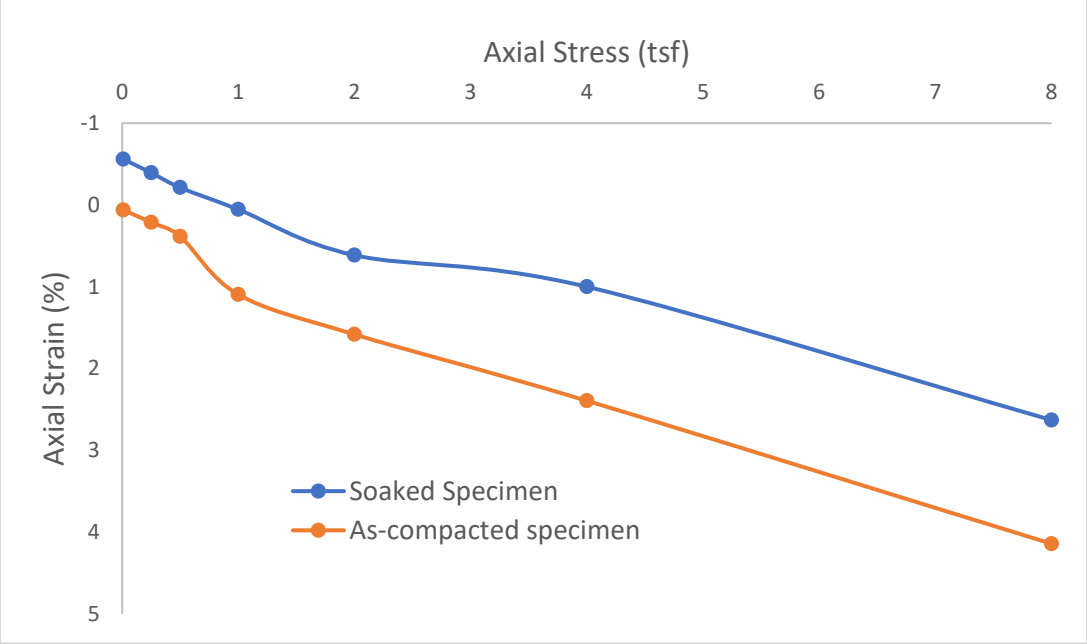

Figure B.26: Comparison of Stress-strain Characteristics Between Soaked and As-compacted Specimens for A-2 (SC) PI>>11 Soil at R_s = 96%, w = 19%

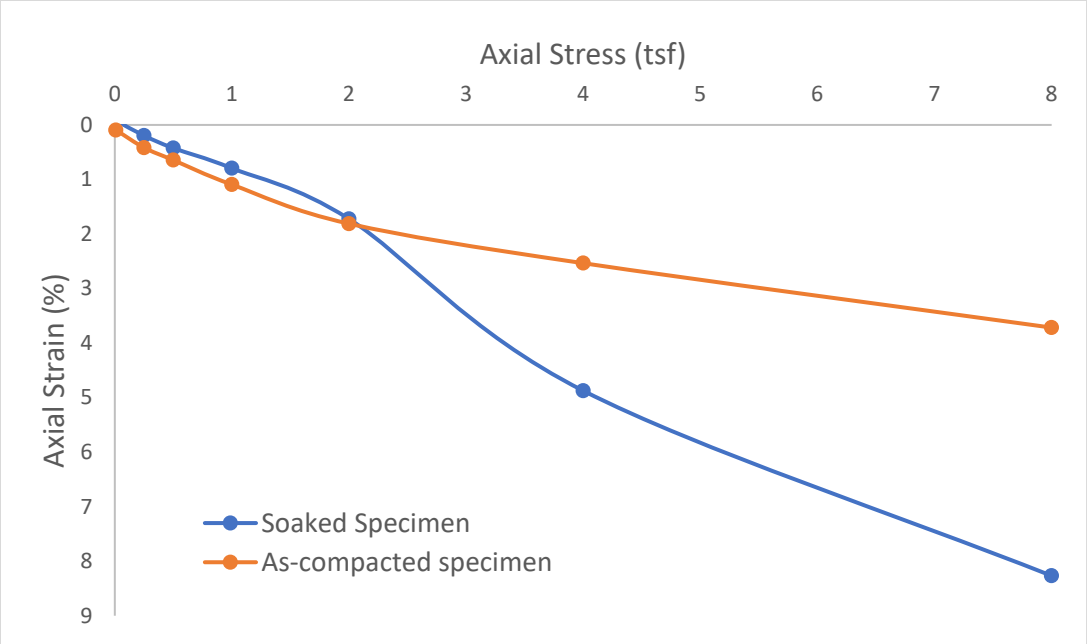

Figure B.27: Comparison of Stress-strain Characteristics Between Soaked and As-compacted Specimens for A-3 (SP-SM) Soil at R_s = 90%, w = 14%

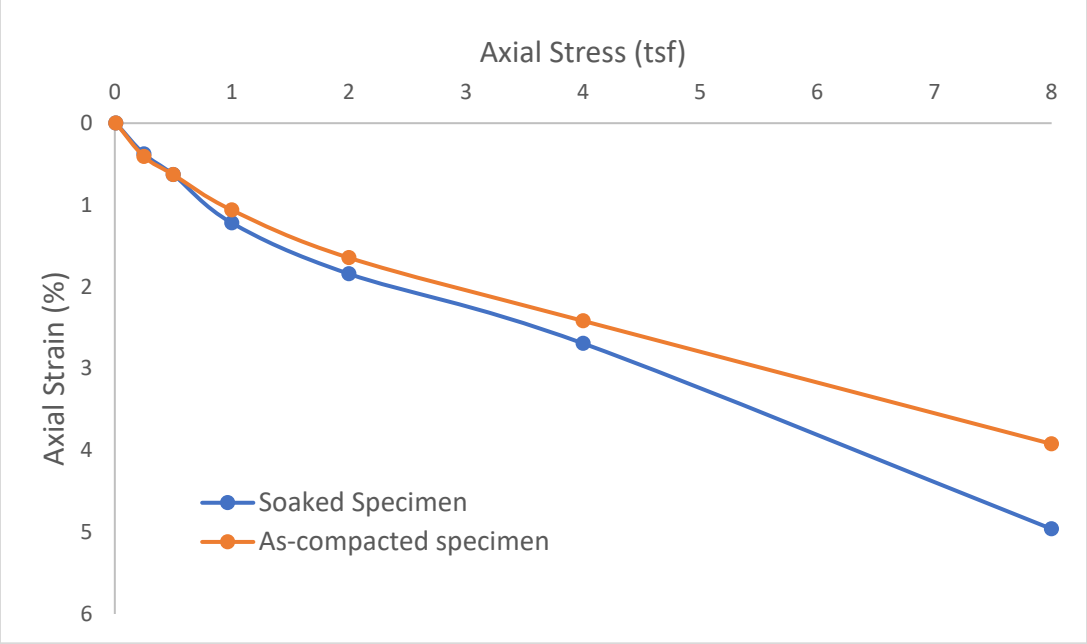

Figure B.28: Comparison of Stress-strain Characteristics Between Soaked and As-compacted Specimens for A-3 (SP-SM) Soil at R_s = 90%, w = 16%

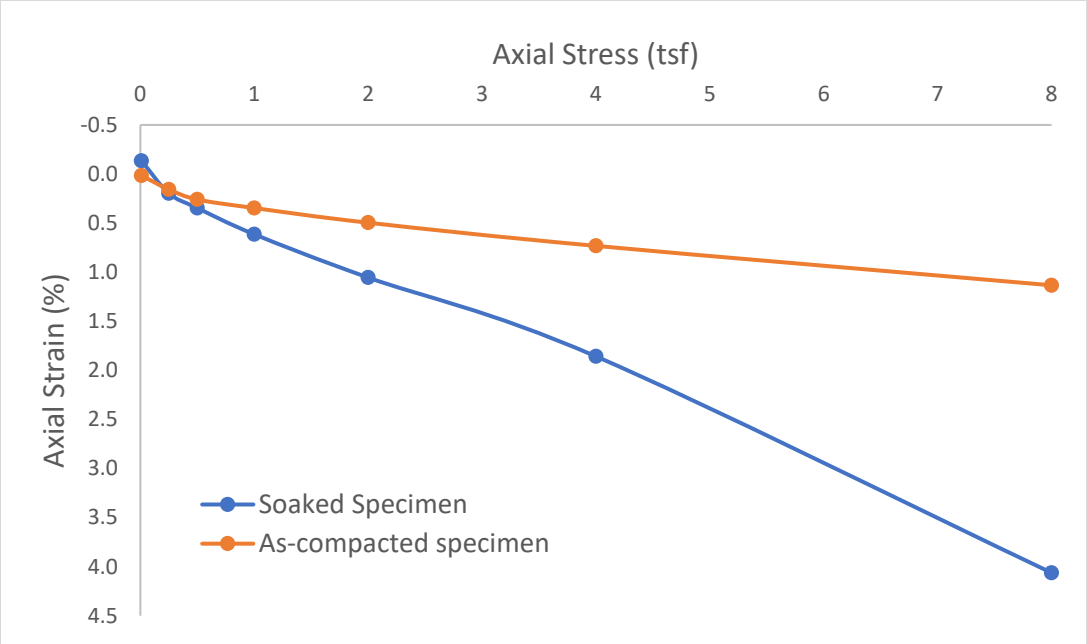

Figure B.29: Comparison of Stress-strain Characteristics Between Soaked and As-compacted Specimens for A-3 (SP-SM) Soil at R_s = 93%, w = 14%

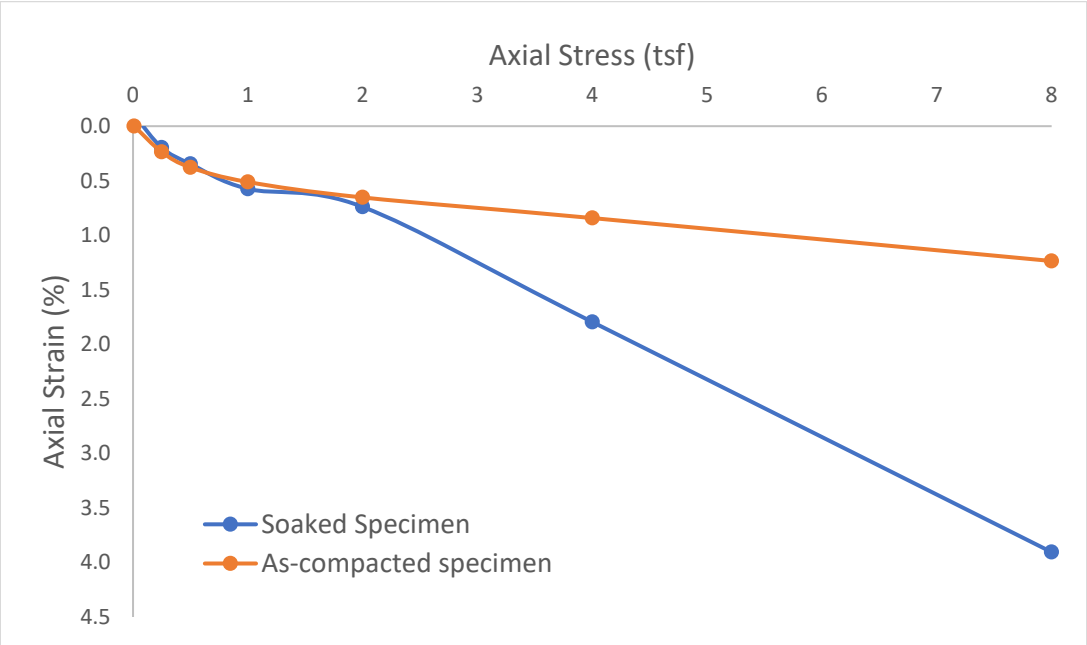

Figure B.30: Comparison of Stress-strain Characteristics Between Soaked and As-compacted Specimens for A-3 (SP-SM) Soil at R_s = 93%, w = 16%

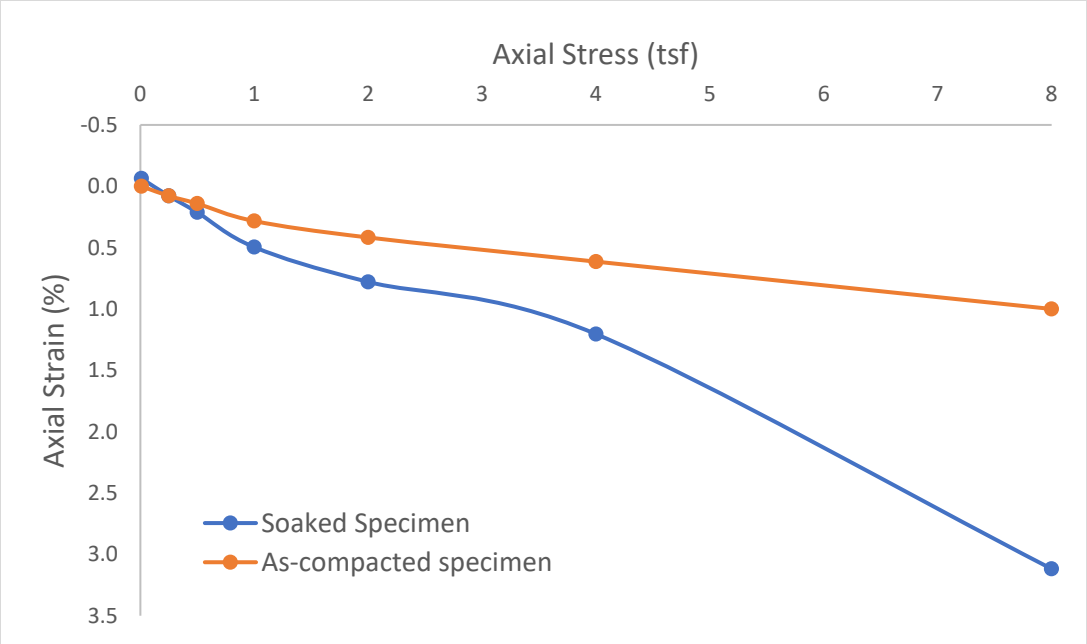

Figure B.31: Comparison of Stress-strain Characteristics Between Soaked and As-compacted Specimens for A-3 (SP-SM) Soil at R_s = 96%, w = 14%

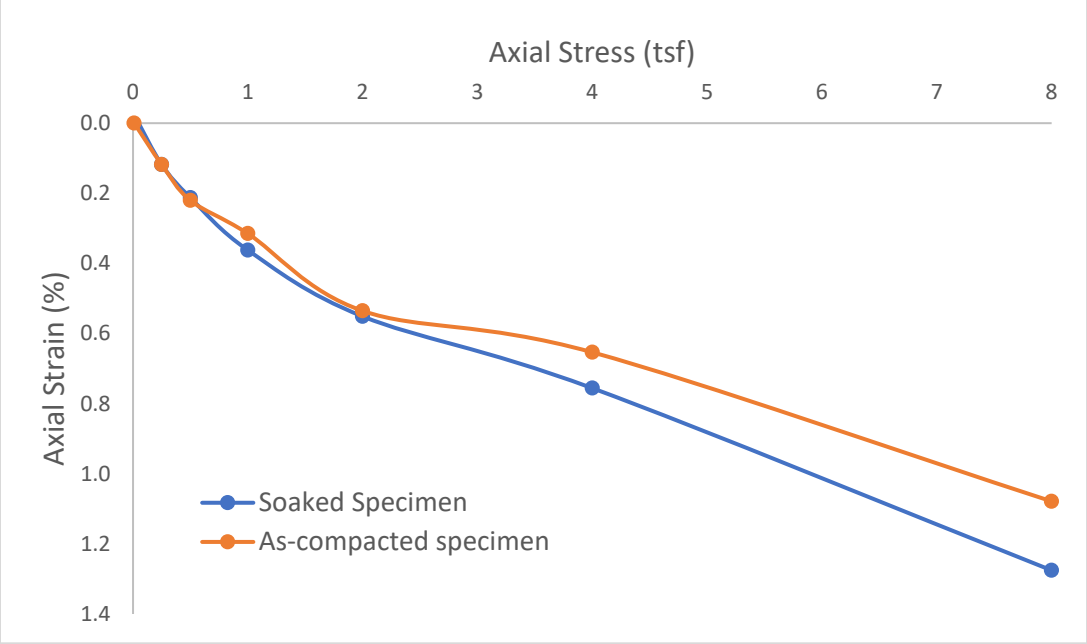

Figure B.32: Comparison of Stress-strain Characteristics Between Soaked and As-compacted Specimens for A-3 (SP-SM) Soil at R_s = 96%, w = 16%

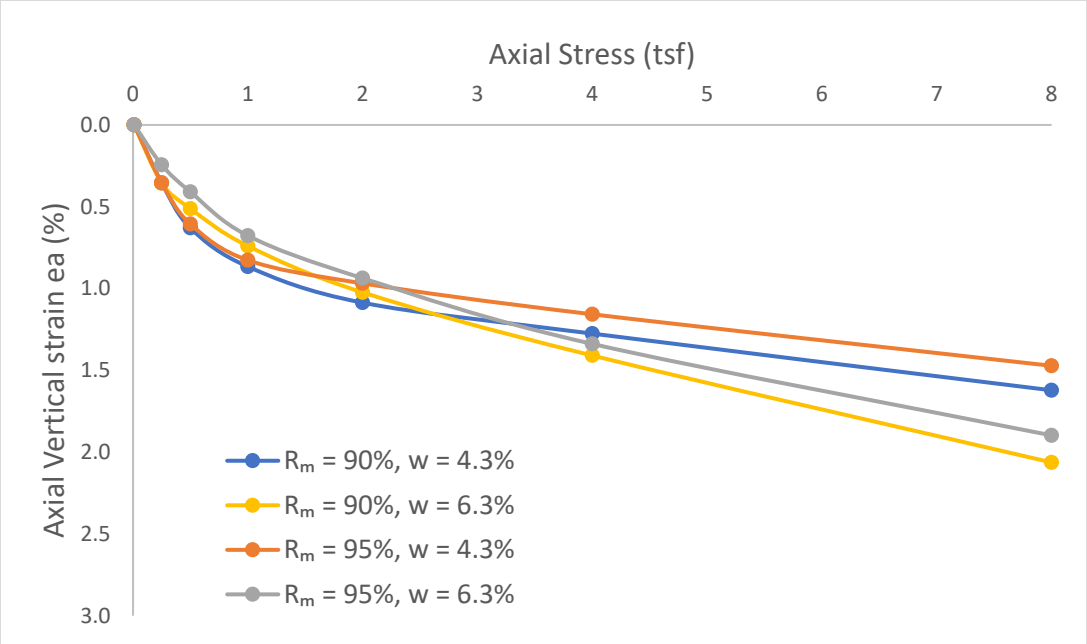

Figure B.33: Loading-induced Stress-strain Characteristics of A-1-a (SC-SM) As-compacted Specimen

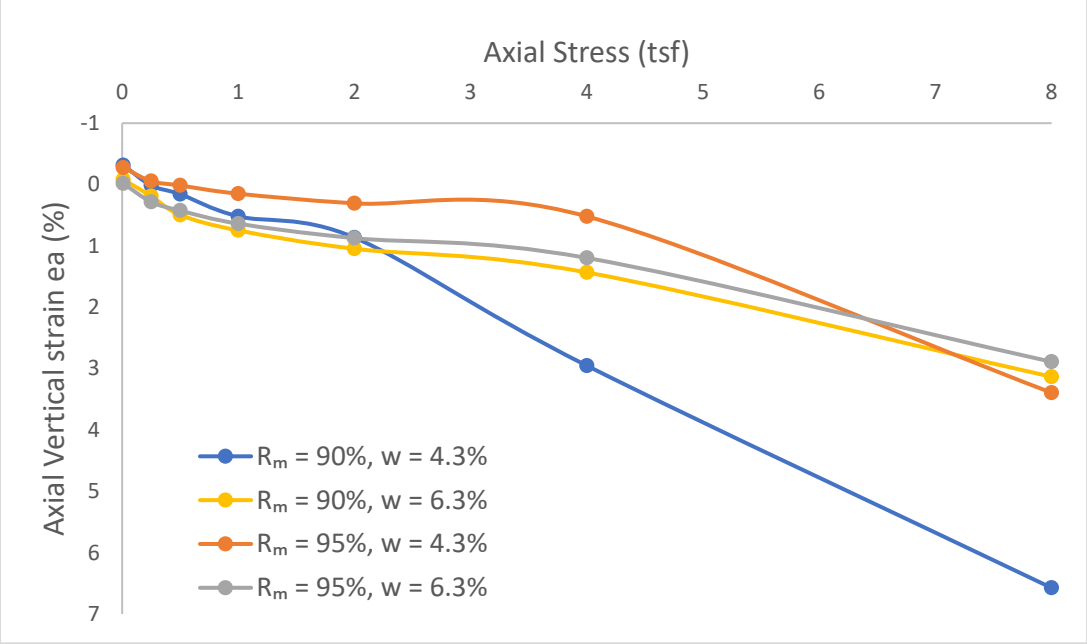

Figure B.34: Loading-induced Stress-strain Characteristics of A-1-a (SC-SM) Soaked Specimen

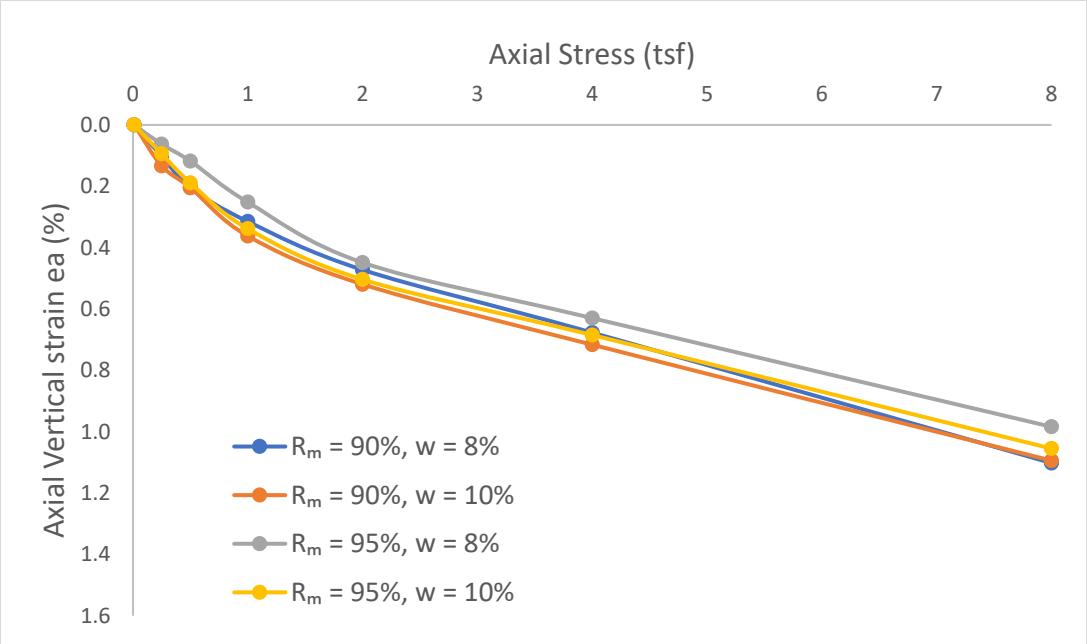

Figure B.35: Loading-induced Stress-strain Characteristics of A-1-a (SM) As-compacted Specimen

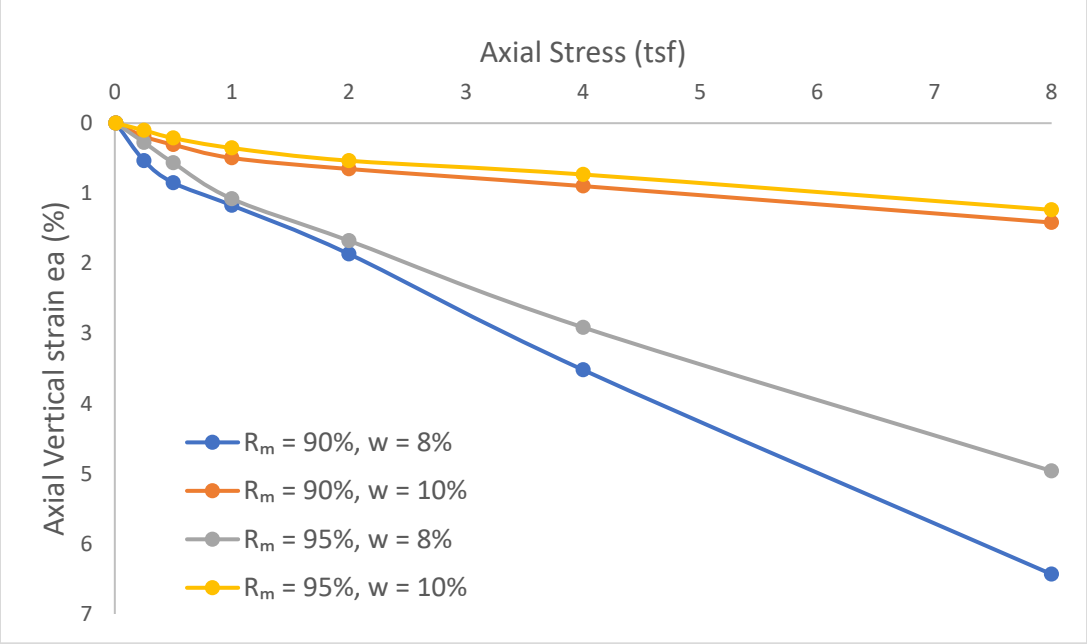

Figure B.36: Loading-induced Stress-strain Characteristics of A-1-a (SM) Soaked Specimen

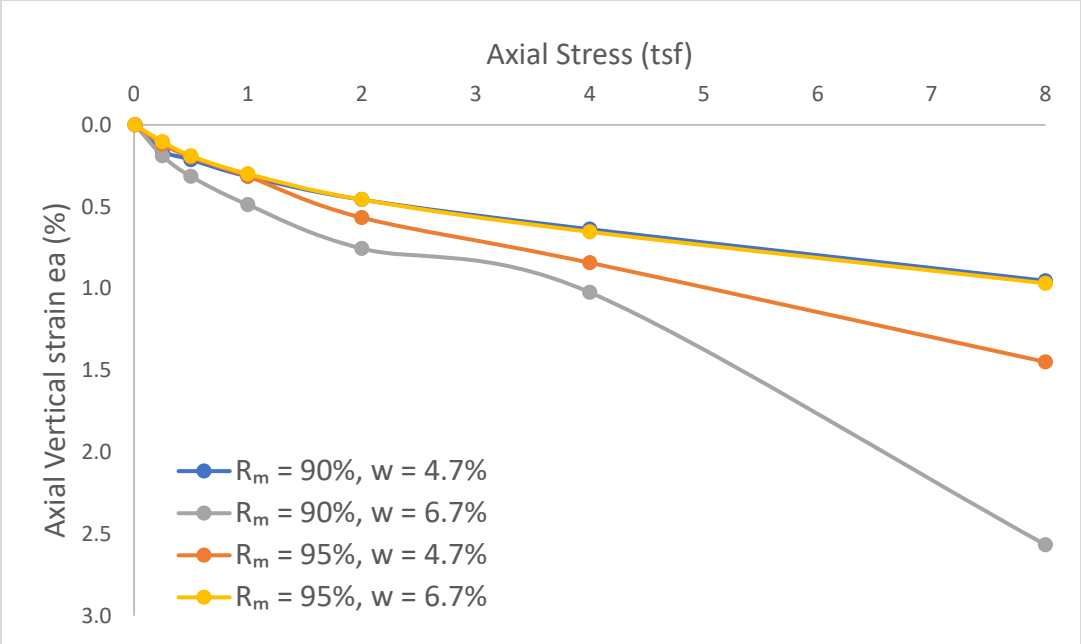

Figure B.37: Loading-induced Stress-strain Characteristics of A-1-b (SC-SM) As-compacted Specimen

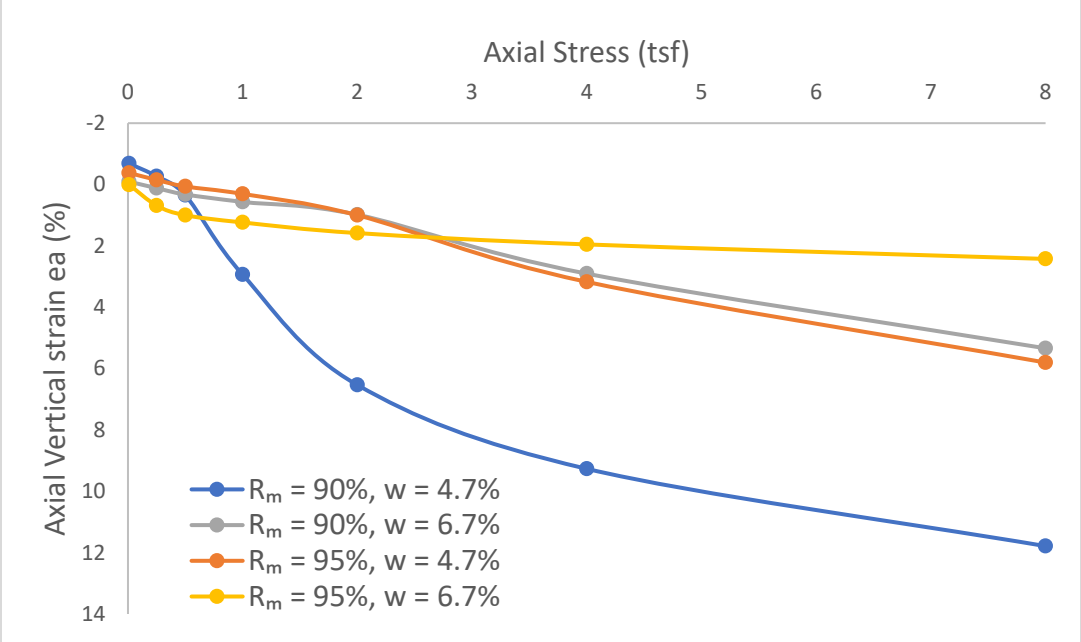

Figure B.38: Loading-induced Stress-strain Characteristics of A-1-b (SC-SM) Soaked Specimen

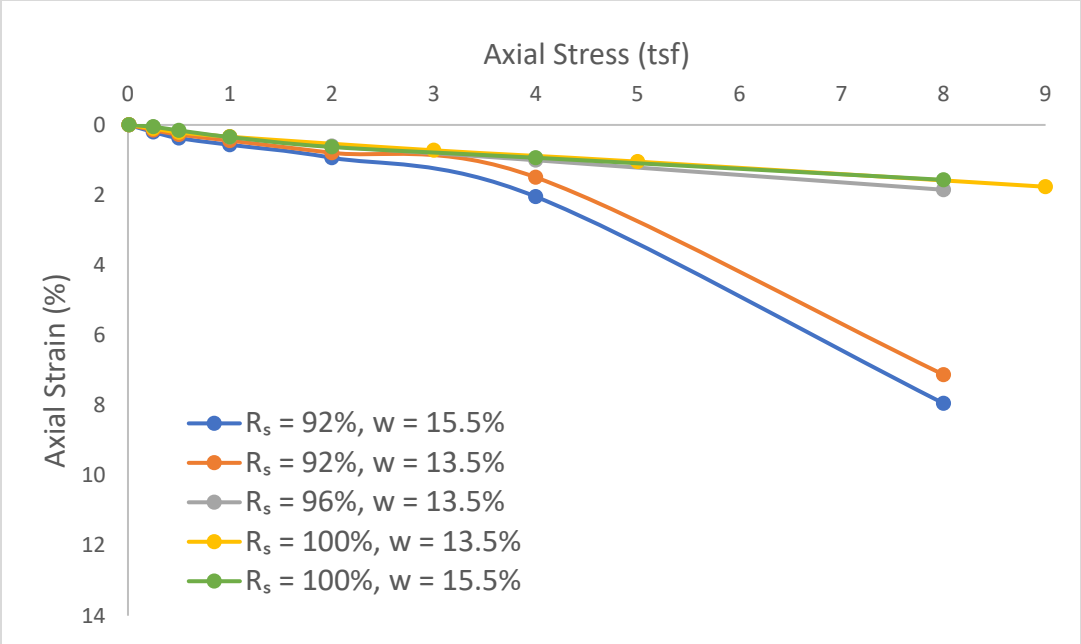

Figure B.39: Loading-induced Stress-strain Characteristics of A-2 (SC) PI=10 As-compacted Specimen

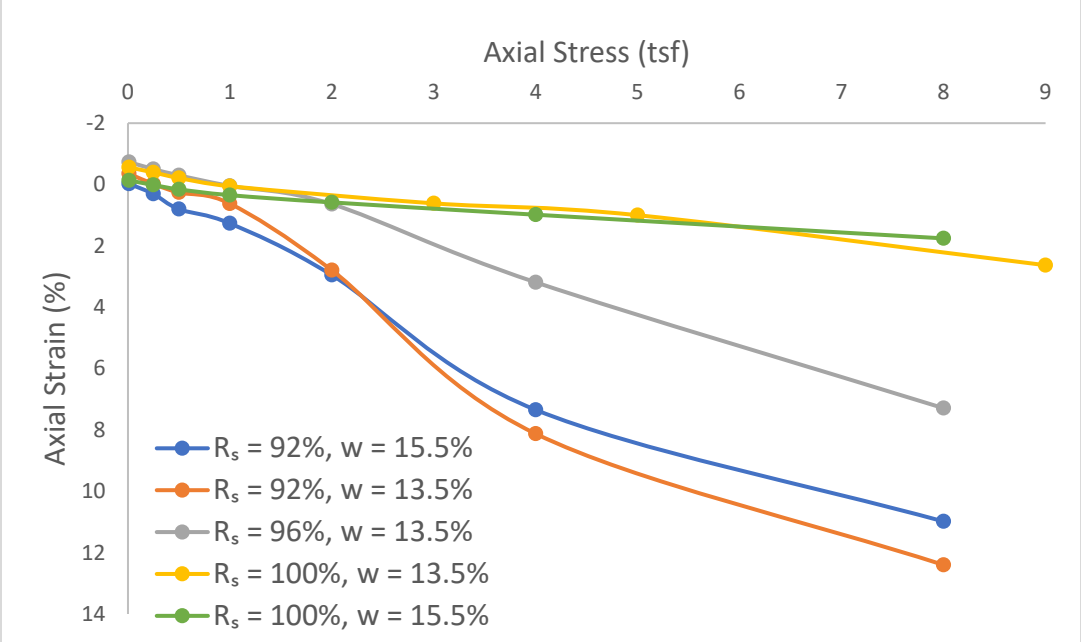

Figure B.40: Loading-induced Stress-strain Characteristics of A-2 (SC) PI=10 Soaked Specimen

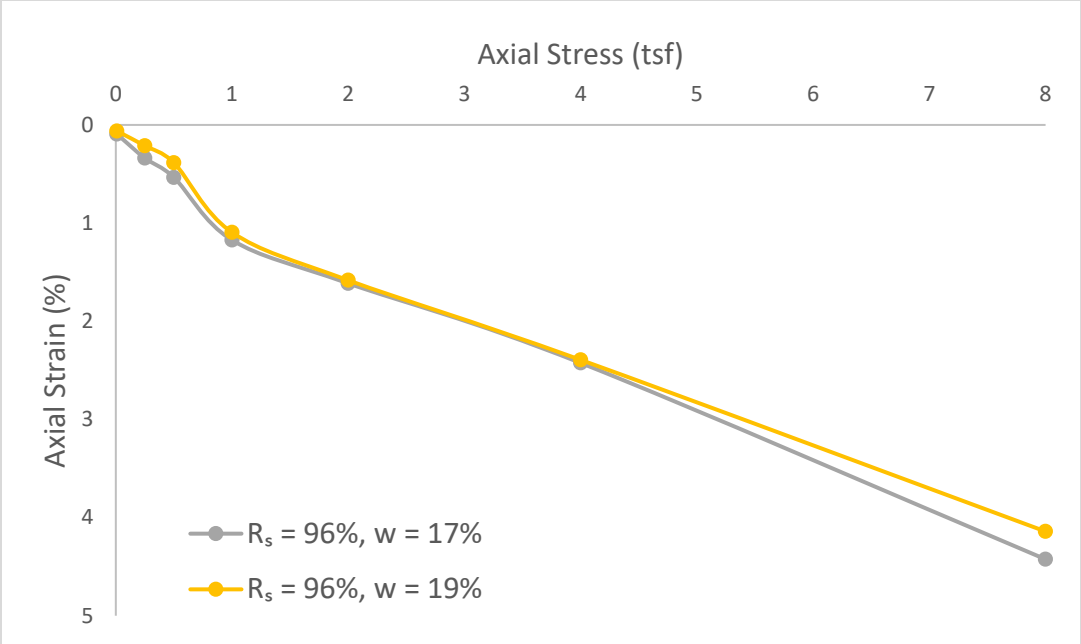

Figure B.41: Loading-induced Stress-strain Characteristics of A-2 (SC) PI>>11 As-compacted Specimen

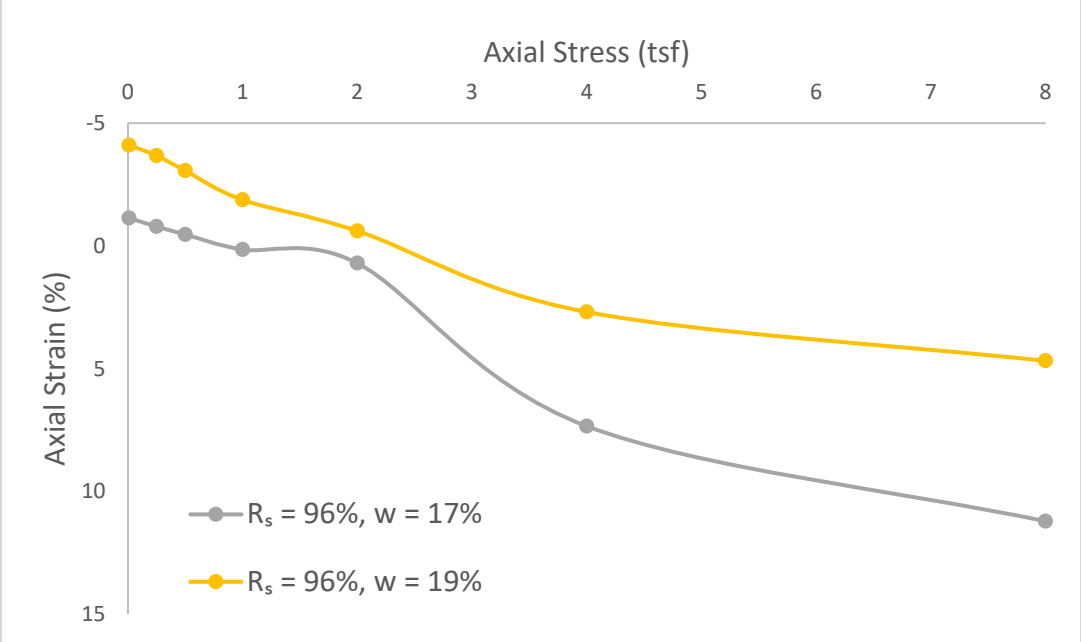

Figure B.42: Loading-induced Stress-strain Characteristics of A-2 (SC) PI>>11 Soaked Specimen

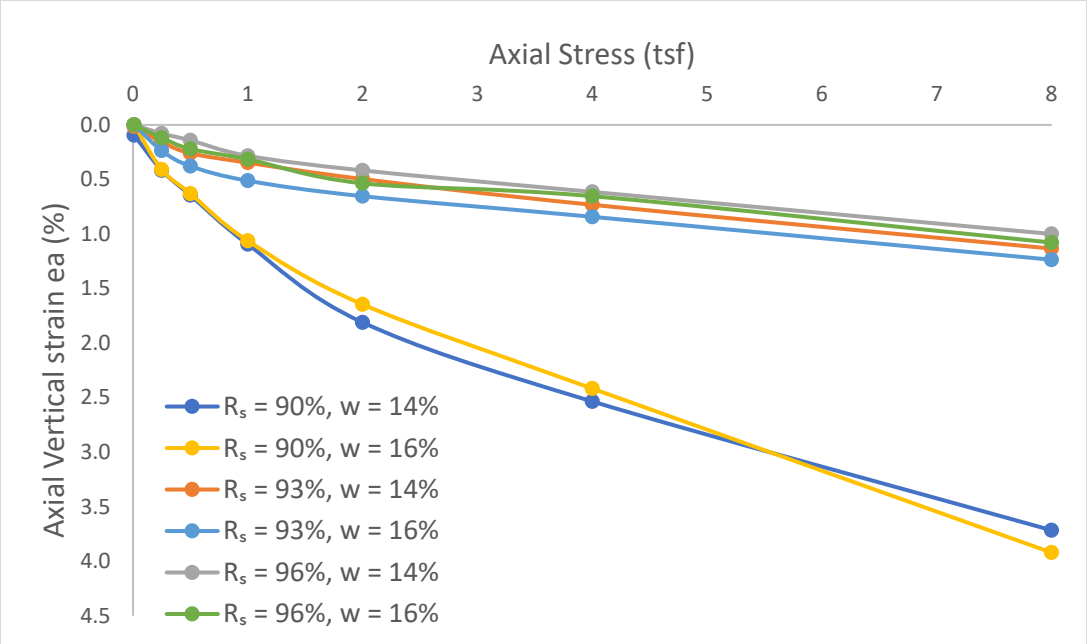

Figure B.43: Loading-induced Stress-strain Characteristics of A-3 (SP-SM) As-compacted Specimen

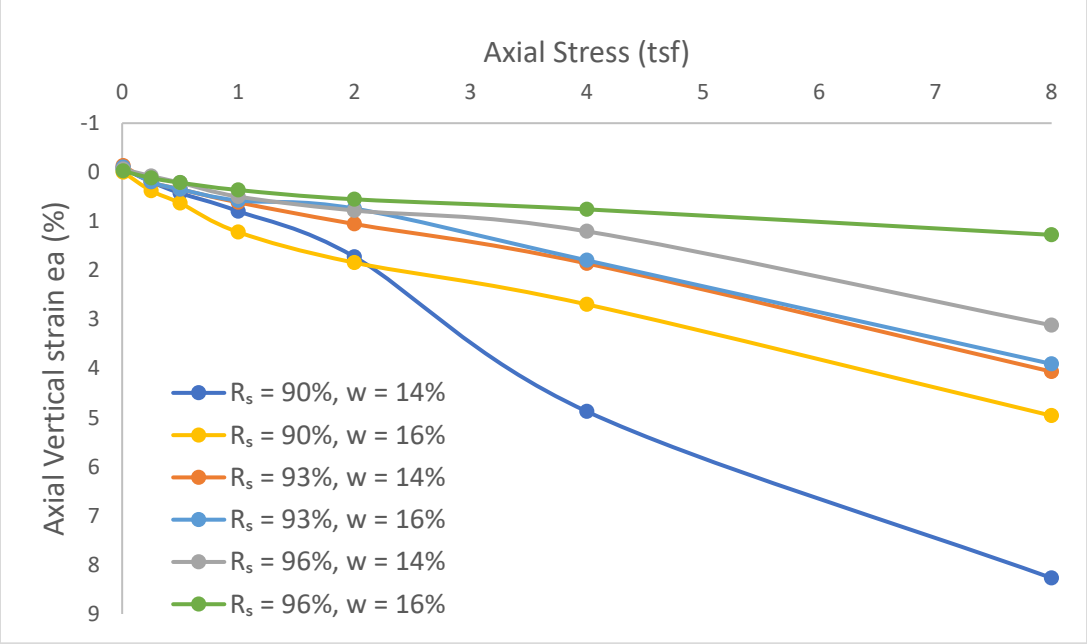

Figure B.44: Loading-induced Stress-strain Characteristics of A-3 (SP-SM) Soaked Specimen

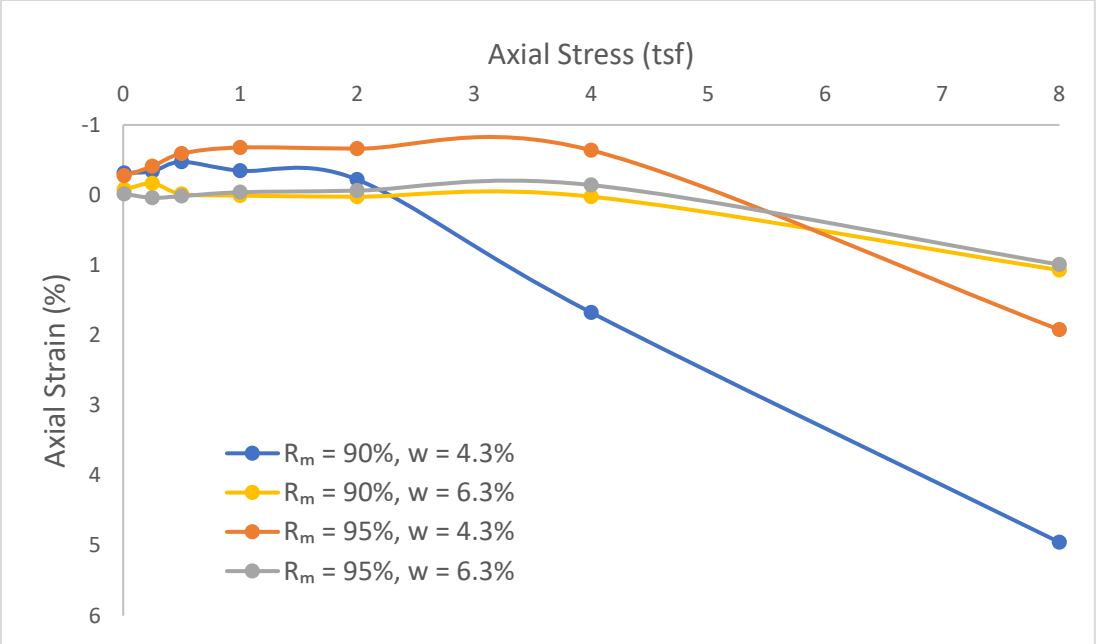

Figure B.45: One-dimensional Double Consolidometer Test Results for A-1-a (SC-SM) Soil

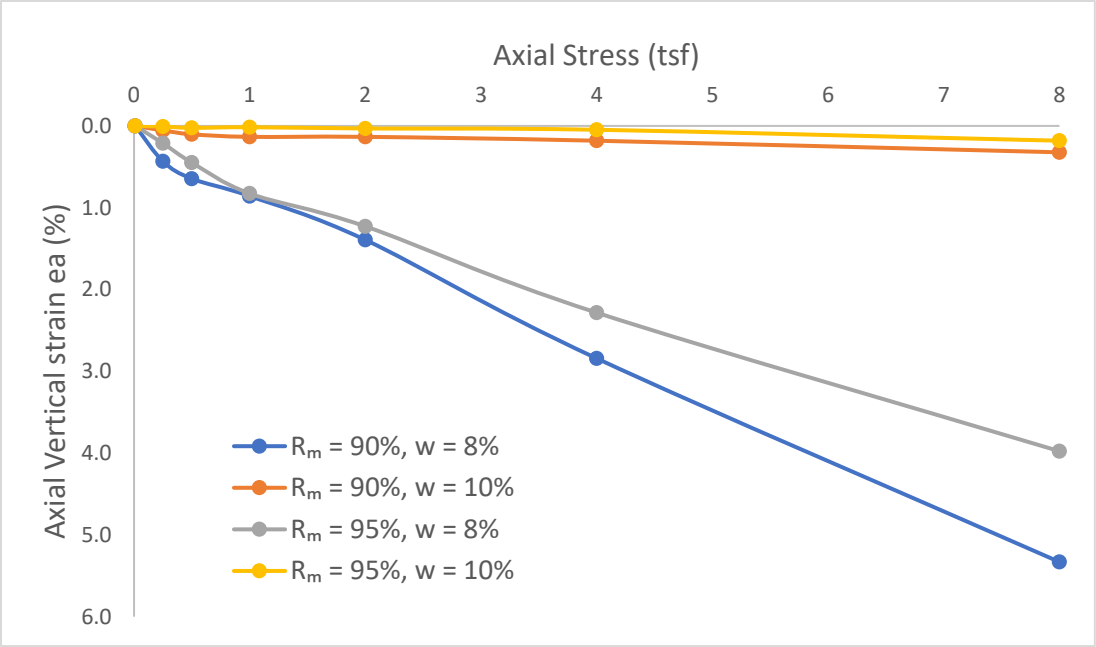

Figure B.46: One-dimensional Double Consolidometer Test Results for A-1-a (SM) Soil

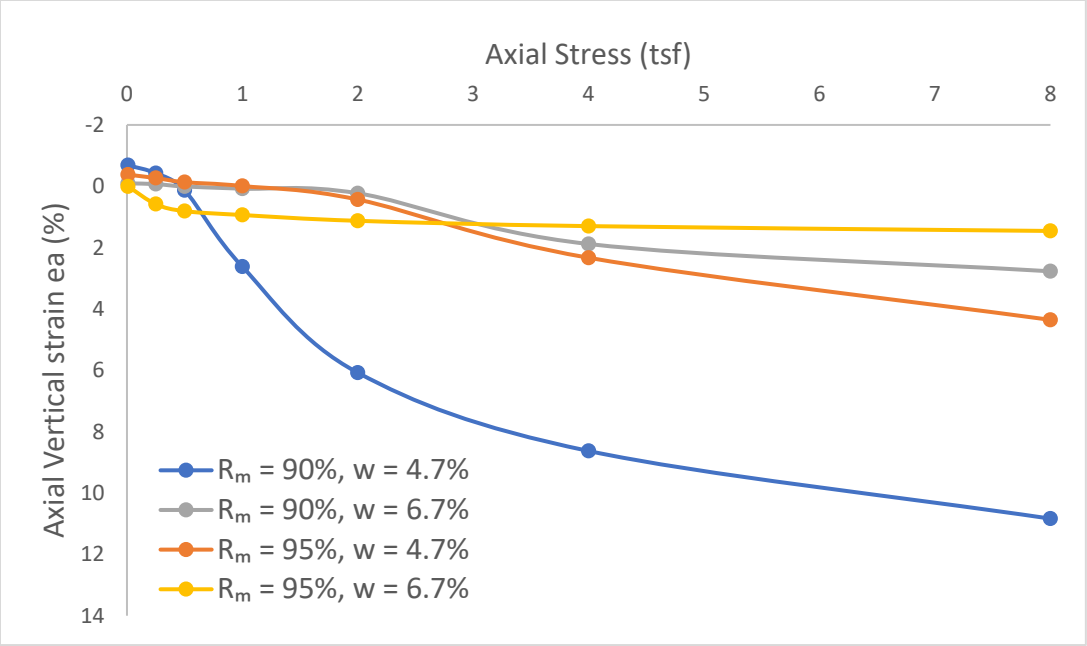

Figure B.47: One-dimensional Double Consolidometer Test Results for A-1-b (SC-SM) Soil

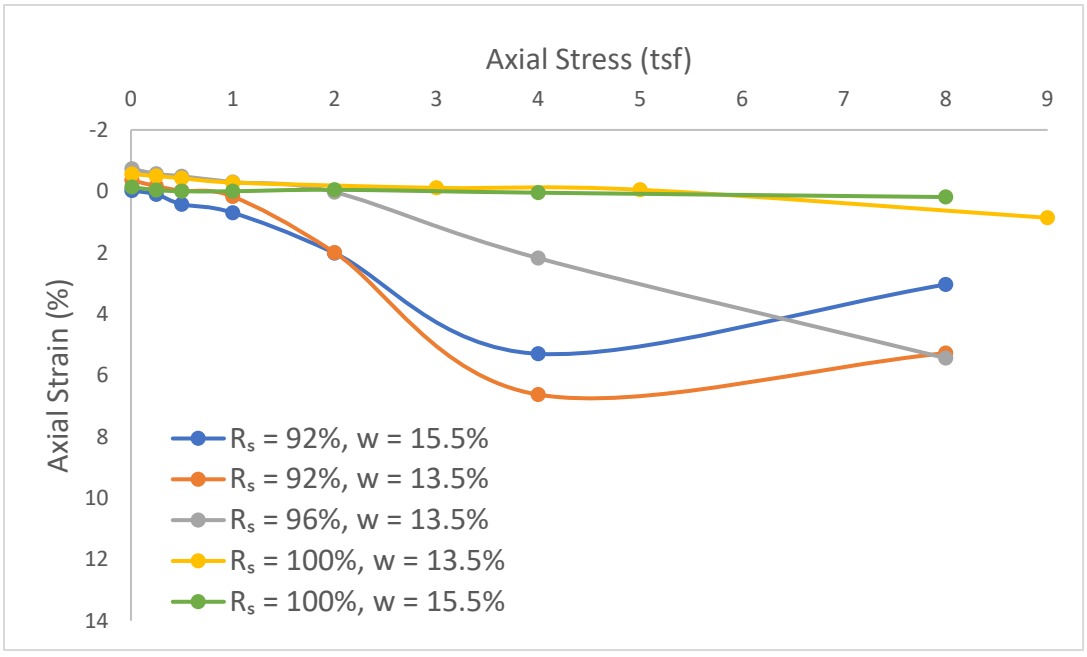

Figure B.48: One-dimensional Double Consolidometer Test Results for A-2 (SC) PI=10 Soil

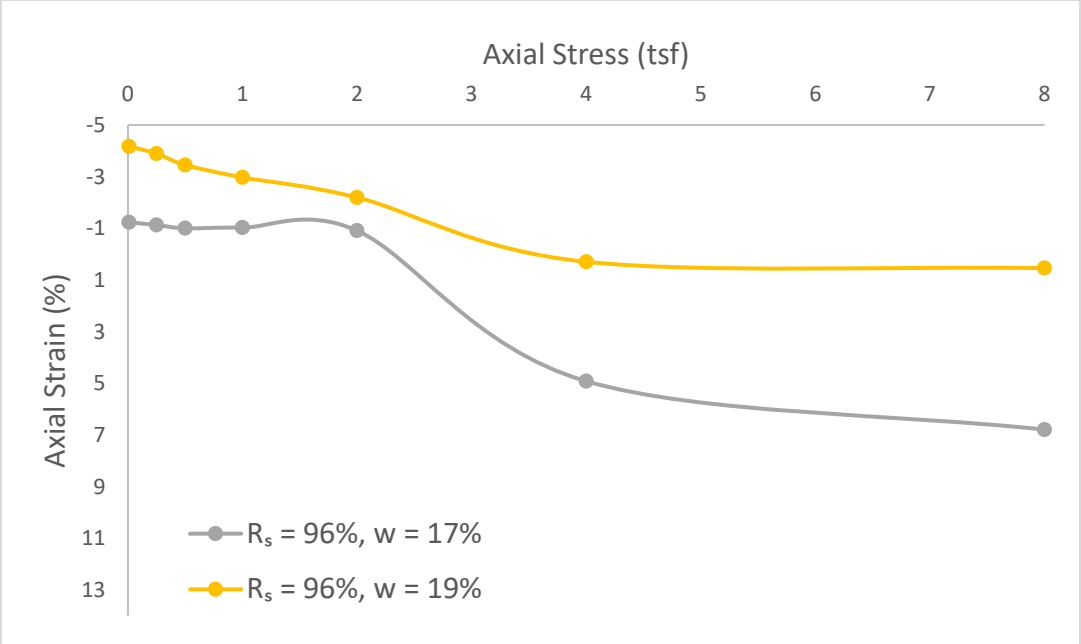

Figure B.49: One-dimensional Double Consolidometer Test Results for A-2 (SC) PI>>11 Soil

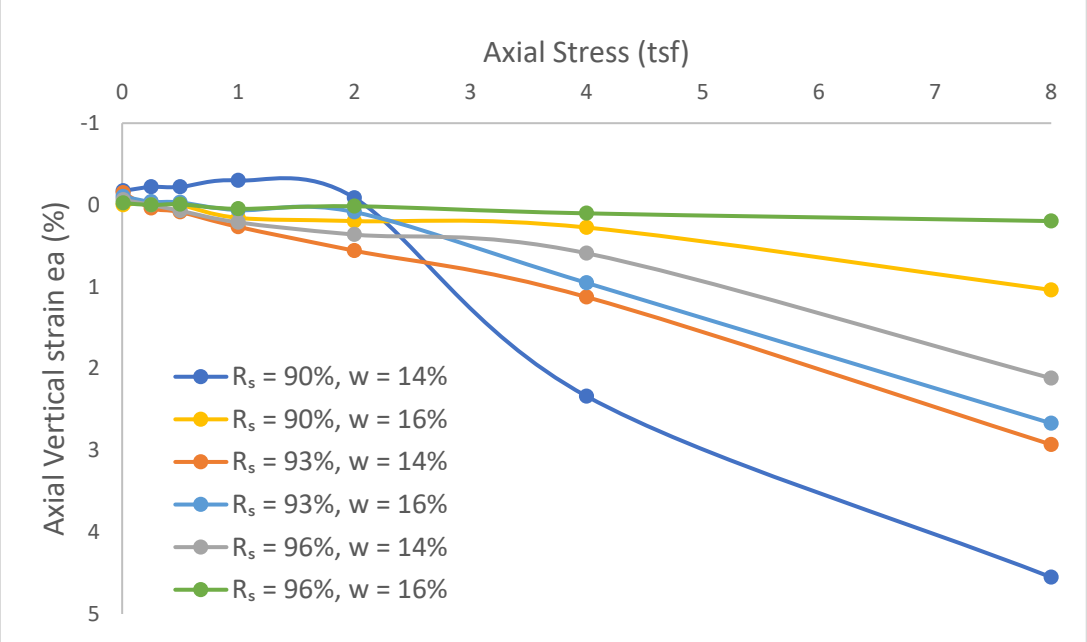

Figure B.50: One-dimensional Double Consolidometer Test Results for A-3 (SP-SM) Soil

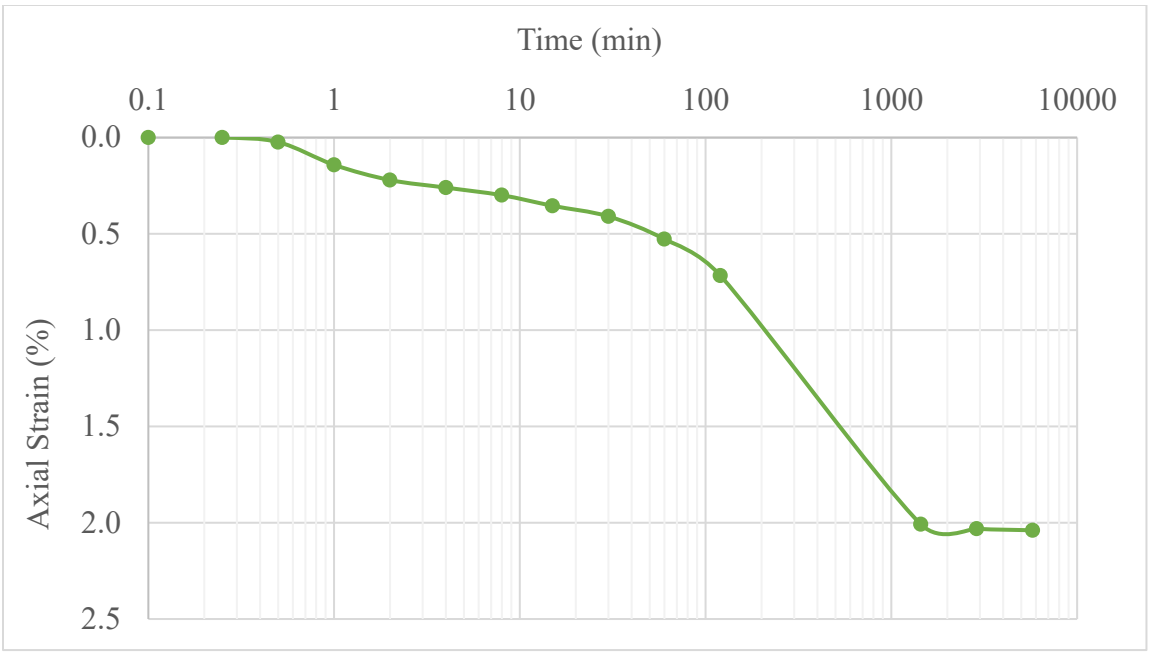

Figure B.51: Strain vs. Logarithm of Time for Single-consolidometer Soaked Specimen A-4 (CL) - R_s = 92%, w = 21%, 2tsf

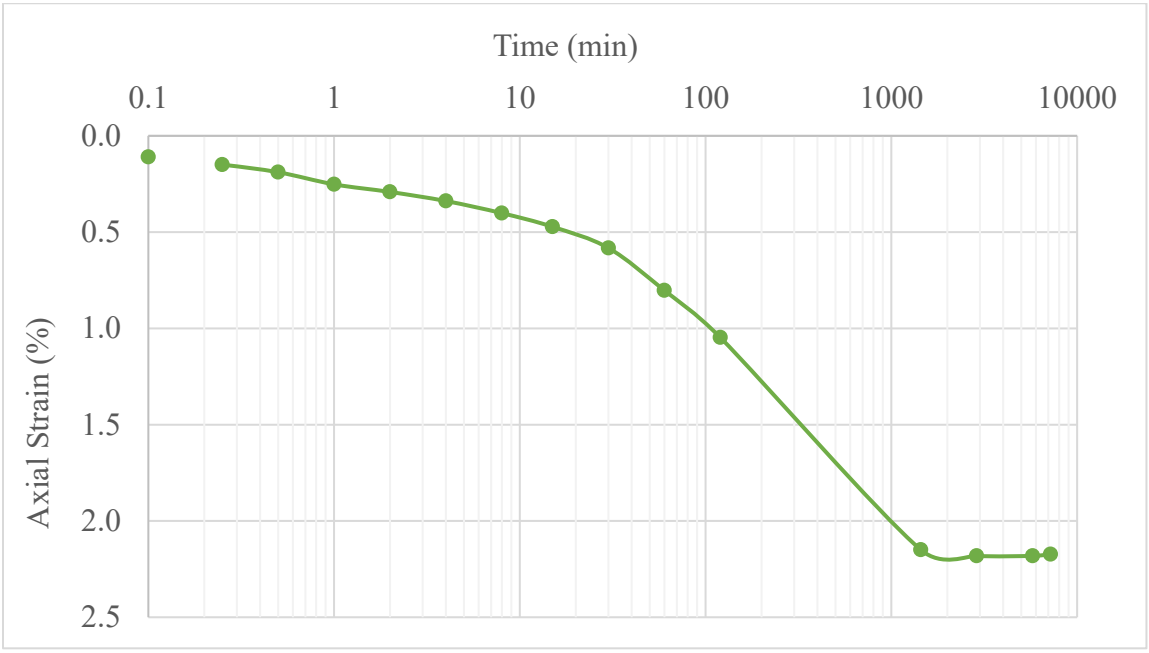

Figure B.52: Strain vs. Logarithm of Time for Single-consolidometer Soaked Specimen A-4 (CL) - R_s = 96%, w = 17%, 2tsf

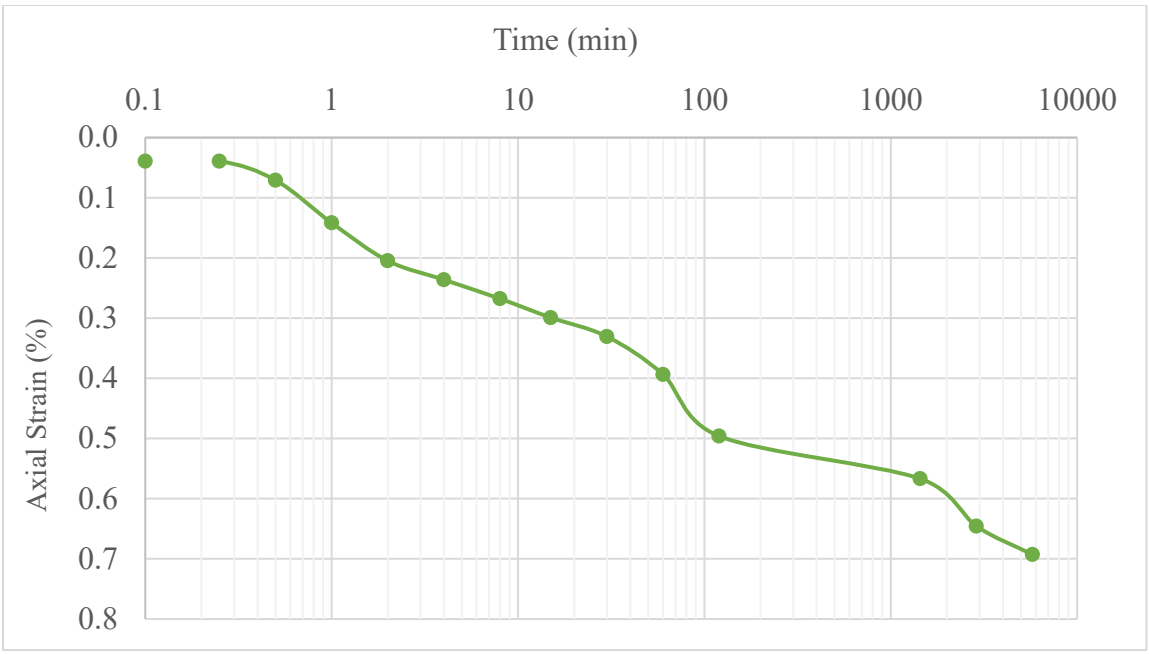

Figure B.53: Strain vs. Logarithm of Time for Single-consolidometer Soaked Specimen A-4 (CL) - Rs = 96%, w = 21%, 2tsf

APPENDIX C: GRAPHS SHOWING THE ACCURACY OF THE CURRENT COLLAPSE PREDICTIVE MODEL

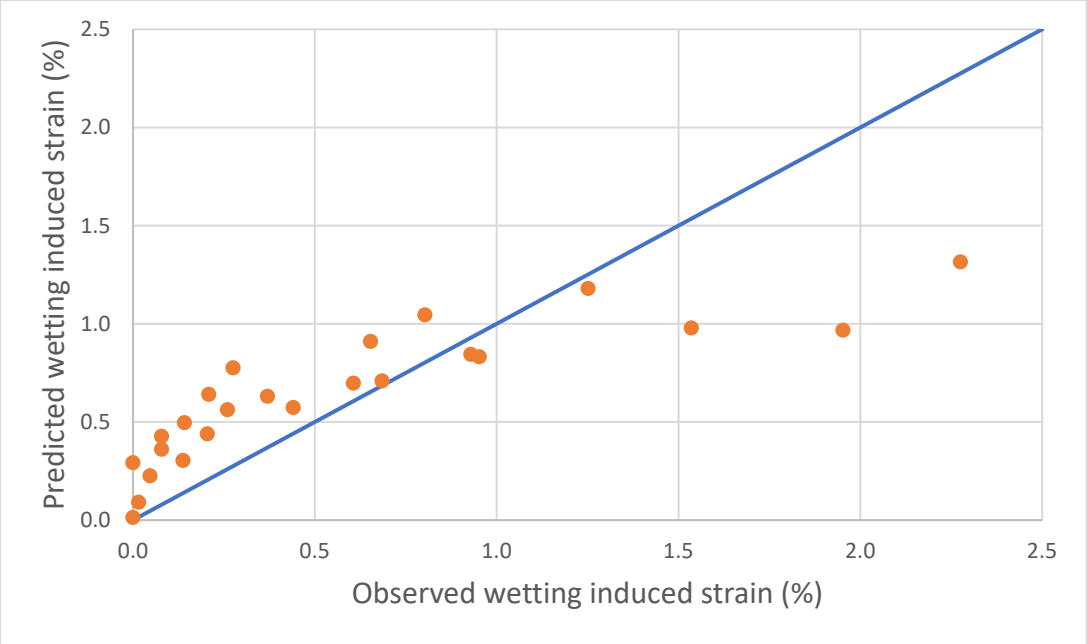

Figure C.1: Predicted vs. Observed Wetting-induced Strain for A-1-a (SP or SW) Soil Using Equation 4.1

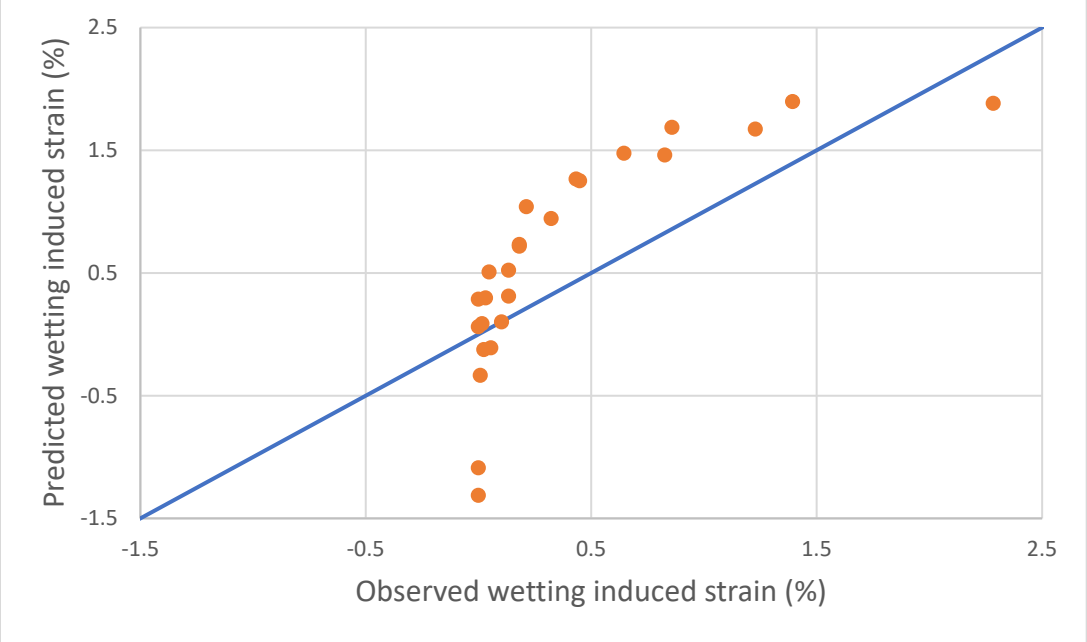

Figure C.2: Predicted vs. Observed Wetting-induced Strain for A-1-a (SM) Soil Using Equation 4.1

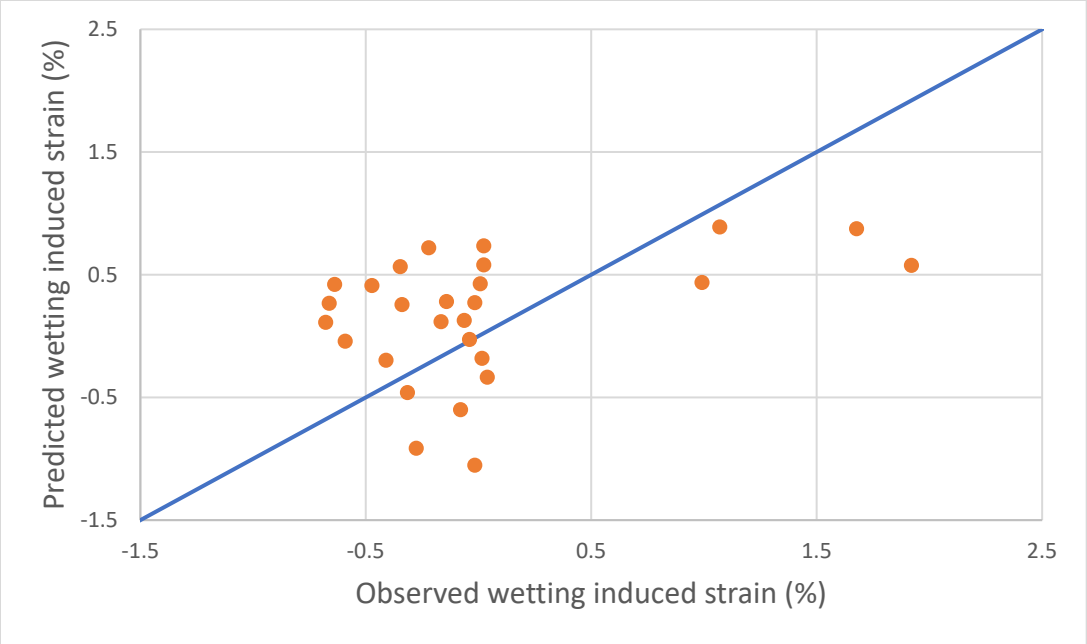

Figure C.3: Predicted vs. Observed Wetting-induced Strain for A-1-a (SC-SM) Soil Using Equation 4.1

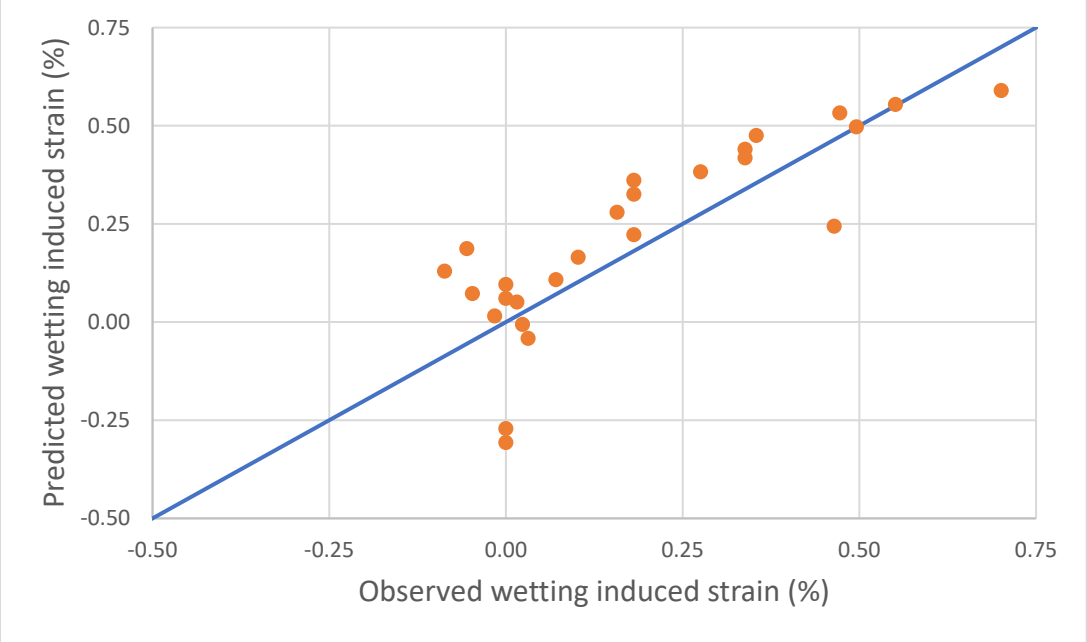

Figure C.4: Predicted vs. Observed Wetting-induced Strain for A-1-b (SM) Soil Using Equation 4.1

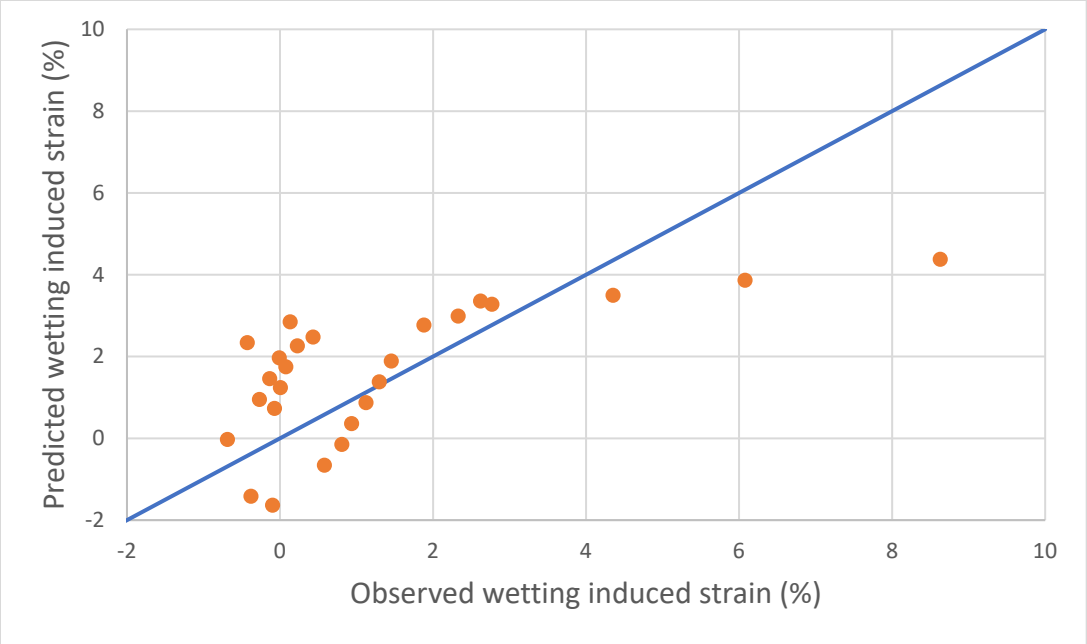

Figure C.5: Predicted vs. Observed Wetting-induced Strain for A-1-b (SC-SM) Soil Using Equation 4.1

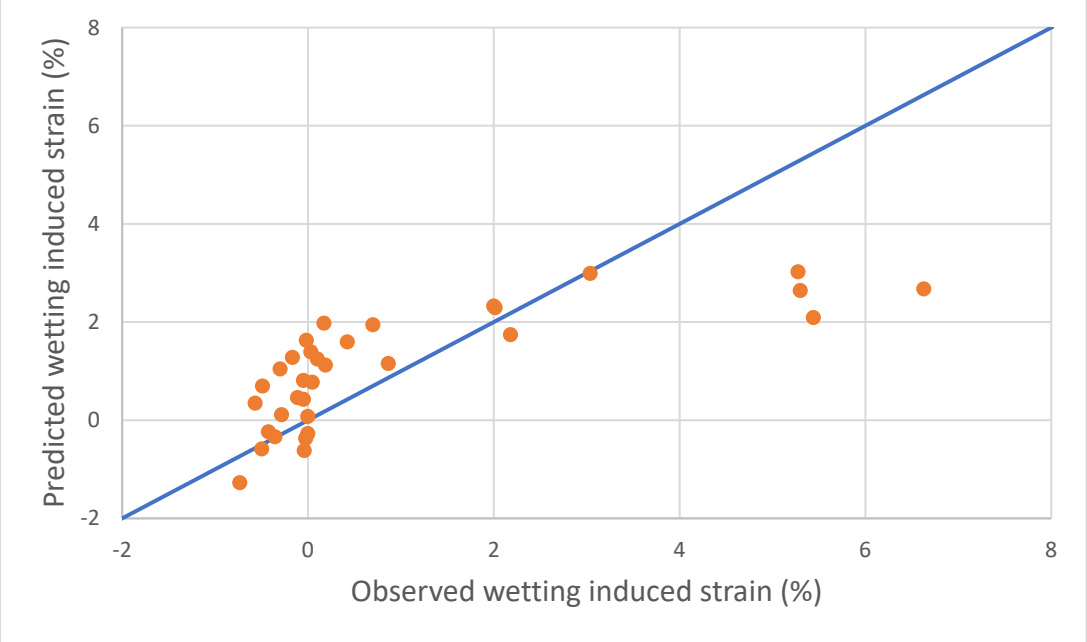

Figure C.6: Predicted vs. Observed Wetting-induced Strain for A-2 (SC) With PI=10 Soil Using Equation 4.1

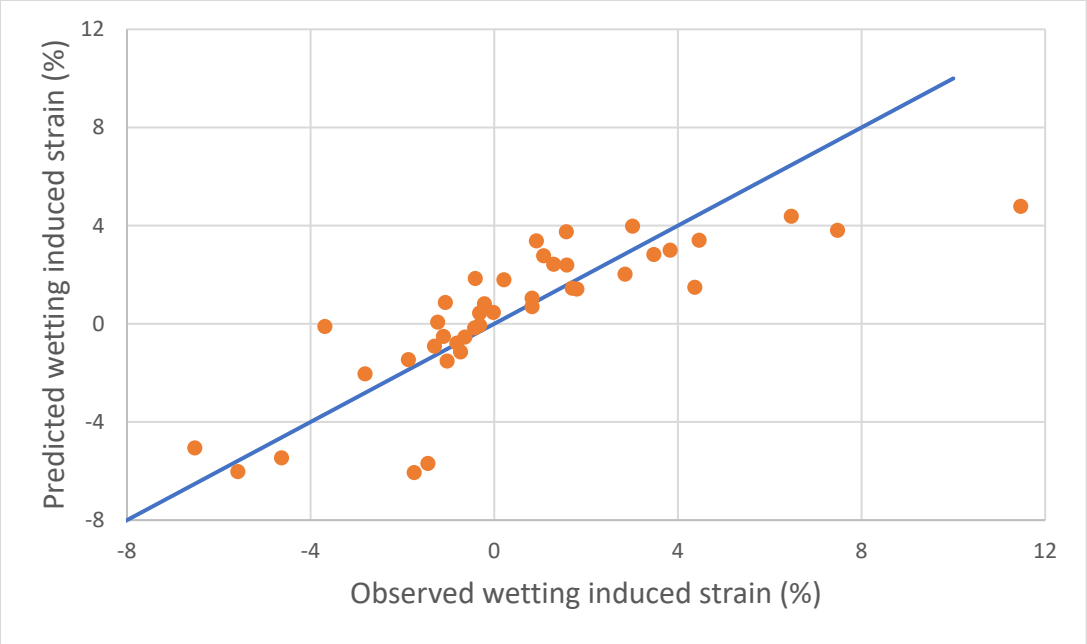

Figure C.7: Predicted vs. Observed Wetting-induced Strain for A-2 (SC) With PI>>11 Soil Using Equation 4.1

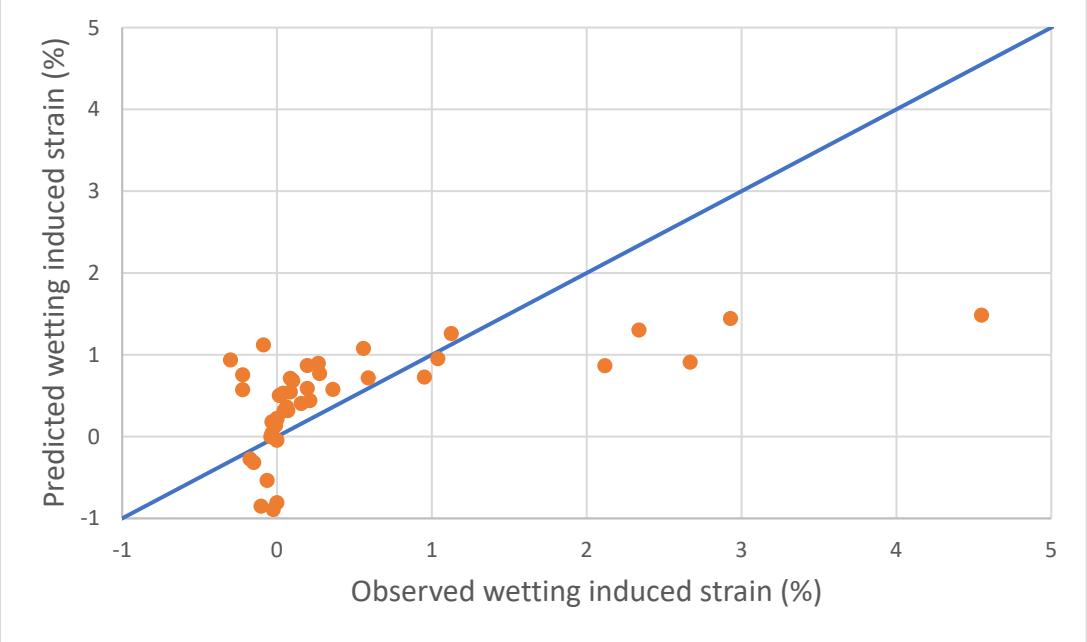

Figure C.8: Predicted vs. Observed Wetting-induced Strain for A-3 (SP-SM) Soil Using Equation 4.1

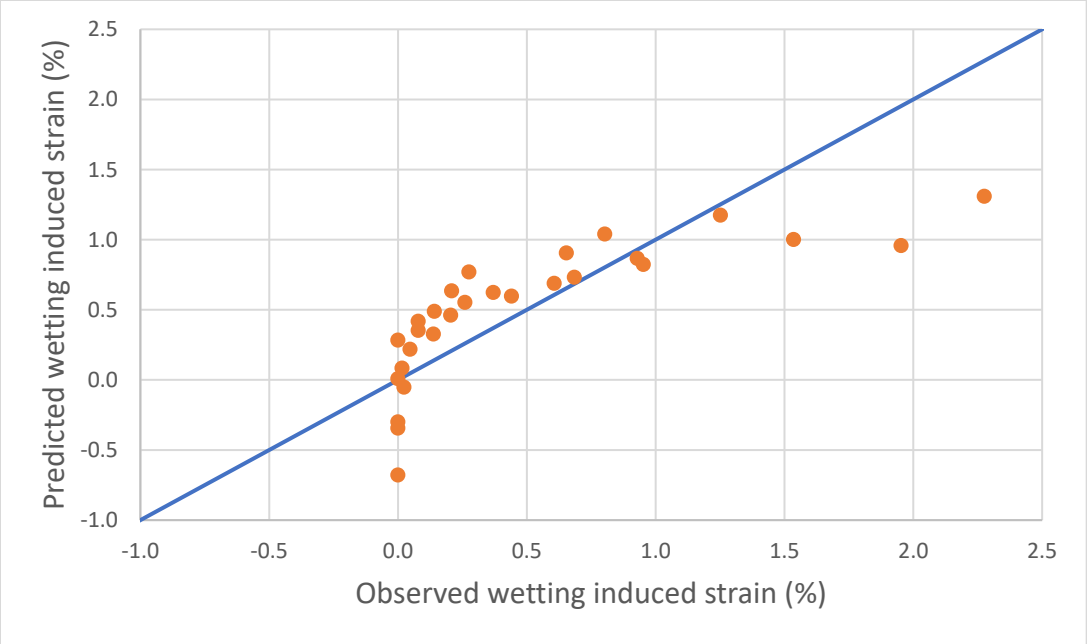

Figure C.9: Predicted vs. Observed Wetting-induced Strain for A-1-a (SP or SW) Soil Using Equation 4.2

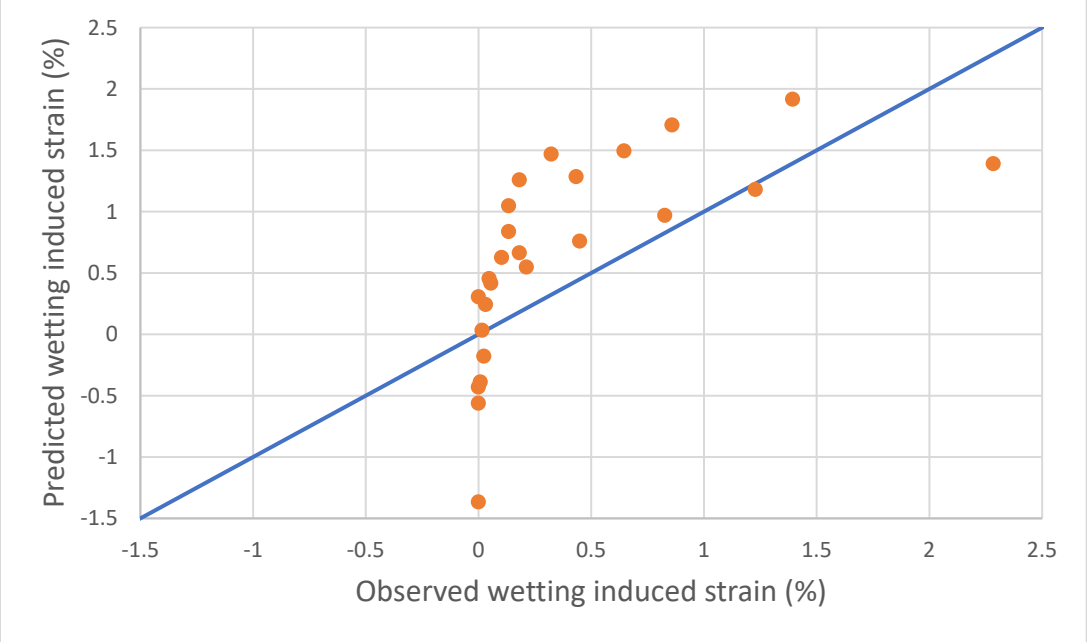

Figure C.10: Predicted vs. Observed Wetting-induced Strain for A-1-a (SM) Soil Using Equation 4.2

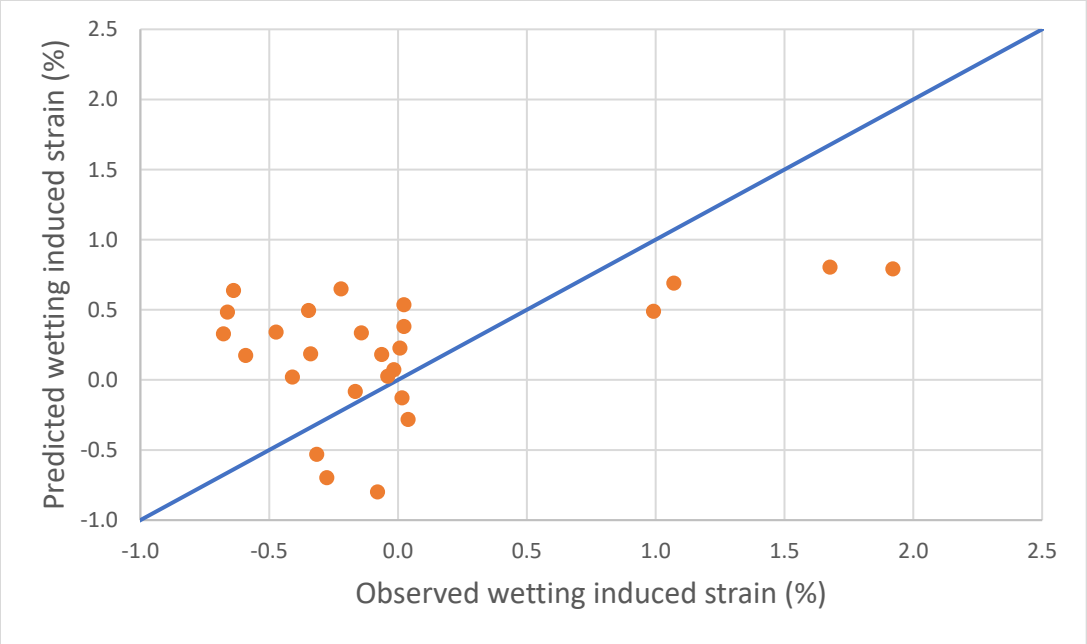

Figure C.11: Predicted vs. Observed Wetting-induced Strain for A-1-a (SC-SM) Soil Using Equation 4.2

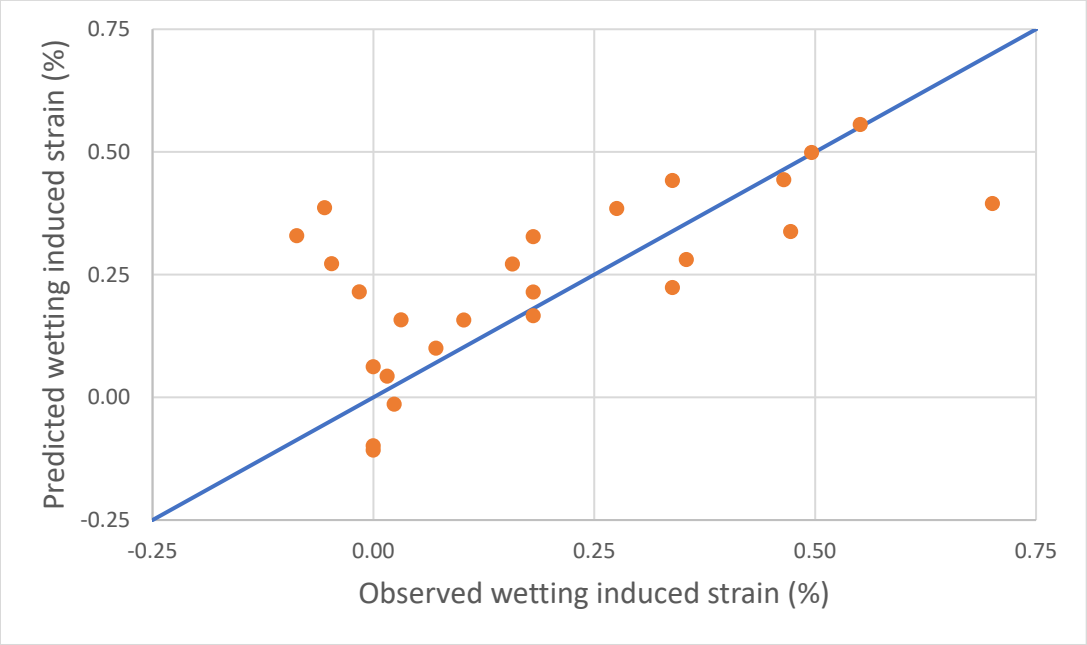

Figure C.12: Predicted vs. Observed Wetting-induced Strain for A-1-b (SM) Soil Using Equation 4.2

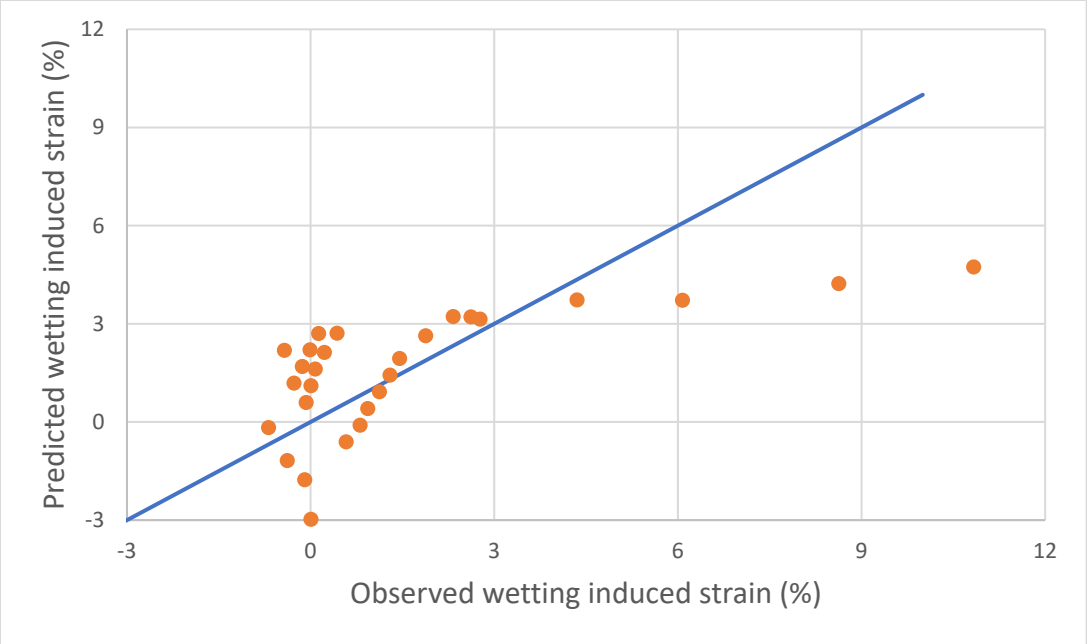

Figure C.13: Predicted vs. Observed Wetting-induced Strain for A-1-b (SC-SM) Soil Using Equation 4.2

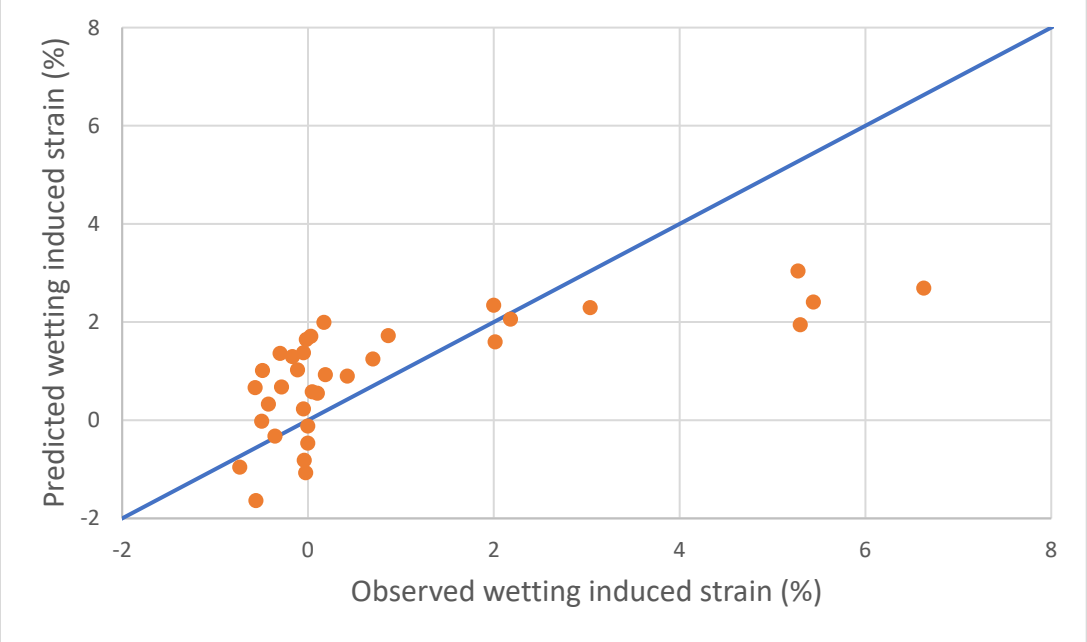

Figure C.14: Predicted vs. Observed Wetting-induced Strain for A-2 (SC) With PI=10 Soil Using Equation 4.2

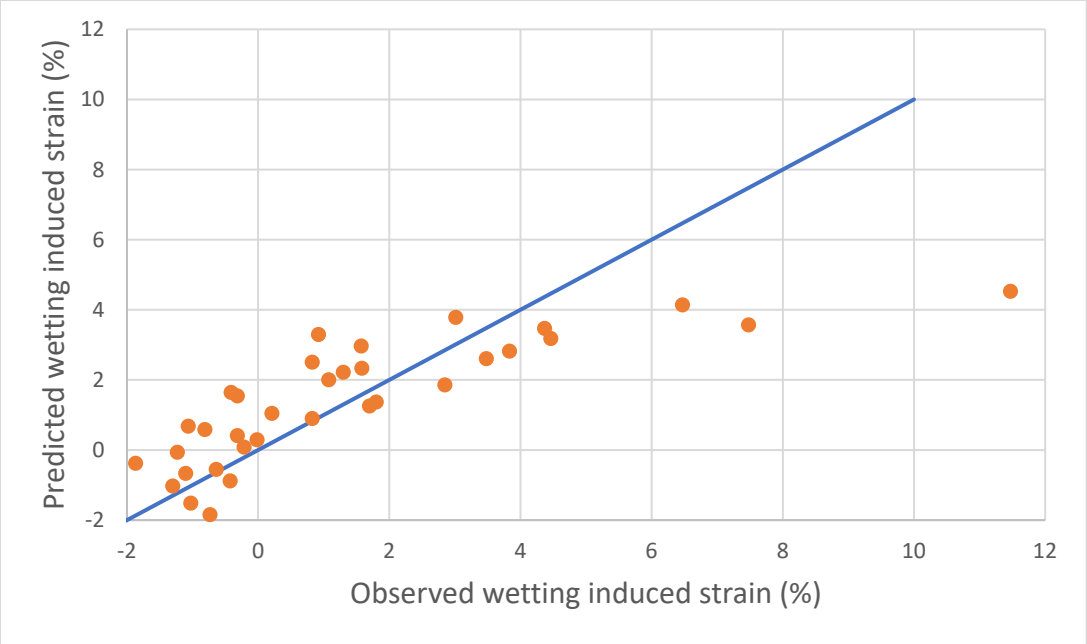

Figure C.15: Predicted vs. Observed Wetting-induced Strain for A-2 (SC) With PI>>11 Soil Using Equation 4.2

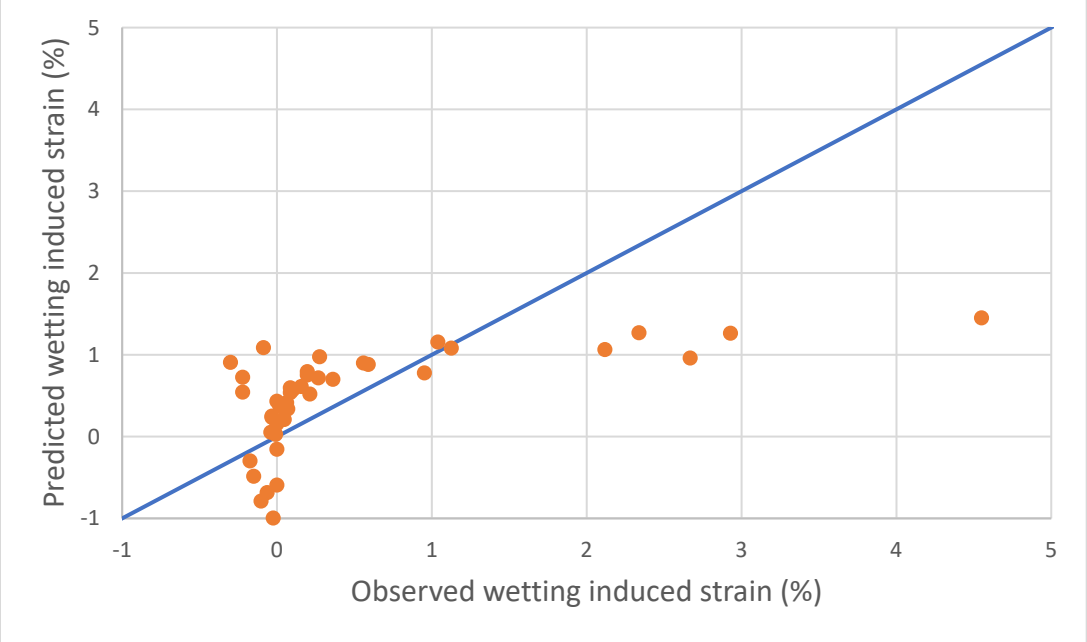

Figure C.16: Predicted vs. Observed Wetting-induced Strain for A-3 (SP-SM) Soil Using Equation 4.2

APPENDIX D: GRAPHS SHOWING THE ACCURACY OF PREVIOUSLY DEVELOPED COLLAPSE PREDICTIVE MODELS

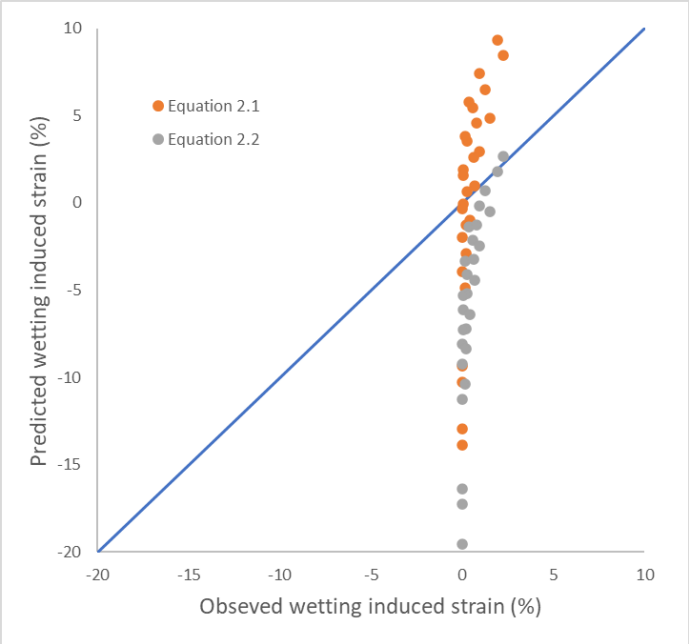

Figure D.1: Predicted vs. Observed Wetting-induced Strain for A-1-a (SP or SW) Soil Using Equations 2.1 and 2.2

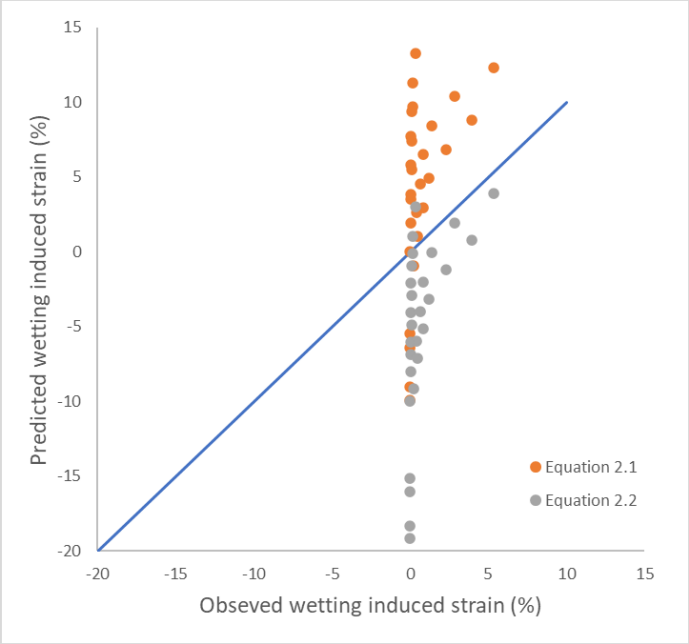

Figure D.2: Predicted vs. Observed Wetting-induced Strain for A-1-a (SM) Soil Using Equations 2.1 and 2.2

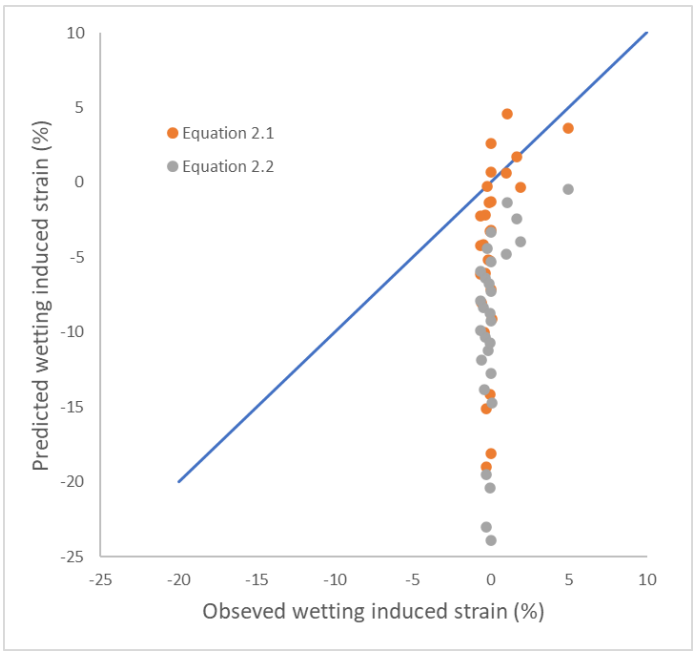

Figure D.3: Predicted vs. Observed Wetting-iInduced Strain for A-1-a (SC-SM) Soil Using Equations 2.1 and 2.2

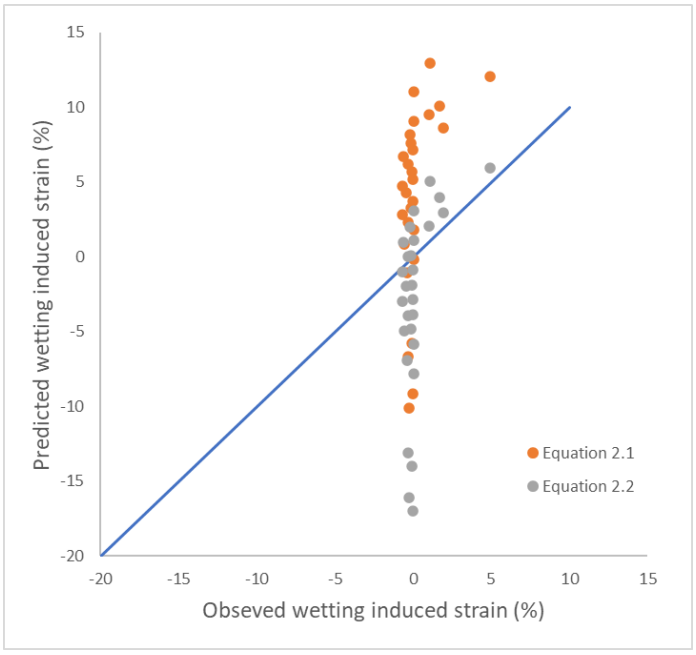

Figure D.4: Predicted vs. Observed Wetting-induced Strain for A-1-b (SM) Soil Using Equations 2.1 and 2.2

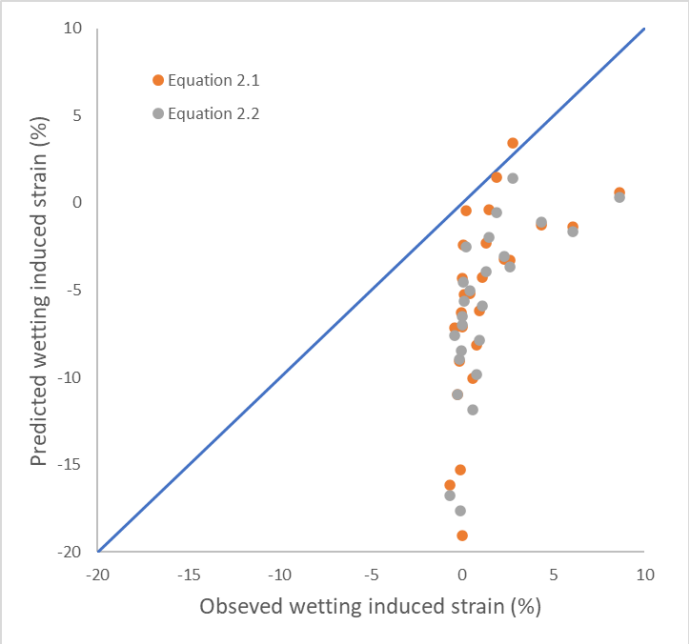

Figure D.5: Predicted vs. Observed Wetting-induced Strain for A-1-b (SC-SM) Soil Using Equations 2.1 and 2.2

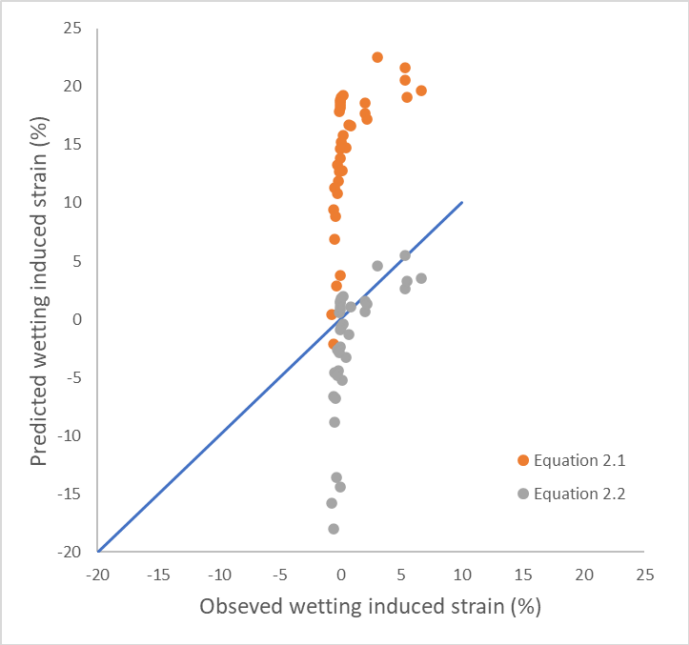

Figure D.6: Predicted vs. Observed Wetting-induced Strain for A-2 (SC) With PI=10 Soil Using Equations 2.1 and 2.2

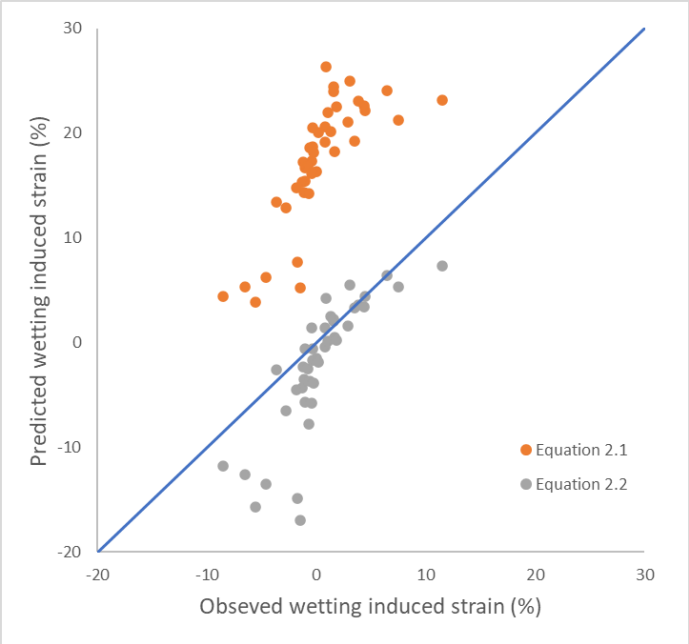

Figure D.7: Predicted vs. Observed Wetting-induced Strain for A-2 (SC) With PI>>11 Soil Using Equations 2.1 and 2.2

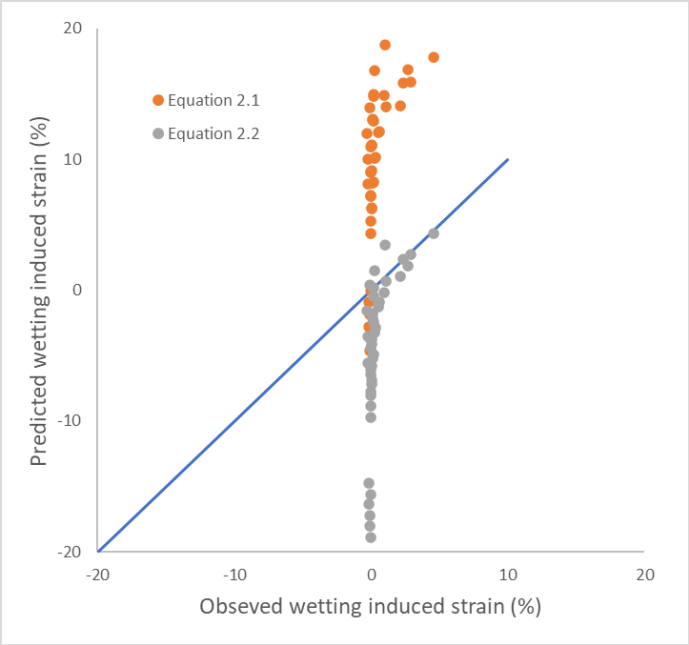

Figure D.8: Predicted vs. Observed Wetting-induced Strain for A-3 (SP-SM) Soil Using Equations 2.1 and 2.2

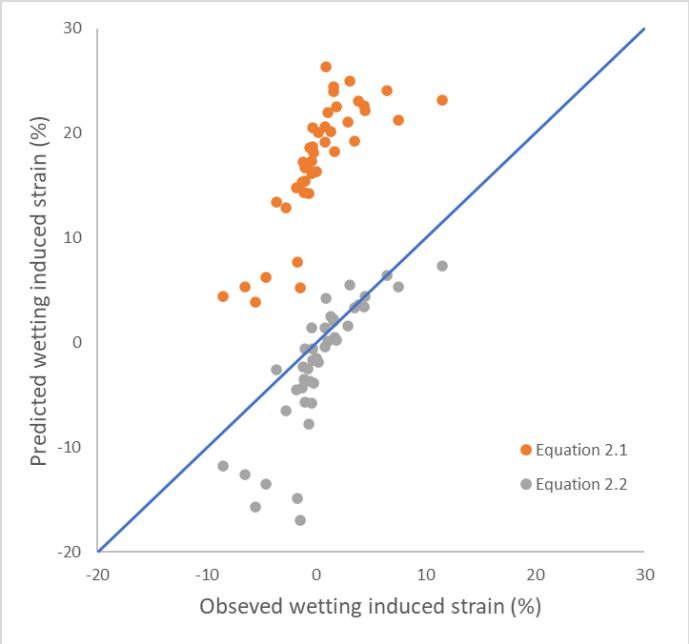

Figure D.7: Predicted vs. Observed Wetting-induced Strain for A-2 (SC) With PI>>11 Soil Using Equations 2.1 and 2.2

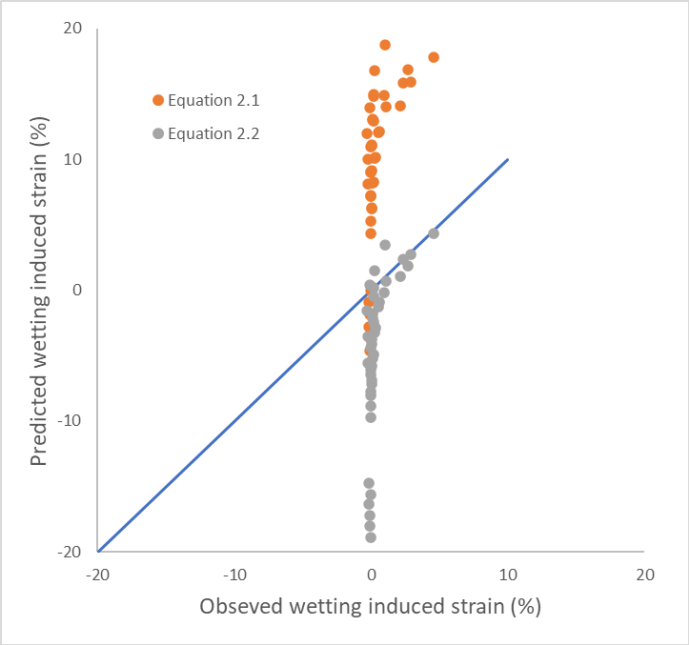

Figure D.8: Predicted vs. Observed Wetting-induced Strain for A-3 (SP-SM) Soil Using Equations 2.1 and 2.2